STRUCTURAL PERFORMANCE OF SELF-CONSOLIDATING CONCRETE IN

AASHTO TYPE I PRESTRESSED GIRDERS

Except where reference is made to the work of others, the work described in this thesis is my own or was done in collaboration with my advisory committee. This thesis does not include proprietary or classified information.

_____
Kurtis McKinley Boehm

Certificate of Approval:

_____
Anton K. Schindler
Gottlieb Associate Professor
Civil Engineering

_____
Robert W. Barnes, Chair
James J. Mallett Associate Professor
Civil Engineering

_____
Mary L. Hughes
Assistant Professor
Civil Engineering

_____
George T. Flowers
Interim Dean
Graduate School

STRUCTURAL PERFORMANCE OF SELF-CONSOLIDATING CONCRETE IN

AASHTO TYPE I PRESTRESSED GIRDERS

Kurtis McKinley Boehm

A Thesis

Submitted to

the Graduate Faculty of

Auburn University

in Partial Fulfillment of the

Requirements for the

Degree of

Master of Science

Auburn, AL

August 9, 2008

STRUCTURAL PERFORMANCE OF SELF-CONSOLIDATING CONCRETE IN

AASHTO TYPE I PRESTRESSED GIRDERS

Kurtis McKinley Boehm

Permission is granted to Auburn University to make copies of this thesis at its discretion, upon requests of individuals or institutions and at their expense. The author reserves all publication rights.

<div style="text-align:right">

_____
Signature of Author

_____
Date of Graduation

</div>

VITA

Kurtis McKinley Boehm, son of Ronald James Boehm and Marsha Renee Boehm, was born July 27, 1983, in Baton Rouge, Louisiana. He graduated with honors from Virgil I. Grissom High School in Huntsville, Alabama, in 2002. He attended Auburn University on an academic scholarship and graduated magna cum laude with a Bachelor of Civil Engineering degree in 2006. He entered the Graduate School at Auburn University in May, 2006 to seek the degree of Master of Science in Civil Engineering (Structures). After graduate school, he began work as a design engineer for BE&K Engineering in Birmingham, Alabama.

THESIS ABSTRACT

STRUCTURAL PERFORMANCE OF SELF-CONSOLIDATING CONCRETE IN

AASHTO TYPE I PRESTRESSED GIRDERS

Kurtis McKinley Boehm

Master of Science, August 9, 2008
(B.C.E., Auburn University, 2006)

281 Typed Pages

Directed by Robert W. Barnes

As part of a larger investigation sponsored by the Alabama Department of

Transportation (ALDOT) into the use of self-consolidating concrete (SCC) in bridge

girders, this thesis documents a structural investigation of SCC in AASHTO Type I

precast, prestressed girders. Six test girders were subjected to transfer length and flexural

testing. Three separate concrete mixtures, two girders per mixture, were used to

construct these specimens. One mixture was a moderate-strength, conventional-slump

concrete mixture, similar to the concrete used in typical ALDOT girders, with a

compressive strength at prestress transfer of approximately 5,000 psi. The other two

mixtures consisted of moderate-strength SCC and high-strength SCC, with compressive

strengths at prestress transfer of approximately 5,000 psi and 10,000 psi, respectively.

No significant difference in transfer bond behavior was found between the full-scale SCC girders and the conventional concrete girders. High-strength SCC girders had shorter transfer lengths than moderate-strength (SCC and conventional) girders. This behavior was accurately estimated by assuming the transfer length was directly proportional to the prestress magnitude and inversely proportional to the square root of the concrete compressive strength at transfer. After normalization for these effects, there was no discernible difference in the magnitude of the transfer lengths between the concrete types. Based on comparisons to smaller specimens in earlier phases of the study, transfer lengths decreased with increasing cross-section size for all concrete types. Significant growth of transfer length over time was found, demonstrating that reliable estimates of long-term transfer lengths are difficult to estimate solely on measurements of initial transfer lengths. In conjunction with the transfer length testing, a strand draw-in program was employed in order to assess its ability to accurately predict transfer lengths.

After a composite, cast-in-place concrete deck was added to each girder, flexural testing was performed near each girder end, resulting in two flexural tests per girder. Embedment lengths were varied for each test in order to bracket the AASHTO strand development length. Results indicated that the SCC mixture proportioning had no adverse effects on the overall flexural performance, and the flexural bond lengths were conservatively predicted by the relevant ACI and AASHTO expressions. Similarly, the SCC girders exhibited comparable service-level performance to the conventional girders. Based on observations of deck separation and slip, deck-to-girder interface shear transfer was less effective for the SCC girders than for the conventional girders. This was attributed to inadequate surface roughening of the SCC girders.

ACKNOWLEDGEMENTS

Style manual used Kate L. Turabian A Manual for Writers of Term Papers, Theses, and

Dissertations. 6th ed.

Computer software used Microsoft Word, Microsoft Excel, and Microsoft PowerPoint

TABLE OF CONTENTS

LIST OF TABLES

LIST OF FIGURES

xxiii

CHAPTER 1

INTRODUCTION

1.1 BACKGROUND

The precast, prestressed industry contributes too many of the structures built today. Structures such as highway bridges, parking decks, and flooring systems make up a vast majority of the structures built from precast, prestressed concrete elements. The ability of this industry to reliably mass-produce elements for these types of structures not only eases the construction process but also makes their products appealing to structural designers. For years the precast, prestressed industry has successfully utilized conventional-slump concrete to construct these structural elements. However, there is much room for improvement, specifically in the consolidation process of the fresh concrete. The successful use of self-consolidating concrete (SCC) in general precast members has generated interest in cost savings potential within the precast, prestressed concrete industry.

Conventional-slump concrete utilizes external/internal vibration procedures to obtain proper consolidation of fresh concrete. This process can be extremely time-consuming and also potentially hazardous, noisy, and tedious, all of which can result in increased costs. In spite of all the effort put forth into vibration, bug holes and voids are often still present on the surfaces of precast, prestressed elements once the forms are

stripped. These results generate additional labor costs in order to patch the unsightly voids and to restore the intended cover to the tendons. SCC, as the name suggests, is designed to consolidate without vibration, thereby eliminating these negative aspects.

SCC was first developed in Japan in the early 1980's by Hajime Okamura, a professor at Kocki University of Technology (Okamura and Ouchi 1999). It is a highly flowable concrete that is able to deform under its own weight, when wet, and completely encapsulate any reinforcement without exhibiting segregation or bleeding (Khayat 1999). The ability of SCC to flow around the reinforcement allows the concrete to be placed without the need for vibration. It is also significant to note that current research has shown that many SCC mixtures can be created by using supplementary cementing materials (SCM), which are industrial by-products such as fly ash and ground-granulated blast-furnace slag, as a partial replacement for cement in the concrete. This reduces some of the negative environmental impacts of producing cement, as well as offers a safe use for waste materials that would otherwise be land filled.

Due to the obvious advantages of SCC over conventional concrete, the precast, prestressed industry is actively pursing its use for their products. Special attention has been given to prestressed bridge girders by many state transportation agencies. However, like any new product, concern has been expressed about its structural performance. SCC is typically created by reducing the amount of coarse aggregate and increasing the amount of total fines relative to conventional concrete mixtures in conjunction with utilizing relatively high amounts of chemical admixtures. As a result, questions concerning time-dependent deformations, prestress losses, shear capacity, and the stiffness of bridge girders cast with SCC have been asked. In addition, concern regarding

2

SCC's ability to effectively bond to the prestressing steel in the anchorage zone of bridge girders has arisen. Until more research is performed regarding the above issues, the widespread implementation of precast, prestressed bridge girders made with SCC will not be achieved.

1.2 RESEARCH OBJECTIVES

The Alabama Department of Transportation (ALDOT) sponsored an investigation by the Auburn University Highway Research Center to evaluate the use of SCC in precast, prestressed concrete bridge girders. The study presented in this thesis is a portion of this investigation. The primary objective of the study described in this thesis was to verify that the structural behavior of SCC observed in extensive small-scale experiments performed in previous phases of the investigation can be extrapolated to full-scale bridge girders constructed with SCC.

Transfer length testing and flexural testing were performed on full-scale prestressed AASHTO Type I girders cast with both SCC and conventional concrete in order to evaluate and compare the general bond behavior, service and ultimate load flexural behavior, and shear capacities. In addition to the primary objective stated above, several other specific objectives were targeted:

1) Assess the feasibility of constructing plant-cast SCC prestressed girders.

2) Determine whether ACI and AASHTO transfer and development length provisions are adequate for SCC girders.

3) Assess the ability of strand draw-in measurements to accurately predict transfer lengths.

3

4) Determine whether the flexural strength of SCC girders is adequately predicted using existing AASHTO provisions.

1.3 RESEARCH SCOPE

This research study consisted of an investigation into the structural performance of SCC in 40-ft long AASHTO Type I prestressed concrete girders. Four of the six bridge girders were cast using SCC and two were cast using a conventional mixture. The conventional mixture was a standard concrete mixture commonly used by ALDOT for precast, prestressed bridge girders in which proper consolidation is achieved by using internal vibration. Transfer length measurements were performed immediately after prestress release, as well as at 3-day, 7-day, 14-day, 28-day, two-month, and three-month ages on all six specimens. Flexural testing was performed on both ends of each specimen separately, resulting in twelve tests. Each test consisted of a flexural loading up to ultimate strength in order to investigate the specimen's response. Strand embedment lengths and span lengths were varied to assess the bonded length necessary to ensure a flexural failure type without strand end slip. The mixing, fabrication, and transfer length measurements of the six bridge girders were performed at the Hanson Prestress Plant in Pelham, Alabama. Flexural testing was performed in the Structural Engineering Laboratory of the Auburn University Department of Civil Engineering. In order to achieve desirable tendon elongations during testing, a cast-in-place, composite deck was added to each bridge girder prior to flexural testing. All composite decks were cast using conventional-slump 4,000 psi concrete.

Three different concrete mixtures, two SCC and one conventional, were used to construct the girder specimens. Two bridge girders were constructed with each mixture. The conventional mixture was a moderate-strength mixture with an average compressive strength at prestress transfer of 4,760 psi. The two SCC mixtures consisted of a moderate-strength mixture and a high-strength mixture. Both SCC mixtures utilized ground-granulated blast-furnace (GGBF) slag as an SCM and had average compressive strengths at transfer of 5,210 psi and 10,430 psi, respectively. All specimens used in this study were pretensioned with 0.5-in. "oversized" prestressing strand because this strand is commonly used in ALDOT prestressed bridge girders and it constitutes a more severe bond stress than a traditional 0.5-in strand.

1.4 ORGANIZATION OF THESIS

Chapter 2 provides an overview of current code provisions relating to transfer and development length from the American Concrete Institute's (ACI) *Standard Building Code Requirements for Reinforced Concrete* (ACI 318-05) and the American Association of State Highway and Transportation Officials' (AASHTO) *Standard Specifications for Highway Bridges* (2002) and *LRFD Bridge Design Specifications* (2007). A discussion of bond theory, including transfer length bond and flexural bond length, is presented. Finally, a review of previous studies involving the structural performance of SCC in precast, prestressed girders is discussed.

Chapter 3 provides a discussion of the design and fabrication of the tested specimens. Specimen details, mixture proportions, material properties, and construction processes are discussed in detail.

A discussion of the transfer length test program is provided in chapter 4. The details and procedures utilized for the measurement and determination of the transfer length are discussed. The transfer length results are presented and compared to previous findings obtained in prior phases of this investigation, as well as to current design provisions.

Chapter 5 provides a discussion of the draw-in test program. The details and procedures utilized for the measurement of strand draw-in and the determination of the transfer length based upon the draw-in results are discussed. The predicted transfer length results are presented and compared to the actual measured transfer lengths and to previous findings obtained from prior phases of this investigation.

Chapter 6 provides a discussion of the flexural test program. The test configurations, instrumentation, and procedures are presented. The results for all 12 flexural tests performed are also presented, along with several relevant discussions. Specifically, the flexural bond performance, service load level performance, and cracking load performance observed for all tests are presented in detail. A discussion concerning the unexpected deck separation and slip observed in several of the SCC specimens is also offered.

Chapter 7 provides a brief summary of this research study and presents conclusions and recommendations based upon its findings. Recommendations for further research are also presented.

1.5 NOTATION

The most commonly used design code for precast, prestressed concrete bridge girders within the United States is the *AASHTO LRFD Bridge Design Specifications* (2007). As a result, the notation employed within this specification is used throughout this thesis. A list of the relevant terms and symbols used in this thesis is presented in the Notation section, which can be found in Appendix A of this thesis.

CHAPTER 2

PRETENSIONED MEMBERS: BOND BEHAVIOR AND PREVIOUS RESEARCH ON SCC IMPLEMENTATION

2.1 INTRODUCTION

The anchorage of prestressing strands to the surrounding concrete is essential in the design and construction of pretensioned members. In precast, prestressed bridge girders, adequate anchorage is provided by bond between the strands and the concrete along the length of the strand. If this anchorage by bond is inadequate, the structural integrity of the girder is compromised and can result in decreased flexural, shear, or torsional resistance. As a result, the structure built with this member will likely exhibit premature failure if actual loads approach those assumed in design. Therefore, there are relevant code provisions in both the ACI building code and the AASHTO bridge design code to ensure adequate anchorage of pretensioned reinforcement.

In this chapter, the current philosophy regarding anchorage of prestressing strands in pretensioned members is discussed. A discussion of key terms, current code provisions and their backgrounds, and transfer bond theory is presented. In addition, a review of recent investigations into the structural behavior of SCC in pretensioned members is presented in this chapter.

2.2 DEFINITIONS

Definitions and descriptions of several key terms required for a discussion of anchorage/bond behavior of steel reinforcement to concrete are presented in this section.

2.2.1 Transfer Length

The transfer length, l_t, is defined as the length of embedded pretensioned strand required to transfer the effective prestress, f_{pe}, to the concrete (ACI 318 2005, Section 2.2). The effective prestress force changes over time due to deformation of the concrete and to relaxation of the prestressing steel. Decreases in effective prestress force are referred to as "prestress losses". Transfer length has no meaning for nonprestressed reinforcement.

2.2.2 Flexural Bond Length

The flexural bond length, l_{fb}, is defined as the additional length, beyond the transfer length, over which the strand must be bonded so that the stress, f_{ps}, in the prestressing steel required to achieve the nominal flexural strength of the member, M_n, can develop (ACI 318 2005, R12.9). In other words, the flexural bond length can be considered the extra length beyond the transfer length required for the strand stress to increase from f_{pe} to f_{ps} under the application of external loads.

2.2.3 Development Length

The development length, l_d, is defined as the length of embedded reinforcement, including pretensioned strand, required to develop the design strength of reinforcement at a critical section (ACI 318 2005, Section 2.2). In other words, the development length is the shortest bonded length of a strand along which the strand stress can increase from

zero to the stress required for achievement of the full nominal strength at the section

under consideration (Barnes et. al 1999). With regards to pretensioned members, the

development length can be considered the sum of the transfer length and the flexural

bond length, or the total bonded strand length, required to fully develop f_{ps}, the full

resistance of the strand at the nominal strength of the member. Figure 2-1 shows the

development of steel stress along the length of a member and the relationship between

transfer length, flexural bond length, and development length.
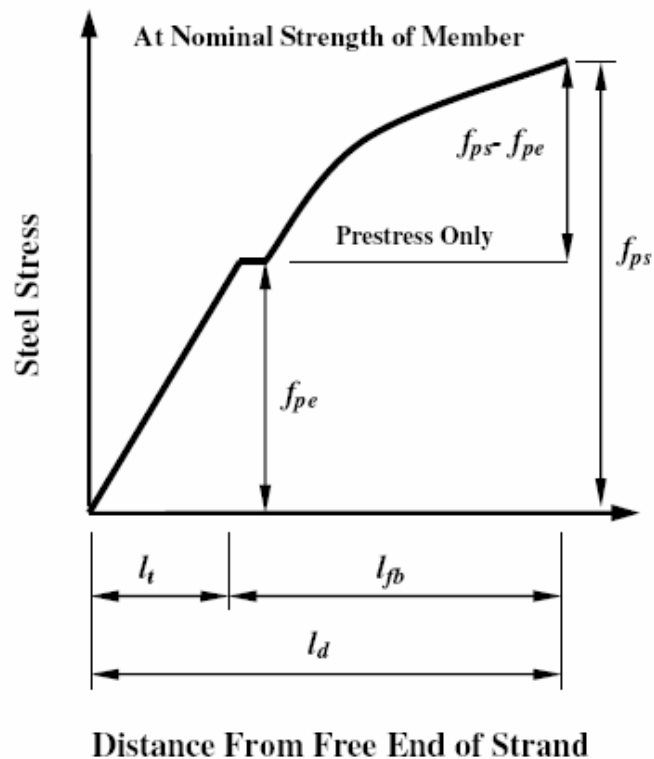
Figure 2-1: Development of Steel Stress in a Pretensioned Member
(Adapted from Barnes et al. 1999)

2.2.4 Embedment Length

The embedment length, l_e, is defined as the bonded length of the pretensioned strand

from the beginning of embedment to a critical cross section at which strength capacity is

being evaluated. If the embedment length at a critical cross section is shorter than the development length of the pretensioned strand, an anchorage/bond failure can be expected to occur before the nominal design flexural capacity of the member is reached. This is due to the fact that the embedded length of the pretensioned strand is not long enough to develop f_{ps}.

2.3 CODE PROVISIONS FOR ANCHORAGE OF STRANDS

This section discusses the current code provisions relating to anchorage of prestressed reinforcement as acknowledged in ACI's *Building Code Requirements for Structural Concrete* (ACI 318-05) and AASHTO's *Standard Specifications for Highway Bridges* (2002) and *AASHTO LRFD Bridge Design Specifications* (2007). The background research that contributed to these code provisions is also discussed. As noted in Chapter 1, the notation used throughout this thesis corresponds to the AASHTO LRFD Specification. However, ACI notation is used for definition and discussion purposes in relevant sections.

2.3.1 Relevant ACI Code Clauses and Commentary

The relevant code clauses and commentary for the development and transfer length of prestressing strand can be found in Section 12.9 of the ACI *Building Code Requirements for Structural Concrete* (ACI 318-05). The existing expression for development length was first incorporated into the ACI code in the 1963 version (Tabatabai and Dickson 1995).

      The provisions of ACI 318-05, Section 12.9 ─ *Development of prestressing strand* that are relevant read as follows:

12.9.1 — Except as provided in 12.9.1.1, seven-wire strand shall be bonded beyond the critical section, a distance not less than

$$l_d = \left(\frac{f_{se}}{3000}\right)d_b + \left(\frac{f_{ps} - f_{se}}{1000}\right)d_b \qquad \textbf{\textit{Equation 2-1}}$$

The expressions in parentheses are used as constants without units.

where, d_b = nominal strand diameter (in.)

    f_{se} = effective stress in prestressing steel, psi

    f_{ps} = stress in prestressing steel at nominal flexural strength, psi.

The ACI 318R-05 Commentary Section R12.9 states that the development requirements for prestressing strand are intended to provide bond integrity for the strength of the member. The expression above can be broken into two distinct parts. According to the ACI 318R-05 Commentary Section R12.9, the first term represents the transfer length (as defined in Section 2.2.1) of the strand and the second term represents the flexural bond length (as defined in Section 2.2.2). Figure 2-1 further illustrates this concept. The steel stress can be seen to vary linearly with distance along the transfer length. Along the flexural bond length, the strand stress continues to increase but at a steadily decreasing rate as the full development length is reached. The ACI 318R-05 Commentary Section R12.9 cites papers by Hanson and Kaar (1959) and Kaar, LaFraugh, and Mass (1963) in the development of Equation 2-1, which results in the following equation for transfer length:

$$l_t = \left(\frac{f_{se}}{3000}\right)d_b \qquad \textbf{\textit{Equation 2-2}}$$

Examination of the shear design provisions presented in ACI 318-05, Sections

11.4.4 and 11.4.5 states that when the critical section for shear lies within the transfer

length of the prestressing strands the reduced prestress shall be considered when

computing web-shear cracking capacity. As a result, the prestress force should be

assumed to vary linearly from zero at the end of the prestressing steel to a maximum at a

distance from the end of the prestressing steel equal to the transfer length, which is

assumed to be 50 strand diameters (ACI 318 2005). Therefore, in this portion of the code

the transfer length is taken equal to $50d_b$. However, no reference is cited in the

Commentary for this section.

2.3.2 Background Research for Relevant ACI Provisions

The relevant ACI code provisions concerning development length, transfer length, and

flexural bond length are based on investigations conducted in the Research and

Development Laboratories of the Portland Cement Association by Hanson and Kaar

(1959) and Kaar, LaFraugh, and Mass (1963). This section summarizes these research

studies.

2.3.2.1 Hanson and Kaar (1959)

The Hanson and Kaar (1959) investigation was performed in the Research and

Development Laboratories of the Portland Cement Association in 1955-57. A total of 47

prestressed beams were tested in flexure to failure. The beam cross sections varied with

the width ranging from 4 to 8 in. and the effective reinforcement depth ranging from 5.5

to 11.5 in. They were pretensioned with seven-wire strand of $^1/_4$, $^3/_8$, and $^1/_2$ in. diameter.

The primary objectives of this study were to develop a theory of bond action predicting

ultimate strength in bond, and to study the influence of various factors on the bond performance of prestressing strand, particularly strand slip. The principal variables investigated were the embedment length and the diameter of the strand. Other variables investigated to a limited extent were percentage of steel reinforcement, concrete strength, and strand surface condition.

Hanson and Kaar found that strand size and embedment length have a considerable influence on the value of the average bond stresses at which bond slip occurs. In general they discovered that as the embedment length decreased, failure occurred at progressively lower moments due to slippage of the strands. Their results produced design curves and charts relating general bond slip to embedment lengths and particular strand diameters. These design aides enabled a quick check of whether or not general bond slip was probable in any particular beam. In addition, they concluded that increased reinforcement percentage or reduced concrete strengths reduce the possibility of general bond slip. Lastly, another relevant finding was that seven-wire strand develops additional bond strength even after general bond slip to the beam end has occurred due to mechanical bond resistance.

2.3.2.2 Kaar, LaFraugh, and Mass (1963)

The Kaar, LaFraugh, and Mass (1963) investigation was performed in the Research and Development Laboratories of the Portland Cement Association as well. A total of 36 prestressed rectangular prisms with varying sizes were used to determine and monitor transfer lengths. They were pretensioned with strand of $^1/_4$, $^3/_8$, and $^1/_2$ and 0.6 in. diameter. The primary objective of this study was to determine the effect of concrete

compressive strength at transfer on transfer lengths. Five different concrete strengths at transfer, ranging from 1,600 psi to 5,000 psi, were evaluated. The same mixture design was used for all specimens; the strengths at prestress transfer were varied by varying the concrete age. Transfer lengths were determined by measuring the changes in concrete surface strains with a Whittemore mechanical strain gauge. Measurements were taken at various ages ranging from immediately after prestress transfer to one year.

Kaar, LaFraugh, and Mass found that concrete strength at transfer had little influence on the transfer lengths of strand sizes up to ½ in. diameter. However, the transfer lengths were reduced with increasing concrete strengths for the 0.6 in. diameter strands. They also found that the transfer lengths at the live end of the strands were twenty to thirty percent higher than at the dead end. The live end refers to the end of the strands adjacent to where the strands were flame-cut. Also it was determined that the transfer lengths increased an average of six percent over a period of one year, with a maximum increase of twenty percent.

2.3.2.3 Evolution of ACI Development Length Expression

The evolution of the ACI development length expression was researched and described by Tabatabai and Dickson (1995) in *The History of the Prestressing Strand Development Length Equation.* Although the ACI code expressions were based upon the research done in the two studies presented above, nothing resembling the current ACI clauses can be found in either report. In fact, Hanson and Kaar recommended development lengths far more conservative than the current ACI code provisions (Tabatabai and Dickson 1995). Tabatabai and Dickson explain how Alan H. Mattock used the results of the previous two

15

studies to develop preliminary transfer length, flexural bond length, and development length expressions. ACI-ASCE Committee 323 (now 423) on Prestressed Concrete then modified Mattock's development length equation to the form originally adopted in the 1963 ACI code.

Mattock's original transfer length equation, however, was not modified and can be still be found in the ACI clauses. Mattock assumed an average transfer bond stress of 400 psi from the studies done by Hanson and Kaar, and used the following equilibrium equation to derive his original transfer length equation.

$$U_t \Sigma_o l_t = A_{ps} f_{pe} \hspace{3cm} \textbf{\textit{Equation 2-3}}$$

where: U_t = Average transfer bond stress (400 psi)

Σ_o = Circumference of prestressing strand (4/3 π D)

l_t = Transfer length

A_{ps} = Area of prestressing strand (0.725 π D^2/4)

D = Nominal strand diameter

f_{pe} = Effective prestress

Solving for the transfer length yields Mattock's original transfer length equation as well as the equation found in the ACI clauses:

$$l_t = (1/3) f_{pe} d_b \hspace{3cm} \textbf{\textit{Equation 2-4}}$$

Except for using units of ksi instead of psi for strand stress, Equation 2-4 can be found in the first part the ACI development length equation (Equation 2-1) presented above.

As stated previously, Mattock's original development length expression was modified before being adopted into the ACI code. The theory reported by Hanson and

Kaar (1959), that general bond slip is caused when the peak of the high bond stress wave reaches the prestress transfer zone, proved to be difficult to codify. Therefore, Mattock performed a "reappraisal" of the data reported by Hanson and Kaar (Tabatabai and Dickson 1995). This "reappraisal" consisted of using an average flexural bond stress approach to determine a flexural bond length. This flexural bond length could then be added to the transfer length to determine the development length.

Using data obtained from Hanson and Kaar, Mattock constructed a straight-line relationship between the flexural bond lengths available in each specimen when general bond slip occurred (Barnes et. al 1999). The relationship he derived to avoid bond slip is given below in Equation 2-5:

$$f_{ps} \leq f_{pe} + 0.9 \left(\frac{l_e - l_t}{d_b} \right) \qquad \text{\textit{Equation 2-5}}$$

This expression represented the *average* flexural bond length required to prevent general bond slip, rather than a conservative value. Therefore, the equation was changed to the less conservative Equation 2-6 before adoption into the 1963 Code.

$$f_{ps} \leq f_{pe} + \left(\frac{l_e - l_t}{d_b} \right) \qquad \text{\textit{Equation 2-6}}$$

Solving for the flexural bond length, the equation results in Equation 2-7.

$$l_{fb} = \left(f_{ps} - f_{pe} \right) d_b \qquad \text{\textit{Equation 2-7}}$$

The final expression for development length can be obtained by adding the flexural bond length (Equation 2-7) with the transfer length equation (Equation 2-4). This equation is functionally equivalent with the development length equation found in the current ACI code (Equation 2-1).

$$l_d = l_t + l_{fb} = \left(\frac{f_{pe}}{3} \right) d_b + \left(f_{ps} - f_{pe} \right) d_b = \left(f_{ps} - \frac{2}{3} f_{pe} \right) d_b \qquad \textbf{\textit{Equation 2-8}}$$

2.3.3 Relevant AASHTO Code Clauses and Commentary

The relevant code clauses and commentary for the development and transfer length of prestressing strand can be found in Section 9.28 of the AASHTO *Standard Specifications for Highway Bridges* (2002), and in Article 5.11.4 of the AASHTO *LRFD Bridge Design Specifications* (2007).

The AASHTO *Standard Specifications for Highway Bridges* (2002), Section 9.28 provisions for development length are identical to those in the ACI Code, besides minor changes in wording and notation. As a result, the same equation for calculating the transfer length as given in the ACI 318-05 Code is present in the AASHTO Standard Specifications. Refer to Equation 2-1 of this thesis.

The AASHTO *LRFD Bridge Design Specifications* (2007) provisions for development and transfer length are slightly different than those in the ACI Code. The AASHTO LRFD, Article 5.11.4 provisions that are relevant read as follows:

5.11.4.1 General

…For purposes of this article, the transfer length may be taken as 60 strand diameters…

5.11.4.2 Bonded Strand

Pretensioning strand shall be bonded beyond the section required to develop f_{ps} for a development length, l_d, in in., where l_d shall satisfy:

$$l_d \geq \kappa \left(f_{ps} - \frac{2}{3} f_{pe} \right) d_b \qquad \textbf{\textit{Equation 2-9}}$$

18

where, $\kappa = 1.0$ for pretensioned panels, piling, and other pretensioned members with a depth of less than or equal to 24.0 in.

$\kappa = 1.6$ for pretensioned members with a depth greater than 24.0 in.

This equation without the κ multiplier is functionally equivalent to the ACI 318-05 equation for development length. The AASHTO LRFD Commentary Section C5.11.4.2 states that the corrected equation, Equation 2-9, is conservative in nature, but accurately reflects the worst-case characteristics of strands shipped prior to 1997.

2.3.4 Background Research for Relevant AASHTO Provisions

As stated, the relevant code clauses and commentary for AASHTO provisions for development length, transfer length, and flexural bond length are very similar to those in ACI. This is primarily due to the fact that they all were based on the investigations conducted by Hanson and Kaar (1959) and Kaar, LaFraugh, and Mass (1963) already reviewed in this thesis. Therefore, this section discusses the evolution of the additional κ multiplier used in the AASHTO LRFD equation. Although not explicitly stated in the AASHTO LRFD Commentary, this κ multiplier was added based on investigations conducted by Cousins, Johnston, and Zia (1990) and Shahawy (2001).

2.3.4.1 Cousins, Johnston and Zia (1990)

The Cousins, Johnston, and Zia (1990) publication describes the investigation completed in the mid 1980's into the effect of epoxy-coated prestressing strand on transfer lengths. A total of 53 prestressed beams with cross-section sizes ranging from 3.5 in. by 3.5 in. to 6 in. by 10 in. were used to determine and monitor transfer lengths. Each beam was prestressed with a single strand of $^3/_8$, $^1/_2$ in., or 0.6 in. diameter. Of the 53 specimens,

19

approximately 35 specimens were tested in flexure in order to determine development

lengths. Transfer lengths were determined by measuring concrete strains using a

Whittemore-type extensometer and measurements were taken periodically up to one year.

Even though the primary objective of this investigation was to determine the

effect of epoxy-coated prestressing strand on transfer and development lengths, the

results from the uncoated prestressing strand proved to be more important. Of the 53

total specimens, 23 were prestressed with uncoated seven-wire prestressing strand.

Sixteen of these 23 were used for development length testing. Experimental results

showed that the transfer lengths for the uncoated strand were longer than the values

calculated using ACI provisions. Similarly, development lengths were also longer than

those calculated using ACI and AASHTO provisions.

This underprediction of transfer and development lengths by the current code

provisions provided personnel at the Federal Highway Administration (FHWA) grounds

to suggest that changes be made to the current AASHTO provisions. On October 26,

1988, the FHWA distributed a memorandum stating that for strands with diameters less

than or equal to 9/16 in., the predicted development length for all members should be

multiplied by a factor of 1.6 (FHWA 1988). This particular event began the evolution of

the additional κ multiplier used in the AASHTO LRFD equation.

2.3.4.2 Shahawy (2001)

Shahawy (2001) describes an evaluation of the AASHTO provisions for strand

development length of prestressed concrete members. This investigation, conducted at

the Florida Department of Transportation (FDOT) Structures Research Center (FSRC),

involved extensive research on the transfer and development lengths of strands in prestressed concrete AASHTO girders, slabs, and piles. The test results of this study were compared with current AASHTO provisions, as well as to proposed changes to the AASHTO provisions based on past studies.

Shahawy reported that shear-flexure interaction, which is more pronounced in deeper members, has a significant effect on the development length of prestressing strands. Shahawy's findings support the conclusions drawn by Peterman et al. (2000) that flexure-shear cracking can significantly influence the required development length in prestressed concrete members. As a result, Shahawy presented design recommendations which account for the effect of shear. His proposal suggested that for members with a depth equal to or less than 24 in., the development length is most accurately predicted by Equation 2-10.

$$l_d = \left(\frac{f_{pe}}{3}\right)d_b + \frac{\left(f_{ps} - f_{pe}\right)d_b}{1.2} \qquad \textbf{\textit{Equation 2-10}}$$

In conjunction, for members with a depth greater than 24 in., Shahawy proposed that Equation 2-11 yielded the closest predictions.

$$l_d = \left(\frac{f_{pe}}{3}\right)d_b + \frac{\left(f_{ps} - f_{pe}\right)d_b}{1.2} + 1.47h \qquad \textbf{\textit{Equation 2-11}}$$

where,   h = depth of member (in.)

It is relevant to note that Shahawy stated that his proposed approach was conservative, but less so than the AASHTO equation as shown in Equation 2-9. Based upon the recommendations of Shahawy (2001) discussed above, the current AASHTO

LRFD provisions for development length stated in section 2.3.3 were adopted utilizing the κ multiplier of 1.6 for members with a depth greater than 24 in.

2.4 BOND THEORY

The bond interaction of the prestressing strand and the surrounding concrete in pretensioned members results in the development of two types of bond stresses. This section defines and discusses both transfer bond stress and flexural bond stress. The mechanisms contributing to these bond stresses, as well as the factors affecting them, are presented.

2.4.1 Transfer Bond Stress

Transfer bond stresses refer to the stresses that develop between the prestressing strand and concrete along the transfer length of the strand. These stresses are responsible for the increase in the steel stress from zero at the free end to the effective prestress, f_{pe}, at the end of the transfer length. As the prestressing strands are detensioned at either end, the strands slip within the concrete along the transfer length, activating bond mechanisms. These bond mechanisms, primarily friction and mechanical resistance defined below, cause a buildup of concrete compressive stress parallel to the axis of the tendon. A linear variation of strand stress is seen over the transfer length due to transfer bond stresses. Since there are no transfer bond stresses outside the transfer length, the strand stress is relatively constant throughout the central portion of an unloaded beam.

2.4.2 Flexural Bond Stress

Flexural bond stresses refer to the stresses that develop between the prestressing strand and concrete as a result of flexural loadings. These stresses are responsible for the increase in steel stress from the effective prestress, f_{pe}, to the ultimate stress, f_{ps}, under applied loads. Under a flexural loading, before the concrete cracks, the flexural bond stresses are minor. However, after the concrete cracks, all of the tensile stresses are transferred to the prestressing strand at the crack locations. This results in high flexural bond stresses on either side of the crack. At the same time, local flexural bond stresses that transfer a portion of the tension back into the concrete, often called "in and out" bond stresses are developed between the cracks. As loading continues, the strand will slip at the cracks, causing increased flexural bond stresses due to mechanical resistance, which is defined below. This increase of flexural bond stresses on either side of cracks along with the "in and out" bond stresses can be described as a "wave" that progresses from the original crack towards the end of the beam (Hanson and Kaar 1959). This is illustrated below in Figure 2-2.

Figure 2-2 illustrates the flexural loading of a simply supported beam with two point loads. The two equal point loads effectively establish a constant moment region during loading. For this diagram, the nominal moment capacity, M_n, has been reached within the constant moment region, and, as a result, the strand stress is equal to f_{ps} at the crack locations. Between the cracks, the steel stress drops slightly due to local flexural bond stresses or "in and out" bond stresses discussed above. Finally, the progression of the local bond stresses, u, in the form of a "wave" can be seen. Note the constant bond stress within the transfer length. Strand slip failures occur when the flexural bond

stresses advance into the transfer length and disrupt this constant bond stress. As a result,

it is vital that, by providing a sufficient embedment length, the transfer zone not be

influenced by cracking.
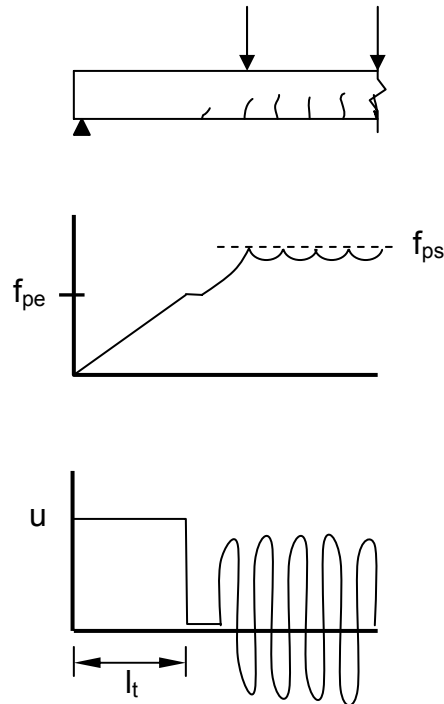
**Figure 2-2: Steel Stress and Bond Stress Diagrams for Portion of Simply Supported
Beam as Cracking Progresses Towards the Support**
(Adapted from Barnes et al. 1999)

2.4.3 Mechanisms Contributing to Bond Stresses

There are three general groups of mechanisms that potentially contribute to the

previously mentioned bond stresses. They are adhesion, friction, and mechanical

resistance (Hanson and Kaar 1959). Adhesion refers to the chemical bond between the

concrete and the steel of the prestressing strand. Due to the relative slip of the strand

upon prestress release along the transfer length, the adhesion between the prestressing

steel and surrounding concrete is destroyed (Barnes et al. 1999). Therefore, it is

universally agreed that adhesion plays a minimal role in transfer bond stresses; however, it can contribute to flexural bond stresses.

Friction refers to the bond developed between the concrete and the prestressing strand due to sliding action of the strand. The frictional resistance is developed due to radial compressive stresses acting between the concrete and the prestressing strand. These radial compressive stresses are primarily attributed to the Hoyer Effect, which is represented in Figure 2-3 (Barnes et al. 1999).
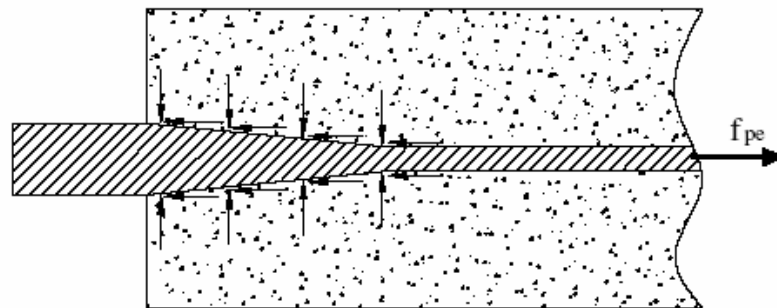
Figure 2-3: Hoyer Effect (Adapted from Haq 2005)

As shown in Figure 2-3, at transfer, the prestressing strand tends to increase in diameter along the transfer length due to decrease in strand tension. As long as the concrete surrounding the prestressing strand stays intact, it will work to resist this expansion of the prestressing strand. This interaction produces the radial compressive stresses necessary to create frictional resistance between the concrete and the prestressing strand. Friction contributes primarily to transfer bond stresses, due to the fact that the Hoyer Effect exists primarily near the free end of the strand where the strand undergoes the largest strain change at transfer (Barnes et al. 1999).

Mechanical resistance, also known as mechanical interlock, refers to the bond developed between the concrete and the prestressing strand due to the cross-sectional

shape of a seven-wire prestressing strand. Since the fresh concrete conforms to the helical shape of a seven-wire strand, the helical ridges prevent the strand from pulling through the concrete without twisting. In many cases, twisting of the strand near the free end is not restrained; therefore, mechanical resistance is dependent upon other mechanisms, particularly the Hoyer Effect, to restrain twisting at one end before transfer bond stresses can be developed (Russell and Burns 1993). Mechanical resistance is critical in developing flexural bond stresses, especially once the concrete has cracked. As the concrete cracks, the strand will slip. This slip activates mechanical resistance, as bearing stresses are formed on either side of the crack between the concrete and the strand's helical grooves, preventing further slip.

2.4.4 Relevant Factors Affecting Bond Stresses

Numerous research investigations throughout the years have been undertaken in order to better understand the factors that affect bond stresses in precast, prestressed members. The factors that affect transfer bond stresses are better known and understood than the factors that affect flexural bond stresses. The factors relevant to this thesis that affect bond stresses in general such as concrete strength, time-dependent deformations, member size, and method of prestress release are briefly discussed in this section. The effects these factors have on the transfer length of precast, prestressed members are given particular attention.

2.4.4.1 Concrete Strength

It has been found that concrete strength can affect both transfer bond stresses and flexural bond stresses. The effect that concrete strength has on transfer length has been

26

investigated and debated for many years. In general it is concluded that higher concrete strengths at transfer result in decreased transfer lengths.

In 1949 Freyssint suggested that transfer bond stresses were dependent on the maximum pressure that the concrete can exert on the steel, which depends on the tensile strength and hardness of the concrete (Guyon 1953). Janney (1954) stated that "one would anticipate some improvement in bonding quality of higher strength concrete." However, the Kaar, LaFraugh, and Mass (1963) study, performed specifically to investigate the effect of concrete strengths at prestress release, concluded that concrete strength had little influence on transfer lengths of members prestressed with strand up to ½ in. in diameter.

A number of research studies over the years have conflicted with the results seen by Kaar, LaFraugh, and Mass. Zia and Mostafa (1977) found that for members with concrete strengths ranging from 2,000 to 8,000 psi, the transfer length was inversely proportional to the strength of the concrete. They proposed a new equation for calculating transfer lengths that was more conservative than the ACI Code equation, particularly where the strength of concrete at transfer was low (Zia and Mostafa 1977). Several other studies have reported that high concrete strengths result in lower transfer lengths (Russell and Burns 1993, Lane 1998, Oh and Kim 2000). It has also been reported that relationships in which the transfer length is inversely proportional to the square root of the concrete strength can yield accurate models (Mitchell et al. 1993, Barnes et al. 1999, Swords 2005, Levy 2007).

2.4.4.2 Time-Dependent Effects

Research has suggested that time can significantly affect transfer bond lengths. It has been found that prestress transfer lengths tend to increase with time, which is most likely attributable to the inelastic behavior of the concrete. Although the strand stress tends to decrease over time with the accumulation of time-dependent losses, the inelastic response of the concrete adjacent to the strands largely prevents the recovery of these stresses (Barnes et al. 1999). At the time of prestress transfer, micro-cracking of the concrete occurs and effectively softens the concrete, resulting in increased transfer lengths over time until crack growth and creep stabilize.

Kaar, LaFraugh, and Mass (1963) reported an average increase in transfer length over one year of 6 percent with a maximum increase of 20 percent. Although its applicability to seven-wire prestressing strand may be argued, Zia and Mostafa (1977) reported increases in transfer lengths with time up to 100 percent for some small size wires. FHWA beam specimens (Lane 1998) experienced an increase in transfer length of 30 percent over the first twenty-eight days after release and an additional 7 percent over the next six months. Oh and Kim (2000) reported smaller increases in transfer length on the order of 5 percent over the first 90 days, but nonetheless acknowledged that transfer length increases with the age after prestress transfer. Barnes et al. (2003) reported an average increase in transfer length of 10 – 20 percent within the first few weeks after prestress transfer, but no definite trend of growth beyond an age of 20 days.

2.4.4.3 Member Size

Although somewhat limited data are available, it has been found that member size can affect both transfer bond stresses and flexural bond stresses. Most of the relevant research has been performed on small-scale rectangular prisms prestressed with single strands. Naturally, one would expect that test data from larger specimens prestressed with multiple strands would more closely reflect the performance of bridge girders in the field.

An investigation conducted by Russell and Burns (1993) into the transfer and development lengths for various cross-section shapes, sizes, and strand patterns revealed that member size has an effect on transfer length. Russell and Burns (1993) concluded that the larger the specimen, the shorter the transfer length. Their results concerning the effects of member size on development length were, to some extent, inconclusive. However, Shahawy (2001) reported that shear-flexure interaction, which is more pronounced in deeper members, has a significant effect on the development length of prestressing strand. It was concluded that larger members (with depths greater than 24 in.) require longer development lengths. Along the same lines, the investigation conducted by Peterman et al. (2000) on single-stranded rectangular beams and multiple-stranded T-beams revealed that the development length, in some cases, depended on the member geometry.

Findings in the previous two phases of this investigation, described by Swords (2005) and Levy (2007) supported the results discussed above. Both studies utilized the same concretes, but different member sizes. The Swords (2005) study consisted of small concentrically prestressed rectangular specimens, whereas, the Levy (2007) study

consisted of larger eccentrically prestressed T-beams. Results indicated smaller transfer lengths in the Levy (2007) specimens. Flexural testing was not performed on the Swords (2005) specimens; as a result, development length comparisons could not be made.

2.4.4.4 Method of Prestress Release

It has been found that the method of prestress release affects primarily the transfer length bond stresses. The two general methods of prestress release are gradual release and sudden release. The most widely used method for detensioning prestressing strands is flame-cutting. Flame-cutting results in a sudden release of prestress at the end of the member adjacent to the cutting and a more gradual release at the opposite end. The two ends of the member are also known as the "cut" or "live" end and the "dead" end, respectively. The majority of research shows that cut ends tend to have longer transfer lengths than the corresponding dead ends.

Kaar, LaFraugh, and Mass (1963) reported that the measured transfer lengths on the cut ends were 20 percent greater than the transfer lengths on the dead ends. Hanson (1969) reported similar findings, stating that transfer lengths were approximately 25 percent greater on the cut ends than on the dead ends. The recommended transfer length expressions developed by Zia and Mostafa (1977) provided for approximately 15 percent longer transfer lengths on the cut ends. In a more recent study, Russell and Burns (1997) reported similar results, stating that transfer lengths measured on the cut ends were on average 34 percent greater than transfer lengths measured on the dead ends. Similarly, Oh and Kim (2000) found that on average the transfer lengths on the cut ends were approximately 15 percent longer.

More recent researchers, namely Swords (2005) and Levy (2007), also observed longer transfer lengths on the cut ends than on the dead ends. Specifically, Swords (2005) reported a 38 percent increase in transfer length on the cut ends over the dead ends. Very similar results were seen in Levy (2007), with increased transfer lengths on the cut ends for all concrete mixtures, with an average increase of 36 percent.

2.5 SCC IN PRECAST, PRESTRESSED MEMBERS

With the increasing popularity of SCC and its economical benefits, it is only natural that the precast, prestressed industry has begun to show interest in using SCC for their products. However, little is known regarding the structural performance of SCC in pretensioned members, particularly regarding the bond performance. As a result, several recent research studies have been conducted. This section provides a review of recent investigations of both small-scale and full-scale pretensioned beams cast with SCC. The topics covered within this section were chosen due to their applicability to the research and testing performed for this thesis, and do not necessarily cover all areas of interest regarding SCC in precast, prestressed members.

2.5.1 Plant Casting Operations

It has been suggested that the use of SCC in precast, prestressed members will provide economic, aesthetic, and safety benefits in the casting process. This is due to its ability to flow freely around reinforcement and into small cavities without the need for external vibration. Several recent studies in which full-scale plant-cast pretensioned girders were constructed have shown these suggestions to be correct. A recent study done in North Carolina in which 54.8-ft-long AASHTO Type III bridge girders were cast using both

conventional concrete and SCC showed that the SCC girders took approximately 20 minutes to cast, whereas the conventional girders took 30 – 45 minutes (Zia et al. 2005). These SCC girders were cast using three consecutive passes along the beam with no vibration and a final product of good quality resulted, according to the authors.

A second study in Minnesota in which 38-ft-long I-girders with a depth of 36 in. were fabricated using SCC produced similar casting time results. The reported casting times were 15 – 20 minutes per girder; however, different casting procedures than those reported in the Zia study were used (Erkmen et al. 2007). One set of SCC girders was cast with two discharge locations, and a second set was cast with only one discharge location along the length of the girder (Erkmen et al. 2007). Erkmen et al. (2007) did report flow segregation while casting one of their girders, but it was later discovered that the aggregate bin had been contaminated with larger aggregate possessing different moisture content and absorption properties. This indicates the sensitivity of SCC to varying moisture content.

There has been some concern that, due to the sensitivity of SCC mixture designs, precast batch plants may have a difficult time reproducing acceptable SCC mixtures. This was the case for a study conducted in Virginia in which 45-in. bulb-T-beams were fabricated using SCC. The first four batches were rejected due to unsatisfactory fresh properties (Ozyildirim and Davis 2007). The authors cited SCC's sensitivity to moisture content as the probable cause. Ozyildirim and Davis (2007) also reported having to use minimal vibration in the top flange, seepage of water and fines through the strand holes of the bulkhead, and a frothy appearance of the concrete with high flow rates. Finally, it

was noted that bug holes were evident on the surface of the SCC girders, but not as large or deep as the ones seen in the conventional concrete girders.

2.5.2 Transfer Length

There are concerns that the ultrafine material content in SCC and the large dosages of superplasticizer and stabilizer in SCC may affect the transfer bond behavior when used in pretensioned members. The current code provisions for transfer length are based upon tests performed with conventional concrete. As a result, the applicability of the ACI and AASHTO provisions for calculating transfer length are in question. The majority of the recent investigations into the transfer lengths of pretensioned members cast with SCC suggest that the current code provisions are ultimately conservative. However, conflicting results have been found concerning comparable transfer lengths between conventional concrete pretensioned members and their counterparts made with SCC, as discussed below.

All three studies previously discussed, Zia et al. (2005), Erkmen et al. (2007), and Ozyildirim and Davis (2007) reported measured transfer lengths less than predicted by the current code provisions. A study performed in Kansas in which small-scale rectangular and T-beam girders were constructed using SCC reported that all of their specimens were in accordance with ACI and AASHTO provisions (Larson et al. 2007). Similarly, small-scale rectangular beams tested by Rueda and Schokker (2007) resulted in transfer lengths well below the AASHTO-recommended 60 diameters. Several other recent investigations, presented in more detail below, reported conservative results for

33

transfer length predictions of SCC pretensioned members when using ACI and AASHTO provisions (Naito et al. 2006, Hamilton et al. 2005, Burgueño and Haq 2005).

Although the consensus is that ACI and AASHTO provisions conservatively estimate the transfer lengths of pretensioned members cast with SCC, there have been conflicting results concerning comparable transfer lengths between SCC and conventional concrete girders. Zia et al. (2005) and Rueda and Schokker (2007) concluded that SCC and conventional concrete girders have comparable transfer lengths. Naito et al. (2006) reported a similar finding from a study in which four 35-ft standard PCEF (Mid-Atlantic States Prestressed Concrete Committee for Economic Fabrication) girders with a depth of 45 in. were cast using SCC in Pennsylvania. A Florida study of 42-ft AASHTO Type II girders also resulted in similar transfer lengths for SCC and conventional concrete specimens (Hamilton et al. 2005). However, conflicting results were reported by Burgueño and Haq (2005). These Michigan State University researchers reported approximately 36 percent longer transfer lengths in their 38-ft small-scale SCC T-beams than in their conventional concrete T-beams of the same size. Erkmen et al. (2007) also reported 75 percent and 10 percent longer transfer lengths in their two sets SCC girders than in the conventional concrete girders.

Transfer length growth over time in pretensioned members made with SCC has not been investigated nearly as thoroughly. Larson et al. (2007) reported an average increase in transfer length of SCC beams of 10 – 20 percent within 21 days after transfer. A transfer length growth of 2 – 24 percent within only 4 days after transfer was reported in a previous phase of this investigation (Levy 2007). As stated previously, there are not

yet enough results to adequately assess the growth of pretensioned SCC transfer lengths

over time; however, relevant results from this investigation can be found in Chapter 4.

2.5.3 Flexural Behavior

The flexural behavior of pretensioned members made with SCC has been investigated in

several recent research studies. Throughout these studies, the reported findings have

been consistent and promising. The majority of the flexural testing conducted on

pretensioned SCC girders/beams resulted in nominal flexural moment capacities

exceeding the predicted moment capacity according to sectional analysis and ACI

provisions (Ozyildirim and Davis 2007; Larson et al. 2007; Burgueño and Haq 2005;

Naito et al. 2006; Rueda and Schokker 2007). In fact, Larson et al. (2007) and Naito et

al. (2006) reported a 10 – 35 percent and a 1 – 4 percent increase in flexural moment

capacity over predicted moment capacities, respectively. Even more specifically, Rueda

and Schokker (2007) reported 22 and 30 percent increases in moment capacity over

predicted capacity for cracking and ultimate moments, respectively.

The findings comparing the flexural moment capacities of SCC girders/beams to

companion conventional concrete girders/beams were almost as consistent as above.

Hamilton et al. (2005) reported no noticeable difference in flexural capacities between

SCC and conventional concrete girders, as well as similar cracking patterns and crack

widths. Similarly, Zia et al. (2005) reported virtually identical load-deflection

relationships up to design service loads with no observed cracks in either type of concrete

and full recovery of deformations upon unloading for all specimens. In one study, even

the progression of damage to the girders during flexural testing was reported to be

consistent between SCC and conventional concrete (Naito et al. 2006). The study

conducted by Rueda and Schokker (2007) resulted in slightly larger cracking and ultimate

flexural moment capacities for SCC beams relative to conventional concrete specimens.

These increases seen in the SCC beams were reported as 5 and 2 percent for cracking and

ultimate moments, respectively.

Unlike the consistent findings pertaining to flexural moment capacities of SCC

girders/beams, results regarding the ductility of SCC pretensioned members are rather

inconclusive. One investigation reports 17.1 percent more deflection at ultimate load for

conventional concrete girders over SCC girders; thus concluding better ductility in

conventional concrete girders (Hamilton et al. 2005). However, Naito et al. (2006)

reported greater ductility in their SCC girders.

2.5.4 Shear Behavior

The shear behavior of pretensioned members made with SCC is more difficult to quantify

than the flexural behavior. The majority of recent studies do not report findings

pertaining to shear behavior, which can be relatively complicated due to the numerous

variables involved. However, the limited literature available suggests that shear

capacities for SCC girders/beams are comparable to conventional concrete specimens

(Naito et al. 2006, Hamilton et al. 2005, Hegger et al. 2007).

Naito et al. (2006) reported that all of their girders, SCC and conventional

concrete, exceeded estimated shear capacities by 6 – 7 percent. Interestingly, one study

reported slightly reduced shear capacities of SCC beams when compared to conventional

concrete beams, especially with increasing shear reinforcement ratios, but suggested that

further research be conducted to clarify this (Hegger et al. 2007). Predominant shear failure modes have included web crushing and compression failures within the top sections of SCC girders (Ozyildirim and Davis 2007, Hamilton et al. 2005).

2.5.5 General Bond Behavior

It has been suggested that the general bond behavior between prestressing strand and SCC is similar to that observed in high-strength concrete (Hegger et al. 2007, Naito et al. 2006). A couple of recent studies have concluded that the general bond performance of SCC depends highly on the mixture proportions (Hegger et al. 2007, Burgueño and Haq 2005). As stated previously, this may be attributed to the increased amount of fine aggregates and chemical admixtures used to produce quality SCC mixtures.

Several recent studies have reported minimal or no strand slip during testing of their SCC girders/beams (Ozyildirim and Davis 2007, Larson et al. 2007, Naito et al. 2006). Specifically, Larson et al. (2007) reported a maximum slip of only 0.01 in. for all of their test specimens. Similarly, Naito et al. (2006) reported a maximum slip of only 0.05 in. for all of their full-scale girders. Furthermore, it was reported that load-carrying capacity was never lost and subsequently increased after the initiation of slip (Naito et al. 2006). It has been concluded that current ACI 318 and AASHTO provisions for strand development length are conservative for pretensioned members made with SCC (Larson et al. 2007).

However, not all recent studies reported such favorable results for SCC. Burgueño and Haq (2005) reported a definite difference in the general bond performance of SCC girders/beams. This conclusion was drawn based upon the results of longer

transfer lengths, flexural bond lengths, and development lengths for the SCC beams over the conventional concrete beams (Burgueño and Haq 2005). The possibility of low bond quality strand was presented as an explanation for these results because rusted strand was used for the conventional concrete beams, but not for the SCC beams.

Hamilton et al. (2005) also reported a significant bond failure during testing of one of their SCC girders. This bond failure consisted of excessive strand slip that led to premature failure of the girder. Hamilton et al. attributed this failure to poor transfer conditions in which sudden release of the strand occurred. Longer transfer lengths were reported for this girder, which may explain the bond failure.

2.5.6 Summary

Despite a few minor issues concerning the ability of precast, prestressed plants to produce and place SCC mixtures consistently, the general consensus is that SCC can improve casting operations. In summary, Hamilton et al. (2005) reports reduced construction times, improved labor efficiency, reduced noise, and improved safety during the construction of SCC girders.

Recent research studies investigating the transfer lengths of pretensioned members made with SCC have shown consistently that the current ACI and AASHTO provisions for predicting transfer lengths are conservative. However, the ability of SCC girders/beams to produce transfer lengths comparable to conventional concrete girders/beams is not as reliable. Transfer length growth over time in SCC pretensioned members has not been investigated thoroughly, but several recent studies have suggested that it occurs.

Recent conclusions concerning the flexural behavior of pretensioned members made with SCC indicate that predicted flexural moment capacities are consistently exceeded. It has also been reported that similar flexural behavior can be seen between pretensioned members made with SCC and conventional concrete. However, possible differences in the ductility of SCC girders/beams over conventional concrete counterparts have been reported.

General bond behavior of pretensioned members made with SCC has been shown to be favorable by recent research studies. The majority of testing performed on SCC girders/beams reported no significant, or minimal, strand slips. However, it has been suggested that general bond behavior of SCC girders/beams is highly dependent on the mixture proportioning of the SCC.

The conclusions drawn by the recent research studies presented above reveal a general trend that SCC is a viable material in the use of pretensioned concrete members. It has been suggested that current code provisions used for design of precast, prestressed bridge girders result in conservative predictions for SCC members. Nonetheless, it is apparent that more research is needed to fully understand the behavior and structural performance of SCC in pretensioned members.

CHAPTER 3

DESIGN AND CONSTRUCTION OF EXPERIMENTAL SPECIMENS

3.1 INTRODUCTION

In this study, a total of six plant-cast AASHTO Type I prestressed girders were used as test specimens. One conventional concrete mixture and two SCC mixtures were used to cast two 40-ft girders per mixture, resulting in a total of six bridge girders. After transportation to the Auburn University Structural Engineering Laboratory, a composite deck was cast on top of each bridge girder using a conventional-slump concrete mixture. The design and fabrication of these specimens are described in this chapter.

3.2 SPECIMEN IDENTIFICATION

A detailed identification system was used to specifically describe each end of the six girders. This specimen identification system is summarized below in Figure 3-1.
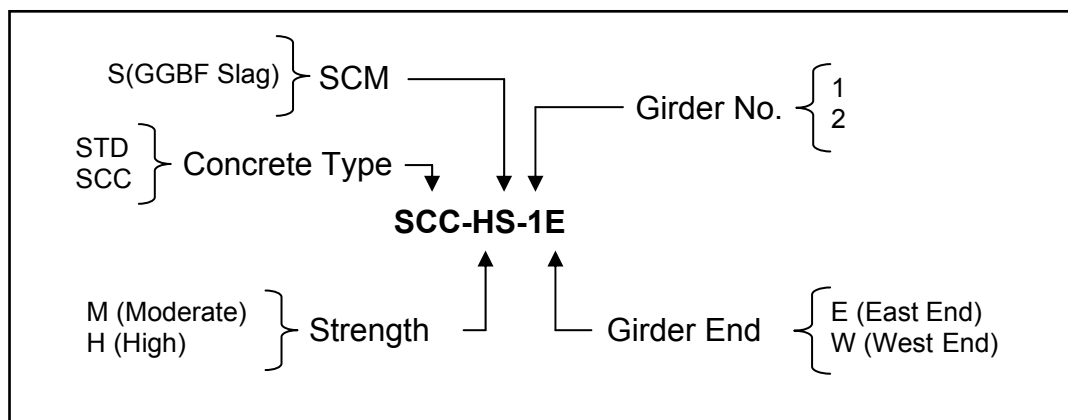
Figure 3-1: Specimen Identification

The six bridge girders were cast in sets of two using a total of three different concrete mixtures. The first term of the identifier denotes whether a standard conventional-slump concrete mixture, "STD," or a self-consolidating concrete mixture, "SCC," was used. The second term identifies the concrete strength and the type of SCM used if applicable. The STD mixture did not include an SCM. The final term in the identifier specifies a particular girder number as well as the particular end of that girder. The girder number and end were identified according to the casting position as seen below in Figure 3-2. Girders 1 and 2 in each pair had different patterns of shear reinforcement and were subjected to different flexural loading configurations and support conditions; therefore, each girder end was uniquely identified. Although the reinforcement and testing geometries varied for each girder end within a girder pair, these parameters did not vary among the three concrete mixtures. In other words, SCC-HS-1W had the same shear reinforcement and flexural testing layout as SCC-MS-1W and STD-M-1W.
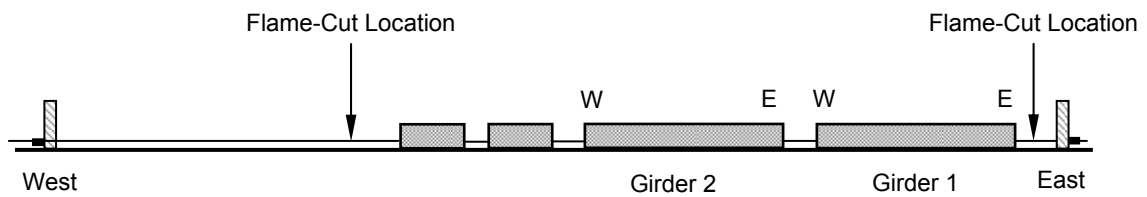
Figure 3-2: Casting Configuration for Typical Beam Pair

Each pair of girders was cast on the same prestressing bed at the Hanson Pipe & Precast prestressing plant in Pelham, Alabama. Casting dates for the "STD-M," "SCC-HS," and "SCC-MS" were May 8, 2007, May 10, 2007, and May 14, 2007, respectively. The strands were torch-cut simultaneously in two different locations as shown in Figure 3-2.

41

3.3 SPECIMEN DESIGN

A total of six bridge girders were used in this study. Each girder was 40 ft long, utilizing the cross section of a typical AASHTO Type I bridge girder. The typical dimensions of this cross section type are shown in Figure 3-3 below. Before the flexural testing was performed, a 48-in.-wide by 3.5-in.-thick cast-in-place reinforced concrete deck was added to the girder in order to ensure a desired elongation of 3.5 percent in the bottom strands prior to failure.
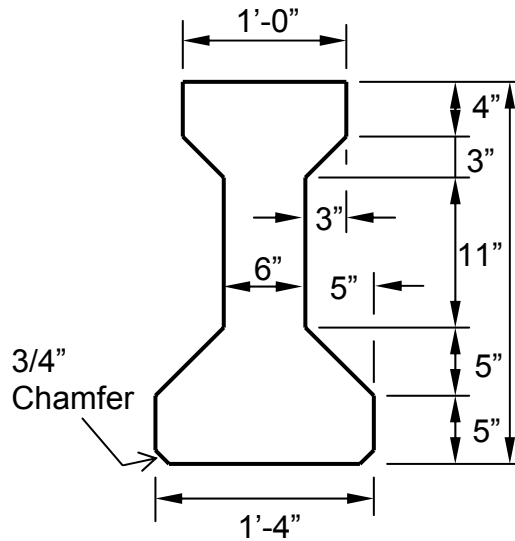
Figure 3-3: Typical AASHTO Type I Cross Section

3.3.1 Strand and Mild Reinforcement Design

All six specimens were prestressed with six strands at the bottom of the girder and two strands at the top, as shown in Figure 3-4. All strands were seven-wire, low-relaxation, 270-ksi, ½-in "special" diameter strands. In accordance with typical ALDOT practice, the bottom six strands were tensioned to 75 percent of the specified tensile strength, f_{pu}. This resulted in a jacking stress, f_{pj}, of 202.5 ksi. The top two strands were not fully

prestressed. Once again, typical ALDOT practice was followed and a jacking stress, f_{pj}, of 30.5 ksi was used. The mild steel reinforcement consisted of that typical to ALDOT bridge girders. This included shear reinforcement throughout the girder and confining steel placed in the ends of the girders. The shear reinforcement consisted of either Grade 60 No. 4 stirrups or Grade 60 No. 5 stirrups. A slightly different stirrup arrangement was used, depending on the girder number and end. The confining steel reinforcement consisted of Grade 60 No. 3 bars. The strand pattern and mild steel reinforcement details can be seen below in Figure 3-4, Figure 3-5, and Figure 3-6.
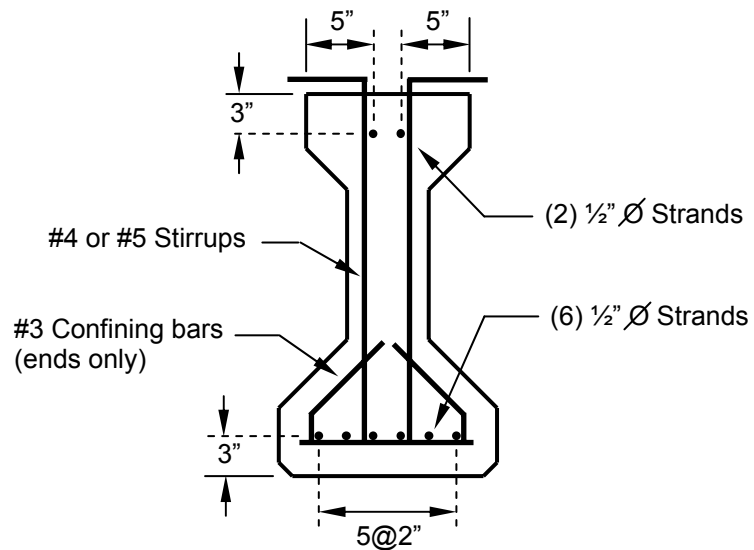
Figure 3-4: Typical Cross Section Detail

Girder 1 Elevation

40'-0"

1 ½" Cl. 4" c-c   26 Spaces @ 18 in. (V #4)   4" c-c 1 ½" Cl.

A   B

7 – Pairs B #3
(Space @ 6 in.)

7 – Pairs B #3
(Space @ 6 in.)

Girder 2 Elevation

Substitute Bars V #5 for Bars V #4

40'-0"

1 ½" Cl. 2@4" 8@7"   5@18   2@13"   8@18"   5@12"   10@8" 8@4" 1 ½" Cl.

A   B

7 – Pairs B #3
(Space w/ Bars V #4)

9 – Pairs B #3
(Space w/ Bars V #5)
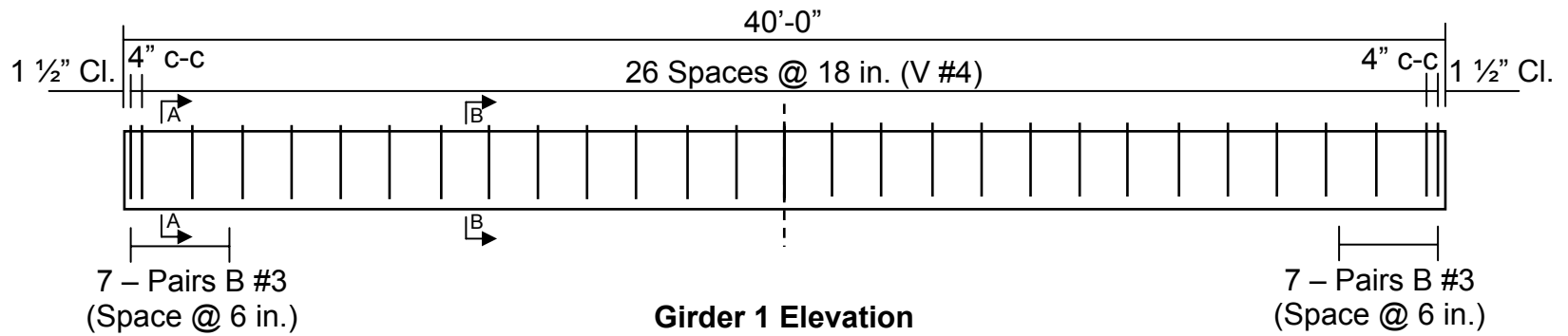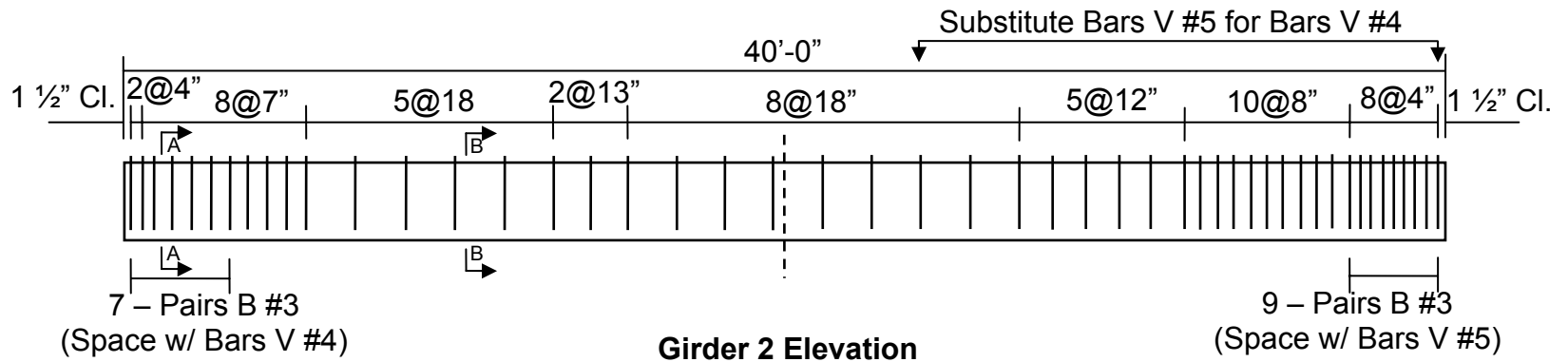
Figure 3-5: Stirrup Spacing for Girders 1 and 2
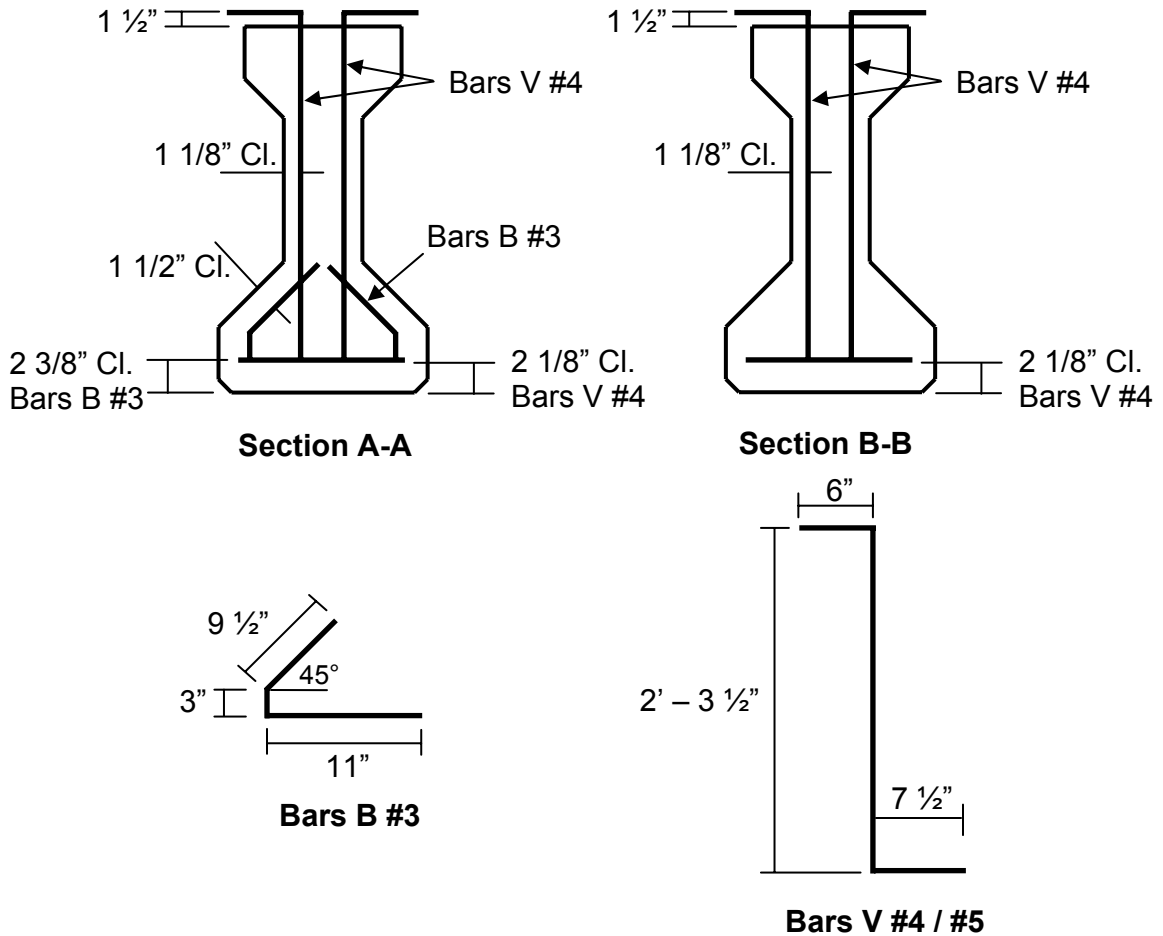
Figure 3-6: Shear Reinforcement Details

As shown in Figure 3-5 the stirrup spacing was different for each girder. Girder 1 was designed with a constant stirrup spacing throughout of 18 in. This corresponds to the maximum stirrup spacing allowed by the AASHTO LRFD design code. Girder 2, on the other hand, did not have a constant spacing throughout. Each end was designed with a slightly different arrangement, with the stirrup spacing increasing to the design code maximum of 18 in. towards the center of the girder. The stirrup arrangement used in the west end of girder 2 is typical of the design used by ALDOT in AASHTO Type I girders. Note #5 bars were used for the stirrups in this region, as specified by ALDOT. The east end of girder 2 was designed to provide the approximate minimum shear strength

necessary (in accordance with AASHTO LRFD provisions) to prevent a diagonal-tension shear failure during the flexural testing planned for this end of the girder. As a result, this girder end had more shear reinforcement than the absolute minimum amount, but less than the typical ALDOT girder design.

The stirrup arrangements were primarily chosen based upon the anticipated flexural testing locations and span lengths. Each girder was to be flexurally tested twice, one test on each end, with varying embedment lengths for each test. The largest embedment lengths were to be used on girder 1 in an attempt to produce flexural failures. As a result, only minimal shear reinforcement was warranted. However, the shorter embedment lengths tested for girder 2 produced larger test shears; therefore, a greater amount of shear reinforcement was warranted in the ends of this girder.

3.3.2 Deck Design

A 48-in. by 3.5-in. cast-in-place reinforced concrete deck was added to the girders in the Auburn University Structural Research Laboratory prior to flexural testing. The purpose of this deck was to model the composite behavior that a typical bridge girder shares with the deck slab. This deck provided a large compression flange for the girder, allowing the neutral axis to be relatively high in the member at flexural failure. As a result, large curvatures and high strains in the tension reinforcement were achieved. The deck was reinforced with a single layer of four Grade 40 No. 4 reinforcing bars longitudinally. Transverse reinforcement spaced at 6 in. to 9 in. center-to-center was also provided in the form of Grade 40 No. 4 reinforcing bars. All decks were cast with conventional-slump

concrete with a specified 28-day compressive strength of 4,000 psi. Figure 3-7 depicts the details of the cast-in-place deck.
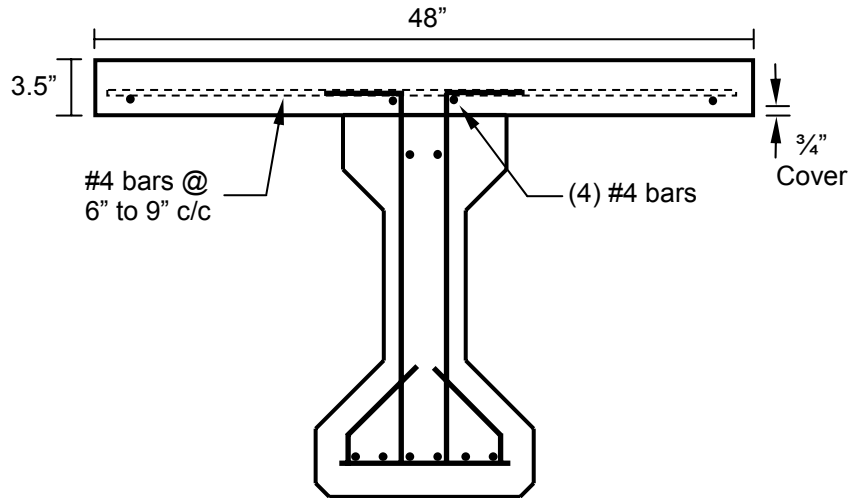
Figure 3-7: Typical Cast-in-Place Deck Details

3.4 MATERIAL PROPERTIES

All materials used to construct the test specimens for this study are discussed in this section. These materials include the concrete for the prestressed bridge girders, the cast-in-place concrete for the deck, the prestressing strand, and the mild reinforcing steel.

3.4.1 Precast Concrete

Three concrete mixtures were used in the fabrication of the precast, prestressed specimens, including one conventional-slump concrete mixture and two SCC mixtures. All three mixtures were batched at the Hanson Pipe & Precast prestressing plant in Pelham, Alabama. Table 3-2 depicts key water-to-cement-ratios, sand-to-aggregate ratios, and fresh concrete properties for each mixture. Similarly, Table 3-2 includes a

comparison of concrete compressive strengths determined from representative 6 in. by 12 in. concrete cylinders. The concrete compressive strength at transfer of prestress, f'_{ci} was reached in approximately eighteen hours. Further mixture proportion details, fresh concrete properties, and hardened concrete properties can be found in Appendix B, Appendix C, and Appendix D of this thesis, respectively. Concrete curing temperature development curves for each girder can be found in Appendix C as well.

Table 3-1: Summary of Fresh Concrete Properties

PROPERTIES	MIXTURE					
	STD-M		SCC-MS		SCC-HS	
	-1	-2	-1	-2	-1	-2
Water / Cement	0.42		0.36		0.28	
Sand / Aggregate	0.37		0.47		0.46	
Slump Flow (in.)	6.75	6.5	26.25	27.75	28	28.25
Unit Weight (lb/ft^3)	Unknown	Unknown	148.5	150.3	153.6	153.2
Air (%)	3.4	3	3.8	1.8	1.5	1.5
VSI	—	—	1.5	1	1	1
T-50 (sec.)	—	—	4.5	3.1	Unknown	5
J-ring (in.)	—	—	26.25	28.6	28	26.25
L-Box (H_1/H_2)	—	—	0.67	0.86	0.8	Unknown

Table 3-2: Precast Concrete Strengths

Concrete Mixture	f'_{ci} (psi)	f'_c (psi) at 28 days
STD-MS	4,760	6,900
SCC-MS	5,210	8,360
SCC-HS	10,430	13,370

The STD-M mixture was representative of conventional-slump concrete used in typical ALDOT precast, prestressed bridge girders with a water-to-cement ratio of 0.42

and a sand-to-aggregate ratio of 0.37. The strength shown in Table 3-2 is typical for use in ALDOT precast, prestressed bridge girders as well.

The SCC-MS mixture was a moderate-strength SCC mixture designed to obtain strengths comparable to the STD-M mixture. A 30-percent Granulated Ground Blast Furnace (GGBF) slag replacement was used, resulting in a water-to-cementitious-materials ratio of 0.36 and a sand-to-aggregate ration of 0.47.

The SCC-HS mixture was a high-strength SCC mixture designed to obtain an 18-hour f'_{ci} of 9,000 psi. A 30-percent Granulated Ground Blast Furnace (GGBF) slag replacement was used, resulting in a water-to-cementitious-materials ratio of 0.28 and a sand-to-aggregate ration of 0.46.

3.4.2 Cast-in-Place Concrete

All concrete used for the cast-in-place deck consisted of conventional-slump concrete. It was delivered to the Auburn University Structural Research Laboratory from ready-mix concrete supplier Twin City Concrete of Auburn, Alabama. The concrete had a specified 28-day compressive strength of 4,000 psi. The concrete slump during casting operations was typically in the range of 2–5 in. Standard 6 in. x 12 in. concrete cylinders were made in order to assess the deck's compressive strength at various ages, including the time of flexural testing. The modulus of elasticity of the deck concrete was also determined in accordance with ASTM C 469-94 at the time of flexural testing. The measured hardened properties of the deck concrete at flexural testing can be found in Appendix D.

3.4.3 Prestressing Strand

The prestressing steel used in this study was ½-in. "special", low-relaxation, Grade 270, seven-wire prestressing strand. Based on manufacturer-reported values, the cross-sectional area, elastic modulus, and diameter of this strand were taken to be 0.164 in^2, 28,900 ksi, and 0.515 in., respectively.

The strand used for all of the specimens in this study came from a single brand new strand pack that was manufactured by American Spring Wire Corporation in Houston, Texas. The strand exhibited slight to no surface weathering and no pitting. As a precautionary measure, prior to prestressing, the strand was wiped with a new cotton cloth to remove any surface debris. Typical prestressing strand surface condition can be seen in Figure 3-8 below.

Figure 3-8: Typical Strand Surface Condition

3.4.4 Mild Steel Reinforcement

The mild reinforcing steel used in this study consisted of ASTM A615 Grade 60 reinforcing bars. For analysis purposes, the modulus of elasticity and yield stress of this reinforcement was taken to be 29,000 ksi and 60 ksi, respectively. The mild reinforcement consisted of #3 bars for the confinement steel, #4 and #5 bars for the shear reinforcement, and #4 bars for the deck reinforcement. Layout of the mild steel reinforcement can be seen in Figure 3-4, Figure 3-7, Figure 3-6, and Figure 3-7.

3.5 SPECIMEN FABRICATION

Six precast, prestressed bridge girders were fabricated for this study. This section presents the fabrication process for the girders, which was conducted at Hanson Pipe & Precast prestressing Plant in Pelham, Alabama, as well as the fabrication process for the cast-in-place deck placed in the Auburn University Structural Engineering Laboratory.

3.5.1 Fabrication of Precast, Prestressed Bridge Girders

All six precast, prestressed bridge girders were fabricated at Hanson Pipe & Precast prestressing plant in Pelham, Alabama. Two girders were cast each casting day, with a separate casting day for each of the three concrete mixtures. Normal casting procedures of the plant were followed as closely as possible. On casting day, operations began by cleaning the prestress bed and pulling the necessary strand. Once all of the strands were placed and the bulkheads were set, tensioning of the strands began one strand at a time. The specified jacking stress, f_{pj}, was verified by checking the hydraulic pressure in the jacking system. However, strand stress was also monitored via load transducers placed on the end of each strand between the chuck and anchor plate. Figure 3-9 illustrates the

strand force transducers. Several individual strand stress readings were taken between

initial jacking and release.

Figure 3-9: Strand Force Transducers

After strand stressing was completed, the mild-steel reinforcing cage was

fabricated. The shear reinforcement and confining steel were placed and secured to the

tensioned strands as shown in Figure 3-10. During this process, a form release agent was

carefully squirted in a thin stream onto the soffit form as well as onto the interior faces of

the side forms. Care was taken to not contact the reinforcement with the release agent,

which could have contaminated the strands, affecting their bond quality. The side forms

were then placed and secured as depicted in Figure 3-11. In order to prevent possible

paste seepage between the bulkheads and the side forms, simple foam weather-stripping

was adhered to the bulkhead perimeter.

Figure 3-10: Mild Steel Reinforcement

Figure 3-11: Placement of Side Forms

53

After batching on site, the concrete was placed. The standard conventional-slump concrete was placed according to standard procedures. This involved slowly moving the concrete delivery vehicle along the length of the girder, discharging concrete through an auger-driven chute, and consolidating the concrete by means of internal vibration as shown in Figure 3-12. This process was not only time-consuming; it was also accompanied by several safety concerns. The constant movement of the concrete delivery vehicle and its chute posed a potential hazard, as well as the walking on top of the slippery formwork during the vibration process, as shown in Figure 3-12.

Figure 3-12: Internal Vibration of Conventional Concrete

On the other hand, the SCC batches were placed using only two discharge points per girder. These discharge points were located at a distance equal to one quarter of the entire length of the girder from each end as shown in Figure 3-13. Concrete was initially placed by the concrete delivery vehicle at the east-end discharge point for each girder as

shown in Figure 3-14 below. Very little potentially hazardous movement of the delivery

vehicle and its chute was necessary.
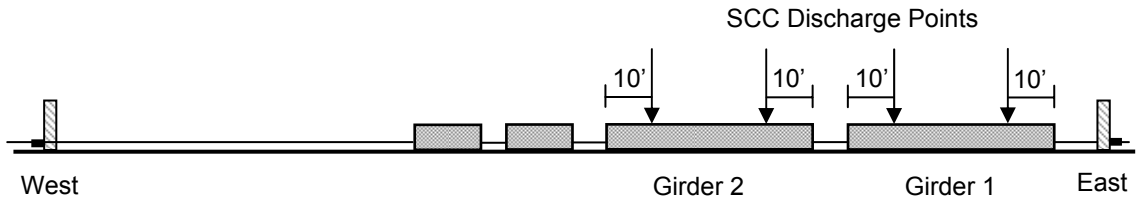
Figure 3-13: SCC Discharge Points

Figure 3-14: Placement of SCC from Concrete Delivery Vehicle at East-End Discharge Point

The SCC flowed easily from this discharge point to the far end of the girder

without segregation as shown in Figure 3-15; however, the girder form could not be

completely filled and leveled from this single point. As a result, the concrete delivery

vehicle was moved to the west-end discharge point and the girders were topped off.

Figure 3-16 below illustrates the state of the girder just prior to cessation of filling at the

east-end. For further illustration, Figure 3-17 depicts the completion of the girder casting

from the west-end discharge point. All SCC girders were cast according to the procedure

described above using a single batch of concrete for each girder. However, several times

a separate smaller batch was required to top off the two girders. Several 6 in. by 12 in.

test cylinders were cast from the concrete batches simultaneously with the girder

castings.

Figure 3-15: SCC Flow from East-End Discharge Point

Figure 3-16: Concrete Level Prior to Relocation to West-End Discharge Point

Figure 3-17: Girder Casting Completion at West-End Discharge Point

Once the concrete casting was completed, the exposed top surface of each girder was raked in order to provide a roughened surface. However, it proved difficult to achieve this on the SCC girders due to the fact that the raked surface would simply reconsolidate into itself. Figure 3-18 and Figure 3-19 illustrate the general difference between the raked surface of the SCC girders and the conventional concrete girders. This reconsolidation resulted in a practically smooth interface between the SCC girders and the cast-in-place deck, which may have contributed to deck separation during flexural testing. (A further discussion of deck separation issues can be found in Chapter 6 of this thesis.) Finally, the entire beam was covered with curing blankets as shown in Figure 3-20. Steam curing was only applied to the standard concrete specimens.

Figure 3-18: Raked Top Surface of Girder SCC-MS-1

Figure 3-19: Raked Top Surface of Girder STD-M-1

Figure 3-20: Placement of Curing Blankets

On the morning after casting, the curing blankets and side forms were removed. Transfer length instrumentation, discussed in further detail in Chapter 4, was then applied. Match-cured 6 in. by 12 in. cylinders were used to monitor the strength of the girder specimens and once the specified release strength was reached, the prestress force was transferred to the concrete via flame-cutting the tensioned strands in two separate places, as shown in Figure 3-2 and Figure 3-21. The strands were flame-cut one at a time. Once initial transfer length testing was performed, the girders were transported, using lift trucks, to storage locations where later-age transfer length testing was performed. The girders were supported at each end on elastomeric bearing pads during the entire storage period.

Figure 3-21: Transfer of Prestress by Flame-Cutting

As discussed previously, SCC has been shown to not only provide cost and safety benefits, but also to provide increased aesthetics in the form of less bugholes and surface blemishes, compared to conventional concrete. In order to demonstrate this, Figure 3-22

and Figure 3-23 illustrate the difference between the formed surfaces of a STD-M girder and a SCC-HS girder. Note the significant decrease in bughole size for the SCC girder.

Figure 3-22: Formed Surface of STD-M Girder

Figure 3-23: Formed Surface of SCC-HS Girder

3.5.2 Fabrication of Cast-in-Place Deck

After each beam pair was transported into the Auburn University Structural Research

Laboratory, preparation for the 48 in. by 3.5 in. deck slab casting began. Both the bridge

girder and the deck formwork were unshored during casting and one deck was cast at a

time. Bridge overhang brackets designed for use on AASHTO Type I precast beams

were secured to the sides of the bridge girder. Reusable plywood formwork sealed with

polyurethane was then secured to the tops of the overhang brackets. Form release agent

was applied to the plywood formwork once it was installed, leveled, and sealed. Slab

reinforcing bars supported on slab chairs were then placed and tied using metal bar ties.

Figure 3-24 and Figure 3-25 depict the operations prior to the casting of the deck

concrete.

Figure 3-24: Bridge Overhang Brackets and Plywood Formwork

Figure 3-25: Slab Reinforcing Steel

The ready-mix concrete was then delivered by Twin Cities Concrete and placed by Auburn University graduate and undergraduate research assistants. The concrete was placed via a crane-suspended bucket as shown in Figure 3-26. Simultaneously, 6 in. by 12 in. test cylinders were cast. Internal vibration was used to consolidate the conventional concrete and a trowel-finish was applied. After initial set, the concrete deck was covered in wet burlap and polyethylene plastic, as shown in Figure 3-27, in order to prevent drying out of the burlap. The burlap was rewetted as needed. The concrete deck was cured underneath the burlap and plastic for approximately three days. At that time, the deck strength was verified and the formwork, along with the overhang brackets, was removed. This process was then repeated on the second girder of the pair.

Figure 3-26: Placement of Deck Concrete

Figure 3-27: Application of Wet Burlap and Plastic

3.6 PRESTRESSING STRAND PULL-OUT TESTING

In order to assess the bond quality of the prestressing strand used in this investigation, a program of strand pull-out testing was performed. Ten strand samples were cast into a concrete test block, pullout testing was performed using a hydraulic jack, and strand performance was monitored. A description of the test procedure and the results of the test program are presented in this section. The strand pull-out testing was performed in accordance with the procedures proposed by Logan (1997).

3.6.1 Specimen Preparation

A single pull-out block was cast with ten strand specimens for the pull-out testing. The ten strand samples were taken from the same roll of American Spring Wire ½" "special" strand used in the AASHTO Type I bridge girders of this study. The samples were cut to 34" lengths, straightened as needed, and inspected in order to ensure they were clean and free of rust.

Preparation prior to casting the pull-out block began with setting of the formwork and installation of the reinforcement cage. Pull-out block dimensions and reinforcement details can be seen in Figure 3-28 and Figure 3-29. The strand samples were then tied securely in place as shown in Figure 3-30. Once the specimen preparation and configuration were checked and approved, concrete placement began. Mixture proportions for the pull-out block concrete can be found in Appendix B. The concrete had a slump of 1.5 in. and an air content of 2.8 percent. Proper consolidation was achieved by means of internal vibration and the top surface was finished using a trowel finish. Curing compound was used on the top of the pull-out block in conjunction with a

curing cover draped over support racks to prevent contact with the tops of the strand samples. The pull-out block and test cylinders were tarp-cured together and no accelerated curing was used.
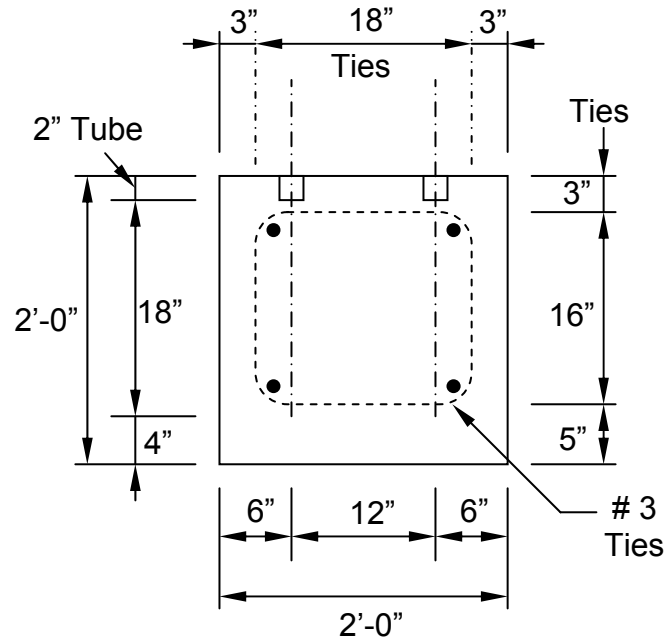
Figure 3-28: Side Elevation of Moustafa Pull-Out Block
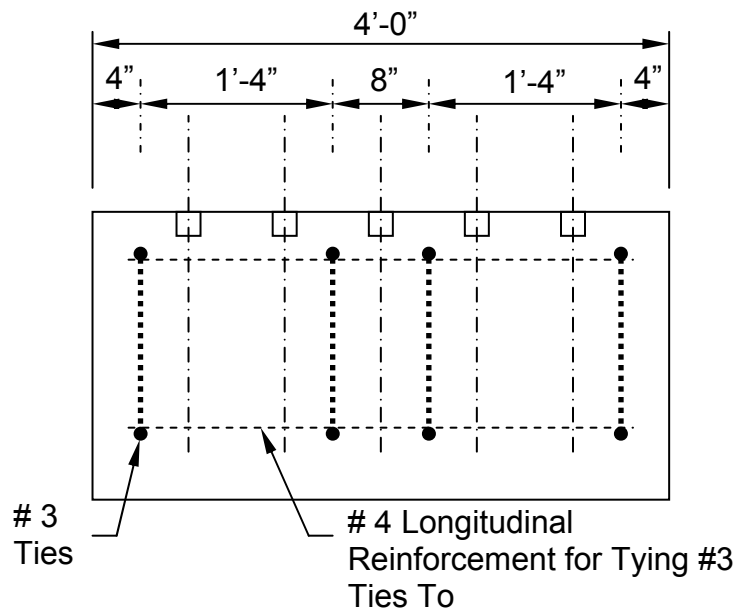
Figure 3-29: Front Elevation of Moustafa Pull-Out Block
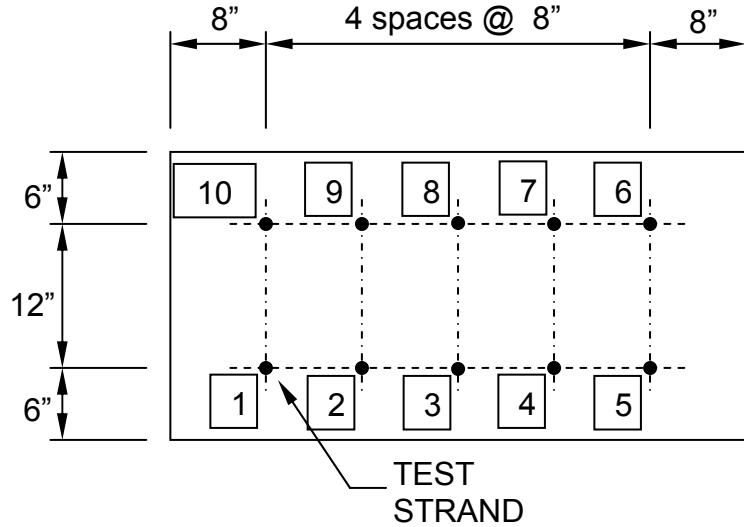
Figure 3-30: Strand Sample Layout and Numbers

3.6.2 Test Procedure

Pull-out testing was performed approximately one day after casting. The average

concrete compressive strength, determined from three 6 in. by 12 in. tarp-cured cylinders,

during the pull-out testing period was 4,300 psi. The average 28-day compressive

strength of the pull-out block concrete measured from three 6 in. by 12 in. moist-cured

(ASTM C 192) cylinders was 7,100 psi. The pull-out test setup is shown in Figure 3-31.

First the bridging device, shown in Figure 3-31, was slipped over the strand and placed

against the concrete surface. Next the strand chuck was slipped over the strand and a

Hercules hydraulic jack typically used for single strand stressing in long-line

pretensioning operations was mounted on the strand. Light pressure was applied to the

jack in order to seat the jaws of the chuck into the strand. The jacking load was then

applied in a single increasing application of load at a rate of approximately 20 kips per

minute until the maximum load was reached. During testing the strand samples were

visually monitored with a video camera and still digital photos were taken.

Figure 3-31: Pull-Out Test Setup

3.6.3 Results and Discussion

During testing, the strand was monitored, noting the approximate load at first noticeable movement, P_{move}, the maximum pull-out force capacity, P_{max}, the approximate distance the strand pulled out at maximum load, Δ_{Pmax}, and the general mode of failure. Table 3-3 presents the pull-out test results for the ten strands.

Table 3-3: Pull-Out Test Results

Strand ID	P_{max} (kips)	P_{move} (kips)	$\Delta P_{P,max}$ (in.)	Failure Description
1	35.0	26.5	2.2	Pullout
2	39.0	23.5	0.6	Pullout
3	37.0	27.0	0.7	Pullout
4	42.6	29.5	0.4	Wire Rupture
5	35.5	29.0	1.1	Pullout
6	38.0	29.5	1.5	Pullout
7	34.0	26.5	NR	Pullout
8	37.0	33.0	2.7	Pullout
9	41.0	31.0	2.2	Pullout
10	38.0	23.0	1.3	Pullout

The average maximum load for this group of ten strand samples was 37.7 kips. Values ranged from 34.0 to 42.6 kips with a standard deviation of 2.7 kips (coefficient of variation = 7.0 percent). The maximum pull-out force, or peak load, corresponded to a pull-out type failure at pull-out distances ranging from 0.4 to 2.7 in.

Based upon the recommendations of Logan (1997), in which pull-out tests were conducted on *standard* ½-in. seven wire prestressing strand in a block with a compressive strength of 4,230 psi, "excellent transfer/development length performance" is defined as an average P_{max} (six samples) of at least 36 kips with a coefficient of variation not exceeding 10 percent. Assuming an equivalent average bond stress at failure for different size strands, the corresponding limiting P_{max} value for ½-in "special" strand is 37.3 kips. The 10-sample P_{max} value obtained in this study exceeds this value, and the coefficient of variation within the recommended 10 percent limit. Thus, it can be concluded that the strand used in this study had comparable bond quality to strand recommended for use by Logan (1997).

CHAPTER 4

TRANSFER LENGTH TEST PROGRAM

4.1 INTRODUCTION

Transfer length testing was performed on all six bridge girders in this study. Each girder had two transfer zones, one at each end. This resulted in twelve total transfer zones available for testing. Transfer lengths were determined by using a mechanical strain gauge to measure concrete compressive surface strains. For all the girders, transfer length testing was performed immediately after transfer of the prestress force, as well as at various later concrete ages ranging from 3 days to 3 months. The transfer length test procedure used for each transfer zone, the results, and the inferences drawn from these results are presented in this chapter. Transfer length results are also compared to transfer length results from previous phases of this investigation.

4.2 PREVIOUS RESEARCH ASSOCIATED WITH THIS STUDY

The research presented in this thesis is part of a larger investigation into the use of SCC in precast, prestressed bridge girders. In previous phases of this project, extensive transfer length testing was conducted on thirty-six concentrically prestressed specimens (Swords 2005) and on sixteen eccentrically prestressed T-beams (Levy 2007). This section presents an overview of the previous transfer length testing conducted prior to the research for this thesis.

70

4.2.1 Concentrically Prestressed Prisms (Swords 2005)

The primary focus of the research reported by Swords (2005) was to determine the effect of SCC on transfer length. Thirty-six concentrically prestressed specimens containing either one or two prestressing strands, as detailed in Figure 4-1, were tested for initial and long-term transfer lengths.
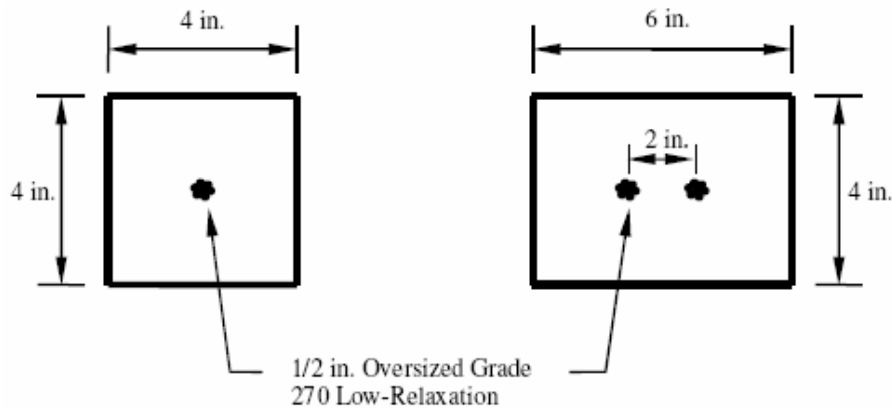
Figure 4-1: Concentrically Prestressed Single- and Double-Strand Cross Sections
(Swords 2005)

Six sets of specimens cast with five different mixtures, one conventional and four SCC mixtures, were investigated. The SCC mixtures included a high- and moderate-strength mixture for each type of SCM: Class C fly ash or ground-granulated blast-furnace (GGBF) slag. Two sets of specimens were cast using the high-strength fly ash mixture due to high air content in the first set. A total of six concentrically prestressed specimens were cast for each set, resulting in 72 transfer zones (two for each specimen). Prestress transfer was achieved by flame-cutting, and concrete compressive surface strains were measured using a mechanical strain gauge. The determination of transfer lengths using measured concrete strains is discussed in detail later in this chapter. Strand

71

draw-in measurements were also used to predict transfer lengths. The results of this phase are discussed in detail by Swords (2005).

4.2.2 Eccentrically Prestressed T-Beams (Levy 2007)

The primary focus of the research reported by Levy (2007) was the transfer and flexural bond behavior of prestressed reinforcement in eccentrically prestressed flexural members cast with SCC. Sixteen T-beams containing two prestressing strands, as detailed in Figure 4-2, were tested for initial and 4-day transfer lengths.
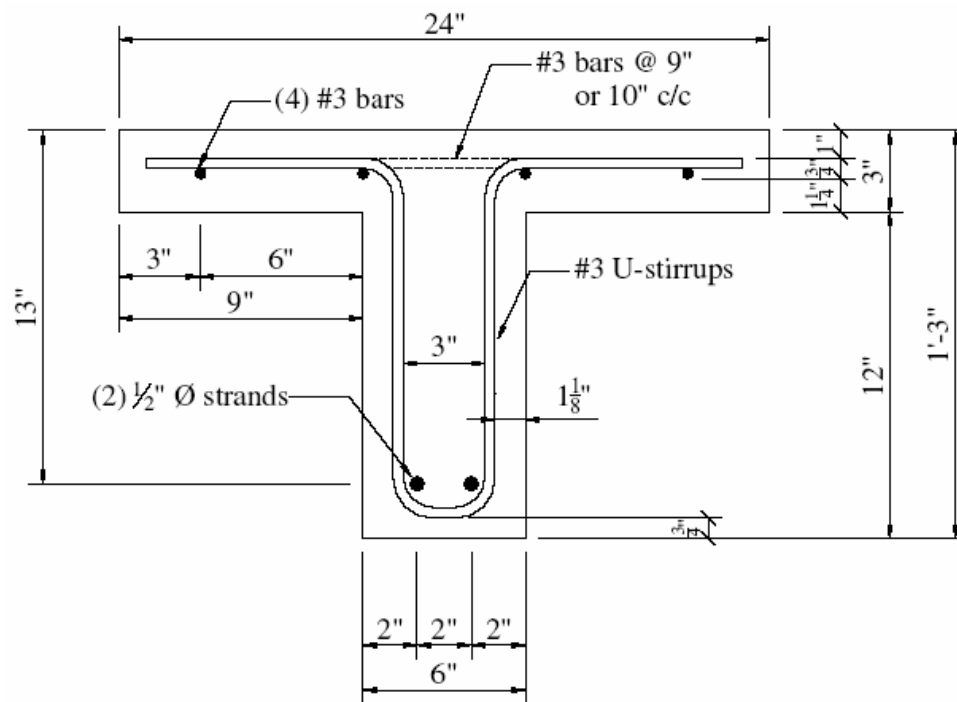
Figure 4-2: T-Beam Cross Section Detail (Levy 2007)

Four sets of specimens cast with four different mixtures, one conventional and three SCC mixtures, were investigated. The SCC mixtures included a high- and moderate-strength mixture utilizing ground-granulated blast-furnace (GGBF) slag as a SCM, and a moderate-strength mixture utilizing Class C fly ash as a SCM. The

conventional mixture and the three SCC mixtures employed the same mixture

proportions as the corresponding mixtures used in the Swords (2005) study. A total of

four eccentrically prestressed T-beams were cast for each mixture, resulting in 32 transfer

zones. Prestress transfer was achieved by flame-cutting, and concrete compressive

surface strains were measured using a mechanical strain gauge. The results of this phase

are discussed in detail by Levy (2007).

4.3 TEST PROCEDURE

This section details the techniques used to measure transfer length in the full-scale

AASHTO Type I girders. The 95% Average Maximum Strain (AMS) Method was

applied to the measured concrete compressive surface strains within the transfer zone in

order to determine transfer lengths. These compressive surface strains were measured

with a demountable mechanical (DEMEC) strain gauge, shown in Figure 4-3. This

method has been well established through many studies for determining transfer lengths

(Barnes et al. 1999). The previous two phases of this study also effectively utilized this

method (Levy 2007, Swords 2005).
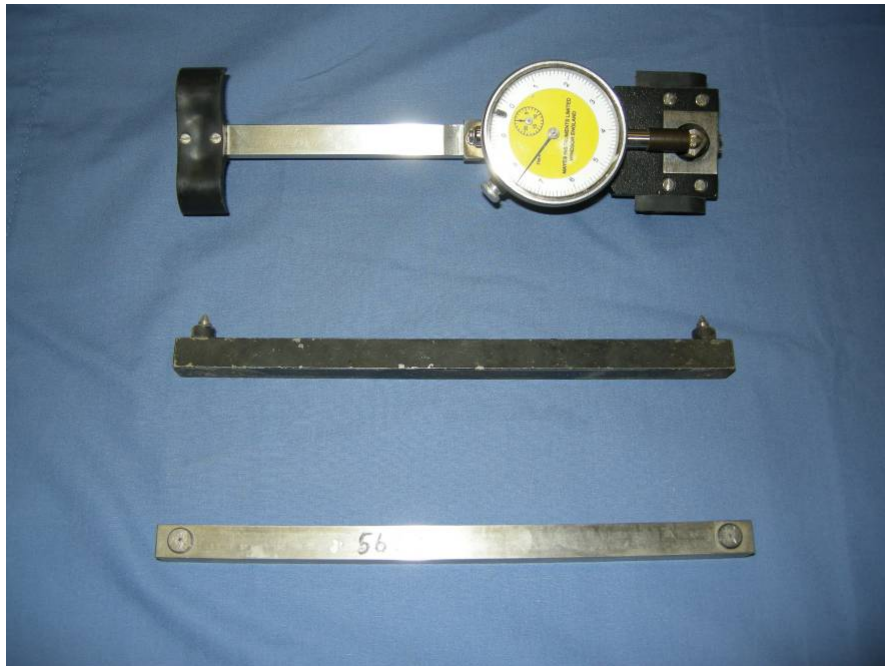
Figure 4-3: DEMEC Instruments

4.3.1 Specimen Preparation

Specimen preparation began with the removal of the side forms early in the morning after

each pair of girders was cast. Figure 4-4 depicts a pair of girders on the prestressing bed

in the middle of the side form removal process. After the side forms were removed, a

chalk line was placed along the length of the bottom flange of the girders on both sides

level with the height of the fully-stressed bottom strands. Then distances equal to 25

mm, 75 mm, 125 mm, and 175 mm were marked along each chalk line from each end of

the girders. DEMEC locating discs were then set at these four locations at each girder

end/face using a five-minute epoxy. This resulted in eight sets of four initial DEMEC

points for the two girders. The stainless steel DEMEC discs had a diameter of 0.25 in.

with a hole drilled in the center for positioning the conical measuring points on the

DEMEC gauge. Once the first four points were set for each series, four more points were

set along the chalk line relative to the first four using a 200-mm setting bar. This process was repeated for all eight series of points until a total of 28 DEMEC discs were set for each. Each line of discs provided a zone, extending well beyond the expected transfer length, in which concrete compressive surface strains were to be measured. Figure 4-5 depicts the placement of the DEMEC discs. Five additional DEMEC discs were placed at 50-mm intervals across the midspan of each girder face at the height of both the bottom and top strands.

Figure 4-4: Side Form Removal
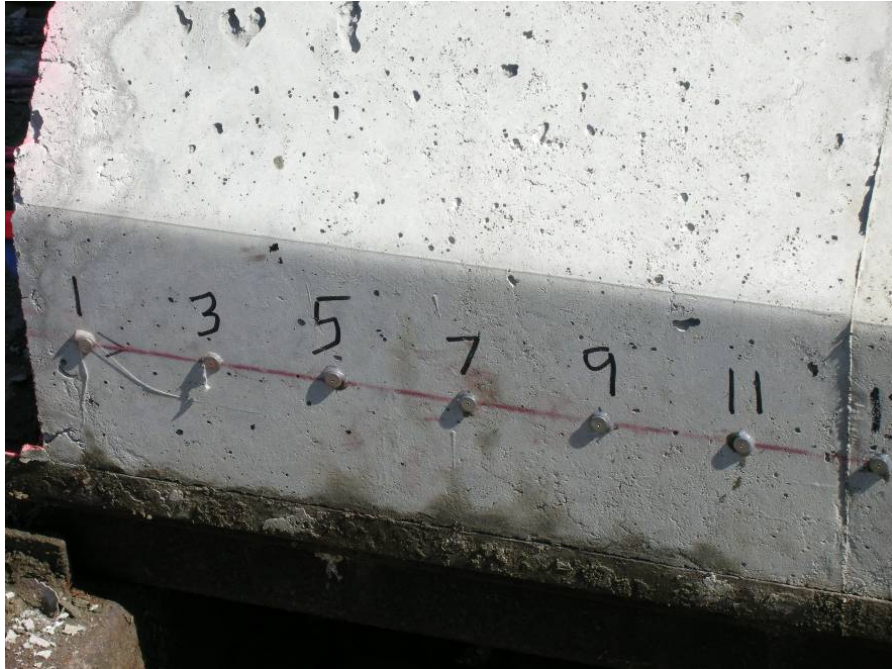
Figure 4-5: DEMEC Discs

After all eight sets of DEMEC discs were placed and the epoxy hardened, initial

readings before prestress transfer were taken with the DEMEC gauge over each 200-mm

length and recorded. Figure 4-6 shows how a DEMEC gauge reading was measured.

Before any set of readings was taken, a reference reading was taken using a

manufacturer-provided reference bar shown in Figure 4-3. Since the DEMEC discs were

spaced only 50 mm apart and the DEMEC gauge had a gauge length of 200 mm,

overlapping measurements were taken for each interval. Each reading was taken twice

and recorded. If a set of discs could not be read due to poor positioning or epoxy quality,

the defective discs were removed, replaced, and re-measured prior to transfer of prestress.

Figure 4-6: Performing DEMEC Gauge Reading

Once all initial readings were taken, the prestress force was transferred to the

girders via flame-cutting the strands at two separate locations, as discussed in Chapter 3

of this thesis. The strands were flame-cut one at a time in two different locations

simultaneously. This method is considered to be a sudden release method as opposed to a

gradual release method, such as might be achieved with a moveable strand anchor block.

This flame-cutting method is typical of the procedure used to produce ALDOT bridge

girders. As a result of the girder placement on the prestressing bed and the flame-cutting

locations, all shown in Figure 3.2, this release method caused only one of the four test

girder ends, 1E, to be a live end (adjacent to flame-cutting). The other three ends were

considered dead ends.

4.3.2 Concrete Surface Strain Measurement

Immediately after the prestress force was transferred to the girders, the DEMEC gauge readings were taken again on all eight sets of DEMEC discs. The procedure followed was identical to the one described for the initial readings. These readings were used to calculate compressive surface strain profiles to and determine initial transfer lengths using the process described in Section 4.4 of this thesis.

For each pair of girders, additional DEMEC gauge readings were taken 3 days, 7 days, 14 days, 28 days, two months, and three months after transfer of prestress. These later-age readings were used to produce compressive strain profiles and to determine later-age transfer lengths. This process made it possible to assess transfer length growth over time.

4.4 TRANSFER LENGTH DETERMINATION

This section describes the process used to construct compressive strain profiles using the DEMEC gauge readings. The determination of initial and long-term transfer lengths from the compressive strain profiles is then detailed. The method is based on the procedure described by Russell and Burns (1997), incorporating the corrections for self-weight and time-dependent deformations proposed by Barnes et al. (1999).

4.4.1 Construction of Surface Compressive Strain Profile

The first step in determining transfer lengths was to construct a surface compressive strain profile for each beam end. The surface compressive strain for each 200-mm interval was calculated by multiplying the DEMEC gauge factor by the difference between the reading at the time under investigation and the preliminary reading recorded

for that interval. All readings were taken relative to the length of the DEMEC reference

bar. As stated previously, overlapping measurements were taken for each 200 mm

interval. This resulted in each disc location being involved in three separate strain

readings. Thus the compressive strain for each disc location was calculated by averaging

the three strain values that included its location. Figure 4-7 illustrates this smoothing

procedure of assigning strain values to individual disc locations. Once strain values were

assigned to individual disc locations, corresponding values on opposite faces of each

girder were averaged to construct one smoothed surface strain profile for each end of

each girder.

Calculated Strain for Interval	15	70	90	120	160	160	185	180	180
Average Strain at Point		58	93	123	147	168	175	182	
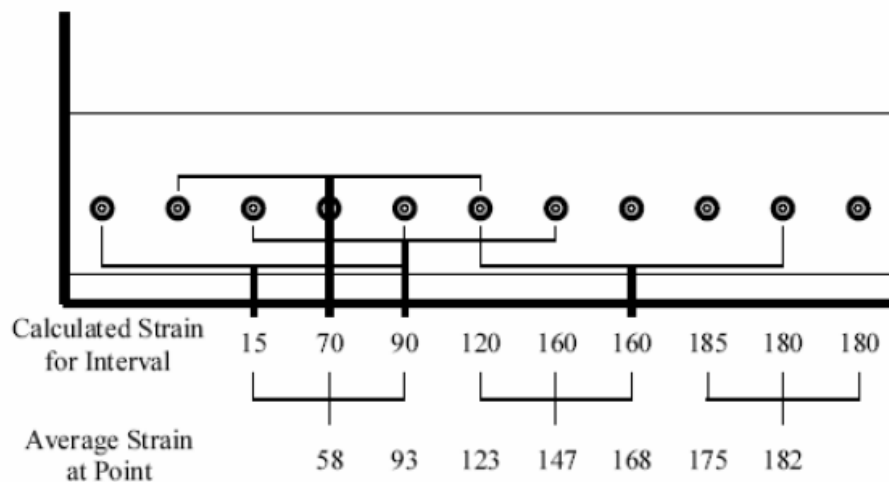
Figure 4-7: Assignment of Surface Compressive Strain Values (Barnes et al. 1999)

Next, in order to isolate the strain resulting from the prestressing, the resulting

surface strain profiles were corrected to account for the flexural strain attributable to the

self-weight of the beam. Due to the eccentricity of prestressing, once the prestressing

was transferred, the girders cambered off of the bed and the girder weight was transferred

to the girder ends through flexural resistance. The girder weight induced a curvature into

the girder which created tensile strains at the level of prestressing, opposing the

79

compressive strains due to prestress force. Once the resulting self-weight-induced tensile

strains were calculated, they were deducted from the measured surface compressive

strains in order to more accurately determine the strain due to the prestressing only. In

general for this procedure, if the strain profile is not corrected to reflect the strain due to

prestress only, a significant error may occur when determining the apparent transfer

length in large members such as full-scale bridge girders.

The self-weight-induced tensile strains were calculated for each disc location on

the basis of engineering beam theory using Equation 4-1.

$$\varepsilon_{weight} = \frac{M * Y_{DEMEC}}{E_c I_{tr}}$$
Equation 4-1

where, ε_{weight} = magnitude of tensile strain due to self-weight

M = moment due to self-weight

Y_{DEMEC} = vertical distance from DEMEC disc to centroid of

transformed section

E_c = modulus of elasticity of concrete

I_{tr} = moment of inertia of transformed section

The presented adjustment for tensile strains induced by the self-weight of the

girders was applied to all strain profiles for all time intervals. However, for long-term

compressive strain profiles, additional creep strains due to self-weight were also

calculated and a similar adjustment was made. Creep strains were estimated by using

creep coefficients experimentally determined for each mixture in previous phases of this

project. For further detail concerning the compensation for self-weight-induced strains

and time-dependent deformations, see Barnes et al. (1999).

4.4.2 Determination of Average Maximum Strain (AMS)

Once the compressive strain profile was constructed for each end of each girder, the next step in determining the transfer length was the establishment of the average maximum strain (AMS) for each end or transfer zone. Determination of the AMS is accomplished by visual inspection of the compressive strain profile. When the strain reaches a plateau, the effective prestress force has been developed in the strand and the strain profile levels out. The strains within this plateau are then averaged in order to determine the AMS. Figure 4-8 illustrates the AMS for a typical compressive strain profile for a specific girder end at two strain measurement ages. The increase in concrete surface strains due to creep and shrinkage during the first few days after transfer is evident in the figure.
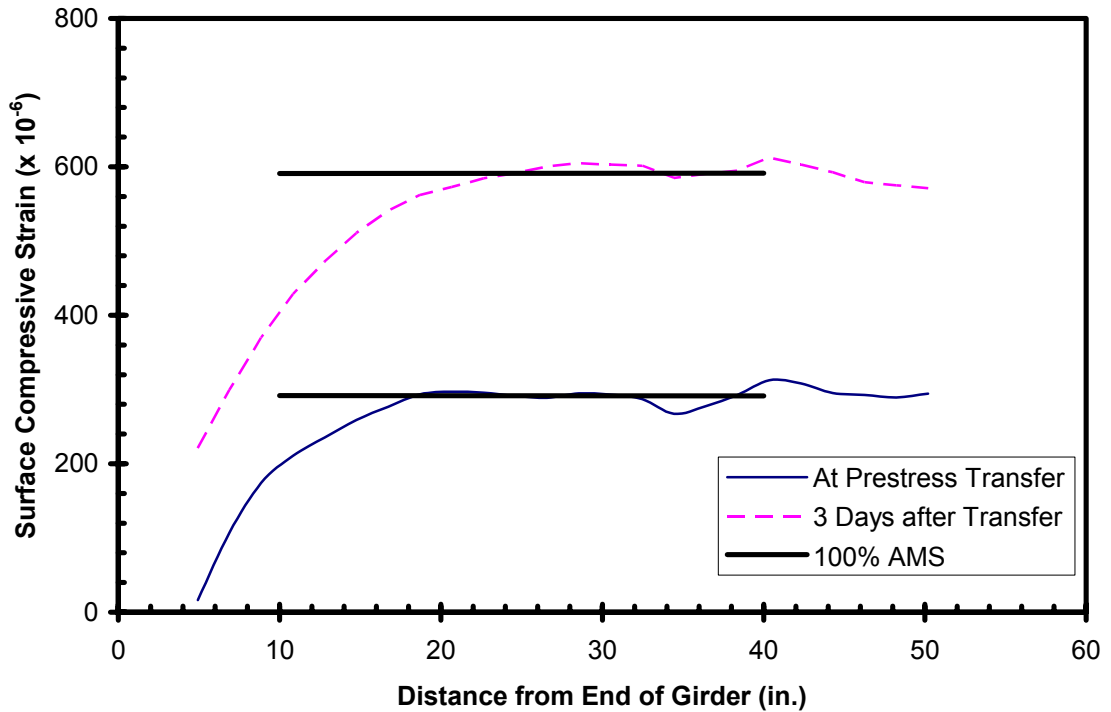
Figure 4-8: Location of Average Maximum Strain Values for Girder SCC-MS-2E

4.4.3 Determination of Transfer Length Using The 95% AMS Method

The transfer length for each girder end was determined by using the 95% AMS Method. According to this method, the apparent transfer length is bounded by the intersection of the compressive strain profile and the horizontal line representing 95% of the average maximum strain for that transfer zone. There are two primary reasons for use of the reduced (95%) limiting value: (1) it provides a clearly identifiable point where the strain profile intersects the limiting value, and (2) it compensates for the slight rounding of the strain profile due to the three-measurement profile smoothing process described earlier. This section details the determination of the 95% AMS value for the initial and long-term strain profiles.

4.4.3.1 Initial Transfer Lengths

The determination of the 95% AMS value for the initial transfer lengths was very simple to achieve. The 100% average maximum strain value already determined was multiplied by 0.95 to obtain a 95% AMS value for each strain profile. This 95% AMS value was then plotted against the corresponding initial compressive strain profiles and the intersection of the two was taken as the end of the transfer length for that girder end transfer zone.

4.4.3.2 Long-Term Transfer Lengths

The determination of the 95% AMS value for the long-term transfer lengths was a more complicated process. Compressive strain profiles for long-term measurements represent elastic strains due to prestress transfer as well as strains due to time-dependent

deformations. These time-dependent deformations due to creep and shrinkage must be accounted for in order to accurately determine long-term transfer lengths.

First of all, consider how creep affects the compressive strain profile. Creep strains are proportional to the applied load; therefore, creep strains will cause an *amplification* of the strain profile. For this type of deformation, one expects the slope of the non-plateau portion of the strain profile to increase at the same rate as the value of the average maximum strain (Barnes et al. 1999). Therefore, when considering only creep strains, multiplying the AMS by a factor of 0.95 will produce consistent transfer length values over time.

However, shrinkage strains are considered to be independent of the applied load; thus they result in a *translation* of the strain profile. Unlike the effect of creep deformations, the slope of the non-plateau portion of the strain profile remains constant and the average maximum strain increases. Applying a five percent reduction to this increased AMS may result in a significantly larger reduction than was used for the initial transfer length estimation. If the actual transfer length remains constant and the strain growth is entirely due to shrinkage, using a fixed percentage AMS value to determine the transfer length will result in an apparent, yet false, decrease of transfer length over time (Barnes et al. 1999).

Individual portions of time-dependent strains attributable to creep and shrinkage for each girder end at each age would be difficult to obtain and would involve inherent uncertainties. Furthermore, varying temperatures from day to day during actual strain measurements can cause a translation or shift of the strain profile. Therefore, a different approach was taken. Instead of simply multiplying the long-term 100% AMS by 0.95,

the long-term average maximum strains were reduced by five percent of the initial 100%

AMS immediately after prestress transfer. In other words, the long-term average

maximum strains were reduced by the same *value* of strain as were the initial average

maximum strains. Although not theoretically ideal, this approach introduces minimal

error and errs on the conservative side for calculated transfer lengths. Figure 4-9

illustrates the 95% AMS for a typical compressive strain profile for a specific girder end

at both initial and long-term strain measurement ages.
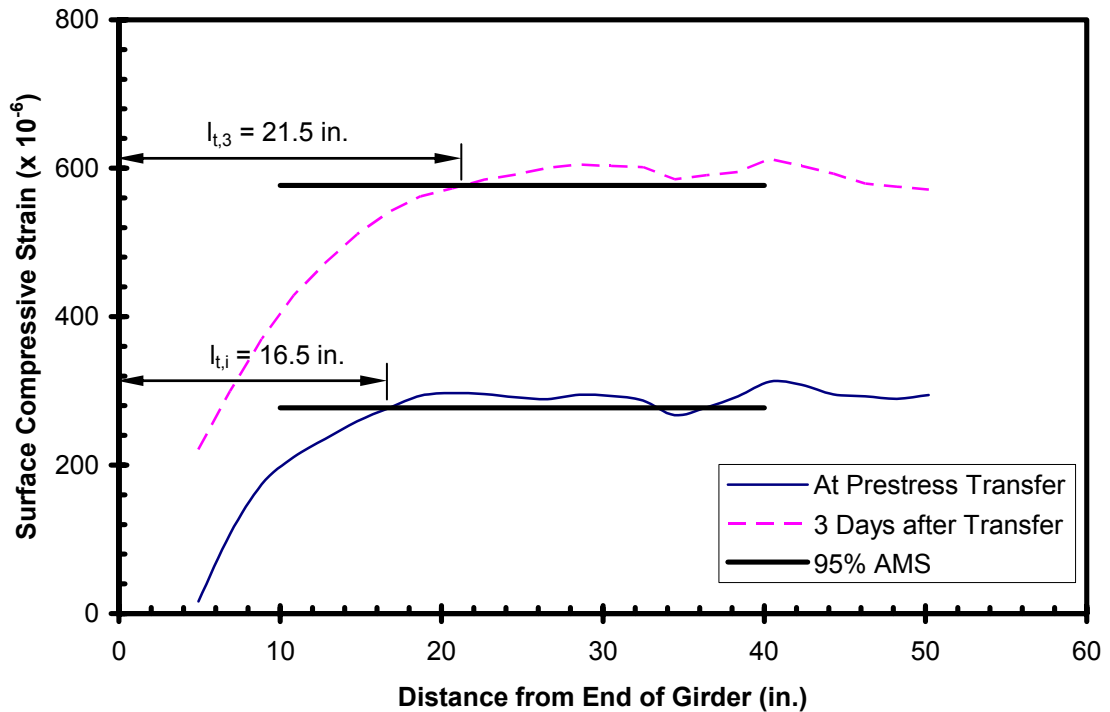
Figure 4-9: Location of 95% AMS Values for Girder SCC-MS-2E

4.4.4 Precision of Results

A precision of 0.5 in. was adopted for all reported transfer length results. This was

determined based upon several factors that affected the accuracy of the transfer length

measurements. First, the spacing of the DEMEC discs was 1.97 in (50 mm). In order to

obtain more precision, values must be smoothed and interpolated. Secondly, researchers were required to perform surface compressive strain measurements in awkward positions outside of laboratory conditions, resulting in less accurate results. Lastly, creep strains were estimated using previously determined creep coefficients (Kavanaugh 2007). Although the transfer length values are not particularly sensitive to the creep values used, this does introduce some uncertainty. In light of these circumstances, researchers concluded it would be misleading to report final transfer length values with a precision better than 0.5 in.

4.5 RESULTS AND DISCUSSIONS

A total of twelve transfer zones were evaluated in this study. The results of the transfer length testing are presented in this section. Details describing trends observed from the results and comparisons to results from previous phases of this project are discussed here.

4.5.1 Transfer Length Results

Twelve different transfer lengths at various ages were determined for the AASHTO Type I girders used in this study. The surface compressive strain profiles for each girder end are presented in Appendix F of this thesis. Using the procedure outlined in Section 4.3, the surface compressive strain profiles were used to determine transfer lengths. The transfer lengths at various ages ranging from immediately after prestress release (initial) to 3 months for all specimens are summarized in Table 4-1. Table 4-1 also reports the concrete compressive strength at transfer, f'_{ci}, the stress in the strand immediately before transfer, f_{pbt}, and the stress in the strand immediately after transfer, f_{pt}, for each girder.

The concrete compressive strength at transfer, f'_{ci}, was calculated as the average compressive strength of three 6 in. by 12 in. match-cured cylinders. For each set of girders, the match-curing for these cylinders was controlled by concrete temperatures in girder 1. However, tarp-cured cylinders cast from girder 1 and 2 produced similar strengths at prestress transfer. Therefore, for each set of girders, it was decided by the researchers to adopt the same f'_{ci} value for girder 2, except in the case of the SCC-MS set. The tarp-cured cylinders from girders 1 and 2 for the SCC-MS set produced significantly different strengths at transfer. As a result, the ratio between the match-cured cylinder strength and the tarp-cured cylinder strength for girder 1 was multiplied by the tarp-cured cylinder strength of girder 2 in order to obtain an accurate f'_{ci} value for girder 2.

The stress in the strand immediately before transfer, f_{pbt}, was calculated as the average of the individual strand force transducer readings discussed in chapter 3. The stress in the strand immediately after transfer, f_{pt}, was calculated by subtracting the product of the modulus of elasticity of the prestressing strand and the peak strain obtained from the DEMEC strain gauge readings immediately after prestress transfer from f_{pbt}. The values of effective prestress in the strands, f_{pe}, corresponding to each transfer length age were calculated similarly to f_{pt}, and can be found in Appendix E. The only difference in the calculation of f_{pe} as opposed to f_{pt} was that the relaxation of the strand stress over time was subtracted as well.

Table 4-1: Summary of Girder End Material Properties and Transfer Lengths

Specimen	f'_{ci} (psi)	f_{pbt} (ksi)	f_{pt} (ksi)	Transfer Length (in.)						
				Initial	3-day	7-day	14-day	28-day	2 month	3 month
STD-M-1E	4,760	200	191	20.5	24.5	25.0	25.5	28.5	28.0	29.0
STD-M-1W		200	193	16.0	21.0	21.5	22.0	23.5	23.0	22.5
STD-M-2E	4,760	200	192	16.5	20.5	21.0	23.5	23.0	26.0	25.0
STD-M-2W		200	192	17.5	20.0	21.5	20.5	20.5	21.0	20.5
SCC-MS-1E	5,540	196	187	17.5	18.5	19.0	19.0	19.0	19.0	19.0
SCC-MS-1W		196	187	17.5	22.5	20.0	22.5	22.5	21.0	22.5
SCC-MS-2E	4,880	196	187	16.5	21.5	21.0	23.0	23.5	19.0	23.5
SCC-MS-2W		196	188	17.5	21.5	21.5	22.5	22.5	22.5	23.0
SCC-HS-1E	10,430	202	195	13.5	15.0	14.5	15.0	14.5	14.5	14.5
SCC-HS-1W		202	195	13.5	15.0	17.0	15.5	18.0	17.5	16.5
SCC-HS-2E	10,430	202	195	13.5	16.5	16.5	18.5	18.5	16.0	17.5
SCC-HS-2W		202	195	14.0	16.5	18.5	17.5	18.5	19.5	21.5

4.5.2 Effects of Concrete Strength

The effect of concrete strength on transfer length has been researched and debated for some time. As discussed in Chapter 2 of this thesis, it has been found that transfer lengths tend to decrease with increased concrete compressive strengths (Russell and Burns 1993, Lane 1998, Oh and Kim 2000, Barnes et al. 2003). Figure 4-10 confirms this relationship for the data obtained in this study by comparing the initial transfer lengths to the compressive strengths at prestress transfer. It has been suggested that the transfer length is inversely proportional to the square root of the concrete compressive strength (Mitchell et al. 1993, Barnes et al. 2003, Swords 2005, Levy 2007). This relationship was explored in the previous two phases of this investigation; therefore, it was investigated for the girder specimens in this study as well.
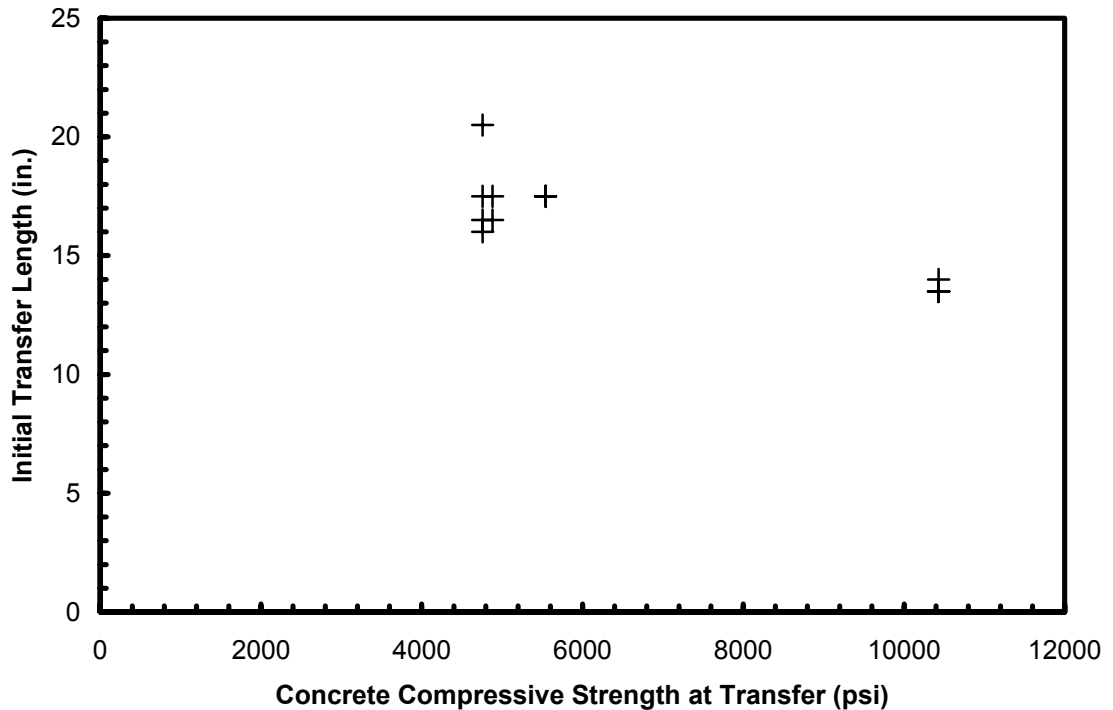
Figure 4-10: Initial Transfer Length vs. Compressive Strength at Transfer

Manipulation of Mattock's original equation for transfer length presented in Equation 2-3 of this thesis shows that the initial transfer length, l_t, is proportional to strand diameter, d_b, and the effective stress in the prestressing tendon, f_{pe}. In addition, it shows that the initial transfer length is inversely proportional to the average bond stress, U_t, along its length. These two relationships result in the following proportional relationship:

$$l_t \propto \frac{f_{pe}}{U_t} d_b \qquad \qquad \textbf{\textit{Equation 4-2}}$$

Barnes et al. (2003) suggest that micro-cracking of the concrete in the inelastic zone creates a softened response, resulting in the stiffness of the concrete being dependent on the tensile strength and the modulus of elasticity. The tensile strength and the modulus of elasticity are often estimated as being proportional to the square root of the concrete compressive strength. Therefore, the average bond stress can be estimated as being proportional to the square root of the concrete compressive strength, which results in the proportional relationship given in Equation 4-3. The α shown in Equation 4-3 is a proportionality constant that depends on many factors (Barnes et al. 2003).

$$l_t = \alpha \frac{f_{pe}}{\sqrt{f'_c}} d_b \qquad \qquad \textbf{\textit{Equation 4-3}}$$

Researchers conducting the previous two phases of this investigation used the aforementioned proportional relationship to relate transfer lengths to concrete compressive strengths. If this relationship accurately reflects the influence of concrete strength and prestress magnitude, the α value in Equation 4-3, which can be calculated for each measured transfer length, gives a measure of the relative transfer bond

performance after normalization for the effects of prestress magnitude and concrete strength. The Swords (2005) study investigated several different combinations of parameters and found that the model that yielded the best correlation was $\dfrac{f_{pt}}{\sqrt{f'_{ci}}}d_b$ in which the stress immediately after prestress transfer, f_{pt}, and the concrete compressive strength at prestress transfer, f'_{ci}, were used. This resulted in the following equation:

$$l_t = \alpha \frac{f_{pt}}{\sqrt{f'_{ci}}}d_b \qquad\qquad \textbf{\textit{Equation 4-4}}$$

As a result, Levy (2007) focused on this form of the relationship for the T-beam specimens. In all cases this relationship proved to be valid for both initial and long-term transfer lengths. Figure 4-11 illustrates the relationship between the measured long-term transfer lengths (3-month) obtained from the full-scale girders used in this study and the corresponding $\dfrac{f_{pt}}{\sqrt{f'_{ci}}}d_b$ values in units of ksi$^{-0.5}$. Based on a linear regression analysis used to determine a "best-fit" line to model the data, an average α value of 0.54 ksi$^{-0.5}$ and a corresponding R^2 value equal to 0.54 were calculated as seen in Figure 4-11. Based upon the precision of the known and measured properties, α values were rounded to the nearest 0.01 ksi$^{-0.5}$. This proportional model seems to work well with the data obtained in this study, and effectively normalizes out the effects of prestress magnitude and concrete strength. Consequently, figures similar to Figure 4-11 will be used for the remainder of this chapter in order to make quantifiable comparisons between transfer lengths.
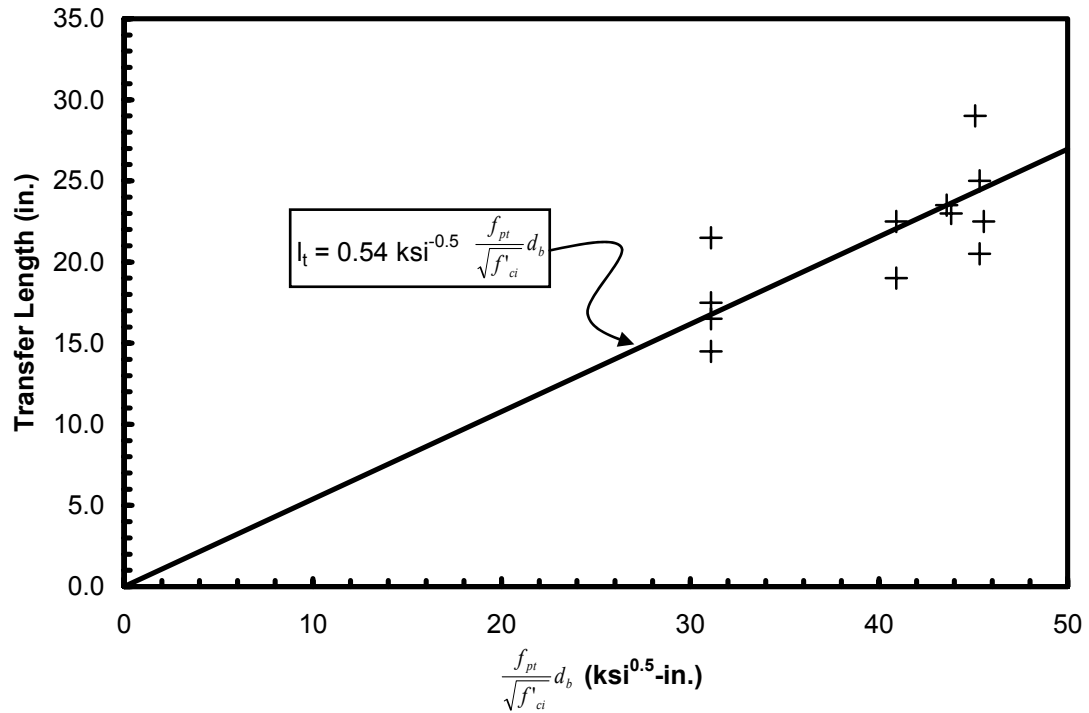
Figure 4-11: Transfer Length as a Function of Strand Prestress and Concrete Strength at Release

4.5.3 Effects of Cross-Section Size

Researchers conducting the previous two phases of this investigation conducted extensive transfer length testing on smaller prestressed specimens. Swords (2005), reviewed in Section 4.2.1, studied concentrically prestressed rectangular specimens and Levy (2007), reviewed in Section 4.2.2, studied eccentrically prestressed T-beam specimens. The purpose of this section is to compare the data obtained in this study to previous results in an effort to establish the effect of cross-section size on transfer length. In order to make the most direct comparison between cross-section size and transfer length, the results from relevant specimens studied by Swords (2005) and Levy (2007) will be presented.

Specifically, only data obtained from Swords' 4 in. by 6 in. specimens prestressed with two strands will be considered. Additionally, only data collected in both studies

91

from specimens constructed with the same concrete mixtures used in this study will be evaluated. Significant differences in dead-end and live-end transfer lengths were noted in both previous studies; therefore, each set of data was analyzed separately. This selection process yielded twelve relevant dead-end transfer lengths from each previous study, as well as six and twelve relevant live-end transfer lengths from Swords (2005) and Levy (2007), respectively, for comparison with the twelve (nine dead-end and three live-end) transfer lengths obtained in this girder study. The sample size from this study was relatively small and no noticeable significant difference was observed between the live- and dead-ends; therefore, all comparisons were made without distinguishing release method for the data obtained in this study.

Unless otherwise noted, the transfer lengths presented in this chapter for the Swords and Levy studies represent seven-day transfer lengths and four-day transfer lengths, respectively. In the Swords study, readings were not taken for all mixtures on a consistent basis until seven days. However, readings were taken at two to four days after transfer for all specimens, and no significant difference between these readings and the seven-day readings was noted. In the Levy study, the only long-term readings taken were four days after prestress transfer. Therefore, it was decided to use Swords' seven-day and Levy's four-day transfer lengths for comparison to the three-day transfer lengths obtained in this study.

As stated previously, Swords (2005) found the best correlation for computing α values resulted from using Equation 4-4. This resulted in Levy (2007) utilizing the same relationship; however, significant differences were noted between live-end and dead-end transfer lengths for both studies, resulting in separate analyses. Considering only relevant

specimens from each study, Figure 4-13 and Figure 4-14 show the comparison between the live-end and dead-end transfer lengths, respectively, to the transfer lengths obtained in this study. As shown in Figure 4-13, the α values for Swords' and Levy's live-end transfer lengths, 1.02 ksi$^{-0.5}$ and 0.74 ksi$^{-0.5}$, are significantly larger than the α value, 0.49 ksi$^{-0.5}$, for all 3-day transfer lengths obtained in this study. Furthermore, the general conclusion that the α value decreases with increasing cross-section size can be drawn.

These general trends are evident, yet less pronounced, in Figure 4-14, in which the dead-end transfer lengths from each previous study are compared to the transfer lengths obtained in this study. The range of α values is not as large as the live-end values; however, the conclusion that α decreases with increasing cross-section size can still be drawn. For further analysis Table 4-2 presents a summary of the α values for each study. Once again it is important to note that no distinction was made between the live- and dead-ends for the transfer lengths from this study. They were analyzed as a whole.
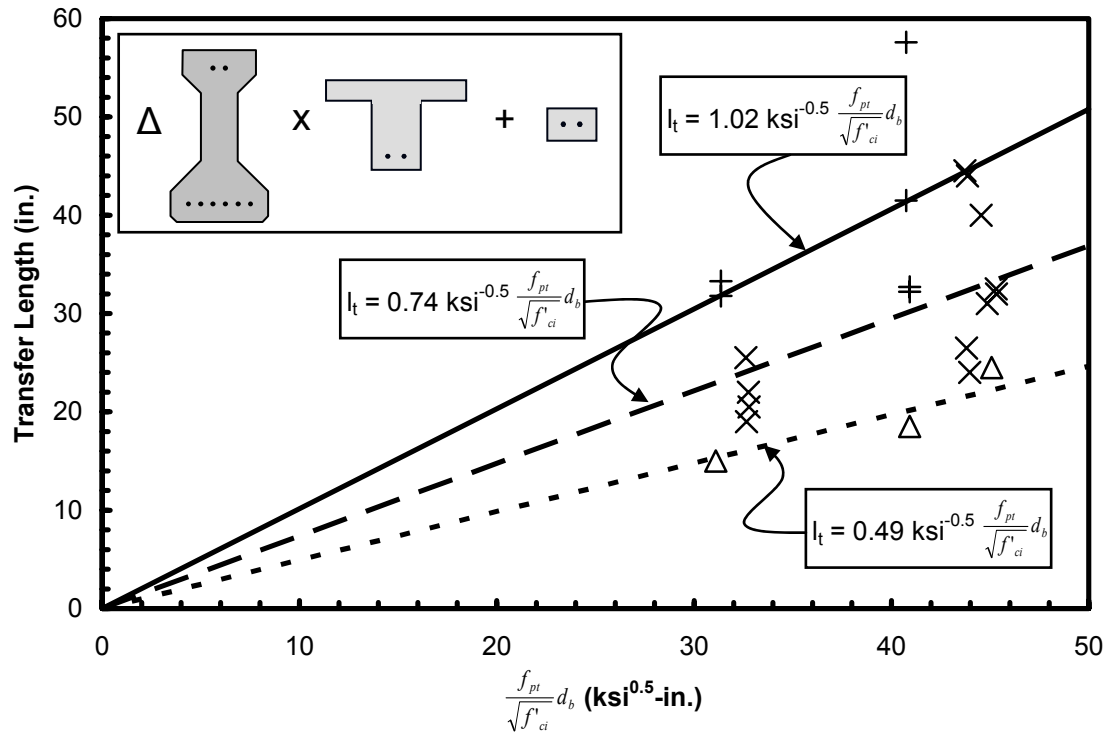
Figure 4-12: Effect of Cross-Section Size Using Live-End Transfer Lengths from Previous Studies

In Figure 4-12, the following relationships are shown:

$$l_t = 1.02 \text{ ksi}^{-0.5} \frac{f_{pt}}{\sqrt{f'_{ci}}} d_b$$

$$l_t = 0.74 \text{ ksi}^{-0.5} \frac{f_{pt}}{\sqrt{f'_{ci}}} d_b$$

$$l_t = 0.49 \text{ ksi}^{-0.5} \frac{f_{pt}}{\sqrt{f'_{ci}}} d_b$$

The horizontal axis is $\frac{f_{pt}}{\sqrt{f'_{ci}}} d_b$ (ksi$^{0.5}$-in.)
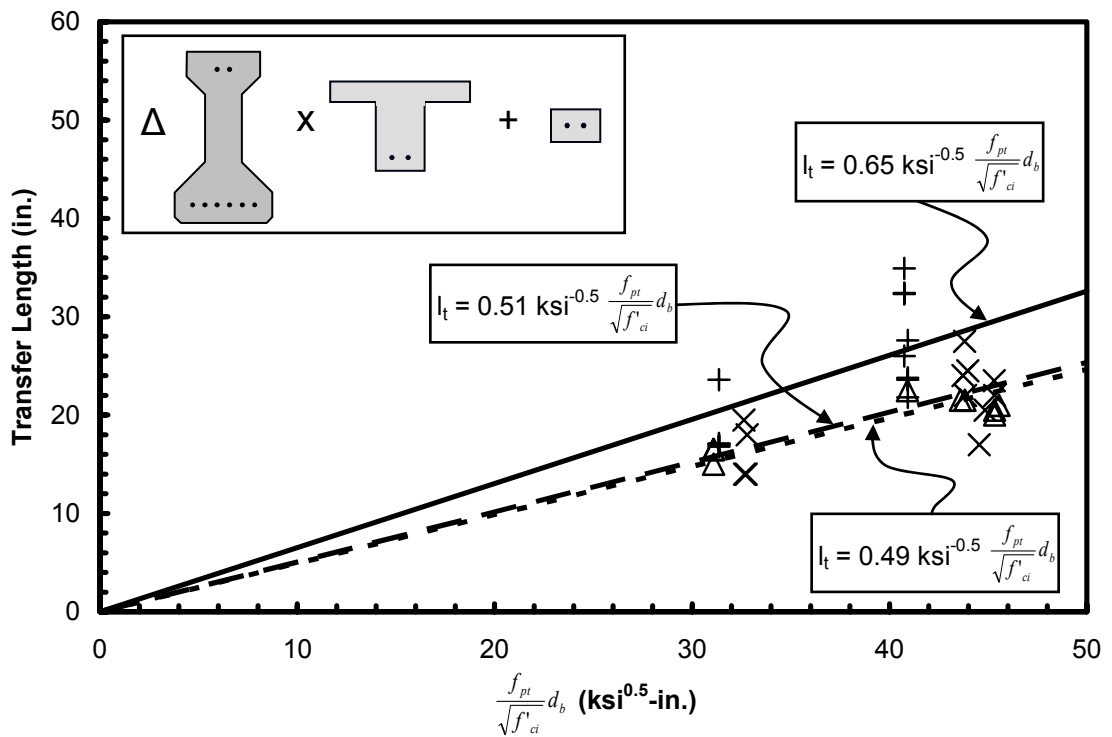
Figure 4-13: Effect of Cross-Section Size Using Dead-End Transfer Lengths from Previous Studies

In Figure 4-13, the following relationships are shown:

$$l_t = 0.65 \text{ ksi}^{-0.5} \frac{f_{pt}}{\sqrt{f'_{ci}}} d_b$$

$$l_t = 0.51 \text{ ksi}^{-0.5} \frac{f_{pt}}{\sqrt{f'_{ci}}} d_b$$

$$l_t = 0.49 \text{ ksi}^{-0.5} \frac{f_{pt}}{\sqrt{f'_{ci}}} d_b$$

The horizontal axis is $\frac{f_{pt}}{\sqrt{f'_{ci}}} d_b$ (ksi$^{0.5}$-in.)

Table 4-2: Summary of α Values

Specimen	α Value	
	Live End	Dead End
(rectangular section)	1.02	0.65
(T-beam section)	0.74	0.51
(I-girder section)	0.49	

As shown in the table, the calculated α values, 1.02 ksi$^{-0.5}$, 0.74 ksi$^{-0.5}$, and 0.49 ksi$^{-0.5}$, tend to significantly decrease as the cross-section size increases when making comparisons using the live-end results from the previous two studies. The same can be stated when making comparisons using the dead-end; however, the α values 0.65 ksi$^{-0.5}$, 0.51 ksi$^{-0.5}$, and 0.49 ksi$^{-0.5}$, are relatively similar with no functional difference between the T-beam specimens and the girders used in this study. This leads to the conclusion that increased cross-section size produces shorter transfer lengths, and, in general, has much more of an effect on the live-end transfer lengths than it does on the dead-end transfer lengths. This conclusion supports the findings of Russell and Burns (1993) in which it was hypothesized that larger cross sections with greater mass can absorb more energy, and will therefore exhibit greater transfer bond.

4.5.4 Comparison of Conventional and SCC Mixtures

In order to compare the transfer lengths of the conventional concrete mixture to the SCC mixtures, it is once again convenient to use Equation 4-4 to produce normalized values of

transfer length. Initial comparisons were made based solely on the transfer length data

obtained from the AASHTO Type I girders used in this study. For each girder end or

transfer zone, a representative α value, which normalizes the effects of prestress

magnitude and concrete strength, was calculated. The corresponding α values for each

concrete mixture were then averaged and used to make quantifiable comparisons between

concrete mixtures. In order to compare SCC transfer lengths to the conventional concrete

transfer lengths, the relationship $\dfrac{\alpha}{\alpha_{STD-M}}$ was employed. Table 4-3 presents the results

of the calculated α values for each mixture and the corresponding comparisons. Once

again, long-term transfer lengths (3-month) were used due to their significance for the

ultimate long-term behavior of prestress members.

Table 4-3: Comparison of Normalized Long-Term α Values

Mixture	α	$\dfrac{\alpha}{\alpha_{STD-M}}$
STD-M	0.54	1.00
SCC-MS	0.52	0.97
SCC-HS	0.56	1.05
All SCC	0.54	1.01

As shown above, the moderate-strength SCC mixture produced transfer lengths 3

percent shorter than the conventional concrete mixture. On the other hand, the high-

strength SCC mixture produced transfer lengths 5 percent longer than the conventional

concrete mixture (after compensating for the effect of concrete strength). Averaged over

all the SCC mixtures, only a 1 percent difference relative to the transfer lengths for the

conventional concrete mixture was observed. This is not a noticeably significant difference, given the small number of girder specimens tested.

In order to make quantifiable comparisons to the data obtained in the previous two phases of this investigation, the three-day transfer lengths were analyzed and compared in the same manner as described above. There was no noticeable significant difference in α values with regard to the effects of concrete mixture type between the three-day and long-term (3-month) transfer lengths obtained in this study. For comparison purposes, the same selection process described in Section 4.5.3 was used to obtain relevant data from the results of Swords (2005) and Levy (2007). As stated previously, significant differences were found between live-end and dead-end transfer lengths for the previous two studies and separate analyses were performed, as is evident in Table 4-4. Table 4-4 summarizes the comparison of the $\dfrac{\alpha}{\alpha_{STD-M}}$ values obtained in this study to the live-end, dead-end, and average (live-end and dead-end) $\dfrac{\alpha}{\alpha_{STD-M}}$ values obtained in the previous two phases of this investigation.

$$\text{Table 4-4: Comparison of } \dfrac{\alpha}{\alpha_{STD-M}} \text{ Values to Previous Data}$$

Mixture	Swords $\dfrac{\alpha}{\alpha_{STD-M}}$			Levy $\dfrac{\alpha}{\alpha_{STD-M}}$			Girder $\dfrac{\alpha}{\alpha_{STD-M}}$
	Live	Dead	Avg.	Live	Dead	Avg.	
STD-M	1.00	1.00	1.00	1.00	1.00	1.00	1.00
SCC-MS	1.53	1.30	1.42	1.40	0.86	1.13	1.05
SCC-HS	1.31	1.00	1.16	1.03	0.92	0.97	1.07
All SCC	1.42	1.15	1.29	1.22	0.89	1.05	1.06

97

Table 4-4 above presents a considerable amount of data from which numerous discussions could be formed. However, the general purpose of this section is to compare the conventional concrete transfer lengths to the SCC transfer lengths. As a result, the average α values for all SCC specimens in each study will be examined. When normalized for the effects of concrete strength, Swords (2005) and Levy (2007) reported a 29 percent and a 5 percent average increase in transfer length of the SCC specimens over the conventional concrete specimens, respectively. The results seen by Levy (2007) are comparable to the 6 percent increase in transfer length for all SCC girders observed in this study. Considering the relatively small sample sizes used in the Levy study and this study, the 5 percent and 6 percent increases have little significance. However, the 29 percent increase seen by Swords suggests that concrete type (conventional concrete or SCC) has a significant effect on the transfer lengths of smaller specimens.

4.5.5 Effects of Time

Although not extensively researched, several studies have suggested significant increases in transfer length with time (Kaar, LaFraugh, and Mass 1963, Lane 1998, Barnes et al. 1999). For mixtures similar to those used in this study, Swords (2005) monitored transfer lengths at various ages ranging from initial to 48 days. It was reported that only a significant growth was observed in the first few days after transfer, with less than a 2 percent increase in transfer length observed from four to forty-eight days. Due to the findings of Swords (2005), Levy (2007) only monitored transfer lengths immediately after transfer and four days after transfer.

Within each of the three mixtures in this study, changes in transfer lengths were determined by comparing each long-term transfer length to the initial transfer length, then taking the averages for each mixture. The results of these comparisons for the previous two phases of this investigation, as well as the results for this study, are shown in Table 4-5.

Table 4-5: Effect of Time on Transfer Length

Mixture	$l_{t,long-term}$ / $l_{t,initial}$		
	3-day (Swords)	**4-day** (Levy)	**3-day** (Girder)
STD-M	1.03	1.06	1.22
SCC-MS	1.04	1.04	1.22
SCC-HS	1.04	1.15	1.16

As can be seen in the table above, significantly greater growth in transfer length over time was observed in this study compared to previous phases of this investigation. The average growth in transfer length at 3 days of 22 percent, 22 percent, and 19 percent for the conventional concrete, SCC-MS, and SCC-HS mixtures, respectively, is considerably higher than the results reported by Swords (2005) and Levy (2007).

In order to further quantify the effects of time on transfer length growth, a more in-depth discussion of the results from this study will be presented. Figure 4-14 illustrates the growth of transfer length over time for each girder end or transfer zone and for each concrete mixture. The first half of the figure illustrates the initial transfer length values while the second half illustrates the corresponding 3-month transfer length values. Several inferences can be made from this figure. The general growth over time for all girder ends and concrete mixtures can be seen. In general, more growth can be seen in the conventional concrete girders, especially the live end (1E). However, the live end

99

does not appear to behave significantly differently relative to the dead ends in the girders

constructed with SCC.
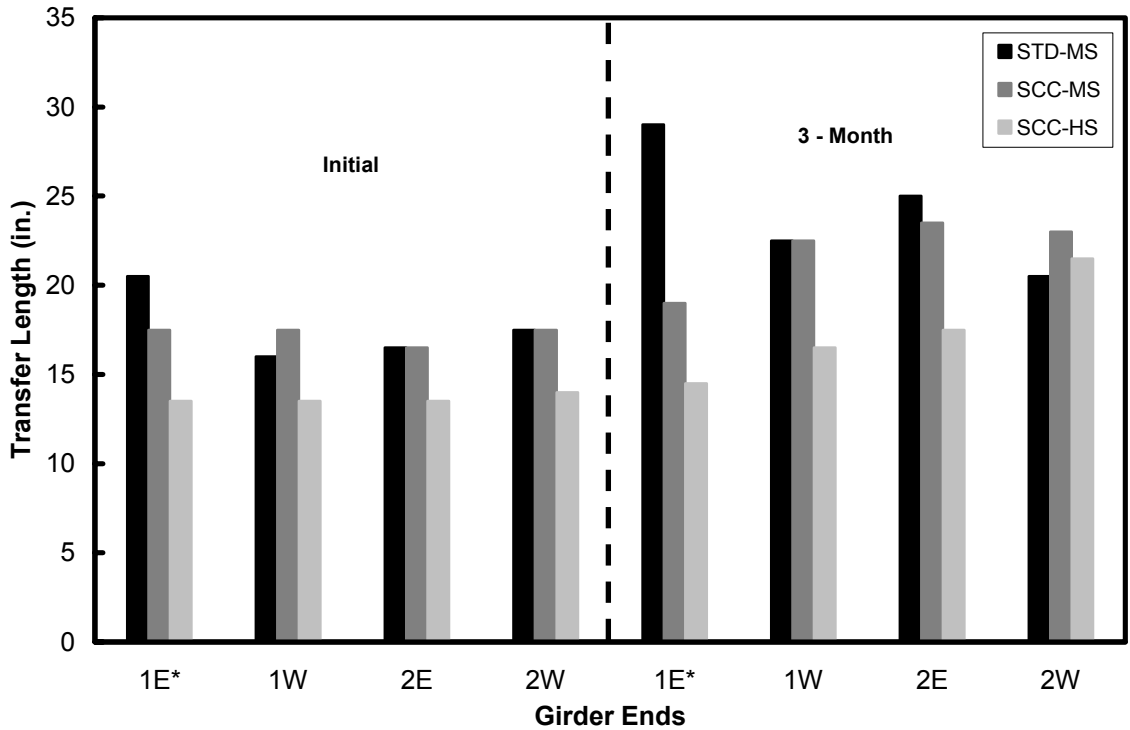
Figure 4-14: Effect of Time on Transfer Length
Note: * Designates cut or "live" end

Further illustration of transfer length growth over time is presented in Table 4-6.

Specific percentage increases in transfer length for each different concrete mixture over

time are tabulated. It can be seen that transfer lengths increased an average of 38 percent

for girders constructed with conventional concrete, and 28 percent for girders constructed

with both SCC mixtures. Although these results are obtained from a relatively small data

set, they suggest more growth of transfer length over time for conventional concrete

specimens than for SCC specimens.

Table 4-6: Transfer Length Growth over Time

Specimen	$l_{t,long\text{-}term}$ / $l_{t,initial}$				
	3-day	7-day	14-day	28-day	3 month
STD-M	1.22	1.27	1.30	1.36	1.38
SCC-MS	1.22	1.18	1.26	1.27	1.28
SCC-HS	1.16	1.22	1.22	1.27	1.28

4.6 COMPARISON OF TEST DATA WITH DESIGN EXPRESSIONS

The purpose of this section is to compare the transfer length data obtained in this study with design expressions for transfer length calculation. Specifically, the recommended expressions from previous phases of this investigation, the ACI 318-05 expression, the ACI 318-05 shear provisions expression, and the AASHTO LRFD expression will be examined. Comparisons will be made, and a brief discussion will be provided.

4.6.1 Recommended Expressions from Previous Phases

Figure 4-15 and Figure 4-16 compare the 3-month transfer length data obtained in this study to the upper bound expressions for predicting transfer length recommended in previous phases of this investigation. All live-end transfer lengths were predicted using the expression $l_t = 0.78\text{ksi}^{-0.5} \dfrac{f_{pt}}{\sqrt{f'_{ci}}} d_b$ and all dead-end transfer lengths were predicted using the expression $l_t = 0.64\text{ksi}^{-0.5} \dfrac{f_{pt}}{\sqrt{f'_{ci}}} d_b$ (Levy 2007). Figure 4-15 is a plot of predicted transfer lengths using the aforementioned expressions versus the corresponding measured transfer lengths. In this type of plot, it is helpful to plot a line of equality representing the points where the predicted transfer length equals the measured transfer

length. Any points falling above the line of equality represent an overestimation by the utilized expressions. Conversely, any points falling below the line of equality represent an underestimation of transfer length, implying that the expression is unsafe for shear and flexure design.
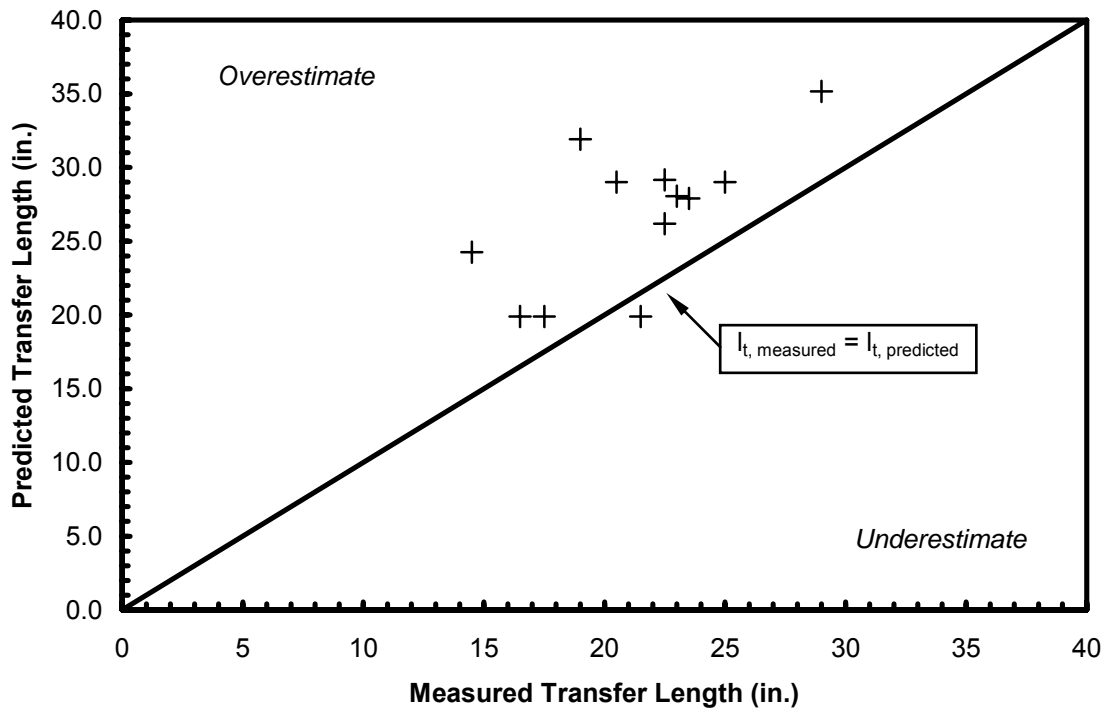
Figure 4-15: Comparison of Levy Expression Values to Measured Long-Term Transfer Lengths

It can be seen in Figure 4-15 that the majority of the datapoints fall above the line of equality, and are therefore conservative estimates. However, one datapoint falls below the line of equality, representing an underestimation using the recommended Levy (2007) expressions. Further analysis and explanation concerning this datapoint will be presented later in this section. In general, the data obtained from this study appears to follow the line of equality suggesting that the Levy (2007) expressions can portray the trends of the data obtained in this study, and produce mostly safe, predictions.

Figure 4-16 shows a plot of the ratio of measured transfer length to the predicted transfer length versus the concrete compressive strength at transfer, f'$_{ci}$. The effectiveness of the expressions in question relative to the concrete strength of the mixture can be assessed in this type of plot. The horizontal line in this type of plot represents perfect agreement between predicted and measured values of transfer length. The closer the data are to the line of equality, the more accurate the expression is in predicting transfer lengths.
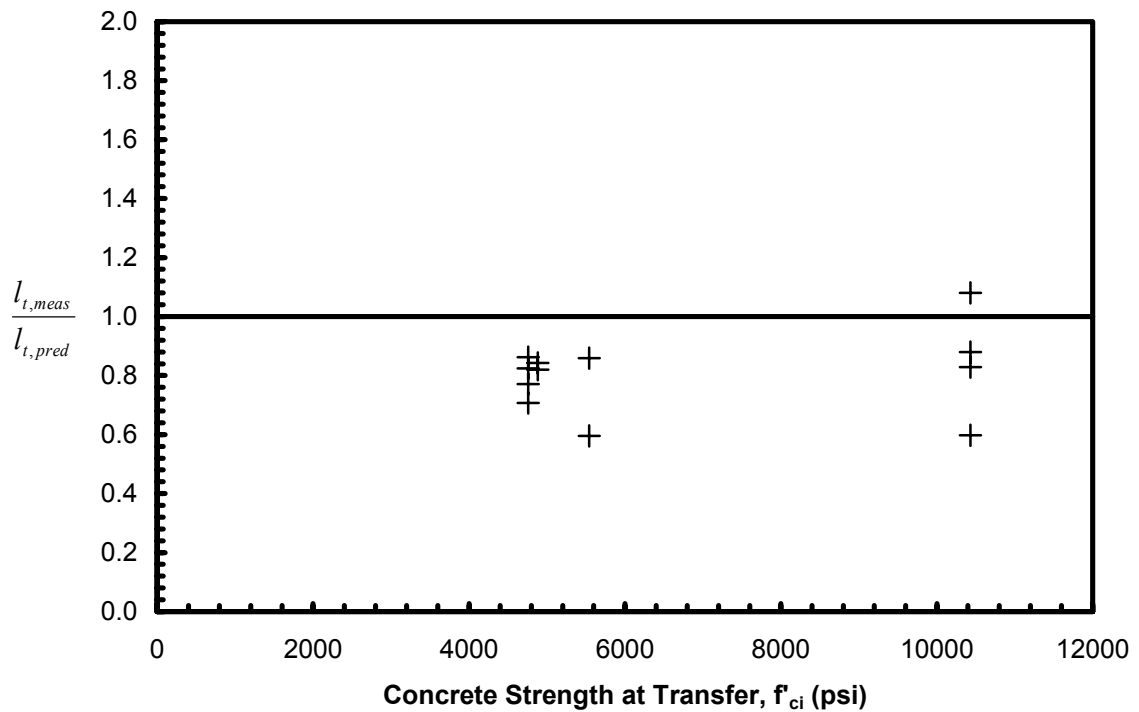
Figure 4-16: Comparison on Levy Expression Values over Concrete Strength Range for Long-Term Transfer Lengths

Upon examination of using Figure 4-16, it can be seen that the one datapoint underestimated by the Levy (2007) expressions corresponds to the high-strength concrete mixture. All other mixtures were conservatively predicted. Although the dataset for this

103

study was relatively small, this one datapoint may suggest that the expressions recommended by Levy (2007) are possibly unconservative for high-strength concrete mixtures.

It was decided to further investigate the Levy (2007) expressions for predicting transfer length by using the 3-day transfer lengths obtained in this study. This was deemed necessary due to the fact that the Levy (2007) expressions were derived based upon 4-day transfer lengths. Figure 4-17 compares the 3-day transfer length data obtained in this study to the Levy (2007) expressions stated above. This comparison effectively eliminated the underestimated datapoint, producing conservative results for all the data obtained in this study.
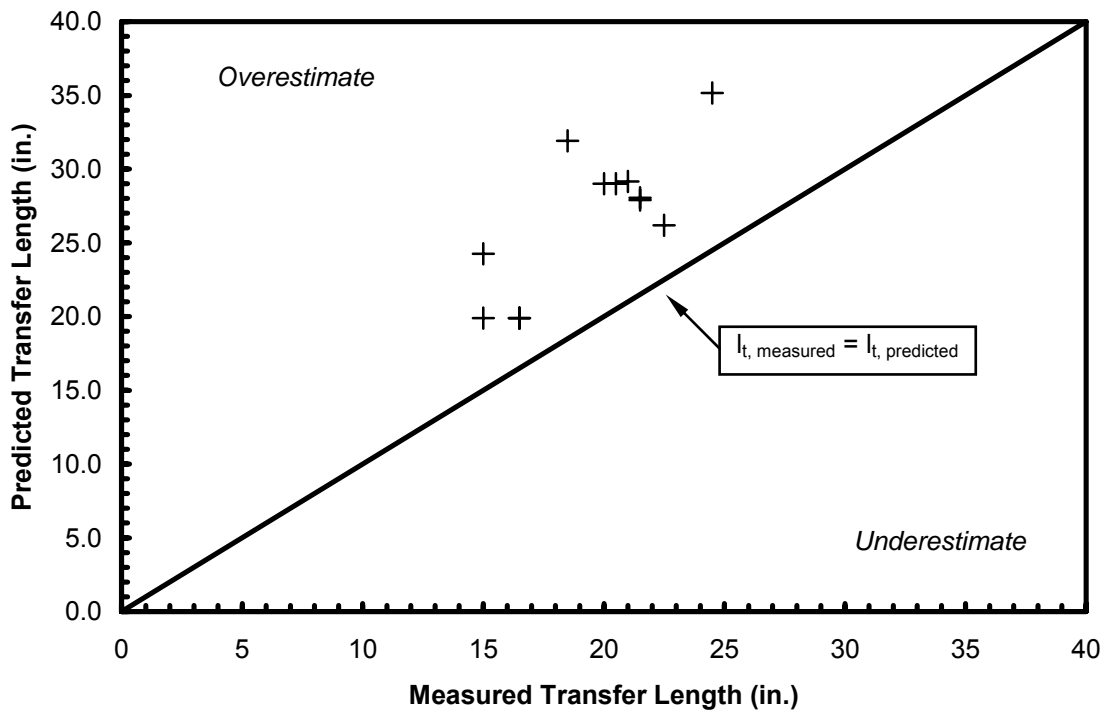
Figure 4-17: Comparison of Levy Expression Values to Measured 3-Day Transfer Lengths

A comparison between Figure 4-15 and Figure 4-17 reveals that some of the data points in Figure 4-17 tend to be located further from the line of equality than the data points in Figure 4-15. This trend suggests a greater overestimation by the Levy (2007) expressions for the 3-day transfer lengths as opposed to the 3-month transfer lengths. It can be shown that a couple of factors contribute to this. First of all, it has been observed that larger cross sections produce shorter transfer lengths. Since the Levy (2007) expressions were derived from smaller specimens than the girders used in this study, the expressions, when applied to data obtained in this study, should theoretically predict longer transfer lengths; i.e. should overestimate transfer lengths. This would account for the overestimation when using the Levy (2007) expressions to predict the 3-day transfer lengths obtained in this study.

In order to explain the fact that the expressions produced a "greater" overestimation of the 3-day transfer lengths than the 3-month transfer lengths, transfer length growth over time must be taken into account. The data presented previously suggests significant growth of transfer length over time; therefore, as time passes, the growing transfer lengths will effectively become closer to the values predicted by the Levy (2007) expressions. It is important to note that all the transfer lengths from this study, except for one, did not grow enough to produce unconservative results using the expressions. Nevertheless, this trend is evident in the data obtained from this study, and it can be concluded that the Levy (2007) expressions derived from smaller specimens at an early age can produce conservative predictions of transfer lengths for larger specimens at later ages.

Further analysis of the one datapoint producing an unconservative result at long-term ages as shown in Figure 4-15 was conducted in order to establish its uncertainty. The datapoint from girder SCC-HS-2W was determined to be underestimated, i.e. the measured transfer length was longer than the Levy (2007) expression predicted. Therefore, the accuracy of the measured transfer length was questioned. In order to facilitate explanation, Figure 4-18 illustrates the surface compressive strain profiles for this girder end at prestress transfer (initial), 3 days after transfer, and 3 months after transfer.
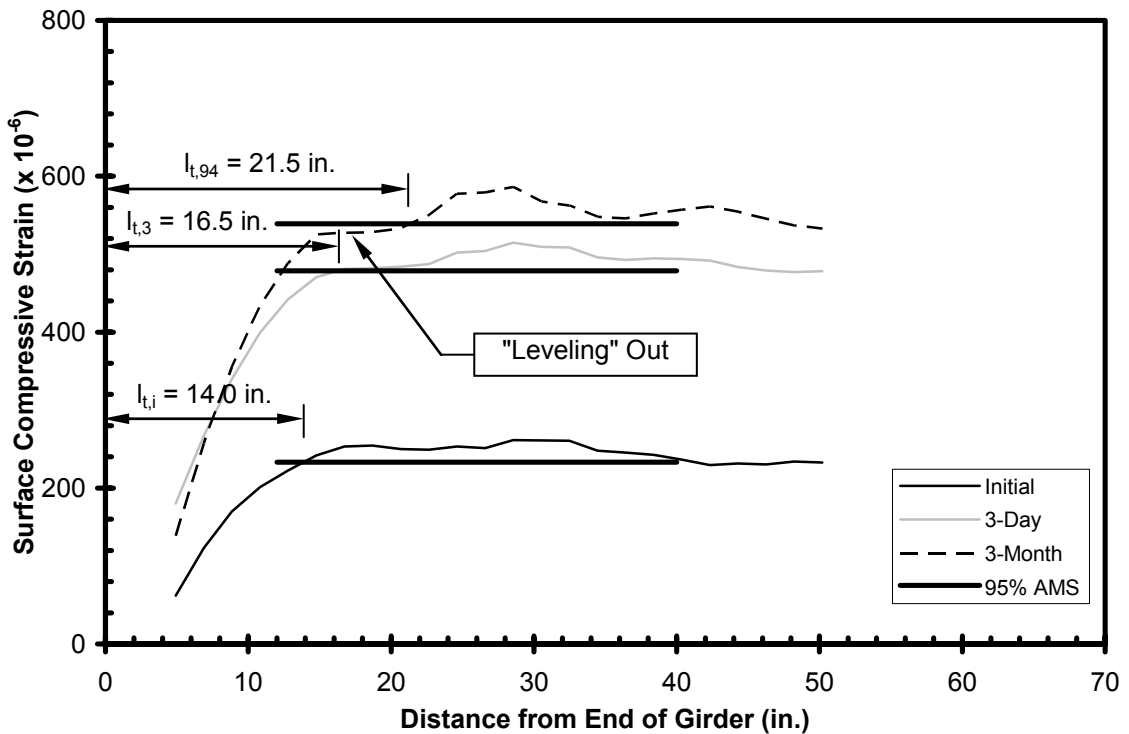
Figure 4-18: Surface Compressive Strain Profiles for Girder SCC-HS-2W

As shown above, the measured transfer length for girder SCC-HS-2W grew from 14.0 in. to 21.5 in. over a 3-month period. This amount of growth was relatively large when compared to other girder ends. The primary factor for the apparent abnormal growth was the surface compressive strain profile at 3 months after transfer. As can be

seen in the figure, the strain profile at 3 months reaches a plateau at approximately 520

microstrain and shows an almost constant strain for several inches. This "leveling" out of

the strain profile makes it difficult to obtain an accurate intersection of the 95% AMS line

and the strain profile. In other words, the apparent transfer length in this case is

extremely sensitive to the slightest change in the 95% AMS value, up or down.

In this particular case, the 95% AMS line happened to be slightly larger than the

plateau value, resulting in an intersection as the strain profile began to slope up again,

and more importantly, a longer apparent transfer length. Had the 95% AMS value been

slightly less, then the intersection would have provided a significantly shorter apparent

transfer length at 3 months after transfer. The 3-day strain profile did not exhibit this

behavior, and its transfer length was previously shown to be conservatively predicted by

the Levy (2007) expressions. If the 3-month strain profile had not been so sensitive to

slight variations in the 95% AMS value, a shorter transfer length that proved to be

conservatively estimated by the Levy (2007) expressions may have been found.

Therefore, it was ultimately decided to not be too concerned by this single unconservative

datapoint.

4.6.2 ACI 318-05 Chapter 12 Expression

Figure 4-19 and Figure 4-20 show comparisons of the 3-month transfer length data

obtained in this study to the expression for transfer length included in article 12.9.1 of the

ACI *Standard Building Code Requirements for Reinforced Concrete*, $l_t = \left(\dfrac{f_{pe}}{3000} \right) d_b$

(ACI 318-05). The history of this expression is discussed in Section 2.3 of this thesis.

Once again, the line of equality has been plotted in order to facilitate comparisons.

Obviously, the data obtained from this study does not follow the line of equality in any way, indicating the expression's ineffectiveness in predicting transfer lengths; however, this expression serves as an adequate upper bound, with all data falling above the line of equality.

Figure 4-20 illustrates that this expression does not follow the general trend of the data with respect to concrete strength. It can be seen that data at higher concrete strengths are further away from the line of equality; this indicates that as concrete strengths increase, this expression becomes increasingly conservative. Nonetheless, this figure reiterates the fact that this expression is conservative for all test data obtained in this study, although not accurate especially for higher strength concretes.
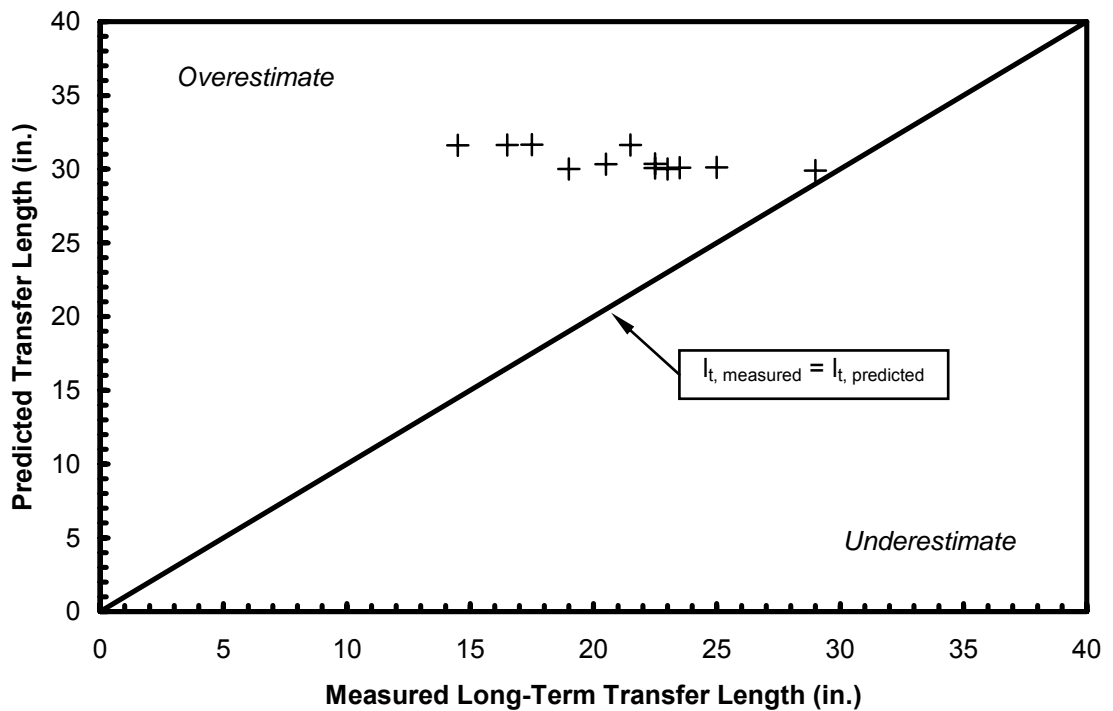
Figure 4-19: Comparison of ACI 318-12.9 Values to Measured Long-Term Transfer Lengths
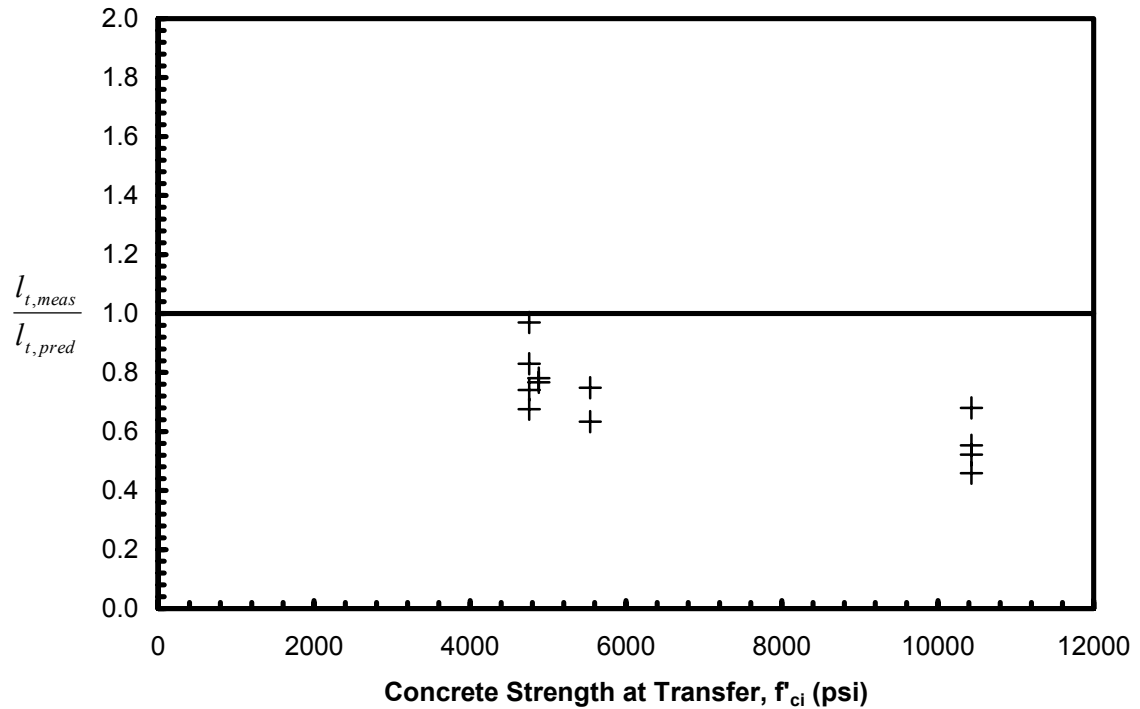
Figure 4-20: Comparison of ACI 318-12.9 Values Over Concrete Strength Range

4.6.3 ACI 318-05 Shear Provisions Expression

Figure 4-21 and Figure 4-22 show comparisons of the 3-month transfer length data

obtained in this study to the expression for transfer length included in the shear

provisions of the ACI *Standard Building Code Requirements for Reinforced Concrete*, l_t

= $50d_b$ (ACI 318-05). Because it only depends on strand diameter, this expression

predicts a constant transfer length for all data obtained in this study. This expression has

a very similar relationship to the data as the one from the ACI 318-05 Chapter 12

expression presented above. The data does not follow the line of equality, and all transfer

length values are overestimated, except for one.

It can be seen in Figure 4-22 that the one underestimated transfer length

corresponded to a moderate-strength concrete mixture. Levy (2007) reported similar

results, stating that this expression proved to be unconservative for lower-strength concrete mixtures. As with the Chapter 12 expression, this expression grows increasingly conservative as concrete strength increases. This expression was conservative for the majority of the test data obtained in this study, although not accurate especially for higher strength concretes.
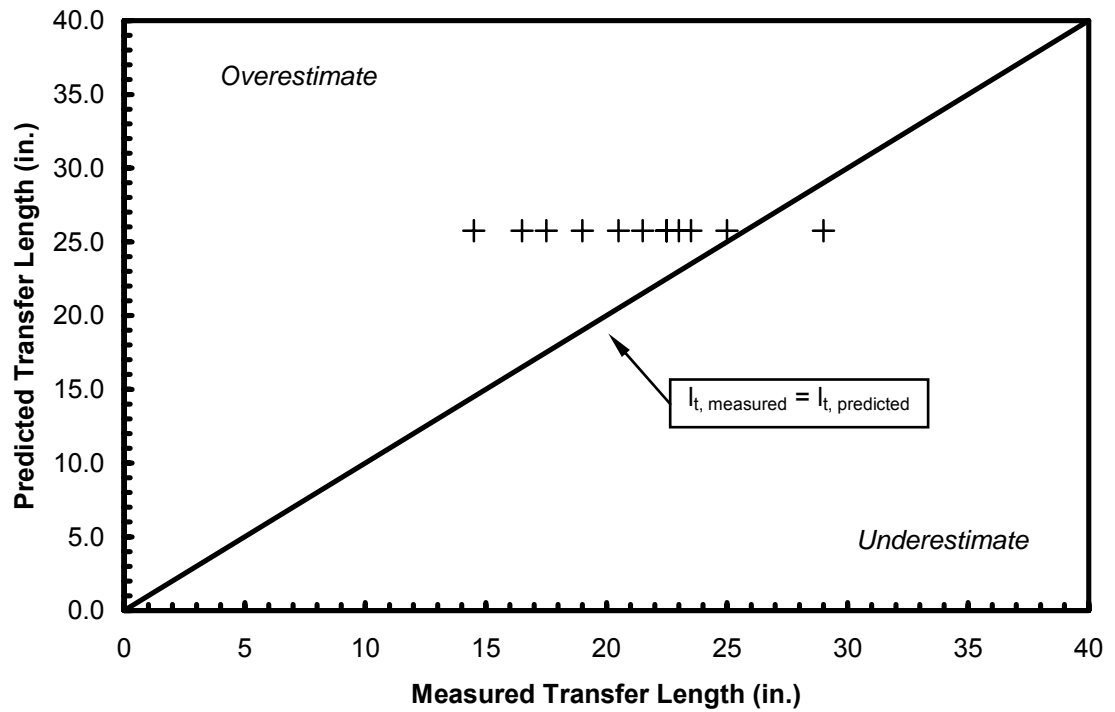
Figure 4-21: Comparison of ACI 318 Shear Provisions To Measured Long-Term Transfer Lengths
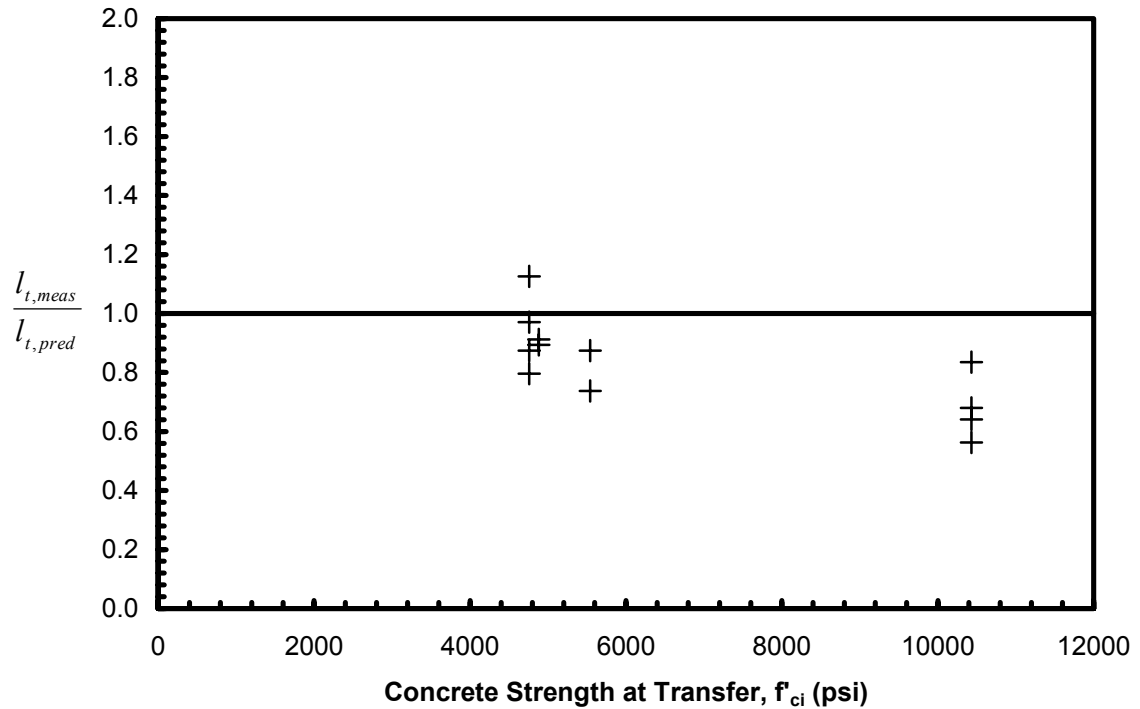
Figure 4-22: Comparison of ACI Shear Provisions over Concrete Strength Range

4.6.4 AASHTO LRFD Expression

Figure 4-23 and Figure 4-24 show comparisons of the 3-month transfer length data

obtained in this study to the expression for transfer length included in the AASHTO

LRFD Specifications, $l_t = 60d_b$ (AASHTO 2007). Very similar to the ACI shear-

provisions expression, this more-recently-developed expression reflects the increased

levels of prestress common in contemporary practice. Consequently, almost identical

results are obtained for the test data obtained in this study, except that this expression

provided conservative estimates for all data points, including the one that was

underpredicted by the ACI shear provisions. Once again, both figures demonstrate

conservative, although not accurate, results—particularly for higher-strength concretes.

111
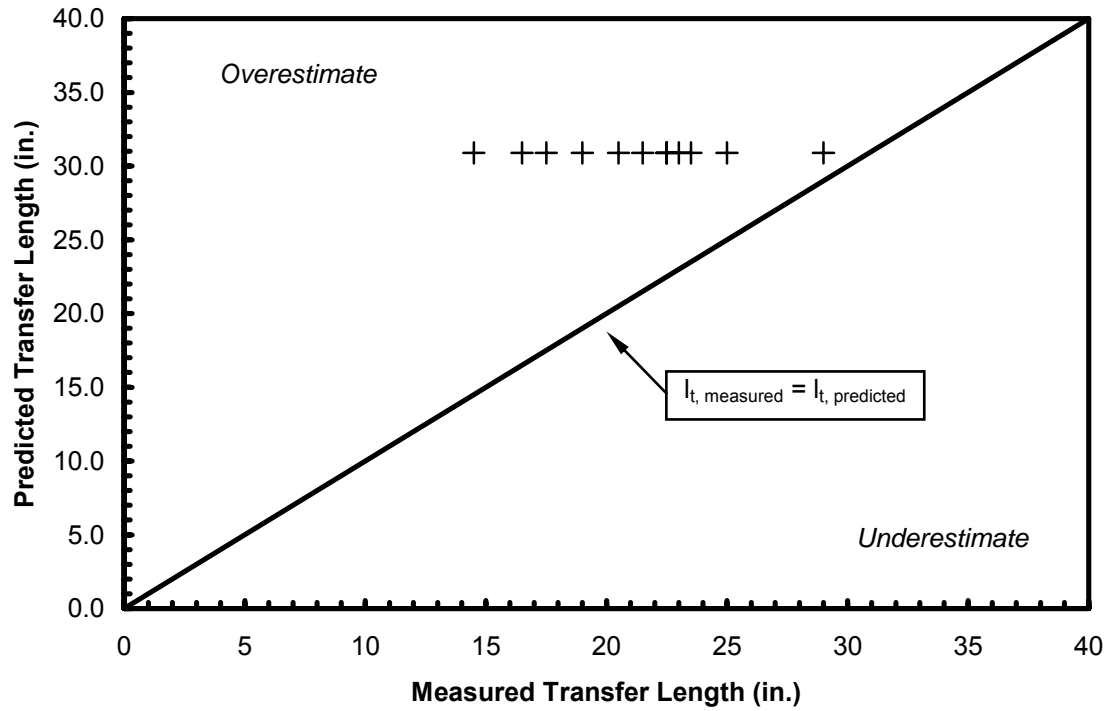
Figure 4-23: Comparison of AASHTO LRFD Provisions to Measured Long-Term Transfer Lengths
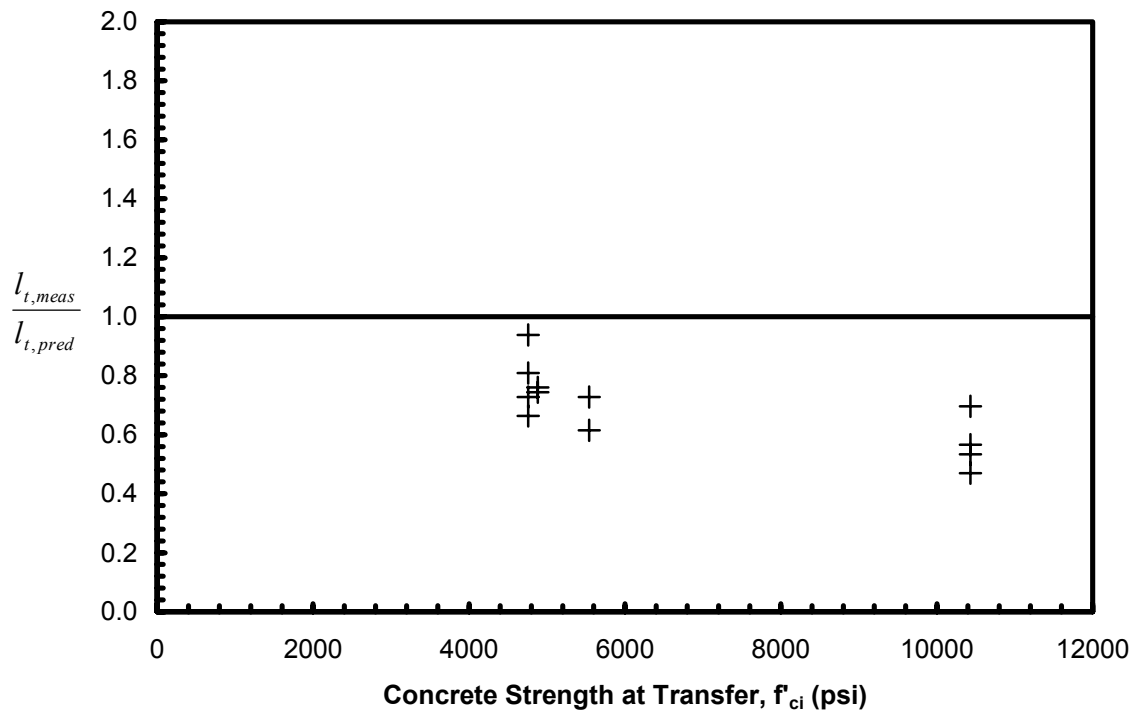
Figure 4-24: Comparison of AASHTO LRFD Provisions over Concrete Strength Range

112

4.7 SUMMARY AND CONCLUSIONS

Transfer length testing was performed on six plant-cast AASHTO Type I bridge girders, resulting in twelve transfer zones (one at each girder end). Concrete compressive strains were measured using mechanical strain gauges immediately after transfer as well as at long-term ages ranging from 3 days after transfer to 3 months. Transfer lengths were then determined by analyzing the surface compressive strain profiles and using the 95% AMS method. The influence of concrete compressive strength, concrete mixture type (conventional concrete or SCC), time, and cross-section size were investigated. Results were also compared to recommended design expressions for predicting transfer lengths.

Several conclusions regarding transfer length resulted from this study:

- Girders cast with higher concrete compressive strengths at transfer had shorter average transfer lengths than girders cast with lower concrete compressive strengths at transfer.

- On average, transfer lengths are proportional to strand stress at transfer and are inversely proportional to concrete strength. The relationship $l_t = \alpha \dfrac{f_{pt}}{\sqrt{f'_{ci}}} d_b$

  proved to effectively describe this trend over a wide range of concrete strengths.

- When normalized against the effects of prestress magnitude and concrete strength, transfer lengths generally tend to decrease with increasing cross-section size. This decrease is more significant at live ends than at dead ends.

- When normalized against the effects of prestress magnitude and concrete strength, the moderate-strength SCC mixture produced transfer lengths 3 percent shorter than the conventional concrete mixture.

- When normalized against the effects of prestress magnitude and concrete strength, the high-strength SCC mixture produced transfer lengths 5 percent longer than the conventional concrete mixture.

- When normalized against the effects of prestress magnitude and concrete strength, there is no significant difference in the transfer lengths of full-scale girders cast with conventional concrete and the transfer lengths of full-scale girders cast with SCC.

- Transfer length increases significantly over time after transfer; therefore, reliable estimates of long-term transfer lengths are difficult to estimate based solely on measurements of initial transfer lengths.

- Transfer lengths increased a total of 38 percent within 3 months after transfer for girders constructed with conventional concrete.

- Transfer lengths increased a total of 28 percent within 3 months after transfer for girders constructed with both moderate- and high-strength SCC.

- The expressions recommended by Levy (2007) for predicting transfer lengths were conservative and portrayed the trends of the data obtained in this study. The expressions proved to effectively reflect the influence of concrete strength.

- The ACI 318-05 12.9 expression for predicting transfer length was conservative for all the data obtained in this study; however it did not portray the trends of the data. This expression does not reflect the influence of concrete strength and becomes less accurate with increasing concrete strengths.

- The ACI 318-05 shear provision expression for predicting transfer length was conservative for all the data except for one transfer length obtained in this study;

however it did not portray the trends of the data. This expression does not reflect the influence of concrete strength and becomes less accurate with increasing concrete strengths.

- The AASHTO LRFD expression for predicting transfer length was conservative for all the data obtained in this study; however it did not portray the trends of the data. This expression does not reflect the influence of concrete strength and becomes less accurate with increasing concrete strengths.

- Although current design provisions for predicting transfer lengths produce conservative results, it is necessary to include a concrete strength parameter in order to predict transfer lengths that portray the trends of data observed across a full range of practical concrete strengths.

CHAPTER 5

DRAW-IN TEST PROGRAM

5.1 INTRODUCTION

A draw-in test program was performed in conjunction with the transfer length test

program described in chapter 4. The objective of this program was to evaluate the

effectiveness of draw-in measurements to predict transfer bond behavior. Strand draw-in,

also known as "free end slip" or "suck-in," is the displacement of the prestressing strand

relative to the end of the girder due to the release of the prestress force. The term draw-in

will be used throughout this thesis in order to prevent confusion with movement of the

strand resulting from the application of external loads, often called "end slip." The draw-

in test procedure, the results, comparisons to the measured transfer lengths from chapter

4, and comparisons to results obtained in previous phases of this project will be presented

and discussed in this chapter.

5.2 BACKGROUND

The theoretical basis for the direct relationship between strand draw-in and transfer

length is thoroughly discussed in Anderson and Anderson (1976) as well as Rose and

Russell (1997). Figure 5-1 illustrates the following derivations and will be referred to

several times for further explanation.
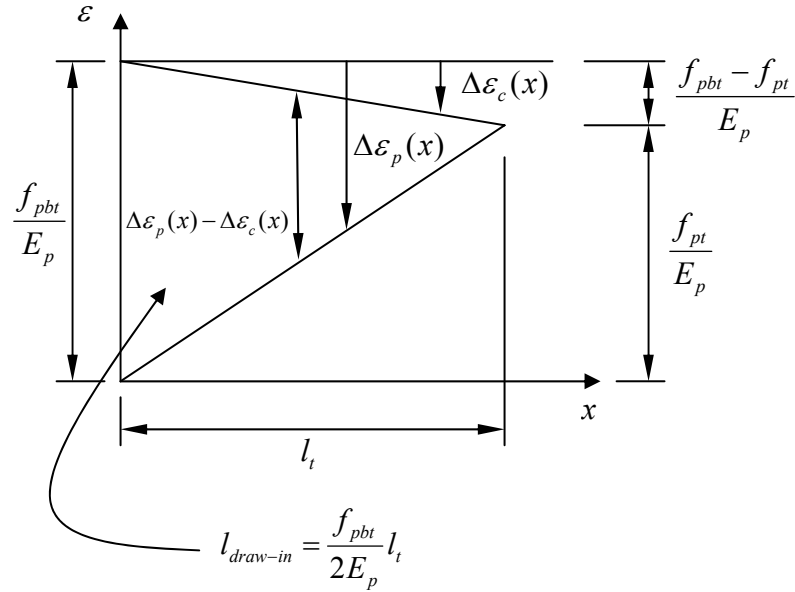
Figure 5-1: Relationship between Draw-In and Transfer Length (Barnes et al. 1999)

Rose and Russell (1997) state that the transfer length of a pretensioned strand can be calculated based on the differences between the concrete and the prestressing strand strains throughout the transfer zone. Theoretically there is no displacement of the steel relative to the concrete at the end of the transfer length; therefore, the initial draw-in length may be calculated as shown in Equation 5-1.

$$l_{draw-in} = \Delta_{pt} - \Delta_{ct} \qquad \textit{Equation 5-1}$$

where, $l_{draw-in}$ = draw-in length

Δ_{pt} = total elastic shortening of the strand along the transfer length

Δ_{ct} = total elastic shortening of the concrete over the transfer length

The values of the total elastic shortening of both the prestressing strand and the concrete can be calculated by integrating the strains that result from the prestress release along the transfer length, l_t. The resulting equation can be seen below.

$$l_{draw-in} = \int_0^{l_t} \left(\Delta\varepsilon_p - \Delta\varepsilon_c \right) dx \qquad\qquad \textbf{\textit{Equation 5-2}}$$

where, $\Delta\varepsilon_p$ = change in steel strain that results from transfer of prestress

                     $\Delta\varepsilon_c$ = change in concrete strain that results from prestress transfer

                     l_t = transfer length

At the free end of the strand, or the "start" of the transfer length (x = 0), $\Delta\varepsilon_c$ is

zero, and the $\Delta\varepsilon_p$ can be taken as $\dfrac{f_{pbt}}{E_p}$ shown in Figure 5-1. At the "end" of the transfer

length (x = l_t), the concrete and steel strains are compatible resulting in the following

relationship, also illustrated in Figure 5-1.

$$\Delta\varepsilon_c = \Delta\varepsilon_p = \frac{\Delta f_p}{E_p} = \frac{f_{pbt} - f_{pt}}{E_p} \qquad\qquad \textbf{\textit{Equation 5-3}}$$

where, Δf_p = decrease in steel stress resulting from transfer of prestress

                     E_p = modulus of elasticity of the prestressing strand

                     f_{pt} = stress in the prestressing strand after transfer

                     f_{pbt} = stress in the prestressing strand immediately prior to transfer

Assuming the concrete and steel strains vary linearly along the transfer length,

Equation 5-2 simplifies to an expression that directly relates draw-in to transfer length:

$$l_{draw-in} = \frac{f_{pbt}}{2E_p} l_t \qquad\qquad \textbf{\textit{Equation 5-4}}$$

The draw-in length of Equation 5-4 is graphically represented as the triangular

area shown in Figure 5-1. Accordingly, the value of the numerical factor (2) in the

denominator of Equation 5-4 is a function of the actual variation of the steel and concrete

strains along the transfer length. If this variation is nonlinear, the value of 2 is not valid.

118

Rearranging Equation 5-4, the transfer length can be estimated based upon
measured draw-in values as indicated in Equation 5-5, which is also only theoretically
valid for linear variations of concrete and steel strain along the transfer length.

$$l_t = \frac{2E_p}{f_{pbt}} l_{draw-in}$$ **Equation 5-5**

Rose and Russell (1997) studied the effectiveness of several proposed bond
performance test methods, including the relationship between transfer length and
measured draw-in values using Equation 5-5. Based on the data from several different
transfer length studies, they reported that actual transfer lengths measured in numerous
test specimens compared very well with predicted transfer lengths from measured draw-
in values.

Barnes et al. (1999) also utilized Equation 5-5 to predict transfer lengths from
measured draw-in values in full-scale bridge girders. On average, the transfer length
values predicted by Equation 5-5 slightly underestimated the actual transfer lengths. It
was concluded that draw-in measurements could be used to indicate overall trends in
bond behavior over a large number of specimens, as well as to indicate gross deficiencies
in bond quality. However, it was difficult to accurately predict *individual* transfer lengths
based on draw-in measurements (Barnes et al. 1999). Similarly, in a previous phase of
this investigation, Swords (2005) reported difficulty in achieving strong correlation
between individual measured transfer lengths and predictions based on draw-in
measurements utilizing Equation 5-5.

5.3 TEST PROCEDURE

Although there are several documented procedures for measuring draw-in data, a single procedure was used for all girder ends in this study. After stripping of the formwork and prior to prestress release, the prestressing strands were spray-painted using masking tape to provide a straight line as shown in Figure 5-2. The resulting lines provided a benchmark for measurements. For each individual strand, a single wire of that strand was chosen and marked. This was to ensure that all measurements were made to a consistent location over time. The distance from the girder end to the spray-painted line was measured with a steel ruler that was graduated in increments of 0.01 in. In order to reduce error, all draw-in measurements were performed by the same researcher and each measurement was taken twice. All measurements were recorded to the nearest 0.01 in.

Prior to prestress release, measurements were taken in order to establish an initial value. Draw-in measurements were then taken again immediately after transfer and at various ages after prestress transfer corresponding to DEMEC measurements of transfer length. The performance of a draw-in measurement is shown in Figure 5-3. The intense shock resulting from the flame-cutting procedure has been known to cause unwrapping of the strand wires and could possibly affect the accuracy of draw-in measurements. Fortunately only one end of each girder set (1E) was affected by this action, as described in chapter 3. The unwrapping of strand wires was mitigated by using hose clamps and duct tape to hold the strand together at the live ends, as shown in Figure 5-3. This procedure proved to be successful.

Figure 5-2: Strand Painted to Provide Benchmarks for Draw-In Measurements

Figure 5-3: Performance of a Strand Draw-In Measurement

5.4 DETERMINATION OF DRAW-IN VALUE

Determination of the draw-in value for each strand, and the corresponding transfer length for each girder end or transfer zone, was a straightforward process. The draw-in values for each time interval were calculated by taking the difference between the measured values before prestress transfer and the measured values at the time of the readings. Additionally, the free contraction of the prestressing strand between the girder end and the measurement benchmark had to be accounted for. This contraction is reflected in the total measured distance change, but it is not part of the actual draw-in along the transfer length. The resulting equation for calculating the draw-in value for each strand is shown below; the final term on the right-hand side represents the free contraction of the strand between the girder end and the measurement mark.

$$l_{draw-in,t} = \Delta_o - \Delta_t - \frac{f_{pbt}}{E_p}\Delta_o \qquad \qquad \textbf{\textit{Equation 5-6}}$$

where, $l_{draw-in,t}$ = draw-in value at time, t

         Δ_o = distance from the benchmark to the end of the girder prior to prestress release

         Δ_t = distance from the benchmark to the end of the girder at time, t

         f_{pbt} = stress in the prestressing strand immediately prior to transfer

         E_p = modulus of elasticity of the prestressing strand

The determination of draw-in values, $l_{draw-in}$, enabled the use of Equation 5-5 shown above to calculate draw-in-predicted transfer lengths for individual girder ends or transfer zones.

5.5 RESULTS AND DISCUSSIONS

As stated previously, draw-in measurements were taken on all girder ends in combination

with the DEMEC transfer length measurements described in Chapter 4 of this thesis. All

values associated with the draw-in measurements were calculated according to the

procedures outlined in the previous section. For comparison purposes, only the initial

and long-term draw-in values will be discussed in this section. Figure 5-4 shows a

representative set of draw-in results (STD-M-2). All other draw-in results are presented

graphically in Appendix G.
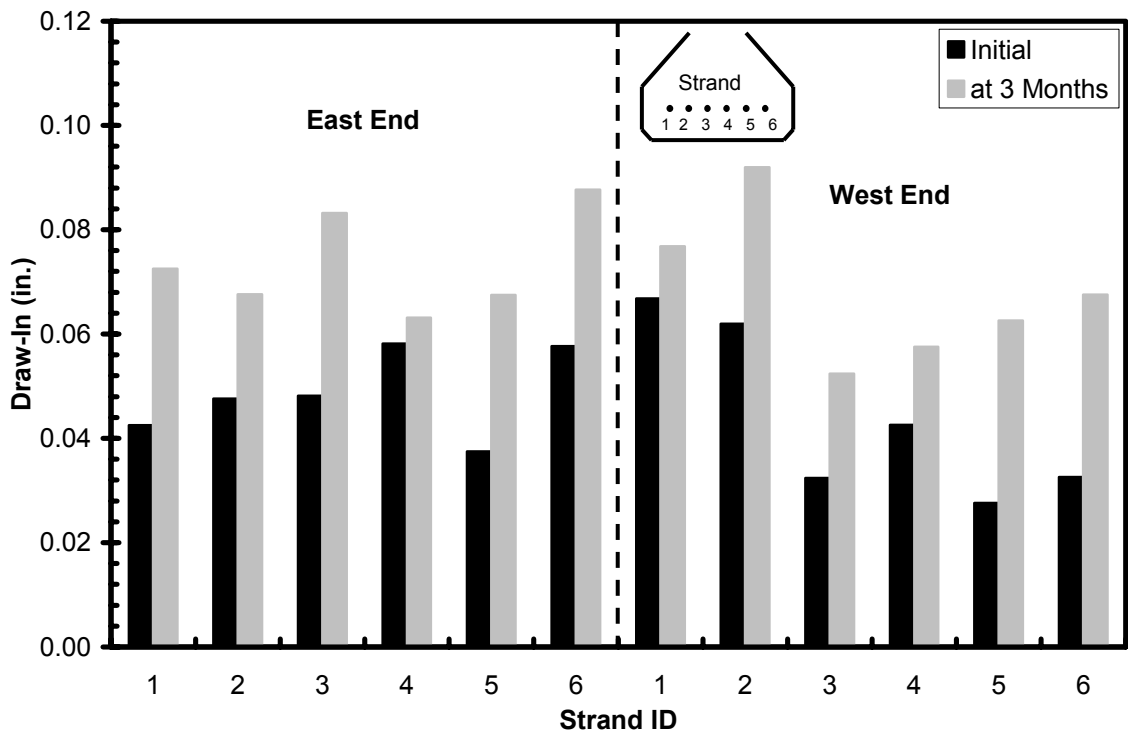
Figure 5-4: Strand Draw-In Results for Girder STD-M-2

Using Equation 5-5, a draw-in-predicted transfer length was calculated for each

girder end based upon the corresponding draw-in, $l_{draw-in}$, value. Comparisons between

the DEMEC-measured transfer lengths and draw-in-predicted transfer lengths were then

made. The modulus of elasticity of the prestressing strand was taken to be 28,900 ksi,

and the stress in the prestressing strand immediately prior to transfer, f_{pbt}, was taken to be

199 ksi. Although each set of girders had slightly different stress values for f_{pbt}, the

differences were minor and a value of 199 ksi represents an average for all girders. Since

the girders used for this study were prestressed with six fully-stressed strands, each girder

end produced six separate draw-in values at each time (initial or long-term). Therefore, it

was unclear which draw-in value should be used with Equation 5-5 to accurately predict

the transfer lengths for a specific girder end. In the comparisons that follow, two

methods were used. The two methods employed were to use (1) the average and (2) the

maximum of the six draw-in values when predicting the transfer length using Equation 5-

5. These two approaches were investigated to determine which one produced the best

correlation with the DEMEC-measured data.

The following six figures illustrate the results of the two approaches mentioned

above to compare the DEMEC-measured transfer lengths with the strand draw-in values.

Different combinations of initial and long-term DEMEC measured transfer lengths were

compared to average and maximum draw-in values at initial and long-term times in order

to produce the best correlation. The dashed line represents the relationship expressed in

Equation 5-5. Using the relevant properties for these girders, the relationship reduces to

$l_t = (290)(l_{draw-in})$ as shown in the figures. Table 5-1 shows a summary of the results from

linear regression analyses of the six different comparisons.
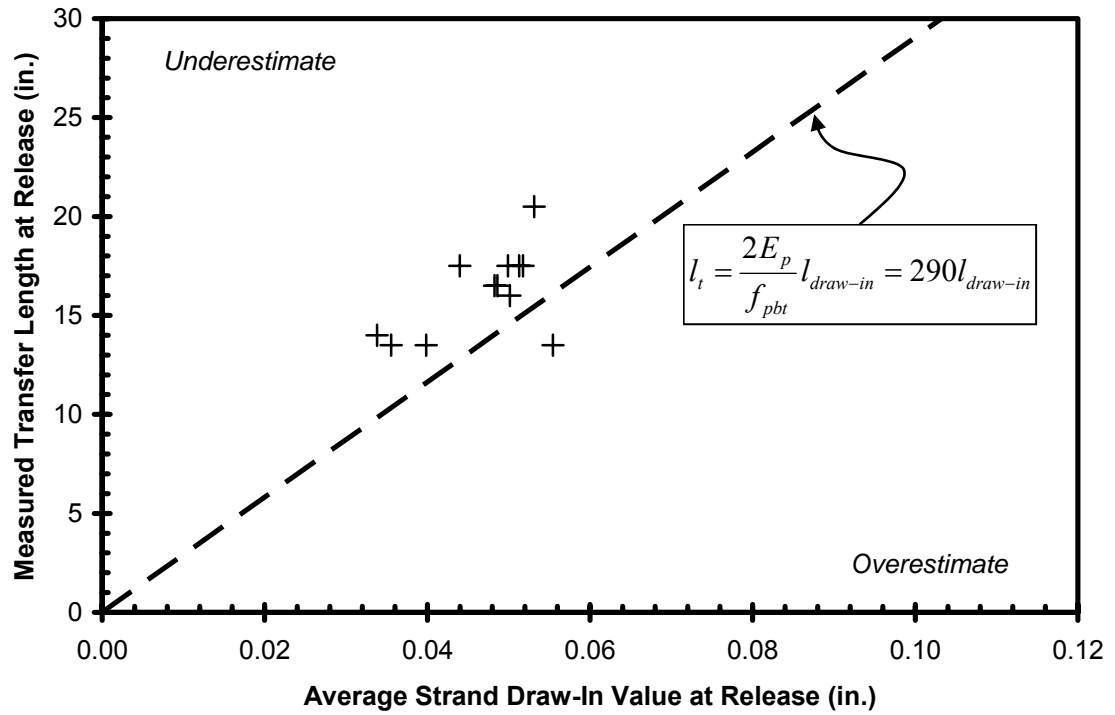
Figure 5-5: Measured Initial Transfer Length vs. Average Initial Draw-In Value
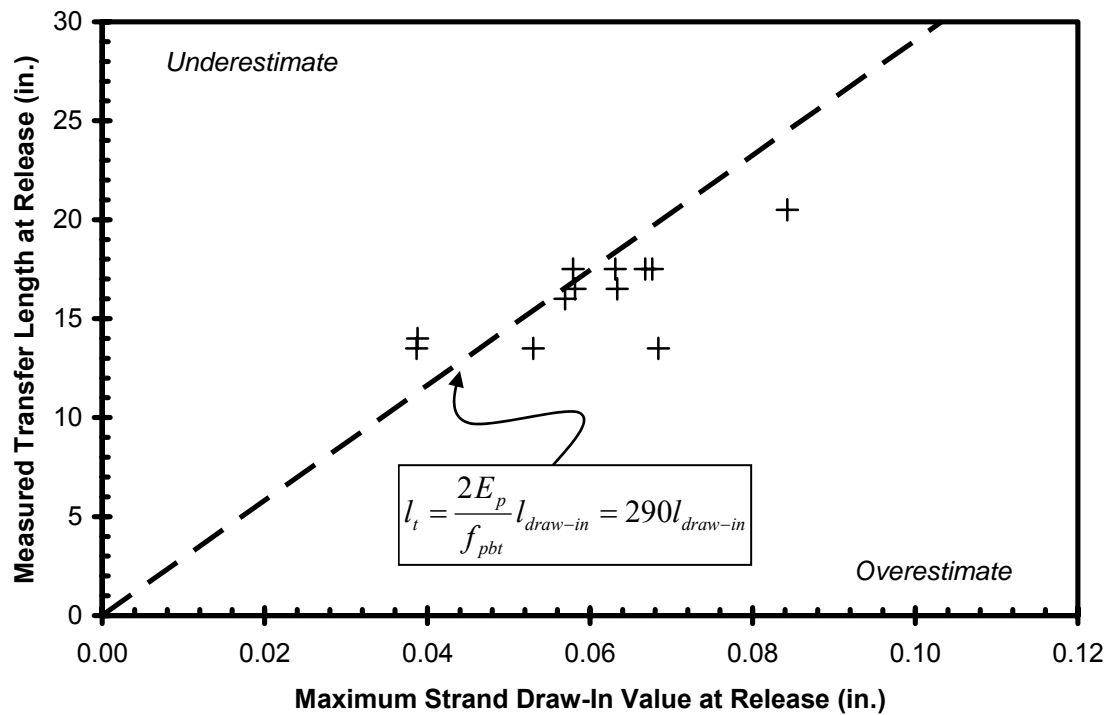
Figure 5-6: Measured Initial Transfer Length vs. Maximum Initial Draw-In Value
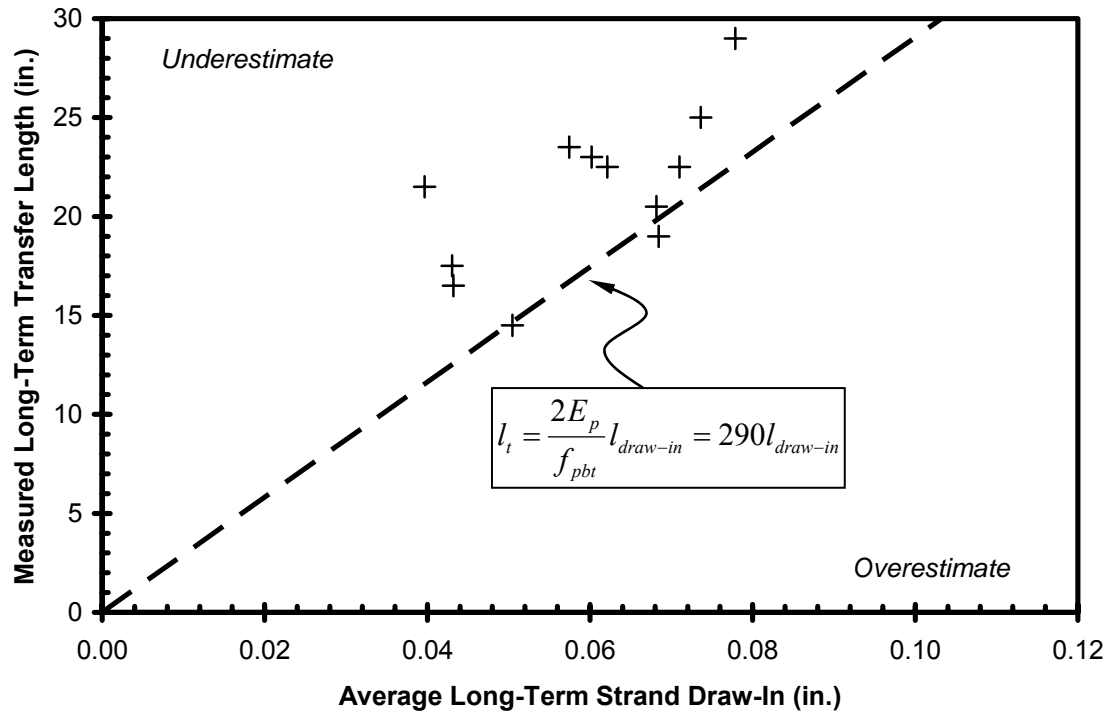
Figure 5-7: Measured Long-Term Transfer Length vs. Average Long-Term Draw-In Value
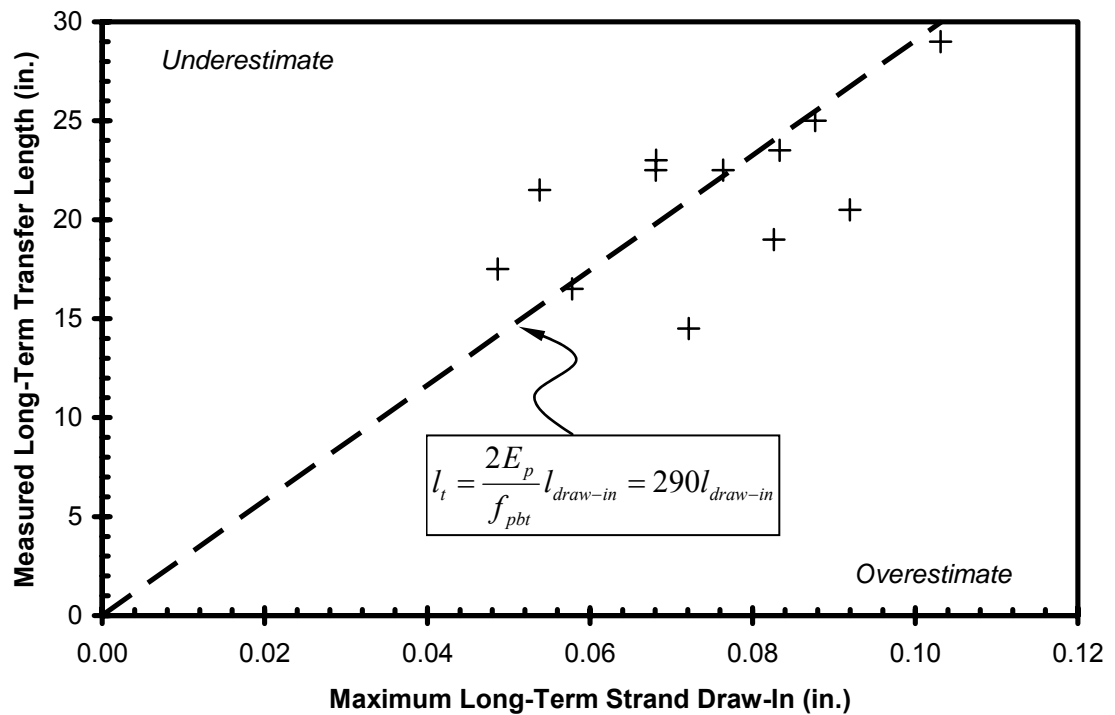
Figure 5-8: Measured Long-Term Transfer Length vs. Maximum Long-Term Draw-In Value

126
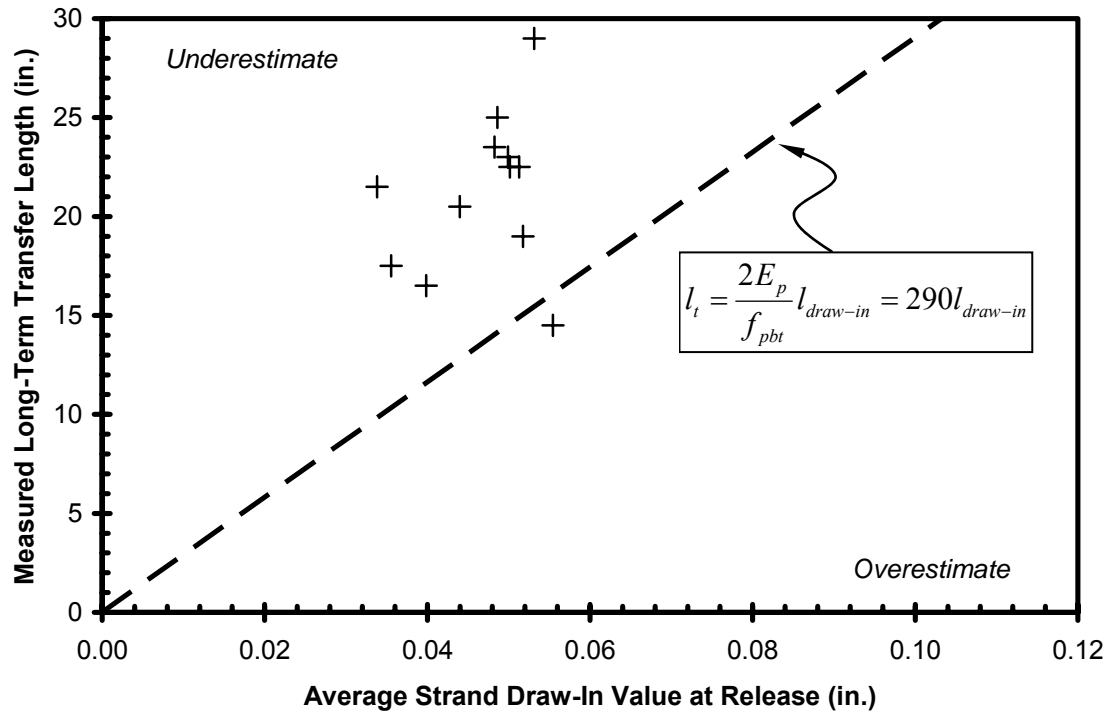
Figure 5-9: Measured Long-Term Transfer Length vs. Average Initial Draw-In Value
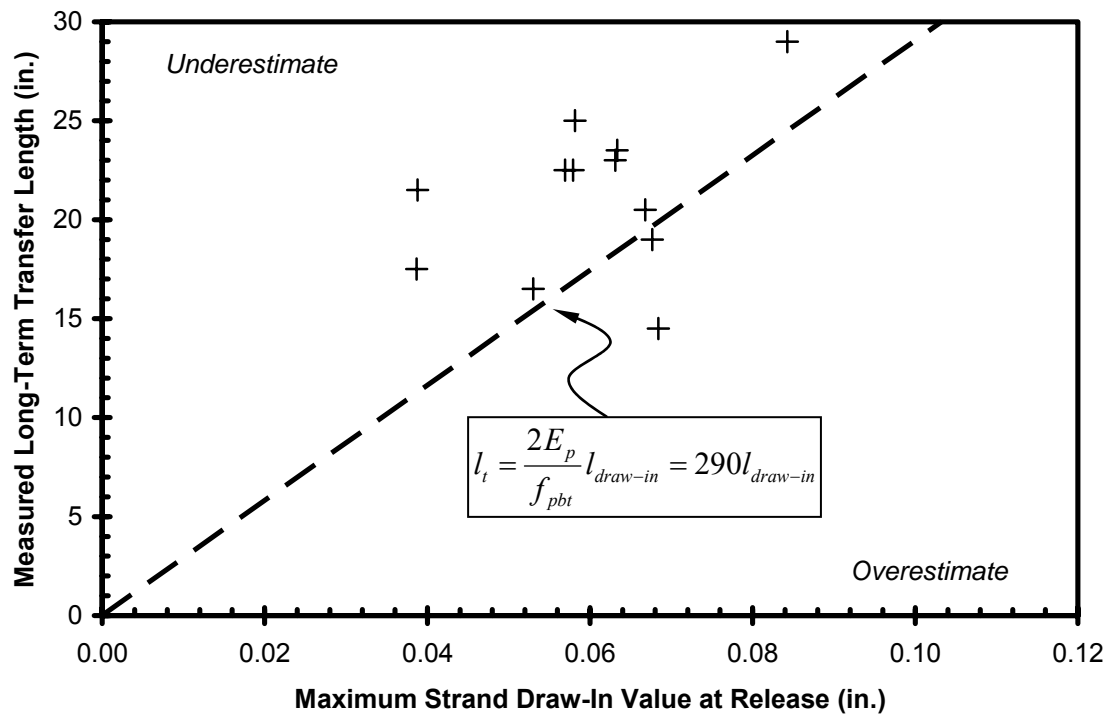
Figure 5-10: Measured Long-Term Transfer Length vs. Maximum Initial Draw-In Value

127

Table 5-1: Results From Linear Regression Analysis for l_t vs. $l_{draw-in}$

Relationship	Proportionality Coefficient	Coefficient of Determination, R^2
$l_{t,initial}$ vs. Average $l_{draw-in,initial}$	342	0.03
$l_{t,initial}$ vs. Maximum $l_{draw-in,initial}$	265	-0.09
$l_{t,long term}$ vs. Average $l_{draw-in,long-term}$	350	0.21
$l_{t,long term}$ vs. Maximum $l_{draw-in,long-term}$	280	0.06
$l_{t,long term}$ vs. Average $l_{draw-in,initial}$	448	-0.22
$l_{t,long term}$ vs. Maximum $l_{draw-in,initial}$	346	-0.37

As Figure 5-5 through Figure 5-10 and Table 5-1 demonstrate, both the average and the maximum draw-in values failed to produce a significant correlation with the measured transfer lengths. This data disagrees with the strong correlation between transfer length and draw-in value reported by Rose and Russell (1997). However, it does agree with the findings of Barnes et al. (1999) and Swords (2005), in which results showed very little reliable proportionality between transfer length and draw-in.

The closest proportionality was obtained between the DEMEC measured long-term transfer lengths and the maximum long-term draw-in value shown in Figure 5-8. As seen in Table 5-1, the coefficient of determination, R^2, and proportionality coefficient for this comparison were 0.06 and 280, respectively. This proportionality coefficient is significantly closer to the theoretical coefficient of 290 than any other comparison, and the correlation value is the second highest.

The following six figures, Figure 5-11 through Figure 5-16, compare the draw-in-predicted transfer lengths, l'_t, based upon Equation 5-5 to the corresponding DEMEC-measured transfer lengths, l_t. The same comparisons between initial and long-term readings as well as average and maximum draw-in values as shown in Figure 5-5 through Figure 5-10 are shown. However, these figures distinguish between the three different

concrete mixtures used for the girders in this study in an effort to draw conclusions about the correlation between draw-in and transfer length based upon concrete mixture. The dashed line intersecting the origin represents the line of equality between the draw-in predicted transfer lengths and the DEMEC measured transfer lengths. Therefore, datapoints falling below the line of equality represent measured transfer lengths longer than predicted from draw-in values, i.e., Equation 5-5 underestimates the measured transfer length for those points. Similarly, data points above the line of equality represent an overestimation by Equation 5-5, as noted on the figures.
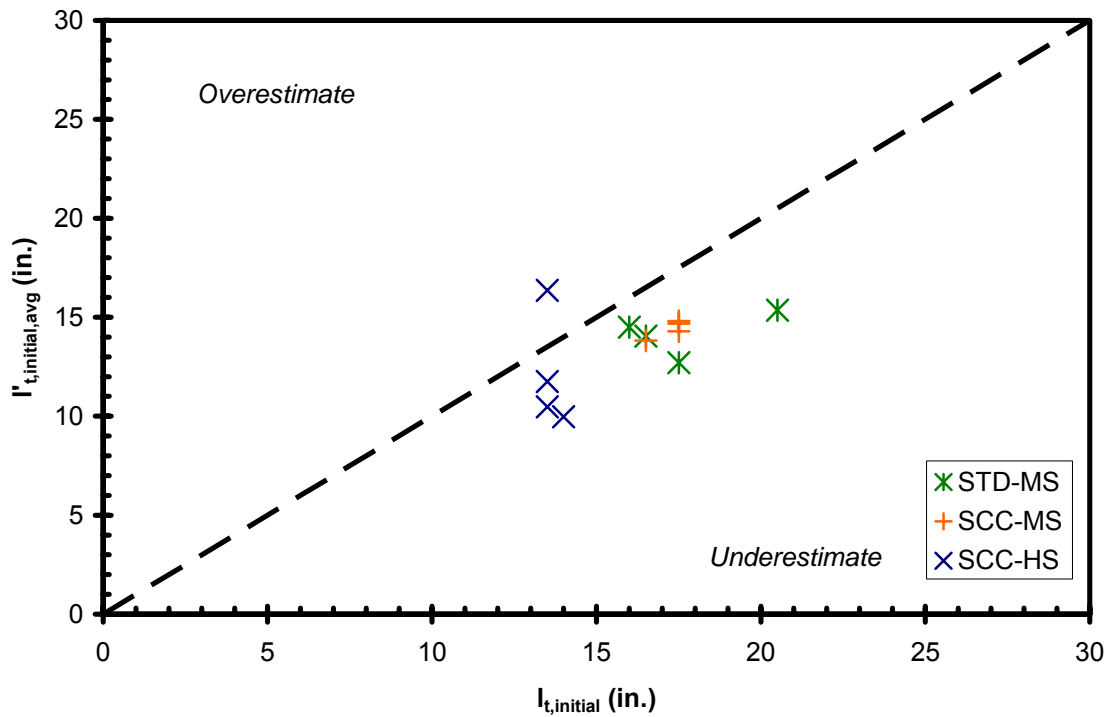
Figure 5-11: Predicted Transfer Length Calculated From Average Initial Draw-In vs. Measured Initial Transfer Length
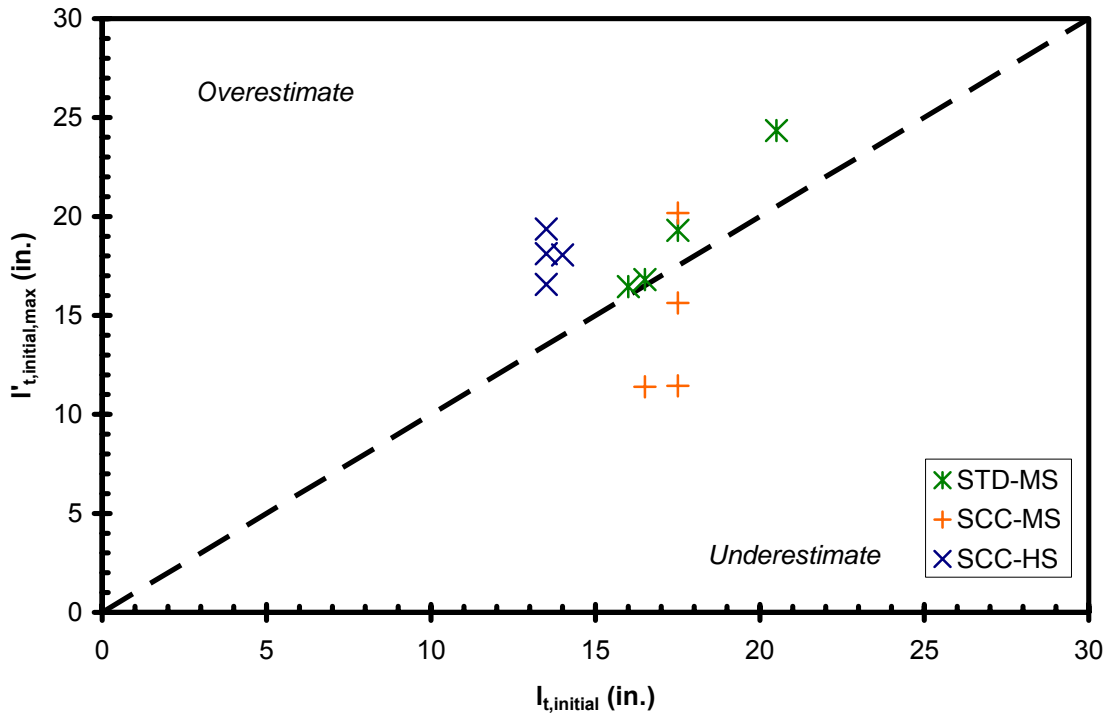
Figure 5-12: Predicted Transfer Length Calculated From Maximum Initial Draw-In vs. Measured Initial Transfer Length
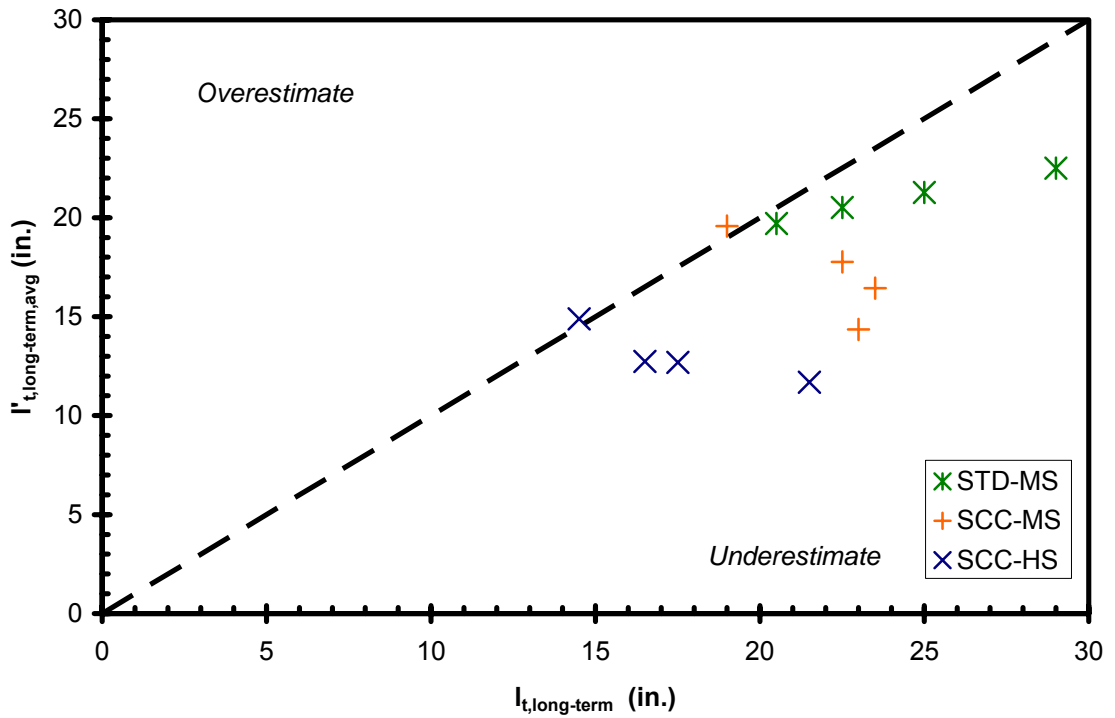
Figure 5-13: Predicted Transfer Length Calculated From Average Long-Term Draw-In vs. Measured Long-Term Transfer Length
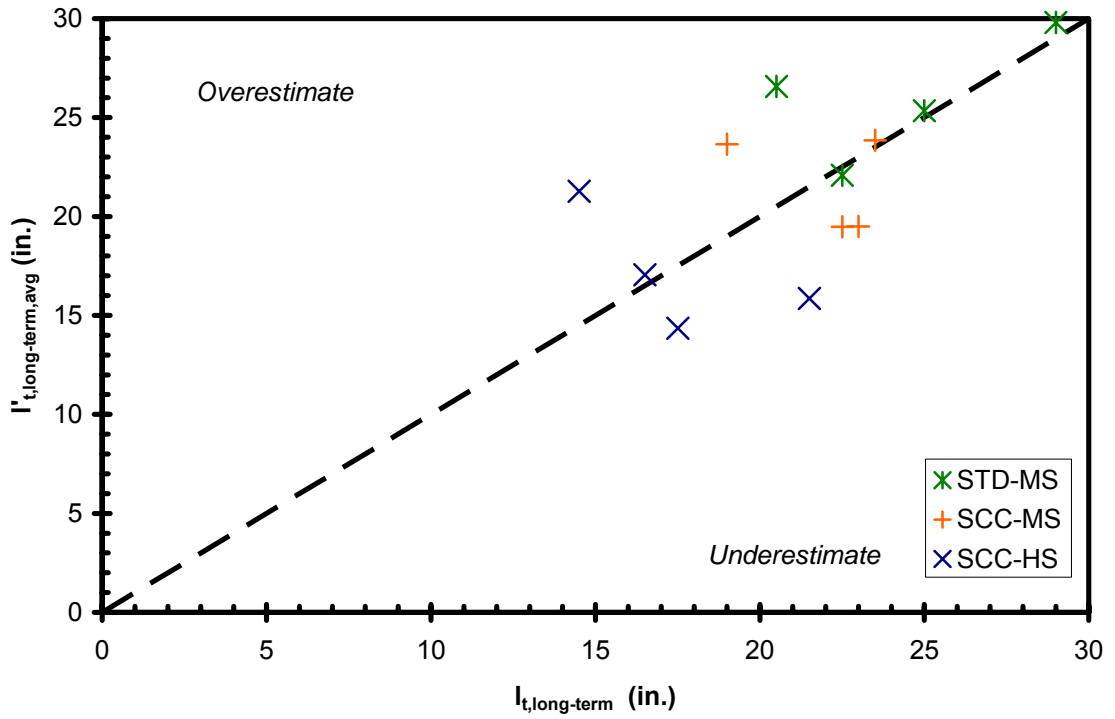
Figure 5-14: Predicted Transfer Length Calculated From Maximum Long-Term Draw-In vs. Measured Long-Term Transfer Length
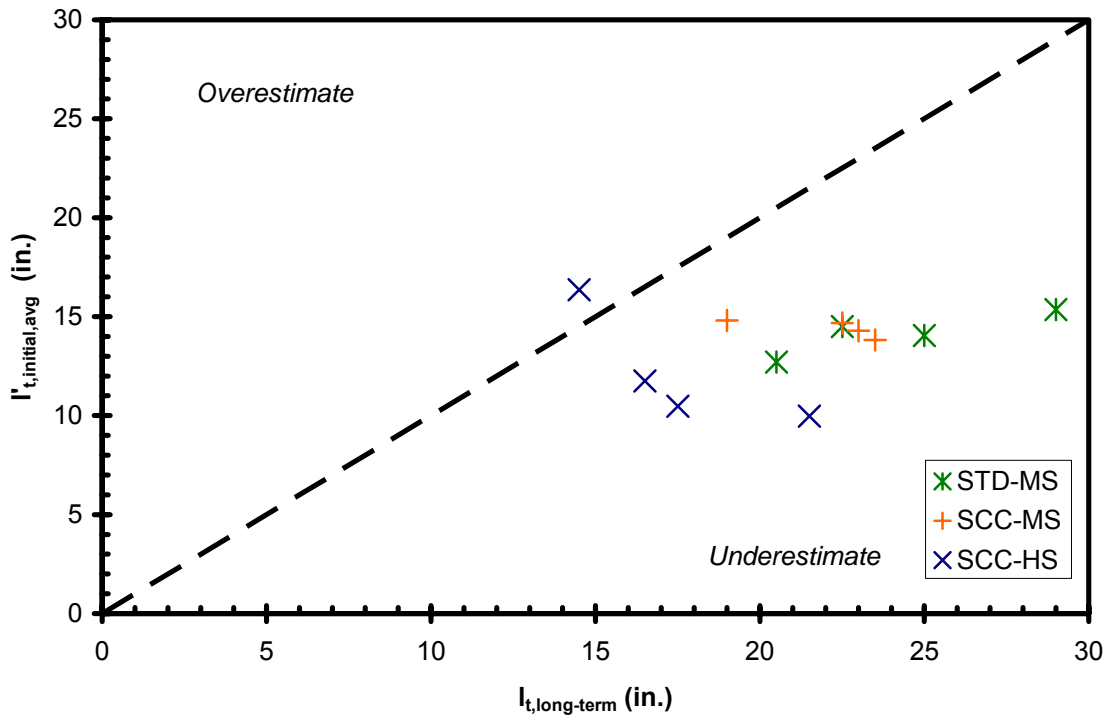
Figure 5-15: Predicted Transfer Length Calculated From Average Initial Draw-In vs. Measured Long-Term Transfer Length

131

Overestimate

$l'_{t,initial,max}$ (in.)

30

25

20

15

10

5

0

0   5   10   15   20   25   30

$l_{t,long-term}$ (in.)

Underestimate

STD-MS
SCC-MS
SCC-HS
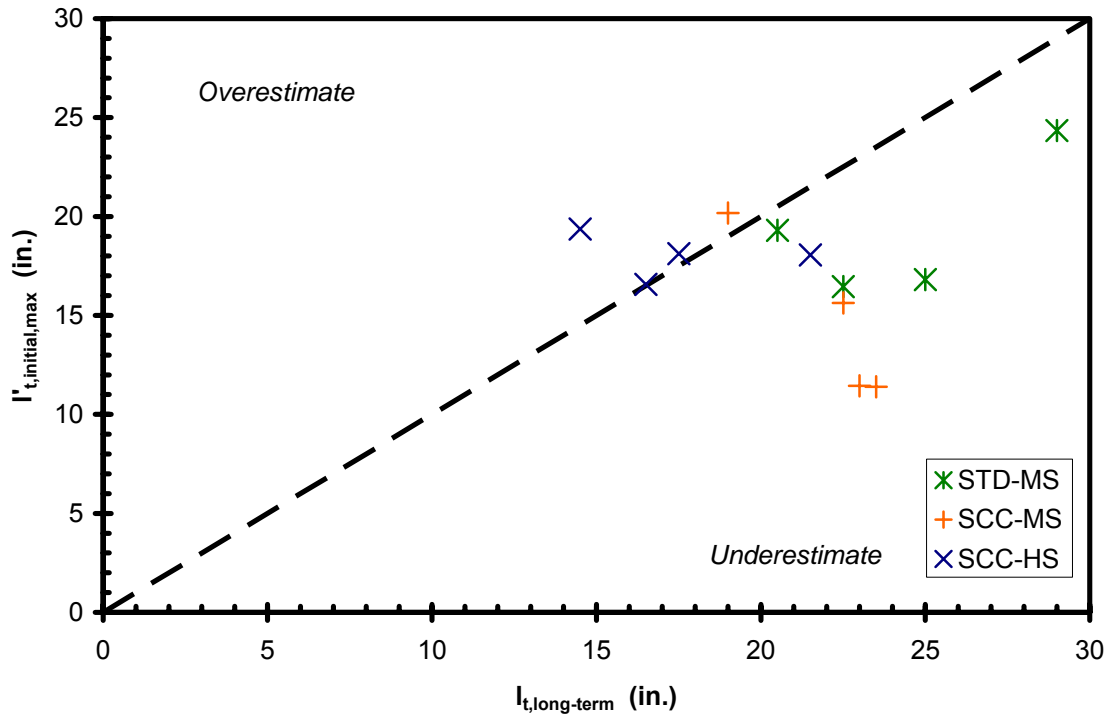
Figure 5-16: Predicted Transfer Length Calculated From Maximum Initial Draw-In vs. Measured Long-Term Transfer Length

As shown in Figure 5-12 and Figure 5-14, it can be seen that using the maximum value of strand draw-in with Equation 5-5 results in an overestimation of the transfer length at corresponding time periods. Similarly, the average value of strand draw-in typically results in an underestimation. This suggests that using a draw-in value between the average and maximum of all the strands would provide a more accurate prediction. Barnes et al. (1999) reported similar findings, citing that the transfer length obtained for a group of strands should lie between the average transfer length of the individual strands and the transfer length of the worst-performing strand.

As for findings concerning the ability of strand draw-in values to accurately predict transfer lengths for the different concrete mixtures used in this study, no obvious trends were apparent.   Swords (2005) reported a similar conclusion; however, he did

132

notice slightly greater correlations with the SCC as compared to the conventional concrete. That does not appear to be evident in the data obtained from this study. However, it is important to note that the sample size for this study was relatively small, which may have resulted in difficulty obtaining significant correlations concerning different types of concrete.

The ability of initial strand draw-in to accurately predict long-term transfer lengths is reflected in Figure 5-15 and Figure 5-16. This comparison was chosen due to the fact that it has been proposed to use initial strand draw-in as a quality control measure for precast, prestressed operations. It would not be feasible for a precast, prestressed plant to store products long enough to perform long-term measurements. Therefore, it has been suggested that initial draw-in measurements may be able to correlate to long-term transfer lengths, which are ultimately the concern of a designer once the prestressed member gets put into service.

Both Figure 5-15 and Figure 5-16 suggest underestimation of actual long-term transfer lengths using initial strand draw-in values. However, using the maximum strand draw-in value rather than the average does appear to provide slightly better results. Once again it is important to note that all correlations were considered to be poor, and this method would not be recommended for use as a quality control measure in the field based upon this study. On the other hand, due to the relatively small sample size of this study, it is recommended that further investigations be conducted into the ability of initial strand draw-in measurements to accurately predict long-term transfer lengths.

5.6 SUMMARY AND CONCLUSIONS

Draw-in testing was performed in conjunction with transfer length testing on all six AASHTO Type I girders. The purpose was to determine if any proportionality existed between strand draw-in values and DEMEC measured transfer lengths. The ability of strand draw-in values to accurately predict transfer lengths, using the expression

$l'_t = \dfrac{2E_p}{f_{pbt}} l_{draw-in}$, was evaluated. Strand draw-in values were determined for all

prestressing strands, resulting in six values for each girder end or transfer zone. Comparisons to the measured transfer length for each transfer zone were made using both the average and the maximum of the six draw-in values. In conjunction, comparisons between initial and long-term readings were also investigated, in an attempt to produce significant correlations. The results were analyzed and compared to previous findings.

Several conclusions regarding strand draw-in were reached for this study:

- Little reliable proportionality existed between the DEMEC-measured transfer lengths and strand draw-in values.

- Equation 5-5 failed to reliably predict transfer lengths comparable to DEMEC-measured transfer lengths.

- The closest proportionality of the data obtained in this study existed between the long-term DEMEC-measured transfer lengths and the long-term draw-in values.

- The use of the maximum strand draw-in value for a group of strands results in an overestimation of the measured transfer length when using Equation 5-5.

- The use of the average strand draw-in value for a group of strands results in an underestimation of the measured transfer length when using Equation 5-5.

- Variation in concrete mixture type (conventional concrete or SCC) failed to produce significantly different results when predicting transfer lengths from draw-in values.

- In general, there was no evident link between initial draw-in values and long-term DEMEC-measured transfer lengths.

- Due to the relatively small sample size and inconsistent correlations of the data collected in this study, it is not recommended that strand draw-in be used as a quality control measure for precast, prestressed operations.

CHAPTER 6

FLEXURAL TEST PROGRAM

6.1 INTRODUCTION

The flexural test program consisted of flexural tests performed on all six AASHTO Type I girders. Each girder end was tested separately, as discussed in more detail later in this chapter, resulting in a total of twelve flexural tests. After the cast-in-place decks were added to each pair of girders, preparation for flexural testing commenced. All girders were at least three months old prior to flexural testing. This chapter includes flexural test configurations and instrumentation, procedures, results, and conclusions.

6.2 TEST APPROACH

The flexural test program was organized in a manner that tested upper and lower bounds of the relevant code-predicted development length for the girders used in this study. As described in Section 2.2.3, the development length is the bonded strand length required to develop the full resistance of the strand, f_{ps}, at the nominal strength of the member. The development length of a particular member cannot be quantified directly from a single experiment; as a result, a more indirect approach was employed.

Using the relevant AASHTO LRFD code provisions described in Section 2.3.3, the development length for the girders used in this study was estimated based on values of 270 ksi, 180 ksi, and 0.515 in. for f_{ps}, f_{pe}, and d_b, respectively. This estimated

development length was then used to select several different embedment lengths for flexural testing. Embedment length, l_e, as described in Section 2.2.4, is the bonded length of the strand from the beginning of bond to the cross section for which strength capacity is being assessed. If the embedment length provided during a flexural test is shorter than the actual development length of that particular member, a bond failure will occur before the critical section can develop its full flexural capacity. As a result, whether or not the actual development length is longer or shorter than the provided embedment length can be assessed by the ultimate bending moment resisted at the critical section and the behavior of the strands during loading.

Each flexural test consisted of loading the girder to failure near one end. The resulting failure type indicated whether the bonded length of the strand (embedment length) was adequate to fully develop the steel stress, f_{ps}, necessary to achieve full flexural strength of the member at the critical cross section. If so, the provided embedment length exceeded the actual development length. Three distinct failure modes were possible: flexural, flexural with moderate strand slip, and bond failure. A failure due to strand slip or bond failure would indicate that the provided embedment length was shorter than the development length of the member. Because all girders were designed to have adequate shear (diagonal-tension) capacity according to AASHTO LRFD provisions, a shear failure in any test would indicate a lack of conservatism of these design provisions for the specimen tested.

Three different embedment lengths were chosen for the flexural testing of the girders in this study. As described previously, two girders were cast from each concrete mixture, resulting in four girder ends to be tested for each mixture (STD-M, STD-MS,

137

and STD-HS). The three embedment lengths were assigned to particular girder ends as shown in Table 6-1. It can be seen that one girder end in each set had an embedment length slightly longer than the AASHTO LRFD code-predicted development length, whereas the other three girder ends had significantly shorter embedment lengths. Two girder ends (2W and 2E) had the same embedment length; however, the shear reinforcement differed significantly between these two ends. As explained in Section 3.1.1, the 2E girder end had approximately the amount of shear reinforcement required to provide adequate shear strength during the test (AASHTO LRFD). There was significantly more shear reinforcement in the 2W girder end—matching the standard ALDOT design for a Type I girder. The tested embedment lengths were varied by utilizing different testing configurations, described in detail in Section 6.3 of this chapter.

Table 6-1: Girder End Development and Embedment Lengths

Girder End	Estimated AASHTO LRFD Development Length (in.)	Embedment Length (in.)
1W	124	135
1E	124	85
2W	124	65
2E	124	65

6.3 TEST CONFIGURATION

Initially, three different testing configurations, one for each embedment length, were chosen for the flexural testing of each set of girders. The primary variables for each configuration consisted of the embedment length and the span length. Each girder end, i.e. 1W, 1E, 2W, and 2E, was designated a particular configuration. However, midway through the testing of girder end SCC-HS-1E, it was realized that one support was

positioned incorrectly. This error, which was corrected prior to final loading of SCC-HS-

1E, will be explained in more detail later in this chapter. As a result, a total of four

different testing configurations were used during the flexural testing of this study. The

configurations were chosen so that the girder end not under investigation was free from

the direct effects of the applied load. In order to maximize flexural behavior in one test

of each set, the 1W test configuration incorporated the full girder in the tested span

length. Conversely, the other three configurations utilized a reduced span length by

cantilevering a portion of the girder. This cantilever portion was effectively free from the

applied load effects, thereby limiting unwanted damage. Flexural testing configurations

for each girder end can be seen in Figures 6-1, 6-2, and 6-3.
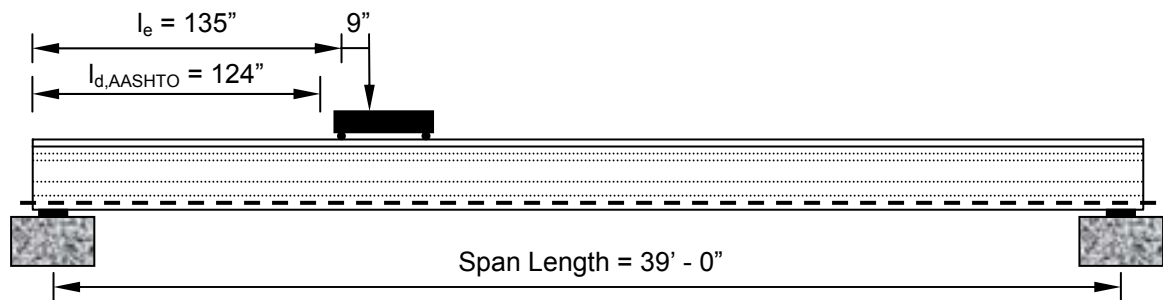
Figure 6-1: Flexural Testing Configuration for Girder End 1W (l_e = 135 in.)
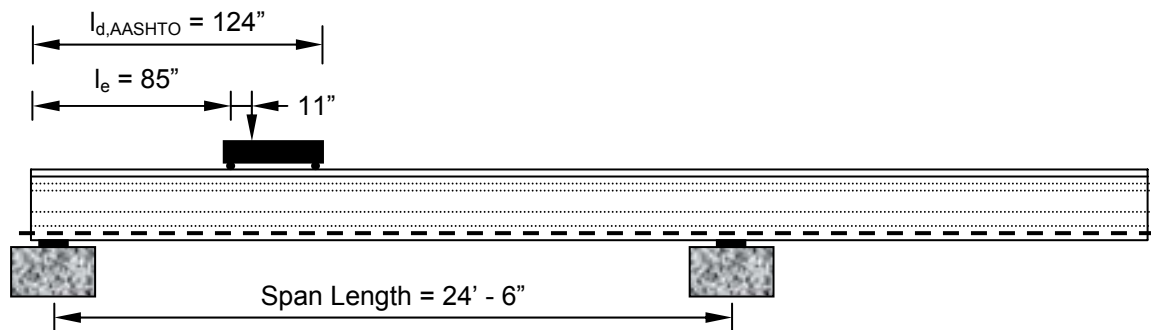
Figure 6-2: Flexural Testing Configuration for Girder End 1E (l_e = 85 in.)
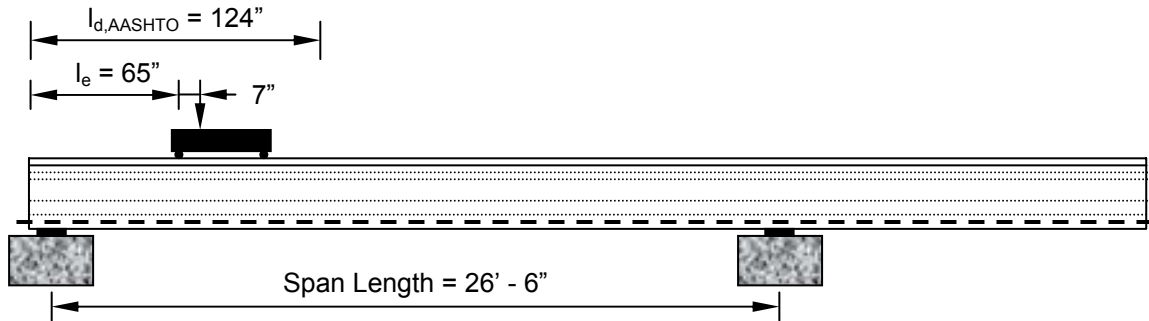
Figure 6-3: Flexural Testing Configuration for Girder End 2W and 2E (l_e = 65 in.)

The girders were directly supported on reinforced, elastomeric bridge bearing pads of 1 ¼ in. thickness. Each bearing pad was 9 in. by 14.5 in. in plan, and matched the ALDOT standard specifications for elastomeric bearing pads at the discontinuous supports of an AASHTO Type I girder. In each flexural test, the center of one bearing pad was located 6 in. from the girder end under investigation; the other bearing pad was positioned to provide the desired span length for the test configuration. The pads were supported by reinforced concrete pedestals designed to safely distribute the girder reaction forces to the laboratory floor.

Flexural loading was applied by piston displacement of a hydraulic cylinder attached to a movable loading frame as shown in Figure 6-4. Hydraulic power was provided using an air-powered pump. The load was transferred from the hydraulic cylinder to a spreader beam resting on steel rollers and plates mounted to the deck of the girder. The steel rollers were located 36 in. apart in the direction of the span. The hydraulic ram was positioned along the spreader beam so as to produce a region of nearly constant moment in the test girder between the two load points (rollers). Self-weight moments and restricted positioning of the loading frame as a whole prevented attainment

140

of a perfectly constant moment in this region. Location of the hydraulic cylinder relative to the load points for each configuration is depicted in Figures 6-1, 6-2, and 6-3.

Figure 6-4: Loading Frame, Hydraulic Cylinder, and Load Application Components

6.4 INSTRUMENTATION

During flexural testing, several instruments were used to monitor the performance and response of each girder to the applied loads. This section provides a description of each instrument used and its purpose.

6.4.1 Measurement of Applied Load

The applied load was measured via a 300-kip shear-type load cell mounted between the hydraulic cylinder and the cross member of the loading frame as shown in Figure 6-4. Prior to flexural testing, the load cell was calibrated over its full scale. The applied load readings obtained from the load cell were used to create load-deflection curves and to calculate sectional shears and bending moments.

6.4.2 Measurement of Displacements

All girder displacements during flexural testing were measured with linear displacement potentiometers. These linear potentiometers were used to measure the displacements of the girder relative to the floor. Potentiometers were positioned underneath the two load points, in the middle of the load points, and underneath the deck overhang on each face at each support. This resulted in a total of seven potentiometers. The latter potentiometers were used to measure vertical support displacements, as well as to monitor any possible rocking of the girder. In order to eliminate inaccurate readings due to surface imperfections, 1 in. x 1 in. glass microscope slides were glued to the surface of the girders at each potentiometer point of contact. The readings obtained from these potentiometers were used to calculate deflections midway between the two load points relative to a straight line connecting the supported girder sections. Unless otherwise noted, displacements reported in this thesis represent these calculated deflections. Figures 6-5 and 6-6 depict the placement and use of linear potentiometers to measure displacements.

Figure 6-5: Linear Potentiometers Used to Monitor Beam Deflections
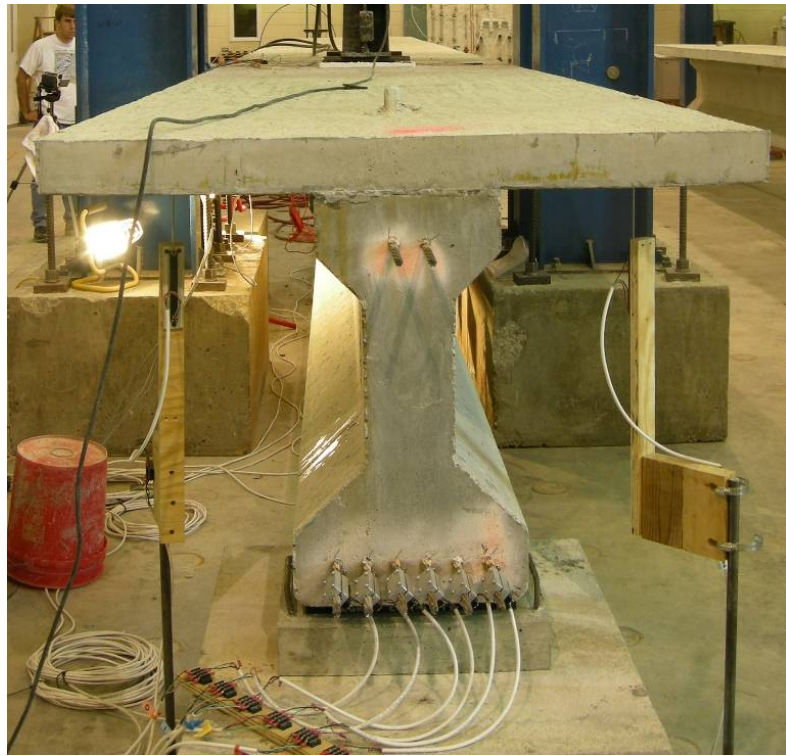
Figure 6-6: Linear Potentiometers Used to Measure Support Deflections

143

6.4.3 Measurement of Strand Slip

Strand slip during flexural testing was also measured with linear displacement potentiometers. These linear potentiometers were attached via brackets to each strand at the girder end being tested as shown in Figure 6-7. The tips of the potentiometers were positioned against concrete girder end face using 1 in. by 1 in. glass microscope slides as before. As a result, if slip occurred, the slip of the strands into the concrete would be registered during flexural loadings. All strand slips were measured relative to the end of the beam.
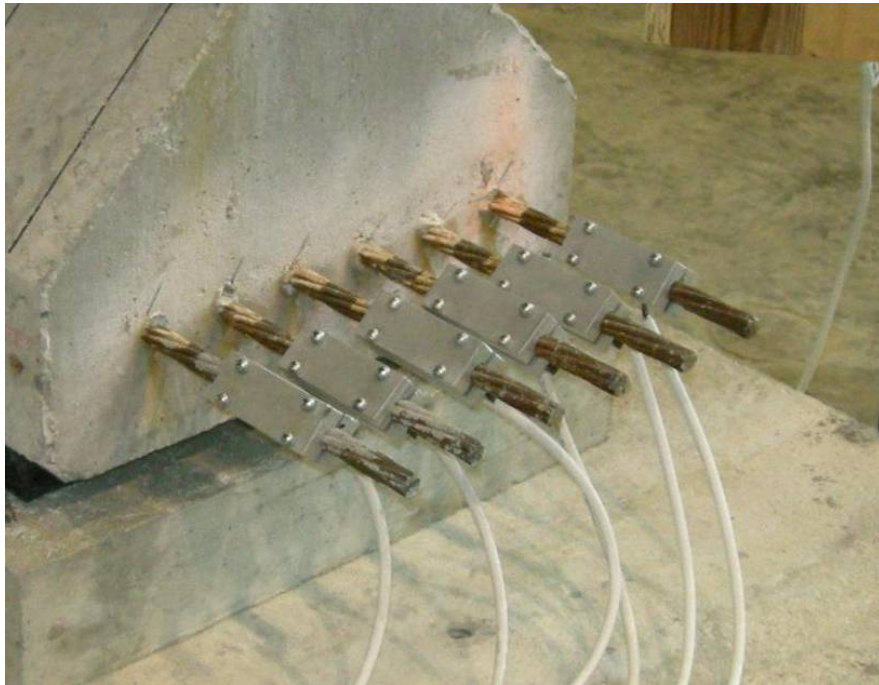
Figure 6-7: Linear Potentiometers used to Measure Strand Slip

6.4.4 Measurement of Strains at Extreme Compression Fiber

Concrete compressive strains at the deck surface during flexural testing were monitored using electrical-resistance strain gauges (ERSGs) with a gauge length of 60 mm. Four ERSGs were bonded to the top surface of the deck within the maximum moment region

for each test. Two gauges were located along the centerline of the girder and two were placed on the deck overhang 6 in. from the edge. The placement longitudinally within the maximum moment region varied based upon the location of stirrups. An attempt was made to locate the strain gauges at critical cross sections containing stirrups in anticipation that flexural cracking would occur at these sections. The readings obtained from these ERSGs were used to anticipate the onset of deck concrete crushing prior to failure. Figure 6-8 illustrates the use of ERSGs to measure strains at the extreme compression fiber.

Figure 6-8: Strain Gauges Used to Measure Extreme Compression Fiber Strains

6.4.5 Data Acquisition

During flexural testing, all instrumentation signals were recorded at 0.2-sec intervals by an Optim MEGADAC Data Acquisition/Signal Conditioning Unit. The data was then transferred to a laptop computer for storage. At critical times during flexural testing,

applied loads, deflections, deck compressive strains, crack widths, and significant slips were recorded by hand in a test log as a backup.

6.5 TEST PROCEDURE

All flexural tests followed a general procedure regardless of support locations or girder end. Prior to the start of each test, the girder end was subjected to several insignificant load cycles in order to confirm that all instrumentation was functioning properly. Once it was determined that all instruments were operating correctly, the sensors were zeroed and the first load was applied. Loading consisted of cyclic loading; after a predetermined load/event was achieved, the applied load was reduced to zero before applying load again. Figure 6-9 below represents the general load levels or cyclic loading scheme utilized for each flexural test.
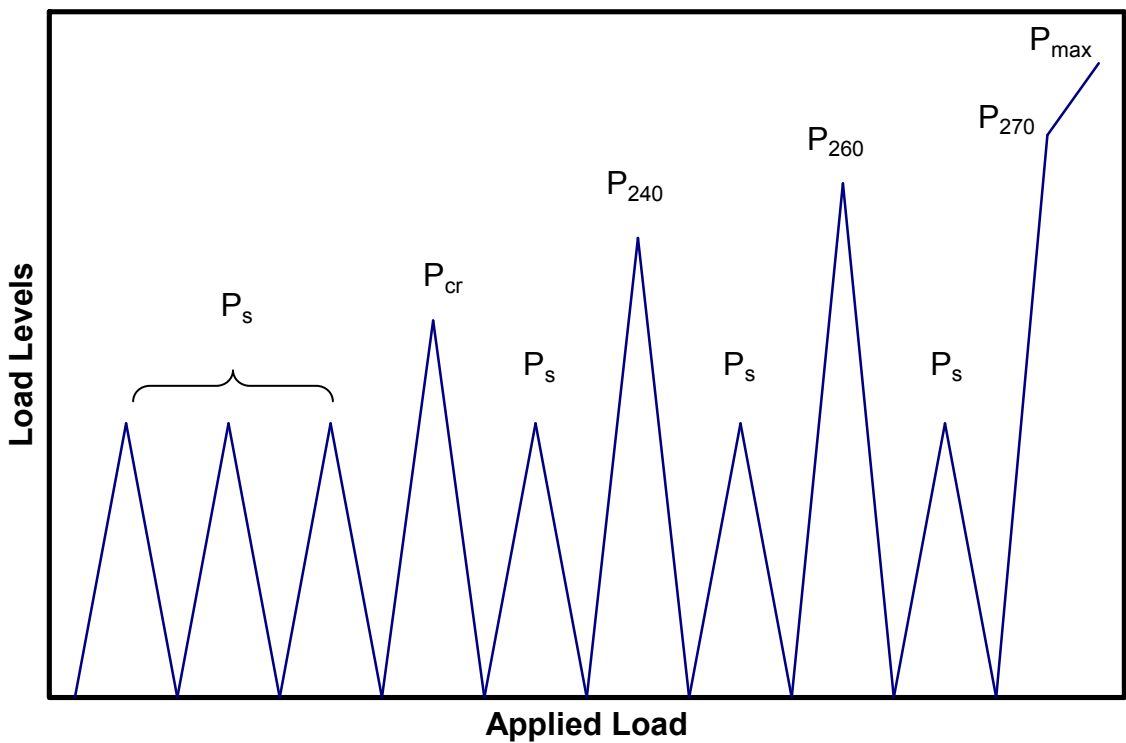
Figure 6-9: Levels of Applied Loading

The maximum load for the first three load cycles, P_s, was approximately equal to the service-level design load for Alabama Department of Transportation (ALDOT) bridge girders. This load represented the applied load necessary to cause zero net stress in the bottom fiber of the girder concrete at the critical (maximum-moment) sections. After each cycle to loads greater than P_s, a single service-load cycle was applied to assess the service-load response after varying levels of damage had occurred.

The next load level applied after first the three P_s cycles was the flexural cracking load, P_{cr}. Assuming that cracking would coincide with a bottom-fiber tensile stress equal to $7.5\sqrt{f'_c}$, an estimated cracking load was calculated. However, the exact cracking load was unknown; therefore, the applied load was steadily increased until cracking occurred. Cracking was signaled by a slight drop in the load accompanied by visible cracking; this was verified by observation of the load-displacement relationship. After this and all subsequent load levels were reached, the load was held, cracks were marked with felt-tip markers, crack widths were measured, and crack patterns were photographed before releasing the load. Measurements from various instruments were also recorded manually as a backup at each load level.

The next two higher load levels applied after cracking corresponded to a calculated stress in the prestressing strands, f_p, of 240 ksi and 260 ksi, respectively. The first load, P_{240}, was select to represent a load just less than that corresponding to yielding of the prestressed strands in the maximum moment region. The 260-ksi load, P_{260}, was selected to represent a post-yielding load less than the nominal strength of the girder. At each of these load levels, the displacement was held during crack documentation, and then the applied load was removed before applying a single service-load cycle again.

The final loading cycle consisted of loading the girder up to a load corresponding to 270 ksi, the nominal strand tensile strength, in the bottom strands. Because the girders were designed to achieve large strand elongations at failure, this level of applied load roughly corresponds to the nominal flexural capacity. After the cracking was documented at this load level, the applied loading was increased until failure or the testing was ceased. Failure was usually indicated by strand rupture or crushing of the deck concrete. In some cases, it was judged by the researchers that further displacement would generate no useful information while jeopardizing the girder usefulness for further testing; therefore testing was ceased. Table 6-2 below presents the specific applied loads for each tested girder end.

Table 6-2: Applied Loads

Test Girder	P_s (kips)	P_{cr} (kips)	P_{240} (kips)	P_{260} (kips)	P_{270} (kips)	P_{max} (kips)
STD-M-1W	40	52	61	69	76	80
STD-M-1E	75	100	115	128	140	159
STD-M-2E	83	116	133	149	164	191
STD-M-2W	83	114	133	149	164	189
SCC-MS-1W	40	51	62	70	75	80
SCC-MS-1E	75	97	115	128	140	152
SCC-MS-2E	83	110	134	149	164	183
SCC-MS-2W	83	111	134	149	164	188
SCC-HS-1W	40	52	62	69	75	81
SCC-HS-1E	75	91	115	127	138	148
SCC-HS-2E	84	113	134	149	164	181
SCC-HS-2W	84	111	134	149	164	188

6.6 ANALYSIS PROCEDURES

Two different analysis procedures were utilized for the flexural tests performed in this study. The first procedure was based upon the recommendations of the relevant AASHTO LRFD code provisions. This analysis resulted in a nominal moment capacity, $M_{n,AASHTO}$, for each flexural test, along with a corresponding strand stress at nominal moment capacity, $f_{ps,AASHTO}$. The second analysis procedure employed was based upon strain compatibility and nonlinear material properties. Similar results including $M_{n,calc}$ and $f_{ps,calc}$ values for each flexural test resulted from this analysis.

6.6.1 AASHTO LRFD Provisions

The relevant AASHTO LRFD provisions can be found in Articles 5.7.3.1 and 5.7.3.2. These provisions provide equations used to calculate $f_{ps,AASHTO}$ and $M_{n,AASHTO}$ values based upon an estimate of the neutral axis location at nominal moment capacity. However, these equations fail to account for the lightly prestressed tendons located in the tops of the girders used for this study. Also, the longitudinal deck reinforcement was estimated to be in tension when subjected to $M_{n,AASHTO}$, but not necessarily beyond the yield strength. As a result, per recommendations found in the AASHTO LRFD commentary, a method based upon conditions of equilibrium and strain compatibility was used to determine $f_{ps,AASHTO}$ and $M_{n,AASHTO}$ values for each flexural test.

For this strain compatibility approach, a maximum usable concrete strain of 0.003 was assumed at the extreme compression fiber. A linear strain profile was then utilized to determine the strains in the three layers of steel reinforcement. The initial prestrain of the prestressing steel due to jacking stresses was used to estimate the difference in

149

prestressing steel strain and the strain in the surrounding concrete. The steel strains were

then used to calculate steel stresses. The prestressing steel stress-strain relationships

found in the PCI Design Handbook were adapted for application to the strand used in this

study (PCI 2004). A rectangular concrete stress block was assumed. The depth of the

stress block was varied until equilibrium of the steel and concrete stresses was achieved

for the cross section. The resulting $f_{ps,AASHTO}$ and $M_{n,AASHTO}$ values were then calculated.

6.6.2 Strain Compatibility and Nonlinear Material Properties

The strain compatibility and nonlinear material properties analysis approach was based

upon the same procedures described in Barnes et al. (1999), as was the procedure used in

the previous phase of this project Levy (2007). As a result, the description of these

procedures is very similar to the descriptions presented within those reports.

Stresses and strains in the girders prior to flexural testing were computed from an

analysis assuming an elastic uncracked response, in which transformed-section properties

were used instead of gross-section properties. A linear elastic stress-strain relationship

for each type of girder concrete was assumed, based on the results of modulus of

elasticity tests conducted on representative 6 in. by 12 in. cylinders, shown in Appendix

D. The linear elastic stress-strain relationship for the prestressed steel was based on the

modulus of elasticity value reported by the strand manufacturer. For the non-prestressed

steel, linear elastic behavior was assumed with a modulus of elasticity equal to 29,000

ksi. Relaxation of the prestressing steel was modeled as described by Collins and

Mitchell (1997) for low-relaxation strand. Creep and shrinkage deformations were

computed using the time-dependent concrete deformation relationships stated in the

150

AASHTO LRFD (1998) code. Although the creep and shrinkage relationships used differ from the provisions of the current code, the AASHTO LRFD (2007) does allow for the use of these older expressions. The stresses and strains in the concrete and steel were calculated for each specimen immediately prior to release, immediately after release, prior to casting the deck concrete, after casting of the deck concrete, and immediately prior to flexural testing (after repositioning of supports, if necessary).

After using the uncracked, linear elastic analysis to estimate the state of stress at the critical cross section (load point closest to the test end of the girder), the general nonlinear, layer-by-layer approach described by Collins and Mitchell (1997) was used to perform flexural analysis of the composite girder when subjected to applied test loads. The composite girder cross section was discretized into thin layers which were analyzed individually as members subjected to axial load, and relative deformations of the layers were constrained by the "plane sections remain plane" hypothesis. In other words, the deformations of the layers were constrained to be proportional to the distance away from the depth of zero strain (neutral axis). The deck concrete was subdivided into thirteen total layers. The bottom layer was 0.5 in. thick and the other twelve layers had a thickness of 0.25 in. The precast girder section was subdivided into twenty-eight layers, each with a thickness of 1.0 in. The two rows of prestressing strands and one row of mild steel deck reinforcement were represented as an additional three layers. The initial stresses and strains in each layer were determined from the elastic, uncracked, time-dependent analysis described above.

For each assumed value of strain at the top fiber of the cross section, the resulting curvature and neutral axis position were determined using an iterative approach which

satisfied equilibrium on the cross section. Equilibrium of the cross section was established when the algebraic sum of the layer forces equaled the applied axial load of zero. Once each combination of curvature and neutral axis position was established, the corresponding total bending moment was calculated by summing the individual moments resulting from the layer axial forces. The full moment-curvature response was obtained by repeating this process for a series of top fiber strains up to a value of 0.003 in./in. in compression. In this manner, the expected cracking moment and flexural capacity of the cross section could be predicted, as well as the stress in the concrete or steel at any level of applied load.

For analysis of the critical section, concrete layers were modeled as resisting tensile stresses up to the modulus of rupture for the cracked section response. Concrete layers with larger strains carried no tensile stress. The stress-strain response of concrete in compression was assumed to follow the nonlinear relationship given in Equation 6-1 (Collins and Mitchell 1997). The concrete compressive strength, f'$_c$, and modulus of elasticity, E$_c$, were based upon tests performed on 6 in. x 12 in. cylinders at the time of flexural testing.

$$\sigma_c = f'_c \left[\frac{n \left(\frac{\varepsilon_c}{\varepsilon'_c} \right)}{n - 1 + \left(\frac{\varepsilon_c}{\varepsilon'_c} \right)^{nk}} \right] \qquad \textbf{\textit{Equation 6-1}}$$

where, σ_c = concrete stress

f'_c = concrete compressive strength at time of test

ε_c = concrete strain

ε'_c = concrete strain when f_c reaches f'_c, as defined below

n = curve-fitting factor, as defined below

k = factor to increase the postpeak decay stress, taken as 1.0 for

$(\varepsilon_c / \varepsilon'_c)$ less than 1.0 and as a number greater than 1.0, as defined

below, for $(\varepsilon_c / \varepsilon'_c)$ greater than 1.0

E_c = concrete modulus of elasticity at test

$$\varepsilon'_c = \frac{f'_c}{E_c} \frac{n}{n-1}$$

$$n = 0.8 + \frac{f'_c}{2500}$$

$$k = 0.67 + \frac{f'_c}{9000}$$

The non-prestressed deck steel was assumed to have a linear stress-strain relationship (E_s = 29,000 ksi) for both compressive and tensile stresses less than the yield stress. For larger strains (tension or compression), the steel was assumed to behave with perfect plasticity, with the stress in the steel taken equal to the yield stress.

A nonlinear stress-strain relationship was used to describe the full range of behavior of the prestressed reinforcement. Based on the manufacturer-supplied modulus of elasticity and previous stress-strain tests of similar strands from the same manufacturer, the tensile stress-strain relationship given in Equation 6-2 was used (Barnes et al. 1999).

$$f_p = 28900\varepsilon_p \left(0.0332 + \frac{0.9668}{\left[1 + \left(114\varepsilon_p \right)^{12} \right]^{\frac{1}{12}}} \right) \qquad \textit{Equation 6-2}$$

153

where, ε_p = strain in prestressing strand

f_p = stress in prestressing strand

The approach outlined above is adequate for predicting the response of an

individual cross section through the complete flexural range of behavior; however, it is

inadequate for predicting the load-deflection behavior of the entire beam because it does

not reflect the increased stiffness that exists between cracked cross sections. Thus a

"tension-stiffened" analysis of the girder cross section was considered for the prediction

of the load-deflection response in accordance with the general procedure described by

Collins and Mitchell (1991). This procedure effectively assigned average tensile stresses

after cracking to concrete fibers located within 7.5 bar or strand diameters of tension

reinforcement. For concrete strains beyond the modulus of rupture, tension-stiffened

concrete stresses were computed in accordance with Equation 6-3 (Collins and Mitchell

1997).

$$f_c = \frac{\alpha_1 f_r}{1 + \sqrt{500\varepsilon_c}}$$ *Equation 6-3*

where, α_1 = 1.0 for deformed reinforcing bars

α_1 = 0.7 for plain bars, wires, or bonded strands

f_r = concrete modulus of rupture or cracking stress

This tension-stiffened model was only used to compute the beam deformations up

to the ultimate load, which was determined based on the unstiffened response of the

cracked section only. Finally, the load-deflection response was generated and plotted.

Each girder was subdivided into 32 segments, and the deflection response was calculated

from the corresponding curvatures in all segments for each level of applied load using the

154

moment-area method. Appendix H contains comparisons of the predicted load-displacement relationships for each flexural test to the experimentally measured load-displacement curves.

A summary of the flexural analysis results is presented in Table 6-3. The nominal moment capacities for each flexural test according to the AASHTO procedure, $M_{n,AASHTO}$, and according to the nonlinear material properties approach, $M_{n,calc}$, are presented. The corresponding strand stresses at nominal moment capacity, $f_{ps,AASHTO}$ and $f_{ps,calc}$, are presented as well. These strand stresses were calculated using the strain compatibility approach previously discussed. In addition, the strain compatibility approach was used to calculate $\varepsilon_{max,calc}$, as an indication of the strand strain necessary to achieve the full flexural capacity of the girder. For a direct comparison to the provided embedment lengths, a precise AASHTO development length, $l_{d,AASHTO}$, for each flexural test was also calculated and reported in Table 6-3. This development length was calculated using Equation 2-9 based on $f_{ps,AASHTO}$ and the effective stress in the strands at the critical section immediately prior to flexural testing, $f_{pe,test}$, which was determined from the linear elastic, uncracked, time-dependent procedure described above.

Table 6-3: Summary of Flexural Analysis Results

Test Girder	l_e (in.)	$l_{d,AASHTO}$ (in.)	$f_{pe,test}$ (ksi)	$f_{ps,AASHTO}$ (ksi)	$M_{n,AASHTO}$ (kip-ft)	$f_{ps,calc}$ (ksi)	$M_{n,calc}$ (kip-ft)	$\varepsilon_{max,calc}$ (in./in.)
STD-M-1W	135	123	180.2	269.0	649	292.3	702	0.0492
STD-M-1E	85	123	178.8	269.0	650	291.9	700	0.0488
STD-M-2E	65	124	178.1	269.0	647	291.0	696	0.0478
STD-M-2W	65	124	178.1	269.0	647	290.7	694	0.0475
SCC-MS-1W	135	124	178.5	269.0	646	291.2	696	0.0481
SCC-MS-1E	85	124	177.0	269.0	648	290.3	691	0.0471
SCC-MS-2E	65	125	176.0	269.0	646	290.2	692	0.0470
SCC-MS-2W	65	125	176.0	268.9	645	289.5	689	0.0462
SCC-HS-1W	135	122	180.8	268.8	631	283.2	663	0.0397
SCC-HS-1E	85	123	179.7	268.7	630	283.4	665	0.0400
SCC-HS-2E	65	123	179.4	268.9	641	287.7	683	0.0444
SCC-HS-2W	65	123	179.4	268.9	642	288.6	686	0.0454

6.7 PRESENTATION OF RESULTS

This section presents the results of the twelve flexural tests performed for this study. For

discussion purposes, the tests have been divided into three groups depending on the

embedment length. Each test is briefly summarized, making note of significant loads,

moments, deflections, strains, and strand slip magnitudes. All reported bending moments

include the applied loads and self-weight of the girder. All reported deflections were

measured at the section midway between the two load points. Experimental and

predicted load vs. displacement plots for individual tests can be found in Appendix H.

Representative crack patterns at maximum load for each test are shown in this section;

however, the progression of crack patterns throughout each individual test can be seen in

Appendix I. Specific crack width values for each flexural test at each load level can be

found in Appendix J.

6.7.1 Specimens with 135-in. Embedment Lengths

Three flexural tests—one for each mixture—were performed with an embedment length (to the maximum moment region), l_e, of 135 in. This embedment length corresponds to approximately 110 percent of the development length, $l_{d, AASHTO}$, calculated using the AASHTO expression. The flexural test setup for these specimens can be seen in Figure 6-1. The load-deflection relationships for these tests can be seen in Figure 6-10.
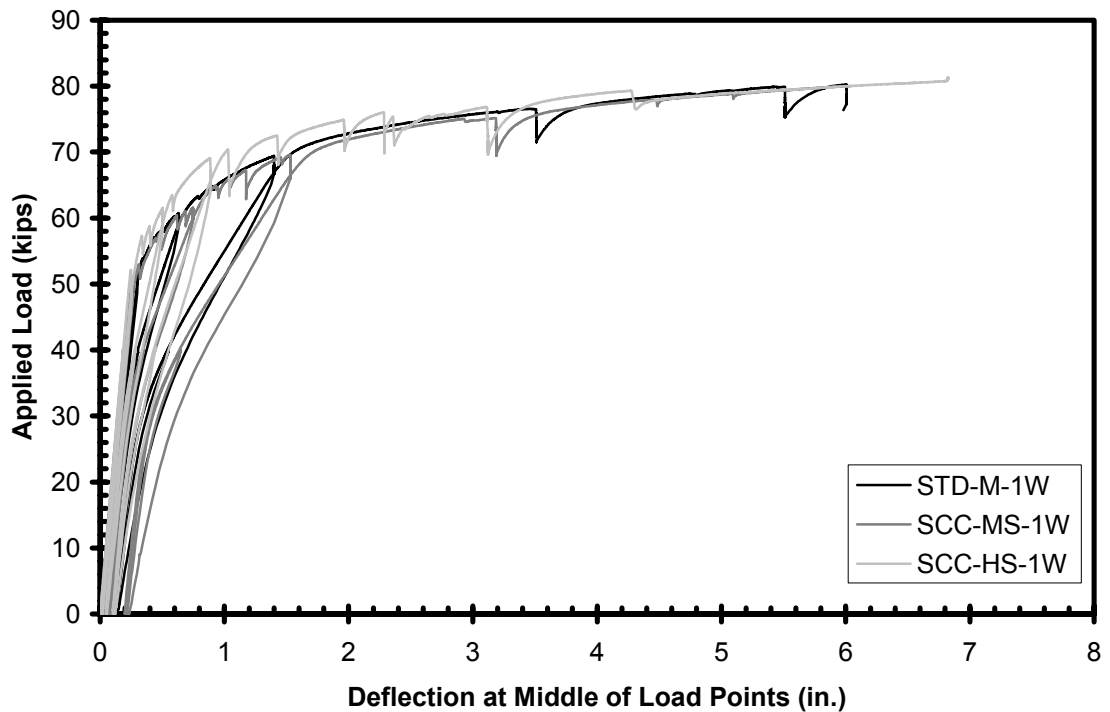
Figure 6-10: Load-Deflection Relationship for Girders with l_e = 135 in. (1W)

6.7.1.1 STD-M-1W

Load-carrying capacity was not exceeded during the flexural test of girder end STD-M-1W. The test was stopped due to deflection limitations. No strand end slip was observed during this test. The first flexural crack was observed at 51.9 kips, corresponding to a deflection of 0.30 in. The cracking moment, M_{cr}, was within 1 percent of the calculated

cracking moment, $M_{cr,calc}$. The maximum load for this girder end was 80.3 kips, corresponding to a maximum deflection of 6.00 in. at the cessation of the test. The maximum moment applied to this girder end, M_{max}, was 5 percent less than $M_{n,calc}$ and 3 percent greater than $M_{n, AASHTO}$. The stress in the strands at the actual maximum moment was estimated to be 280 ksi from the nonlinear flexural analysis. A residual deflection of approximately 2.4 in. was observed after unloading. This flexural test did not result in any web-shear cracking. The crack pattern corresponding to the maximum load for this girder end can be seen in Figure 6-11.
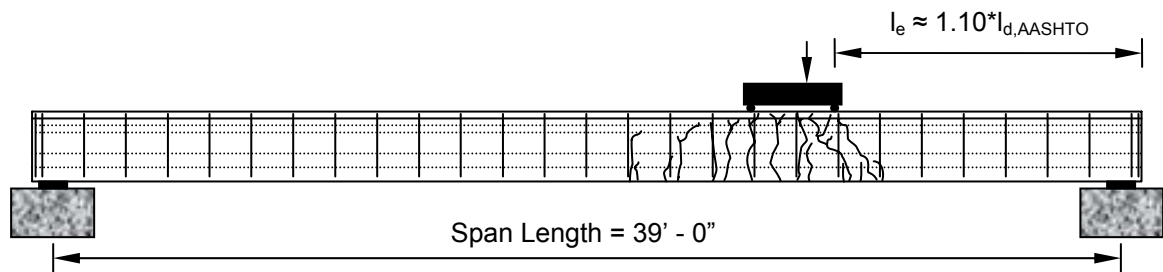

Figure 6-11: Crack Pattern for STD-M-1W at Maximum Load

6.7.1.2 SCC-MS-1W

Load-carrying capacity was not exceeded during the flexural test of girder end SCC-MS-1W. The test was stopped due to deflection limitations. Relatively small amounts of strand end slip on the order of 0.0011 – 0.0019 in. were observed. The first flexural crack was observed at 50.7 kips, corresponding to a deflection of 0.26 in. The cracking moment, M_{cr}, was 8 percent less than the calculated cracking moment, $M_{cr,calc}$. The maximum load for this girder end was 80.0 kips, corresponding to a maximum deflection of 6.03 in. The maximum moment applied to this girder end, M_{max}, was 4 percent less than $M_{n,calc}$ and 3 percent greater than $M_{n, AASHTO}$. The stress in the strands at the actual

158

maximum moment was estimated to be 280 ksi. A residual deflection of approximately

3.0 in. was observed. This flexural test exhibited shear-type cracking over the support,

which was first observed at an applied load of approximately 75 kips. This cracking

appeared to occur in conjunction with deck separation (relative horizontal displacement

between the deck and girder); however, this separation was not noticed until the end of

the test. The crack pattern corresponding to the maximum load for this girder end can be
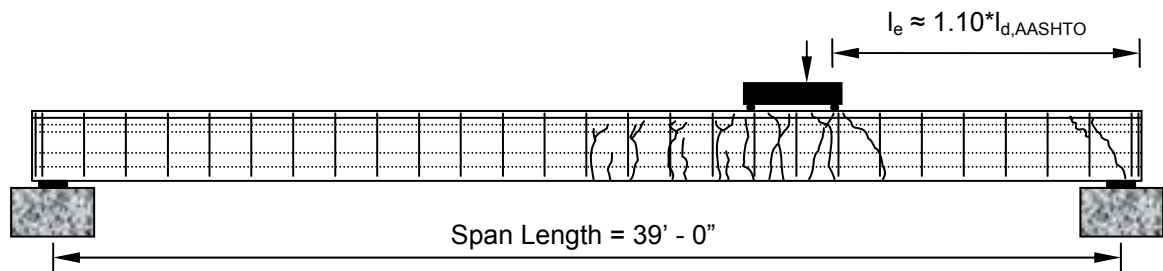
seen in Figure 6-11.

$l_e \approx 1.10 * l_{d,AASHTO}$

Span Length = 39' - 0"

Figure 6-12: Crack Pattern for SCC-MS-1W at Maximum Load

6.7.1.3 SCC-HS-1W

Load-carrying capacity was not exceeded during the flexural test of girder end SCC-HS-

1W. The test was stopped was at an applied load greater than the predicted ultimate load

due to the fact that the load was increasing but the concrete deck strains were not. This

was believed to be attributed to the yielding and displacement of the stirrups as the deck

separated and slid along the girder/deck interface. Relatively small amounts of strand

end slip on the order of 0.0010–0.0014 in. were observed. The first flexural crack was

observed at 52.1 kips, corresponding to a deflection of 0.25 in. The cracking moment,

M_{cr}, was 7 percent less than the calculated cracking moment, $M_{cr,calc}$. The maximum load

for this girder end was 81.3, kips corresponding to a maximum deflection of 6.83 in. The

maximum moment applied to this girder end, M_{max}, was 2 percent greater than $M_{n,calc}$ and 7 percent greater than $M_{n,\,AASHTO}$. The stress in the strands at the actual maximum moment was estimated to be at least 283 ksi. A residual deflection of approximately 3.9 in. was observed. This flexural test did not exhibit any web-shear cracking except for a crack over the end support associated with the deck separation (similar to SCC-MS-1W). The crack pattern corresponding to the maximum load for this girder end can be seen in Figure 6-11.
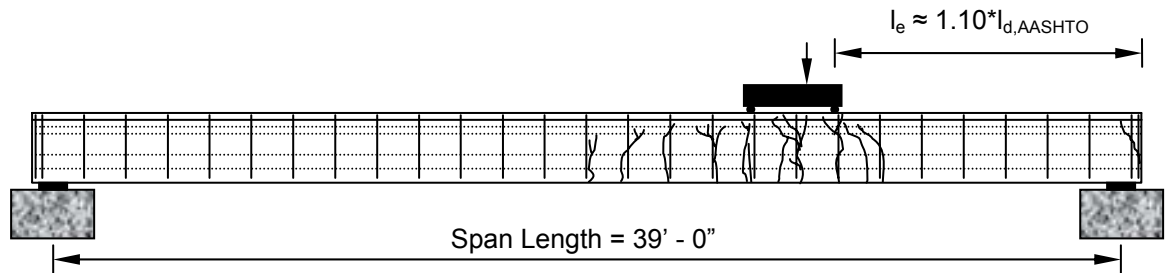

$l_e \approx 1.10 \cdot l_{d,AASHTO}$

Span Length = 39' - 0"

Figure 6-13: Crack Pattern for SCC-HS-1W at Maximum Load

6.7.2 Specimens with 85-in. Embedment Lengths

Three flexural tests were performed with an embedment length, l_e, of 85 in. This embedment length corresponds to approximately 68 percent of the development length, $l_{d,\,AASHTO}$, calculated using the AASHTO expression. The flexural test setup for these specimens can be seen in Figure 6-2. The load-deflection relationships for these tests can be seen in Figure 6-14. As noted earlier, SCC-HS-1E was tested with an unintended span length for deflections up to approximately 1.5 in.
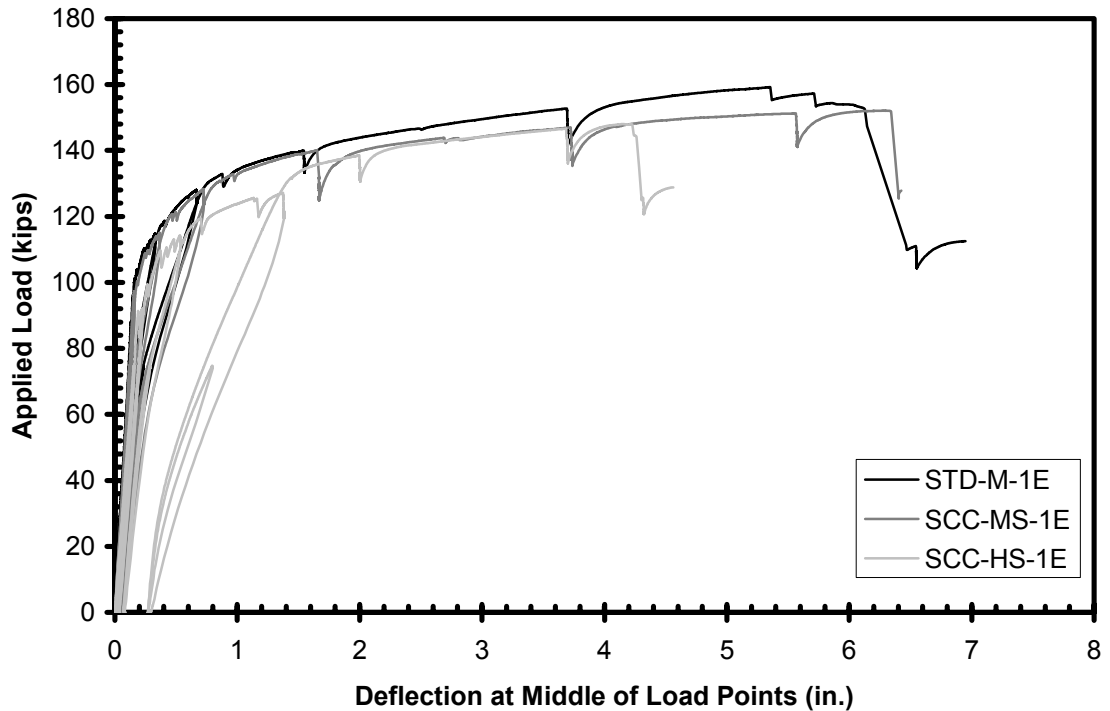
Figure 6-14: Load-Deflection Relationship for Girders with l$_e$ = 85 in. (1E)

6.7.2.1 STD-M-1E

Girder end STD-M-1E failed in a flexural manner. Load-carrying capacity was lost for this girder end due to crushing of the deck concrete. Relatively small amounts of strand end slip on the order of 0.003 in. were observed at the very end of the test. The first flexural crack was observed at 100.0 kips, corresponding to a deflection of 0.16 in. The cracking moment, M$_{cr}$, was within 1 percent of the calculated cracking moment, M$_{cr,calc}$. The maximum load for this girder end was 159.3 kips, corresponding to a maximum deflection of 5.35 in. The maximum moment for this girder end, M$_{max}$, was 3 percent greater than M$_{n,calc}$ and 11 percent greater than M$_{n, AASHTO}$. The stress in the strands at the actual maximum moment was estimated to be at least 292 ksi. A residual defection was not recorded. This flexural test did not experience any web-shear cracking. The crack

pattern corresponding to the maximum load for this girder end can be seen in Figure 6-11.
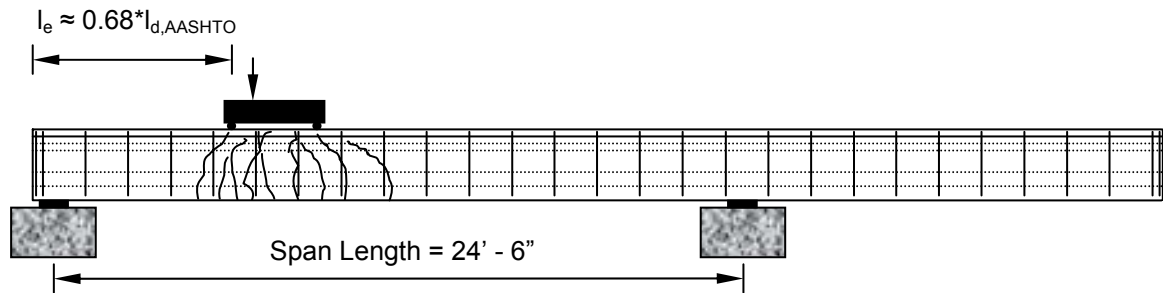

$l_e \approx 0.68*l_{d,AASHTO}$

Span Length = 24' - 6"

Figure 6-15: Crack Pattern for STD-M-1E at Maximum Load

6.7.2.2 SCC-MS-1E

Girder end SCC-MS-1E failed in a flexural manner. Loss of load-carrying capacity for this girder end was attributed to the rupture of one or more prestressing strands. Relatively small amounts of strand end slip, on the order of 0.001 in., were observed at the very end of the test. The first flexural crack was observed at 97.0 kips, corresponding to a deflection of 0.16 in. The cracking moment, M_{cr}, was 8 percent less than the calculated cracking moment, $M_{cr,calc}$. The maximum load for this specimen was 152.1 kips, corresponding to a maximum deflection of 6.31 in. The maximum moment applied to this girder end, M_{max}, was within 1 percent of $M_{n,calc}$ and 6 percent greater than $M_{n, AASHTO}$. The stress in the strands at the actual maximum moment was estimated to be 289 ksi. A residual deflection of approximately 3.9 in. was observed. This flexural test exhibited web-shear cracking that was first observed at an applied load of approximately 144 kips. Deck separation also occurred and was observed at approximately 144 kips. The crack pattern corresponding to the maximum load for this girder end can be seen in Figure 6-11.
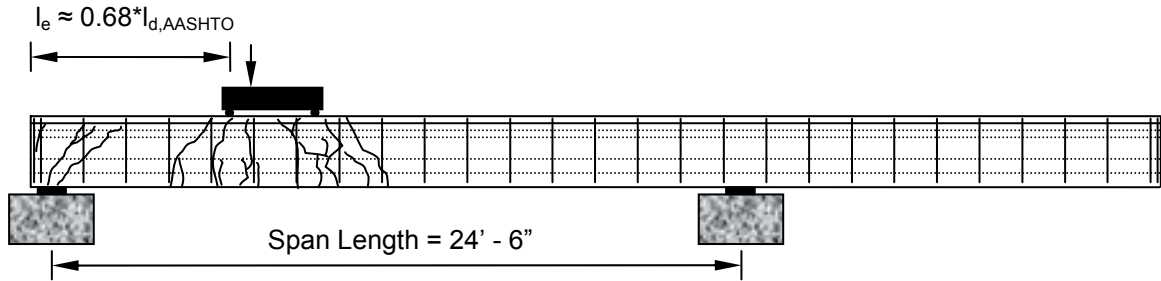
162

$l_e \approx 0.68*l_{d,AASHTO}$

Span Length = 24' - 6"

Figure 6-16: Crack Pattern for SCC-MS-1E at Maximum Load

6.7.2.3 SCC-HS-1E

The initial test setup was incorrect for this specimen, however this was not recognized until during the test. The embedment length and load point location were correct, but the span length was initially set at 26.5 ft rather than 24.5 ft. As a result, the testing of this girder end was interrupted after the service-load cycle prior to the load corresponding to approximately 270 ksi in the bottom strands. The far support block was moved 2 ft to shorten the span to the correct length of 24.5 ft. All sensors and other instrumentation were rezeroed, and testing to failure was completed.

Girder end SCC-HS-1E failed in a flexural manner. Loss of load-carrying capacity for this girder end was attributed to the rupture of one or more prestressing strands. Relatively small amounts of strand end slip on the order of 0.0003–0.0007 in. were observed. The first flexural crack occurred while testing with the incorrect span length at 91.4 kips, corresponding to a deflection of 0.19 in. The cracking moment, M_{cr}, was 7 percent less than the calculated cracking moment, $M_{cr,calc}$. Note $M_{cr,calc}$ was calculated based upon the incorrect, but actual, span length. The maximum load for this girder end, obtained using the correct span length, was 148.0 kips, corresponding to a maximum deflection of 4.16 in. The maximum moment applied to this girder end, M_{max},

163

was 1 percent greater than $M_{n,calc}$ and 7 percent greater than $M_{n, AASHTO}$. The stress in the strands at the actual maximum moment was estimated to be 283+ ksi. A residual deflection of approximately 3.7 in. was observed. This flexural test did not experience any web-shear cracking. Slight deck separation also occurred at the end of the test, accompanied by a crack in the girder above the end support. The crack pattern corresponding to the maximum load for this girder end can be seen in Figure 6-11.
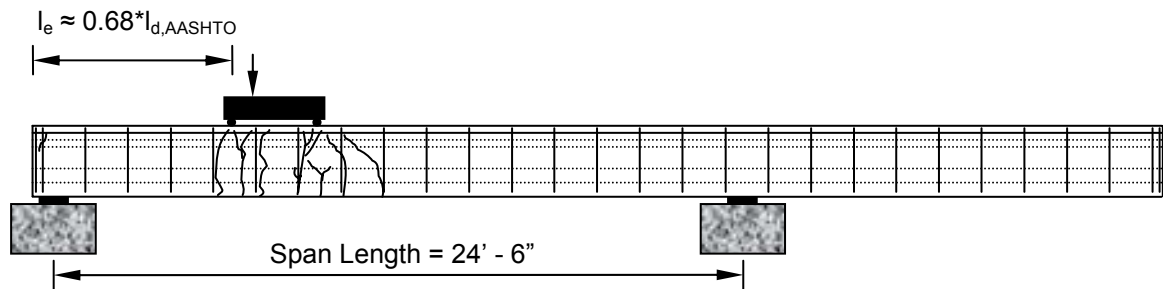

$l_e \approx 0.68 * l_{d,AASHTO}$

Span Length = 24' - 6"

Figure 6-17: Crack Pattern for SCC-HS-1E at Maximum Load

6.7.3 Girders with 65-in. Embedment Lengths

Six flexural tests were performed with an embedment length, l_e, of 65 in. This embedment length corresponds to approximately 52 percent of the development length, $l_{d, AASHTO}$, calculated using the AASHTO expression. The flexural test setup for these specimens can be seen in Figure 6-3. The load-deflection relationships for these tests can be seen in Figure 6-18 and Figure 6-19.
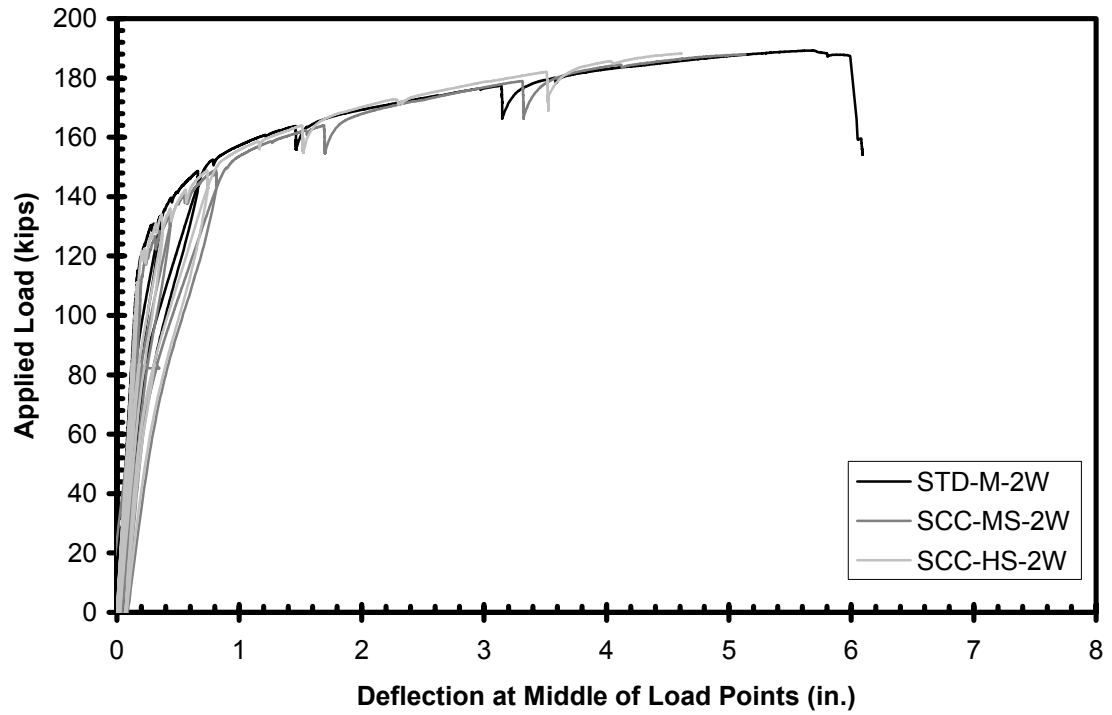
Figure 6-18: Load-Deflection Relationship for Girders with l_e = 65 in. (2W)
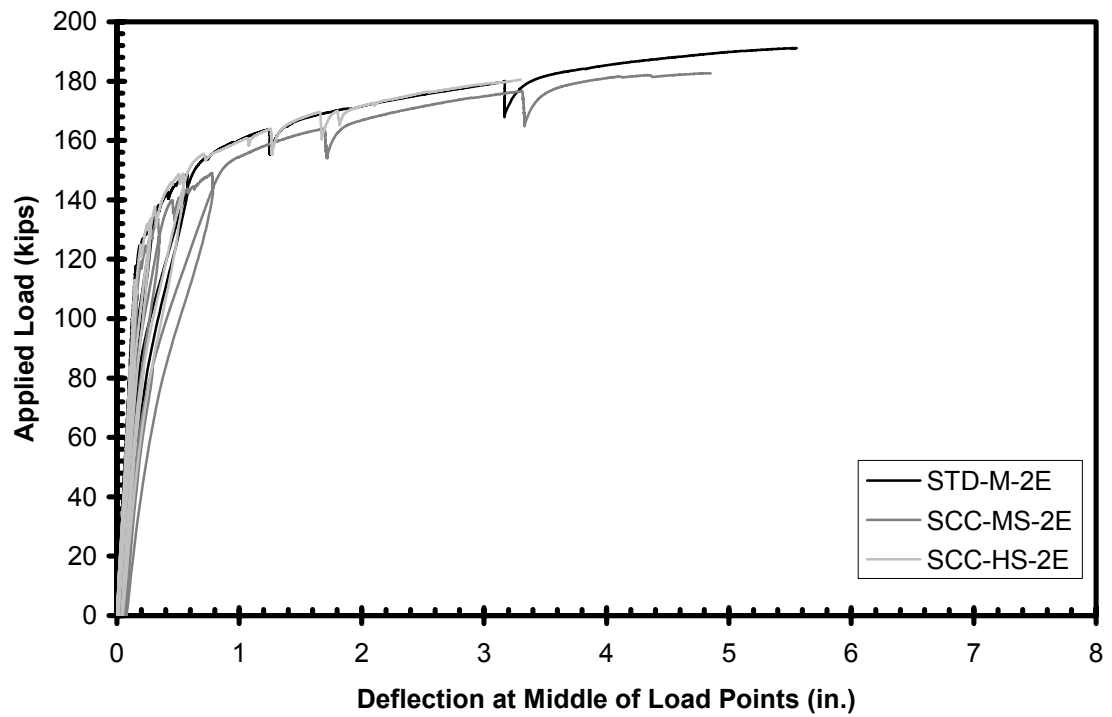

Figure 6-19: Load-Deflection Relationship for Girders with l_e = 65 in. (2E)

165

6.7.3.1 STD-M-2W

Load-carrying capacity was not exceeded during the flexural test of girder end STD-M-2W. The test was stopped to prevent excessive damage after exceeding the predicted flexural capacity. Relatively small amount of strand end slip on the order of 0.0005 in. were observed. The first flexural crack was observed at 114.1 kips, corresponding to a deflection of 0.17 in. The cracking moment, M_{cr}, was 3 percent less than the calculated cracking moment, $M_{cr,calc}$. The maximum load for this girder end was 189.3 kips, corresponding to a maximum deflection of 5.69 in. The maximum moment applied to this girder end, M_{max}, was 5 percent greater than $M_{n,calc}$ and 13 percent greater than $M_{n,\ AASHTO}$. The stress in the strands at the actual maximum moment was estimated to be at least 291 ksi. A residual deflection was not recorded for this test. This flexural test exhibited web-shear cracking, which was first observed at an applied load of approximately 149 kips. The crack pattern corresponding to the maximum load for this girder end can be seen in Figure 6-11.
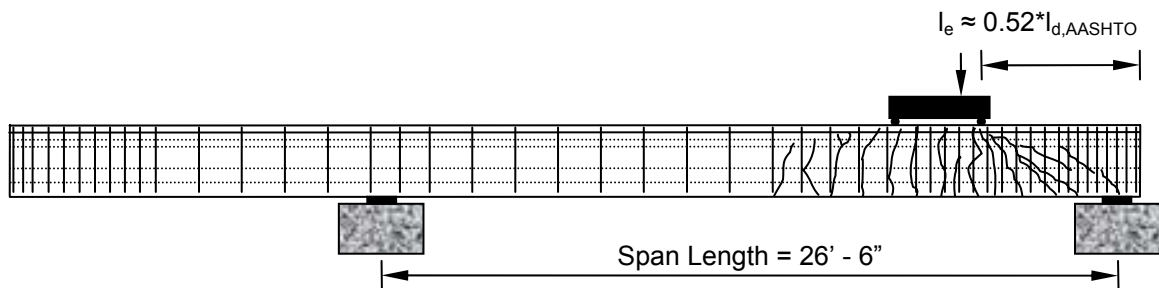

Figure 6-20: Crack Pattern for STD-M-2W at Maximum Load

6.7.3.2 SCC-MS-2W

Load-carrying capacity was not lost during the flexural test of girder end SCC-MS-2W. The test was stopped due to deflection limitations. Relatively small amounts of strand

end slip on the order of 0.0003–0.0006 in. were observed during this test. The first

flexural crack was observed at 111.1 kips, corresponding to a deflection of 0.19 in. The

cracking moment, M_{cr}, was 9 percent less than the calculated cracking moment, $M_{cr,calc}$.

The maximum load for this specimen was 187.9 kips, corresponding to a maximum

deflection of 5.14 in. The maximum moment applied to this girder end, M_{max}, was 5

percent greater than $M_{n,calc}$ and 12 percent greater than $M_{n, AASHTO}$. The stress in the

strands at the actual maximum moment was estimated to be at least 290 ksi. A residual

deflection of approximately 3.2 in. was observed. This flexural test exhibited web-shear

cracking, first observed at an applied load of approximately 145 kips. Deck separation

also occurred; however, it was located in the lightly reinforced, long shear span (away

from the girder end) and was not noticed until after completion of the test. The crack

pattern corresponding to the maximum load for this girder end can be seen in Figure
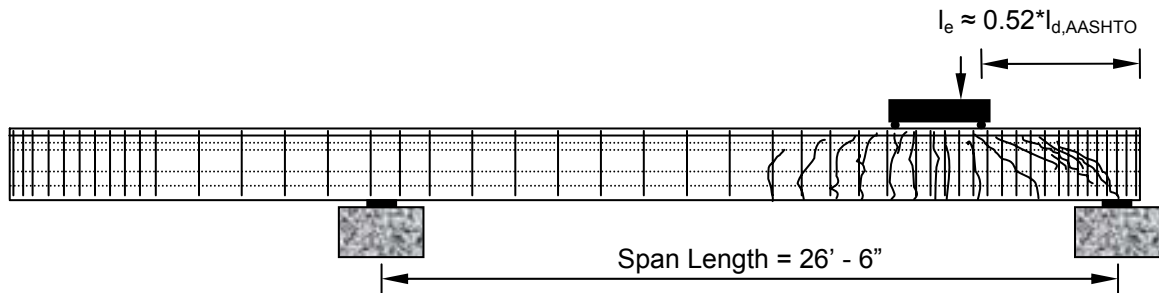
6-11.

Figure 6-21: Crack Pattern for SCC-MS-2W at Maximum Load

6.7.3.3 SCC-HS-2W

The flexural test of girder end SCC-HS-2W failed in a flexural manner. Loss of load-

carrying capacity for this girder end resulted from rupture of prestressed strands.

Relatively small amounts of strand end slip on the order of 0.0007 in. were observed

during this test. The first flexural crack was observed at 111.0 kips, corresponding to a deflection of 0.17 in. The cracking moment, M_{cr}, was 11 percent less than the calculated cracking moment, $M_{cr,calc}$. The maximum load for this girder end was 188.2 kips, corresponding to a maximum deflection of 4.62 in. The maximum moment applied to this girder end, M_{max}, was 6 percent greater than $M_{n,calc}$ and 13 percent greater than $M_{n,AASHTO}$. The stress in the strands at the actual maximum moment was estimated to be at least 289 ksi. A residual deflection of approximately 3.6 in. was observed. This flexural test exhibited web-shear cracking, which was first observed at an applied load of approximately 173 kips. The crack pattern corresponding to the maximum load for this girder end can be seen in Figure 6-11.
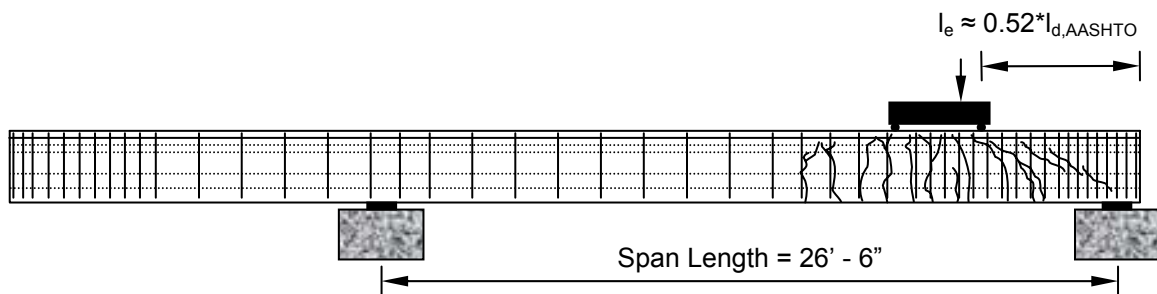

Figure 6-22: Crack Pattern for SCC-HS-1W at Maximum Load

6.7.3.4 STD-M-2E

The flexural test of girder end STD-M-2E failed in a flexural manner. Load-carrying capacity was lost for this girder end due to crushing of the deck concrete. Relatively small amounts of strand end slip on the order of 0.0005–0.0026 in. were observed. The first flexural crack was observed at 116.2 kips, corresponding to a deflection of 0.15 in. The cracking moment, M_{cr}, was within 1 percent of the calculated cracking moment, $M_{cr,calc}$. The maximum load for this girder end was 191.1 kips, corresponding to a

maximum deflection of 5.55 in. The maximum moment applied to this girder end, M_{max}, was 6 percent greater than $M_{n,calc}$ and 14 percent greater than $M_{n, AASHTO}$. The stress in the strands at the actual maximum moment was estimated to be at least 291 ksi. A residual deflection was not recorded for this test. This flexural test exhibited web-shear cracking, which was first observed at an applied load of approximately 149 kips. The crack pattern corresponding to the maximum load for this girder end can be seen in Figure 6-11.
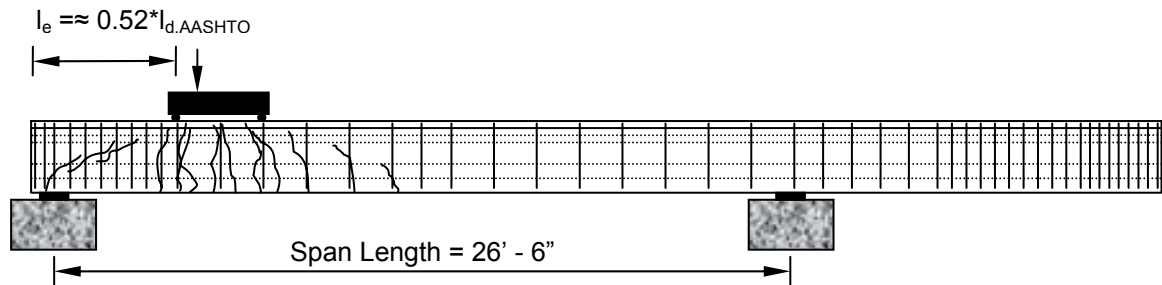

Figure 6-23: Crack Pattern for STD-M-2E at Maximum Load

6.7.3.5 SCC-MS-2E

The flexural test of girder end SCC-MS-2E failed in a flexural manner. Loss of load-carrying capacity for this girder end was attributed to rupture of one or more prestressed strands. No strand end slip was observed during this test. The first flexural crack was observed at 110.0 kips, corresponding to a deflection of 0.16 in. The cracking moment, M_{cr}, was 9 percent less than the calculated cracking moment, $M_{cr,calc}$. The maximum load for this girder end was 182.7 kips, corresponding to a maximum deflection of 4.81 in. The maximum moment applied to this girder end, M_{max}, was 2 percent greater than $M_{n,calc}$ and 9 percent greater than $M_{n, AASHTO}$. The stress in the strands at the actual maximum moment was estimated to be at least 290 ksi. A residual deflection of approximately 3.9

in. was observed. This flexural test exhibited web-shear cracking, which was first observed at an applied load of approximately 140 kips. Deck separation also occurred; however, it was located in the lightly reinforced, long shear span (away from the girder end) and was not noticed until after completion of the test. The crack pattern corresponding to the maximum load for this girder end can be seen in Figure 6-11.
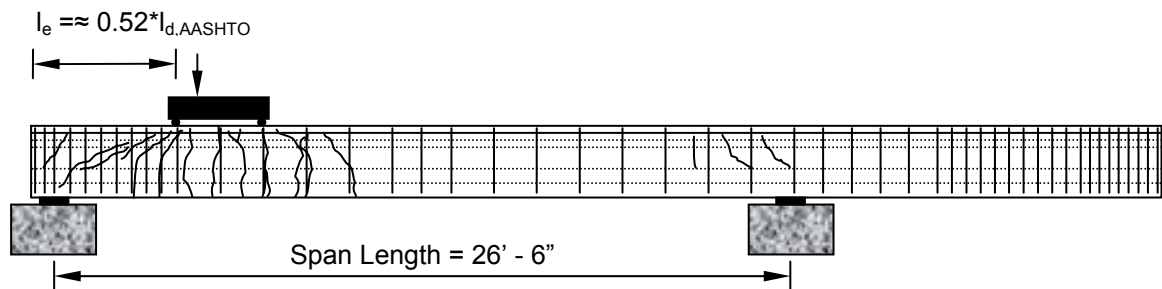

Figure 6-24: Crack Pattern for SCC-MS-2E at Maximum Load

6.7.3.6 SCC-HS-2E

Load-carrying capacity was not exceeded during the flexural test of girder end SCC-HS-2E. The test was stopped for safety concerns due to relatively high compressive strains in the deck concrete. Relatively small amounts of strand end slip on the order of 0.0008–0.0024 in. were observed at the very end of this test. The first flexural crack was observed at 112.9 kips, corresponding to a deflection of 0.15 in. The cracking moment, M_{cr}, was 9 percent less than the calculated cracking moment, $M_{cr,calc}$. The maximum load for this girder end was 180.5 kips, corresponding to a maximum deflection of 3.29 in. The maximum moment applied to this girder end, M_{max}, was 2 percent greater than $M_{n,calc}$ and 9 percent greater than $M_{n, AASHTO}$. The stress in the strands at the actual maximum moment was estimated to be 293 ksi. A residual deflection of approximately 1.5 in. was observed. This flexural test exhibited web-shear cracking, which was first observed at an

applied load of approximately 169 kips. The crack pattern corresponding to the

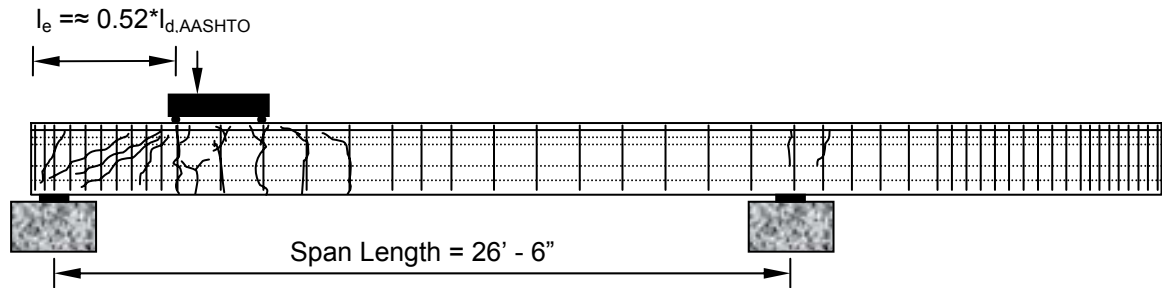maximum load for this girder end can be seen in Figure 6-11.

$l_e = \approx 0.52 \cdot l_{d.AASHTO}$

Span Length = 26' - 6"

Figure 6-25: Crack Pattern for SCC-HS-2E at Maximum Load

6.8 DISCUSSION OF TEST RESULTS

This section presents a summary of the flexural test program results and a discussion of

the flexural bond performance of all tested girders. Discussions about the service-load-

level performance and the cracking-load performance of the tested girders are also

offered.

6.8.1 Summary of Test Results at Maximum Load

Table 6-3 presents a summary of the results from the flexural test program at maximum

load for each girder end. For reference purposes, ratios of embedment length to

AASHTO-predicted development length are presented for each test. The maximum

moment, M_{max}, obtained for each test is compared to both the predicted nominal moment

capacities $M_{n,calc}$ and $M_{n,AASHTO}$ calculated based upon the flexural analysis procedures

described in Section 6.6 of this thesis. The computed strain in the bottom prestressing

strands at the maximum applied moment, ε_{max}, is also presented. Four of the twelve

flexural tests were ceased prior to exceeding load-carrying capacity. Reasons for this

included deflection limitations, safety concerns, and limiting the damage to the opposite

end of the girder. The other eight tests were stopped due to the failure types listed in

Table 6-4.

Table 6-4: Summary of Flexural Testing Results at Maximum Load

Test Girder	$\dfrac{l_e}{l_{d,AASHTO}}$	$\dfrac{M_{Max}}{M_{n,calc}}$	$\dfrac{M_{max}}{M_{n,AASHTO}}$	ε_{max} (in./in.)	Failure Description
STD-M-1W	1.10	0.95	1.03	0.037	Test Ceased
STD-M-1E	0.69	1.03	1.11	0.049+	Deck Crushed
STD-M-2E	0.53	1.06	1.14	0.048+	Deck Crushed
STD-M-2W	0.53	1.05	1.13	0.048+	Test Ceased
SCC-MS-1W	1.09	0.96	1.03	0.036	Test Ceased
SCC-MS-1E	0.68	1.00	1.06	0.046	Strand Rupture
SCC-MS-2E	0.52	1.02	1.09	0.047+	Strand Rupture
SCC-MS-2W	0.52	1.05	1.12	0.046+	Test Ceased
SCC-HS-1W	1.11	1.02	1.07	0.040+	Horizontal Shear
SCC-HS-1E	0.69	1.01	1.07	0.040+	Strand Rupture
SCC-HS-2E	0.53	1.02	1.09	0.044+	High Deck Strains
SCC-HS-2W	0.53	1.06	1.13	0.045+	Strand Rupture

Table 6-4 indicates that the ultimate load behavior for all tested girder ends was

well predicted. In all but two tests, STD-M-1W and SCC-MS-1W, the maximum

moment exceeded the nominal moment capacity predicted by the strain compatibility

approach using nonlinear material properties. The two tests that did not reach the

predicted capacity were prematurely ceased due to deflection limitations. It was also the

researcher's discretion to limit the amount of damage inflicted upon the 1E end of these

girders by not continuing to load the 1W ends. Based on the performance of the same

girders when tested with a shorter embedment length (STD-M-1E and SCC-MS-1E,

respectively), it is reasonable to assume that both STD-M-1W and SCC-MS-1W would

have surpassed the predicted moment capacity if loaded to failure. The maximum

moment obtained for all flexural tests was even more conservatively predicted using the AASHTO moment-capacity computation than from the strain compatibility approach using nonlinear material properties, with exceedance ranging from 3 to 14 percent.

Flexural failures were exhibited even in all eight flexural tests in which the embedment length was significantly less than the predicted development length. These results suggest that the AASHTO development length equation is quite conservative for the strands and concrete mixtures tested. In order to ensure attainment of ultimate strand strength and high strand strains, a total elongation of at least 3.5 percent was targeted for the bottom row of prestressing strands. It can be seen in Table 6-4 that all flexural tests resulted in a greater computed total elongation, ranging from 3.6 to at least 4.9 percent.

Table 6-4 also indicates that the SCC girders performed comparably to the girders cast with the conventional concrete mixture. All of the maximum moment exceedance percentages over the nominal moment capacities are within similar ranges when comparing the SCC values to the STD values. This suggests that the SCC mixture proportioning had no adverse effect on the flexural performance at ultimate load for these girders with respect to current design procedures or with respect to a comparable conventional concrete mixture.

6.8.2 Flexural Bond Performance

The flexural bond performance of each girder end tested was assessed by comparing the flexural bond length for each test to the flexural bond lengths implied by both ACI 318 and AASHTO LRFD design provisions. In order to calculate the predicted flexural bond lengths, the flexural bond portion of the development length equations presented in the

173

ACI 318 and AASHTO LRFD design codes were isolated. The experimental flexural

bond length was simply calculated as the difference between the tested embedment length

and measured long-term transfer length. The relevant development length equations and

a discussion on flexural bond length, transfer length, and embedment length can be found

in Chapter 2 of this thesis. Figure 6-26 and Figure 6-27 illustrate the flexural bond

performance of the tested girder ends with respect to the ACI and AASHTO equations,

respectively.

Represented on the y-axis of Figure 6-26 and Figure 6-27 is the expression

$\dfrac{f_{p,\max} - f_{pe,test}}{f_{ps,calc} - f_{pe,test}}$. The change in stress from the calculated effective stress in the strands

immediately prior to testing, $f_{pe,test}$, to the stress in the strands at maximum moment,

$f_{p,\max}$, is represented in the numerator of this expression. Normalization of the numerator

for all tests is achieved by dividing by the difference between the predicted ultimate

stress in the strands, $f_{ps,calc}$, and the $f_{pe,test}$. Ultimately, this expression represents the total

flexural bond stress achieved at the maximum moment relative to the flexural bond stress

required for development of predicted nominal flexural capacity, $M_{n,calc}$.

Represented on the x-axis of Figure 6-26 and Figure 6-27 are the expressions

$\dfrac{l_e - l_t}{l_{fb,ACI}}$ and $\dfrac{l_e - l_t}{l_{fb,AASHTO}}$, respectively. The numerator in these expressions, the difference

between the tested embedment length and the 3-month measured transfer length,

represents the available flexural bond length for each tested girder end. Once again,

normalization for each test is achieved by dividing by the flexural bond length portions of

the ACI or AASHTO development length equations. In other words, this expression

174

represents the actual tested flexural bond length relative to the flexural bond length required by ACI or AASHTO to develop the full flexural capacity of the member.

As mentioned above, the implied flexural bond lengths $l_{fb,ACI}$ and $l_{fb,AASHTO}$ were calculated based upon the relevant development length equations in each design code. The ACI 318 provisions calculate the transfer length and the flexural bond length separately, and then add them together in order to calculate a development length. Therefore, the flexural bond length portion of the equation was simply isolated to calculate $l_{fb,ACI}$. On the other hand, the AASHTO LRFD development length equation does not explicitly distinguish between a transfer length portion and a flexural bond length portion. As a result, $l_{fb,AASHTO}$ was calculated by subtracting the AASHTO LRFD transfer length of $60d_b$ from the calculated AASHTO LRFD development length. For both formulations, ACI and AASHTO, the ultimate stress in the strands was taken as $f_{ps,calc}$ and the effective stress was taken as $f_{pe,test}$.
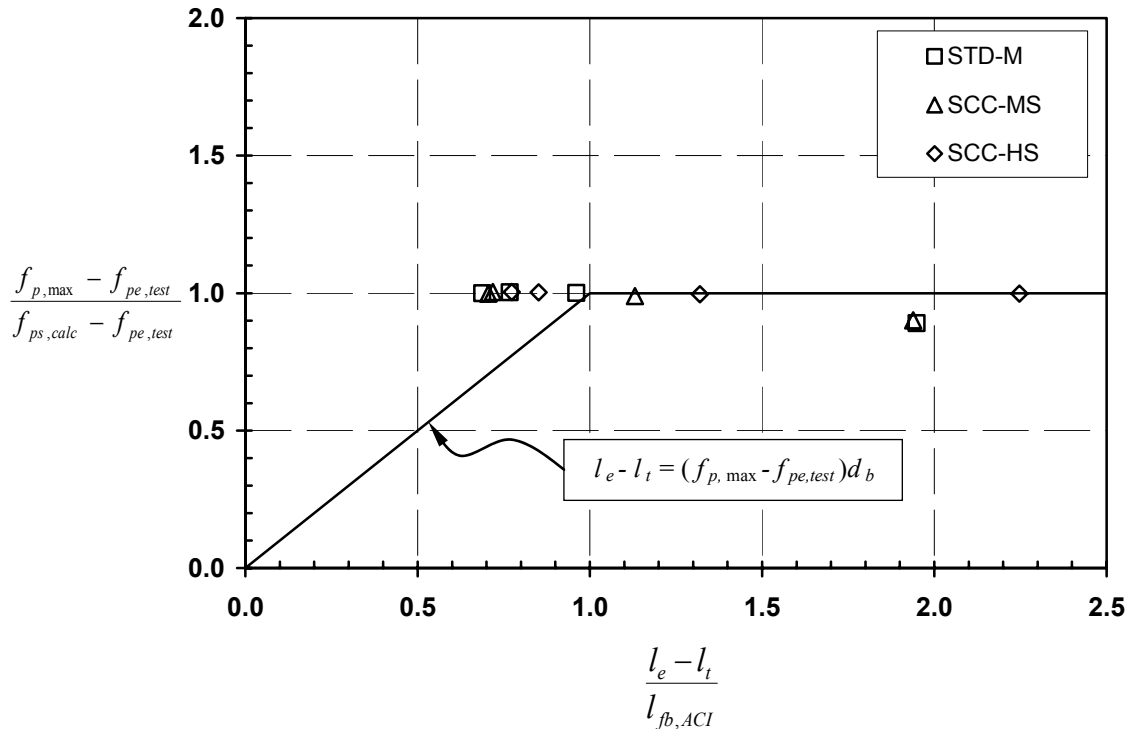
Figure 6-26: Flexural Bond Performance Relative to ACI 318 Flexural Bond Length

Figure 6-26 illustrates the flexural bond performance of the tested girder ends

with respect to the ACI implied flexural bond length. The solid line shown in Figure

6-26 represents the flexural bond length expression, $l_e - l_t = (f_{p,max} - f_{pe,test})d_b$ from ACI

318 as discussed in Chapter 2 of this thesis. In other words, this line represents the

assumed linear strand stress build up between the measured transfer length and the code-

predicted development length. For analysis purposes, the data that falls above or to the

left of this solid line indicate that the expression is conservative for predicting the flexural

bond length required at ultimate strength of the member. Figure 6-26 suggests that, for

the majority of the tested girder ends, the expression for the flexural bond length is

conservative. Only the STD-M-1W point and SCC-MS-1W point fall below, but not far

removed from, the line; however, testing of these two girder ends was stopped before the

176

full $f_{ps,calc}$ was achieved. Regardless, the achievement of $f_{ps,calc}$ at shorter embedment

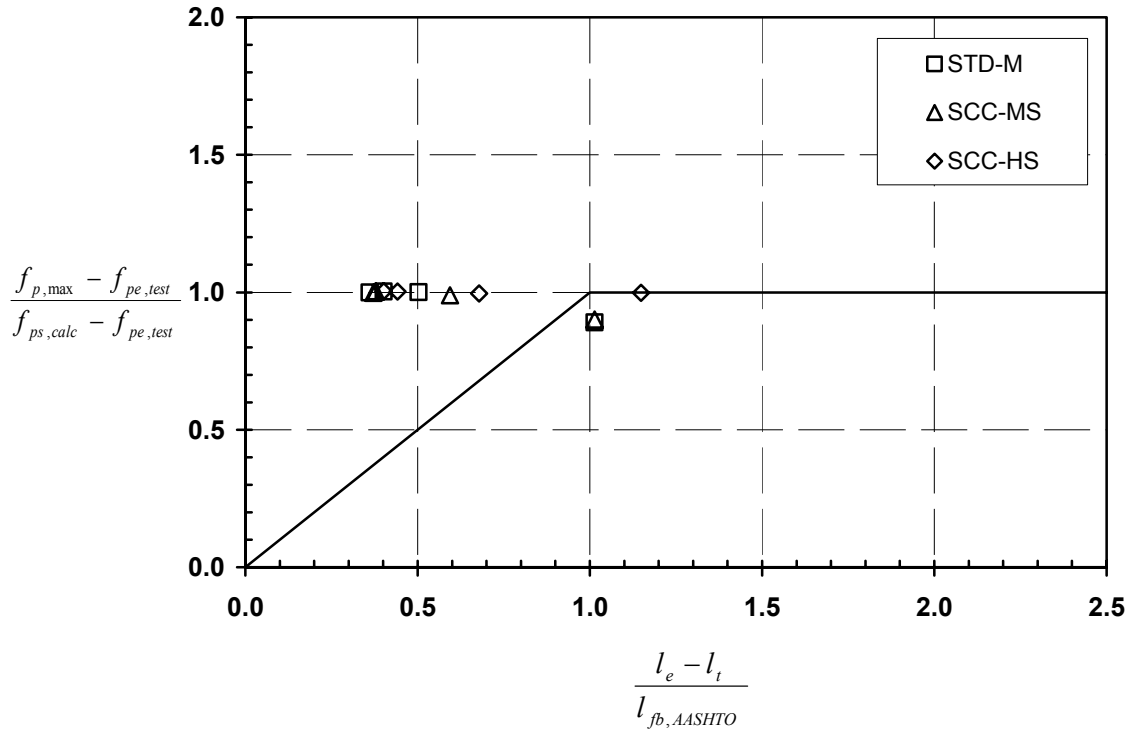lengths indicates excellent bond performance for all of the concrete mixtures.

Figure 6-27: Flexural Bond Performance Relative to AASHTO LRFD Flexural Bond Length

Figure 6-27 illustrates the flexural bond performance of the tested girder ends

with respect to the AASHTO LRFD flexural bond length. The majority of the points fall

above and to the left of the line, representing conservative results. These tests exhibited

flexural bond lengths shorter than the AASHTO LRFD flexural bond length, yet full

development of the maximum strand stress was achieved. Once again, the line represents

the build up of the strand stress from the effective stress to the maximum stress over the

flexural bond length. As discussed above, the two points falling below the line represent

two tests that were prematurely stopped before the maximum strand stress could be

achieved.

177

6.8.3 Service Load Level Performance

As discussed previously, each flexural test included loading the girder up to a predetermined service level load several times within the test. This load corresponded to the service-level design load used by ALDOT for bridge girders, which represents the applied load necessary to cause zero stress in the bottom fiber of the girder at the critical sections. The objective of this was simply to investigate the girder's response to service level loads before and after being damaged. For discussion purposes, the deflections at the three service load cycles applied at the beginning of each test are presented in Table 6-5. As stated previously, all reported deflections were measured at the middle of the two load points. The average of these deflections was calculated for each test as $\Delta_{s,avg}$ and then compared to the predicted deflection at service load, $\Delta_{s,calc}$. The predicted deflections at service load were calculated based upon a moment-curvature analysis.

Table 6-5: Initial Service Load Deflections
Note: *Indicates Deflections Measured with Incorrect Span Length

Test Girder	Initial Service Load, Δ_s (in.)			$\Delta_{s,avg}$ (in.)	$\Delta_{s,calc}$ (in.)	$\dfrac{\Delta_{s,avg}}{\Delta_{s,calc}}$
	1	2	3			
STD-M-1W	0.204	0.207	0.207	0.206	0.186	1.11
STD-M-1E	0.116	0.121	0.121	0.119	0.089	1.34
STD-M-2E	0.106	0.105	0.105	0.105	0.082	1.28
STD-M-2W	0.119	0.121	0.122	0.121	0.081	1.49
SCC-MS-1W	0.187	0.193	0.194	0.191	0.186	1.03
SCC-MS-1E	0.118	0.121	0.122	0.120	0.089	1.35
SCC-MS-2E	0.118	0.120	0.120	0.119	0.082	1.46
SCC-MS-2W	0.134	0.142	0.143	0.140	0.081	1.72
SCC-HS-1W	0.186	0.187	0.188	0.187	0.180	1.04
SCC-HS-1E*	0.154	0.157	0.158	0.156	0.103	1.52
SCC-HS-2E	0.107	0.111	0.112	0.110	0.076	1.45
SCC-HS-2W	0.125	0.126	0.127	0.126	0.076	1.66

Table 6-5 indicates that, for all tests, the observed deflections during flexural testing were not accurately predicted, especially for the shorter embedment length tests. For the test in each set with the longest embedment and span length, i.e. the most "flexural" tests (1W), the observed deflections were only 3 to 11 percent higher than the predicted deflection. However, for the shorter embedment length tests, the observed deflections ranged from 28 to 72 percent higher than the predicted deflections. The primary reason for the large discrepancy is that, for the shorter embedment length tests, shear deformations contribute significantly to the overall deflection at the location of measurement. However, shear deformations were neglected when computing the predicted deflections.

As shown above, the "flexural" (1W) tests produced reasonably accurate deflection results when compared to the usual "plane sections remain plane" type of analysis. The loading and support configuration during these tests was most representative of the loading that will generate significant deflections in an actual bridge girder. As a result, further discussion of the stiffness characteristics observed during only these (1W) tests is warranted. Figure 6-28 through Figure 6-30, shown below, illustrate load vs. deflection plots for the three most deflection-sensitive tests. The data on these plots represent only the first three load cycles up to the service load, P_s.
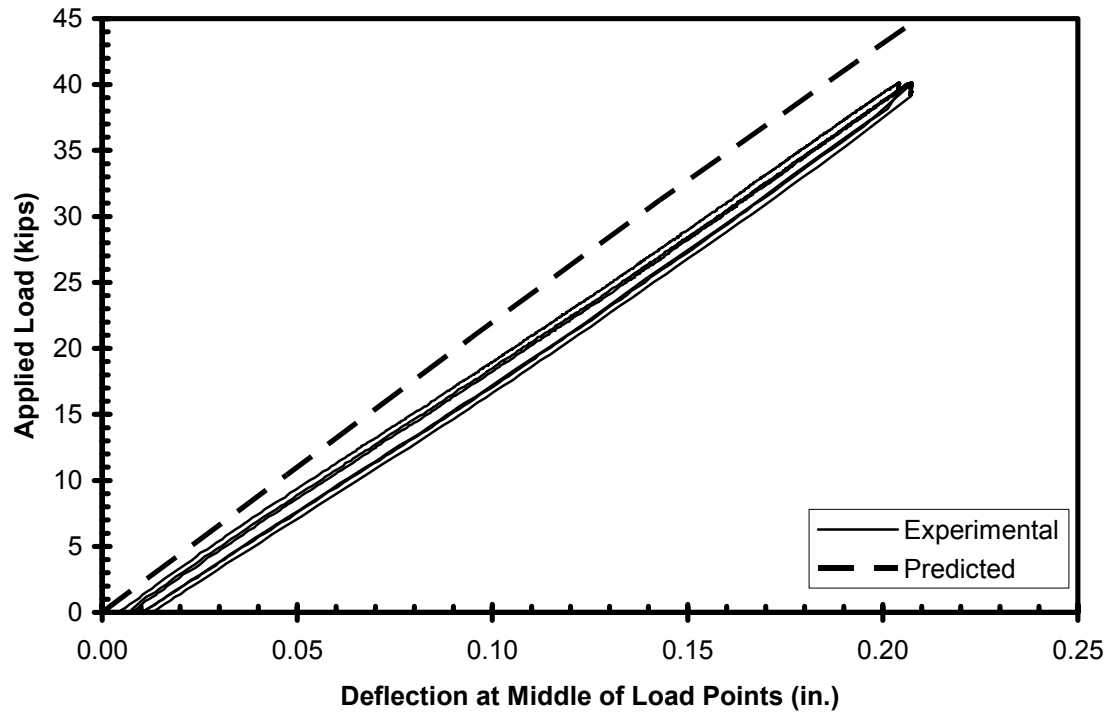
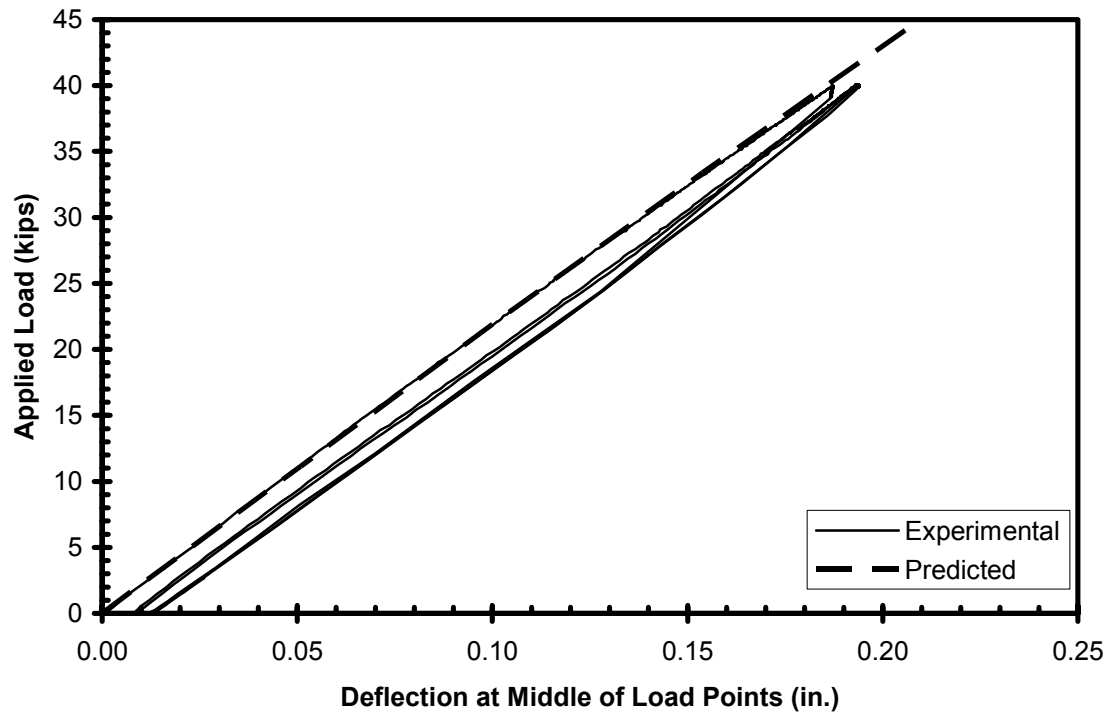**Figure 6-28: Service Loads vs. Deflection for STD-M-1W**

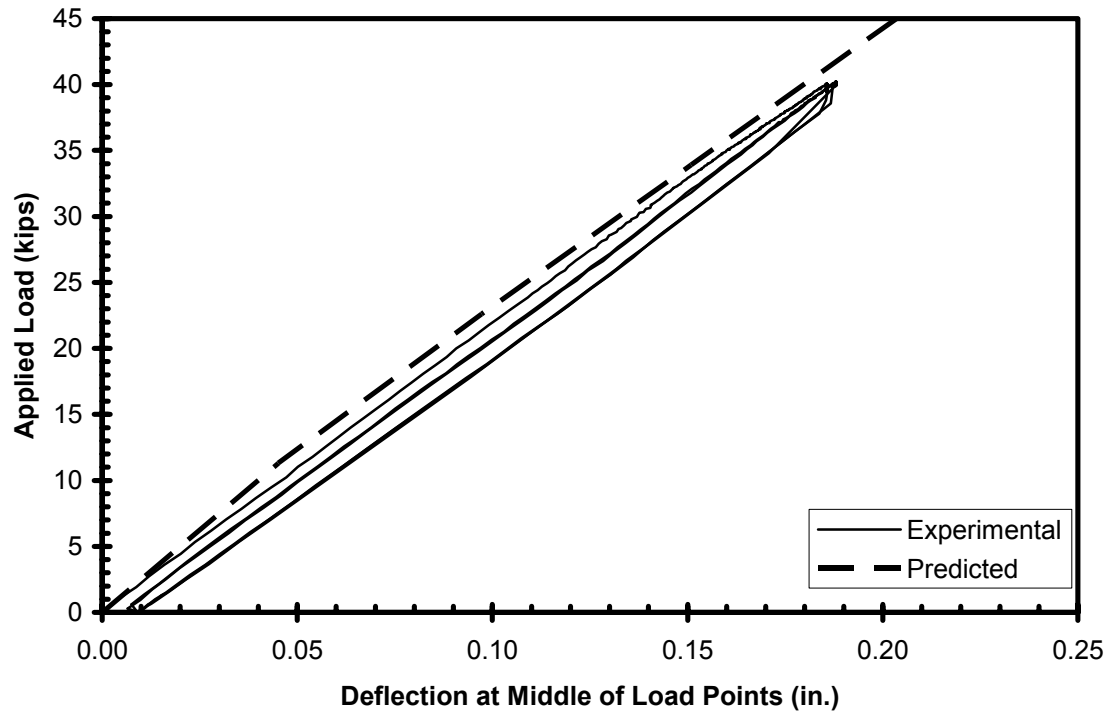**Figure 6-29: Service Loads vs. Deflection for SCC-MS-1W**

Figure 6-30: Service Loads vs. Deflection for SCC-HS-1W

The three load vs. deflection plots above are within the elastic region, and can be used to illustrate the stiffness of the tested girder end. Ideally, the experimental plot should fall on top of the predicted line for both loading and unloading. It can be seen that the plots are only slightly underneath the predicted line, but follow it very well. This suggests that the stiffness of these girders was very well predicted. It can also be seen that although the girder was loaded several times, the plot does not deviate significantly. This suggests no loss of stiffness within the girder due to service level loadings. A slightly higher and more accurately predicted stiffness is apparent for the two SCC girders when compared to the conventional concrete girder.

181

6.8.4 Cracking Load Performance

Table 6-6 presents a summary of the results from the flexural test program at the cracking moment for each tested girder end. The experimental cracking moment, M_{cr}, observed during each test and the predicted cracking moment, $M_{cr,calc}$, are shown. The predicted cracking moment, $M_{cr,calc}$, was calculated based upon the strain compatibility analysis using nonlinear material properties described previously. A modulus of rupture or cracking stress at the extreme tensile fiber was assumed to be $7.5\sqrt{f'_c}$ for the analysis, where f'_c was obtained from compressive strength tests of 6 in. by 12 in. cylinders performed at the time of flexural testing. The ratio of the actual cracking moment to the predicted cracking moment is presented. In addition, the apparent modulus of rupture, $f_{r,test}$, which was back-calculated based upon the actual test cracking moment, is reported. The apparent modulus of rupture is also reported as a multiple of $\sqrt{f'_c}$ for each test. For comparison purposes, the modulus of rupture obtained from third-point loading tests, according to ASTM C 78, of 6 in. by 6 in. by 20 in. beams cast at the time of girder casting is reported as a multiple of $\sqrt{f'_c}$ for each type of concrete. Each value reported is the average of three beams cast from the same concrete as girder 1 for each set of girders. Both air-cured simple beams and moist-cured simple beams were tested for each concrete mixture as evident in the table.

Table 6-6: Summary of Cracking Load Performance

Test Girder	M_{cr} (kip-ft)	$M_{cr,calc}$ (kip-ft)	$\dfrac{M_{cr}}{M_{cr,calc}}$	$f_{r,test}$ (ksi)	$\dfrac{f_{r,test}}{\sqrt{f'_c}}$	$\dfrac{f_{r,air}}{\sqrt{f'_c}}$	$\dfrac{f_{r,moist}}{\sqrt{f'_c}}$
STD-M-1W	473.1	474.1	1.00	0.611	7.5		
STD-M-1E	485.8	484.6	1.00	0.619	7.5	11.0	13.5
STD-M-2E	490.6	492.8	1.00	0.595	7.4		
STD-M-2W	481.8	495.6	0.97	0.547	6.8		
SCC-MS-1W	462.9	501.0	0.92	0.543	5.8		
SCC-MS-1E	471.7	511.7	0.92	0.536	5.7	8.9	15.1
SCC-MS-2E	465.4	514.1	0.91	0.508	5.3		
SCC-MS-2W	469.8	516.3	0.91	0.520	5.4		
SCC-HS-1W	474.0	507.7	0.93	0.702	6.1		
SCC-HS-1E	475.7	512.4	0.93	0.687	6.0	8.2	17.3
SCC-HS-2E	477.2	523.0	0.91	0.640	5.7		
SCC-HS-2W	469.4	524.5	0.89	0.598	5.3		

Table 6-6 indicates that cracking moments for the conventional concrete girders were very well predicted. The cracking moment was predicted within 1 percent for three of the four tests on the conventional concrete girders, and the fourth was only 3 percent high. However, the cracking moments for the SCC girders were not as well predicted. Actual cracking moments were 8 to 11 percent lower than the predicted values. For all tests, the apparent modulus of rupture was less than the values obtained from the simple flexural beam tests.

The apparent modulus of rupture values ranging from $5.3\sqrt{f'_c}$ to $6.1\sqrt{f'_c}$ for the SCC girders were significantly less than the conventional concrete mixture apparent modulus of rupture values. A decrease in the values obtained from the flexural tests of the air-cured 6 in. by 6 in. by 20 in. beams was also seen for the SCC mixtures with modulus of rupture values of $8.9\sqrt{f'_c}$ and $8.2\sqrt{f'_c}$ for the SCC, as compared to

$11.0\sqrt{f'_c}$ for the conventional concrete mixture. The exact opposite results were seen in the flexural tests of the moist-cured 6 in. by 6 in. by 20 in. beams. Modulus of rupture values of $15.1\sqrt{f'_c}$ and $17.3\sqrt{f'_c}$ for the SCC mixtures were greater than the $13.5\sqrt{f'_c}$ value obtained from the conventional concrete mixture

This data suggests a possible decrease in flexural tensile strength or modulus of rupture associated with SCC mixture proportioning, except in the case of moist-cured specimens. It can also be seen that apparent modulus of rupture values tend to be less than predicted values. However, the effects of deck shrinkage over time were not accounted for. As the deck concrete dries, shrinkage of the deck concrete relative to the girder concrete can impose tensile stresses on the bottom concrete fibers of the girder. Without accounting for this induced tensile strain, an apparent modulus of rupture less than anticipated will be observed. Nevertheless, this does not explain why the SCC girders resulted in an apparent decrease in flexural tensile strength over the conventional concrete girders. All in all, it is important to note that current ALDOT design practices for bridge girders result in zero stress in the bottom fiber at service level loads. This effectively nullifies the issue of possible decreased modulus of rupture associated with bridge girders cast with SCC.

6.9 DISCUSSION OF DECK SEPARATION AND SLIP

During six of the twelve flexural tests, a separation and horizontal displacement, or "slip", of the cast-in-place (CIP) deck relative to the girder was observed. This separation and slip were only observed in SCC girders and can be attributed to inadequate shear transfer between the girder and the CIP deck. More specifically, it is believed that

the failure to achieve proper interface surface roughness on the finished top surface of the SCC girders was a significant factor. This section presents a discussion concerning horizontal shear resistance, relevant code design methods, and the results obtained in this study.

6.9.1 Horizontal Shear Resistance

Whenever two elements of a concrete member are cast at separate times, adequate bond along the interface of the two elements is essential if the composite member is to resist externally applied loads as a single structural element. Horizontal shear resistance refers to a composite member's ability to transfer shear stresses across an interface. Factors contributing to the transfer of shear stresses and resistance against shear displacements (slip) along the interface are cohesion, interlock, and shear friction developed by the force in the reinforcement crossing the plane of the interface (MacGregor and Wight 2005).

Cohesion refers to the chemical bond formed between the two concrete elements of the member. As long as the interface surface is free of laitance prior to casting of the second element, cohesion can provide a significantly strong bond. When the interface surface is intentionally roughened prior to casting of the second concrete element, bond between the two elements is enhanced by interlock. After the cohesion bond has failed and interface separation begins to occur, a tension force is induced into the reinforcement, if any, crossing the plane of the interface. This tension force is balanced by compressive stresses on the interface surfaces, which, in turn, are accompanied by frictional forces. These frictional forces then work to resist further shear displacements.

185

This phenomenon is referred to as shear friction (MacGregor and Wight 2005). It is important to note that the effects of shear friction are amplified with increased interface surface roughness.

The structural performance of a composite bridge girder is highly dependent on its ability to adequately transfer shear stresses across its deck interface. In members with large interfacial contact areas, bond through cohesion and interlock alone may be sufficient. However, the top surface of an I-shaped bridge girder is usually relatively thin and requires the use of transverse reinforcement to produce shear-friction forces adequate to sufficiently transfer the shear stresses. In the design of this interface shear reinforcement, the structural designer should take into account not only the total amount of steel crossing the interface, but also the surface condition of the interface prior to casting of the second element.

6.9.2 Segmental Shear Friction Approach

The design for horizontal shear resistance of the Type I AASHTO girders used in this study can be approached two different ways. The first will be referred to as the segmental shear friction approach and can be found in both the AASHTO LRFD (Section 5.8.4) and the ACI 318-05 (Section 11.7.4) design codes. For this method, a total number of reinforcement ties needed to adequately transfer shear stresses along a particular segment of the girder is determined. This segment is most commonly taken as a length between a point of inflection and a point of maximum moment. In other words, individual segments of the girder are examined separately and are separately designed to provide sufficient horizontal shear resistance based upon the interface shear demand.

In order to fully comprehend this method, a discussion concerning the calculation of the interface shear demand, V_{ui}, for each segment must be presented. Figure 6-31 represents a free-body diagram of an individual girder segment. The interface region between the girder and the CIP deck, along with the shear forces transferred between the two can be seen. In this method a segment of the girder between the inflection point (i.e. support location of a simply supported beam) and the point of maximum bending moment is considered. Because the moment is zero at the inflection point, equilibrium of the deck element dictates that the total amount of interface shear force, V_{ui}, that must be transferred over this segment is equal to the net compressive force resisted by the slab at the maximum-moment section as shown. Upon examination of the maximum-moment section, it can be seen that the net compressive force can be calculated by simply dividing the maximum moment, M_{max} by d_v. Per AASHTO LRFD Commentary (C5.8.4.2), d_v can be taken as the distance between the centroid of the tension steel and the mid-thickness of the slab.
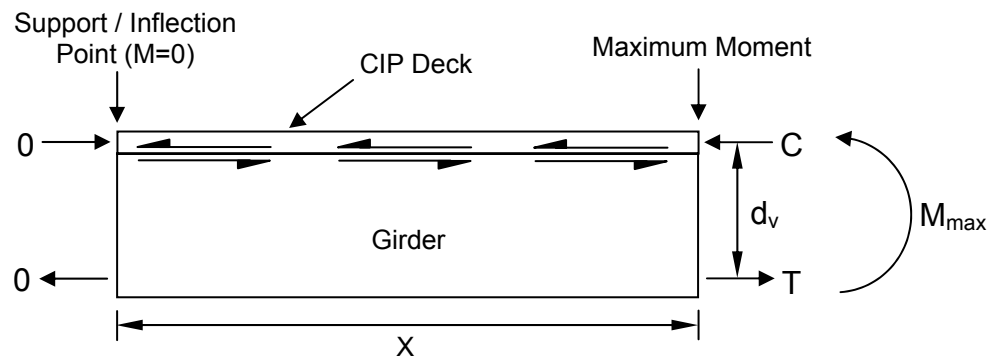
Figure 6-31: Segmental Shear Friction Approach

Therefore, the calculation for the interface shear force demand, V_{ui}, along this segment is as given below in Equation 6-4. It is important to note that this method of

reasoning requires the neutral axis to be located within the CIP deck, which at ultimate

strength was the case for all girders used in this study.

$$V_{ui} = \frac{M_{max}}{d_v}$$ **Equation 6-4**

The calculation of the interface shear resistance, V_{ni}, is similar for both the

AASHTO LRFD and the ACI 318-05 design codes. Both codes assume that the interface

shear resistance for the segment is directly proportional to the net normal clamping force

provided by the total amount of interface reinforcement through the use of a friction

coefficient. This friction coefficient is dependent upon the surface condition of the

precast interface region, i.e. roughened or not roughened. However, the AASHTO LRFD

code assumes additional resistance from cohesion and interlock through the use of a

cohesion term. The relevant AASHTO LRFD and ACI 318-05 interface shear resistance

equations are presented below in Equation 6-5 and Equation 6-6, respectively.

$$V_{ni} = cA_{cv} + \mu\left(A_{vf}f_y + P_c\right)$$ **Equation 6-5**

$$V_n = A_{vf}f_y\mu$$ **Equation 6-6**

where, A_{cv} = area of concrete engaged in interface shear transfer

A_{vf} = area of interface shear reinforcement

P_c = permanent net compressive force normal to shear plane

c = cohesion factor

μ = friction factor

f_y = yield strength of shear reinforcement

The resistance values, V_{ni}, calculated using the AASHTO LRFD provisions are

considerably greater than the ACI 318-05 resistance values. In other words, ACI 318-05

188

provides more conservative estimates of the total interface shear resistance. Table 6-7

below presents the results of using the segmental shear friction approach to determine the

interface shear demand, V_{ui}, and the interface shear resistance, V_{ni}, at the maximum

moment for each flexural test performed in this study. Note that V_{ni} is dependent on

girder geometry and the total amount of reinforcement; therefore, the values for each

girder end (1W, 1E, 2E, 2W) are identical, regardless of girder concrete type.

Table 6-7: Segmental Shear Friction Interface Shear Demand and Resistance

Test Girder	Deck Slip	$V_{ui,max}$ (kips)	AASHTO V_{ni} (kips)		ACI V_{ni} (kips)	
			Rough	Not Rough	Rough	Not Rough
STD-M-1W	No	305				
SCC-MS-1W	Yes	304	603	218	168	101
SCC-HS-1W	Yes	308				
STD-M-1E	No	332				
SCC-MS-1E	Yes	318	363	129	96	58
SCC-HS-1E	Yes	309				
STD-M-2E	No	342				
SCC-MS-2E	Yes	327	391	169	192	115
SCC-HS-2E	No	323				
STD-M-2W	No	339				
SCC-MS-2W	Yes	336	646	322	446	268
SCC-HS-2W	No	337				

The relative conservatism of the ACI 318-05 code provisions is apparent in Table

6-6. All of the ACI-predicted shear resistance values, V_{ni}, are significantly less than the

corresponding AASHTO LRFD values. It is important to note that the V_{ni} values

represent ultimate shear strength levels and if exceeded, should theoretically result in

failure. Only one of the flexural tests, SCC-HS-1W, exhibited anything remotely

resembling a possible failure of load-carrying capacity due to horizontal shear. Recall for

this test at ultimate load, as the load increased, the strains in the extreme compression fiber remained relatively constant, suggesting yielding of the horizontal shear reinforcement. The test was ceased at that point.

Although no definite failure due to horizontal shear was evident, based upon the design code resistance values, it is not surprising that separation and slip of the CIP deck occurred. All of the maximum horizontal shear demand values, $V_{ui,max}$, exceeded the ACI 318 "not roughened" V_{ni} values, as well as all but one (2W) of the ACI "roughened" values. For all of these cases, except possibly SCC-MS-2W in which slip occurred, this suggests conservatism of the design code provisions, especially in ACI 318-05.

Alternatively, the AASHTO LRFD "roughened" V_{ni} values proved to exceed all of the applied $V_{ui,max}$ values. This suggests that none of the flexural tests theoretically should have failed due to horizontal shear. However, the applied $V_{ui,max}$ values were significantly high enough compared to the AASHTO LRFD "roughened" V_{ni} values to suggest possible separation. Once again, after analysis of the data and code provisions, it was not surprising to the researchers that separation and slip occurred.

6.9.3 Sectional Shear Stress Approach

The second approach applicable to the design of the horizontal shear resistance of the girders used in this study will be referred to as the sectional shear stress approach. This method can only be found in ACI 318-05 (Section 17.5). Similar to the segmental shear-friction approach, full transfer of horizontal shear between two concrete elements cast at two different times is ensured by horizontal shear strength of the contact surfaces or

properly anchored ties. Analytically, this method is focused on individual cross sections of the member for the magnitude of shear stress across the interface.

The computation of the horizontal shear force for this method is simpler than for the segmental shear friction approach. The horizontal shear force, V_{uh}, is simply taken as the magnitude of the vertical shear force at the cross section in question. This is based upon the mechanics of materials approach that the shear stress on the vertical face of an individual stress element is equal in magnitude to the shear stress on the horizontal face of that element. For the flexural testing performed in this study, the largest vertical shears were seen at the face of the supports; therefore, this cross section is ultimately the most significant.

According to the ACI 318-05 design code, the horizontal shear strength, V_{nh}, is computed based upon the conditions provided at the interface shear plane. Three separate conditions are considered: the interface surface is intentionally roughened, the interface surface is *not* intentionally roughened but minimum ties (transverse reinforcement) are provided, and the interface surface is intentionally roughened and ties are provided. The significance of this method is that it provides a means of calculating a horizontal shear resistance based upon cohesion and interlock alone (intentionally roughened). Therefore, the load event at which the CIP deck first separated can be examined. This is due to the fact that, until separation begins, the reinforcing ties provide no significant shear strength. Table 6-8 below presents the results of using the sectional shear stress approach to determine the interface shear demand, V_{uh}, and the interface shear resistance, V_{nh}, at the maximum moment for each flexural test performed in this study and at the point where

191

separation occurred in a few of the tests. It was unclear exactly when separation occurred

for several of the tests; therefore, interface shear values at separation are not reported.

Table 6-8: Section Shear Stress Interface Shear Demand and Resistance

Test Girder	Deck Slip	$V_{uh,sep}$ (kips)	$V_{uh,max}$ (kips)	V_{nh} (kips)		
				Rough	Min. Ties	Rough & Ties
STD-M-1W	No	—	66			
SCC-MS-1W	Yes	—	65	27.4	27.4	112
SCC-HS-1W	Yes	63	66			
STD-M-1E	No	—	114			
SCC-MS-1E	Yes	83	109	27.4	27.4	112
SCC-HS-1E	Yes	105	106			
STD-M-2E	No	—	156			
SCC-MS-2E	Yes	—	149	27.4	27.4	148
SCC-HS-2E	No	—	148			
STD-M-2W	No	—	155			
SCC-MS-2W	Yes	—	154	27.4	27.4	171
SCC-HS-2W	No	—	154			

While examining Table 6-8, it is important to note that for girder ends 1W and 1E

"minimum ties" that satisfied the ACI 318-05 design code were not provided. However

several relevant comparisons and conclusions can still be drawn from these values. Most

importantly, note that the shear resistance value, $V_{nh} = 27.4$ kips, for a roughened

interface surface is less than the shear demand values at initial separation, $V_{uh,sep}$. This

suggests that the actual horizontal shear resistance from cohesion and interlock alone

exceeded the code-predicted resistance without ties.

For three of the flexural tests (STD-M-1E, STD-M-2E, and SCC-MS-2E), the

$V_{uh,max}$ value exceed the "roughened-and-ties-provided" V_{nh} resistance values. This

would suggest failure due to horizontal shear in these tests; however, this was not

192

observed. In general, it can be concluded that the ACI 318-05 provisions provide

conservative predictions of interface shear strengths for all the girders tested.

6.9.4 Deck Separation and Slip Due to Interface Surface Roughness

As shown in the discussion of horizontal shear resistance and the relevant code

provisions, the interface surface condition is a major contributing factor to the horizontal

shear strength of composite members. Both the AASHTO LRFD and ACI 318-05 design

codes distinguish between a surface roughened to a ¼-in. amplitude and a *not*-roughened

surface for strength calculations. This surface roughness is typically achieved by raking

the top surface of the girder after casting. However, during the casting of the SCC

girders used for this study, surface roughening was difficult to achieve due to the fact that

the SCC simply re-consolidated after raking. This is believed by the researchers to be the

primary cause of the deck separation and slip seen during flexural testing of the SCC

girders.

Deck separation was only observed in the SCC girders: specifically, all four of the

SCC-MS girders and two of the SCC-HS girders. Figure 6-32 and Figure 6-33 show the

difference between the typical conventional concrete girder (STD) surface condition and

the typical SCC girder surface condition. The difference in effective roughening is

evident.

Figure 6-32: Typical Conventional-Slump Concrete Girder Surface
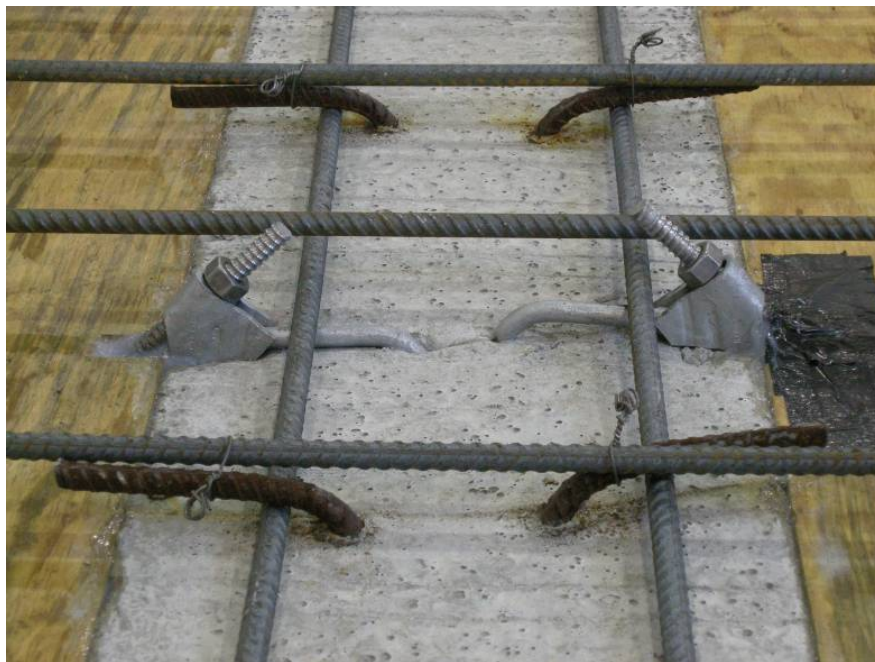
Figure 6-33: Typical SCC Girder Surface

194

As discussed previously and summarized in Table 6-6, the AASHTO LRFD "roughened" horizontal shear resistance values exceeded the applied horizontal shear for all tests. Therefore, it would be expected that the girders that were properly roughened (STD-M) would not experience any horizontal shear problems, as was the case. The SCC girders, which were not roughened properly, did exhibit horizontal shear problems, suggesting that the designers would not be able to rely on the roughened shear resistance values obtained from the relevant code provisions. This was particularly evident in the SCC-HS-1W test, in which it appeared that all of the horizontal shear capacity of the interface was exhausted, but the applied shear was only about half of the AASHTO LRFD roughened value shown in Figure 6-7. The ACI 318-05 resistance values for both cases proved to be more conservative than the AASHTO LRFD resistance values. This suggests that roughening may not be such a problem when using ACI provisions.

Considering all relevant factors in analyzing the results of this study, it must be emphasized that the girders cast with conventional concrete did not experience horizontal shear problems. However the SCC girders, especially the SCC-MS mixture, did. It is proposed by researchers that the most important factor contributing to this was the lack of interface surface roughness in the SCC girders. As a result, for AASHTO Type I girders used as composite members with a cast-in-place deck, special precautions should be taken in order to ensure that proper surface roughness is achieved. Raking of the girder top surface should be postponed until the concrete has begun to set, and the finished surface condition for the SCC girders should be inspected carefully. This will eliminate the tendency of the SCC to reconsolidate.

6.10 SUMMARY AND CONCLUSIONS

Twelve flexural tests were conducted on the six plant-cast AASHTO Type I girders used for this study. A composite, cast-in-place concrete deck was added to the girders prior to flexural testing in order to ensure a total elongation of at least 3.5 percent in the bottom row of tensile reinforcement at flexural failure. All flexural testing was conducted at the Auburn University Structural Research Laboratory in Auburn, Alabama.

Based upon an estimated development length using the relevant AASHTO LRFD code provisions, three different embedment lengths were chosen for the twelve flexural tests. These three embedment lengths were approximately equal to 110, 68, and 52 percent of the code-predicted development length. After the embedment lengths for each flexural test were determined, test configurations for each girder end were established based upon the desired failure response. Flexural loading was applied to create a region of relatively constant maximum bending moment, and consisted of cyclic loading. During flexural testing, crack patterns, crack widths, strand slip, and deflections were monitored and recorded. A summary narrative containing the relevant events and values for each flexural test was presented.

Comparisons between predicted nominal moment capacities and achieved moment capacities, as well as predicted load-displacement relationships and experimentally observed load-displacement relationships were made. Along with the presentation of the results, discussions concerning the flexural bond performance of each flexural test, the service load level performance, cracking performance, and the separation and slip of the cast-in-place concrete deck were also presented.

Several conclusions regarding flexural performance of the girders are warranted base on the results of this study:

- The ultimate load behavior of the conventional and SCC girders was well-predicted using a strain compatibility approach with nonlinear material properties.

- All tested girder ends exceeded the nominal moment capacity predicted according to the AASHTO LRFD provisions, even for strand embedment lengths approximately equal to one half of the required AASHTO LRFD development length.

- Except for issues related to interface shear resistance, the girders cast with SCC performed comparably to the girders cast with conventional concrete, which suggests that the SCC mixture proportioning had no adverse effect on the flexural testing performance at ultimate load for these girders.

- Flexural bond performance was comparable for conventional and SCC girders. These results compared favorably to flexural bond provisions of the ACI 318 and AASHTO LRFD design provisions.

- Service load deflections were well predicted for the most flexural test for each type of concrete. A slightly higher and more accurately predicted stiffness was apparent for the two SCC girders when compared to the conventional concrete girder.

- The cracking moment proved to be well-predicted for girders cast with conventional concrete, but not as well-predicted for girders cast with SCC.

- The apparent modulus of rupture for girders cast with SCC ranged from $5.3\sqrt{f'c}$ to $6.1\sqrt{f'c}$. Due to the fact that ALDOT bridge girder designs are based on a condition of no tensile stress in the bottom fiber of concrete under service load conditions, the decreased effective modulus of rupture seen in the SCC girders is not a practical problem.

- Six of the twelve flexural tests (all SCC girders) experienced deck separation and horizontal displacement relative to the girder (slip) at applied loads greater than service loads.

- Deck separation and slip was attributed to insufficient transfer of horizontal shear resulting from a lack of effective roughening of the SCC girder surfaces.

- Due to the fact that SCC can reconsolidate after raking, special precautions should be taken in order to ensure proper roughening of SCC girder surfaces.

CHAPTER 7

SUMMARY AND CONCLUSIONS

7.1 SUMMARY

The general use of self-consolidating concrete (SCC) is becoming increasingly popular within the concrete industry. Its ability to flow freely and consolidate around reinforcement without the need for external vibration makes it an attractive alternative. However, few research studies have been employed to investigate its use in precast, prestressed members. Specifically, little data quantifying the structural performance of SCC is available. The ability of the industry to consistently produce satisfactory plant-cast SCC members must also be investigated. When approved, implementation of SCC within the precast, prestressed industry can provide benefits such as increased productivity, increased worker safety, lower labor costs, and improved product aesthetics.

This study was performed as part of a larger investigation undertaken by the Auburn University Highway Research Center and sponsored by the Alabama Department of Transportation (ALDOT) of the use of SCC for precast, prestressed bridge girders. Extensive evaluation of the bond behavior between SCC and the prestressing strands was explored in the previous two phases in the form of transfer length and development length testing on small-scale specimens. The results of these two studies were reported by Swords (2005) and Levy (2007). The testing described in this thesis was performed to

determine whether the results of the earlier phases are applicable to full-scale precast, prestressed bridge girders. The general structural performance of SCC in prestressed girders, and the ability to successfully produce these girders at a standard prestressing plant, was also examined.

The research performed in this study encompassed transfer length and flexural testing of six precast, prestressed AASHTO Type I bridge girders. One conventional-slump concrete mixture and two SCC mixtures were used to cast these girders. Two 40-ft girders were cast for each mixture. The conventional concrete mixture was a moderate-strength mixture—similar to that used by ALDOT for precast, prestressed members—with a compressive strength at prestress transfer of approximately 4,800 psi. The two SCC mixtures consisted of a moderate- and a high-strength mixture with compressive strengths at prestress transfer of approximately 5,500 psi and 10,500 psi, respectively. Both SCC mixtures utilized Type III cement, 30-percent replacement with ground-granulated blast-furnace (GGBF) slag, No. 78 crushed dolomitic limestone, and natural river sand. Sand-to-aggregate ratios for the conventional concrete mixture and the SCC mixtures were approximately 0.37 and 0.46, respectively.

All girders were pretensioned with the 0.5-in. "oversized" prestressing strand commonly used in ALDOT prestressed girders. Concrete batching and girder casting were performed at the Hanson Pipe & Prestress Plant in Pelham, Alabama. A standard Moustafa pull-out test was performed in an effort to verify strand bond quality. Transfer length testing was performed at the plant as well; both immediate and long-term transfer lengths were measured. Each girder had two transfer zones, one at each end, resulting in twelve total transfer lengths. Transfer lengths were measured immediately after prestress

release and at a series of ages ranging from three days to three months after prestress transfer. The influence of concrete strength, concrete mixture type, cross-section size, and time were examined. Comparisons were made to design expressions developed in previous phases of this investigation and to current code provisions.

A strand draw-in measurement program was conducted in conjunction with the transfer length test program. Draw-in measurements were performed simultaneously with transfer length measurements and then used to predict corresponding transfer lengths. Transfer-length predictions from draw-in measurements were compared with measured transfer lengths to assess the validity of using draw-in to measure transfer length.

Flexural testing was performed on all six girders at the Auburn University Structural Research Laboratory. Prior to flexural testing, a cast-in-place composite deck was added to each girder in order to achieve large strand elongations during testing to ultimate strength. Each girder was tested twice, one test at each end, resulting in a total of twelve flexural tests. Load-displacement relationships were predicted and compared to the experimentally observed load-displacement relationships. In order to evaluate the flexural bond performance of the SCC, embedment length was varied for each test. The service-load performance and cracking strength of all twelve flexural tests was also examined. Unanticipated deck separation and slip was observed during flexural testing of several SCC girders. This behavior was investigated relative to design provisions for horizontal shear strength.

7.2 CONCLUSIONS

The conclusions presented in this section were drawn based upon the background research and experimental data of this study. Several well-established analysis techniques and procedures were utilized to analyze the experimental data. Further discussion and explanation of the analysis techniques and the conclusions drawn can be found in the relevant chapters.

7.2.1 Plant Casting of SCC Girders

Several conclusions regarding the plant casting of SCC girders are justified by the results of this study:

- Plant casting of SCC girders is feasible without the use of internal or external vibration techniques.

- Proper quality control measures must be implemented for SCC mixing and placement.

- The SCC mixtures used in this study flowed 20–30 ft. and encapsulated strands and stirrups with adequate stability.

- The girders cast with SCC exhibited smaller and shallower bug holes and surface defects than the girders cast with the conventional-slump concrete mixture.

- Formwork joints must be adequately sealed prior to casting girders with SCC.

- SCC girder top surfaces should be carefully raked after sufficient setting to ensure retention of desired surface roughening.

7.2.2 Transfer Length Testing

Several conclusions regarding transfer length were reached for this study:

202

- Transfer lengths are approximately inversely proportional to the square root of the concrete compressive strength at release.

- When normalized against the effects of prestress magnitude and concrete strength, transfer lengths tend to decrease with increasing cross-section size. This decrease is more significant at member ends subjected to sudden prestress transfer than at ends where prestress force is transferred gradually.

- When normalized against the effects of prestress magnitude and concrete strength, there is no significant difference in the transfer lengths of full-scale girders cast with conventional concrete compared to girders cast with SCC.

- Significant increases in transfer length over time were measured; long-term transfer length is difficult to accurately estimate solely based on initial transfer length measurement.

- When normalized against the effects of prestress magnitude and concrete strength, measured transfer lengths for girders cast with conventional concrete grew 10 percent more than for girders cast with SCC.

- The ACI 318-05 12.9 expression and the AASHTO LRFD expression for predicting transfer length were conservative for all the data obtained in this study; however it did not portray the trends of the data.

- The ACI 318-05 shear provision for predicting transfer length was conservative for all data with concrete strengths at prestress transfer greater than 4,800 psi; however it did not portray the trends of the data.

- Although current design provisions for predicting transfer lengths produce conservative results, it is necessary to include a concrete strength parameter in

order to predict transfer lengths that portray the trends of data observed across a full range of practical concrete strengths.

- The expressions recommended by Levy (2007) for predicting transfer lengths are conservative for strength design of ALDOT bridge girders and portray the trends of the data obtained in this study. The expressions proved to effectively reflect the influence of concrete strength, and are given in Table 7-1.

Table 7-1: Transfer Length Expressions Recommended for Strength Design

Release Method	Concrete Type	Transfer Length
Gradual	Standard & All SCC	$l_t = 0.64 ksi^{-0.5} \dfrac{f_{pt}}{\sqrt{f'_{ci}}} d_b$
Sudden	Standard & SCC w/ ≤ 30% slag	$l_t = 0.78 ksi^{-0.5} \dfrac{f_{pt}}{\sqrt{f'_{ci}}} d_b$
	Standard & SCC w/ > 30% slag	$l_t = 1.02 ksi^{-0.5} \dfrac{f_{pt}}{\sqrt{f'_{ci}}} d_b$

7.2.3 Draw-In Testing

Several conclusions regarding strand draw-in were reached for this study:

- Little reliable proportionality existed between the DEMEC-measured transfer lengths and strand draw-in values.

- The equation $l_t = \dfrac{2E_p}{f_{pbt}} l_{draw-in}$ failed to reliably predict transfer lengths comparable to DEMEC-measured transfer lengths.

- Concrete mixture type (conventional concrete or SCC) failed to produce significantly different results when predicting transfer lengths from draw-in values.

- In general, there was no evident link between initial draw-in values and long-term DEMEC-measured transfer lengths.

- Due to the relatively small sample size and inconsistent correlations of the data collected in this study, it is not recommended that strand draw-in be used as a quality control measure for precast, prestressed operations.

7.2.4 Flexural Testing

Several conclusions regarding flexural performance of the girders were reached for this study:

- All tested girder ends exceeded the nominal moment capacity predicted according to the AASHTO LRFD provisions, even for strand embedment lengths approximately equal to one half of the required AASHTO LRFD development length.

- SCC mixture proportioning had no adverse effect on the flexural testing performance at ultimate load for the girders used in this study.

- The ultimate load behavior of the conventional and SCC girders was well-predicted using a strain compatibility approach with nonlinear material properties.

- Flexural bond performance was comparable for conventional and SCC girders. These results compared favorably to flexural bond provisions of the ACI 318 and AASHTO LRFD design provisions.

- A slightly higher and more accurately predicted service-load stiffness was apparent for the SCC girders when compared to the corresponding conventional concrete girder.

- The cracking moment proved to be well-predicted for girders cast with conventional concrete, but slightly overpredicted for girders cast with SCC.

- The SCC girders exhibited less horizontal shear resistance than the conventional concrete girders; therefore, proper roughening of SCC girder surfaces needs to be addressed.

7.3 RECOMENDATIONS FOR FUTURE STUDY

Although the research presented in this study and the previous two phases of this investigation provided a comprehensive study of SCC for use in prestressed members, further work/research is recommended to supplement this work before SCC can be implemented into ALDOT bridge girder productions.

Future work should include:

- Construction of a multi-span bridge on a low-importance road with SCC girders supporting one span and conventional concrete girders supporting the rest. Instrumentation of all spans, load testing, and long-term monitoring should be used to make quantifiable comparisons.

- Development of implementation recommendations/guidelines for the use of SCC in ALDOT precast, prestressed bridge girders based upon the results of all the relevant studies performed in this investigation.

- Development of training workshops for ALDOT to present relevant properties of SCC, its production, and precautions that need to be followed in order to ensure a high-quality end product.

REFERENCES

AASHTO. 2007. *AASHTO LRFD Bridge Design Specifications: Customary U.S. Units.* 3rd ed. Washington D.C.: American Association of State Highway and Transportation Officials (AASHTO).

AASHTO. 2002. *Standard Specifications for Highway Bridges.* 16th ed. Washington D.C.: American Association of State Highway and Transportation Officials (AASHTO).

AASHTO. 1998. *AASHTO LRFD Bridge Design Specifications: Customary U.S. Units.* 2rd ed. Washington D.C.: American Association of State Highway and Transportation Officials (AASHTO).

ACI 318. 2005. "Building Code Requirements for Structural Concrete (ACI 318-05) and Commentary (ACI 318R-05)." Farmington Hills, Michigan: American Concrete Institute (ACI).

Anderson, A. R., and R. G. Anderson. 1976. An Assurance Criterion for Flexural Bond in Pretensioned Hollow Core Units. *ACI Journal, Proceedings* 73, no. 8: 457 – 464.

Barnes, R. W., J. W. Grove, and N. H. Burns. 2003. Experimental Assessment of Factors Affecting Transfer Length. *ACI Journal* 100, no. 6: 740 – 748.

Barnes, R. W., N. H. Burns, and M. E. Kreger. 1999. "Development Length of 0.6-Inch Prestressing Strand in Standard I-Shaped Pretensioned Concrete Beams." *Research Report No. 1388-1.* Austin: Center for Transportation Research, The University of Texas at Austin.

Burgueño, R., and M. Haq. 2005. Development Length of Prestressing Strands in Precast/Prestressed Girders using Self Compacting Concrete. 2005 ASCE Structures Congress, New York, NY.

Collins, M. P. and Mitchell, D. 1997. Prestressed Concrete Structures. Response Publications, Montreal, Canada.

Cousins, T., D. Johnston, and P. Zia. 1990. Transfer and Development Length of Epoxy Coated Prestressing Strand. *PCI Journal* 35, no. 4: 92 – 103.

Erkmen, B., C. K. Shield, and C. E. French. 2007. Time-Dependent Behavior of Full-Scale Self-Consolidating Concrete Precast Prestressed Girders. In *Self-Consolidating Concrete for Precast Prestressed Applications*, ed. A. Schindler, D. Trejo, and R. Barnes. SP-247-12. Farmington Hills, Michigan: American Concrete Institute: 139 – 154.

FHWA. 1988. Prestressing Strand for Pretension Applications-Development Length Revisited. Memorandum, Chief, Bridge Division, Washington, D.C.

Guyon, Y. 1953. Prestressed Concrete. John Wiley and Sons, New York, N.Y.

Hamilton, H. R., T. Labonte, and M. H. Ansley. 2005. "Behavior of Pretensioned Type II AASHTO Girders Constructed with Self-Consolidating Concrete." In *Ned H. Burns Symposium on Historic Innovations in Prestressed Concrete,* ed. B. W. Russell and S. P. Gross. Farmington Hills, Michigan: American Concrete Institute: 252 – 270.

Hanson, Norman W. 1969. Influence of Surface Roughness of Prestressing Strand on Bond Performance. *PCI Journal* 14, no. 1: 32 – 45.

Hanson, N. W. and P. H. Kaar. 1959. Flexural Bond Tests of Pretensioned Prestressed Beams. *ACI Journal. Proceedings* 55, no. 7: 783 – 802.

Haq, M. 2005. Effect of Self Consolidating Concrete Mix Proportioning on Transfer and Development Length of Prestressing Strands. M.S. Thesis, Michigan State University.

Hegger, J., S. Bülte, B. Kommer. 2007. Structural Behavior of Prestressed Beams Made With Self-Consolidating Concrete. *PCI Journal* 52, no. 4: 34 – 42.

Janney, J. R. 1954. Nature of Bond in Pre-Tensioned Prestressed Concrete. *ACI Journal. Proceedings* 50, no. 9: 717 – 736.

Kaar, P. H., R. W. LaFraugh, and M. A. Mass. 1963. Influence of Concrete Strength on Strand Transfer Length. *PCI Journal* 8, no. 5: 47 – 67.

Kavanaugh, Bryan. 2007. Creep Behavior of Self-Consolidating Concrete. M.S. Thesis, Auburn University.

Khayat, K. H. N. Petrov, E. K. Attiogbe, and H. T. See. 2003. "Uniformity of Bond
Strength of Prestressing Strands in Conventional Flowable and Self-Consolidating
Concrete Mixtures." In *Self-Compacting Concrete: Proceedings of the Third
International RILEM Symposium,* ed. O. Wallevik and I. Nielsson. Bagneux,
France: RILEM Publications, 703 – 709.

Lane, S. N. 1998. "A New Development Length Equation For Pretensioned Strands in
Bridge Beams and Piles." *Report No. FHWRA-RD-98-116.* McLean, Virginia:
Federal Highway Administration.

Larson, K. H., R. J. Peterman, and A. Esmaeily. 2007. Bond Characteristics of Self-
Consolidating Concrete for Prestressed Bridge Girders. *PCI Journal* 52, no. 4: 44
– 57.

Levy, Kelly. 2007. Bond Behavior of Prestressed Reinforcement in Beams Constructed
with Self-Consolidating Concrete. M.S. Thesis, Auburn University.

Logan, D. R. 1997. Acceptance Criteria for Bond Quality of Strand for Pretensioned
Prestressed Concrete Applications. *PCI Journal* 42, no. 2: 52 – 90.

MacGregor, J. G., and J. K. Wight. 2005. *Reinforced Concrete: Mechanics and Design.*
4th Edition. Prentice Hall.

Mitchell, D., W. D. Cook, A. A. Kahn, and T. Tham. 1993. Influence of High-Strength
Concrete on Transfer and Development Length in Pretensioning Strand. *PCI
Journal* 38, no. 3: 52 – 66.

Naito, Clay, G. Parent, and G. Brunn. 2006. Performance of Bulb-Tee Girders Made with
Self-Consolidating Concrete. *PCI Journal* 51, no. 6: 72 – 85.

Oh, B. H., and E. S. Kim. 2000. Realistic Evaluation of Transfer Lengths in Pretensioned, Prestressed Concrete Members. *ACI Journal* 97, no. 6: 821 – 830.

Okamura, H. and Ouchi. 1999. "Self-Compacting Concrete, Development, Present Use and Future." In *Self-Compacting Concrete: Proceedings of the First International RILEM Symposium,* ed. A. Skarendahl and O. Petersson. Cachan Cedex, France: RILEM Publications, 3-14.

Ozyildirim, C. and R. T. Davis. 2007. Bulb-T Beams with Self-Consolidating Concrete on Route 33 in Virginia. *Transportation Research Record: Journal of the Transportation Research Board,* no. *2020.* 76 – 82.

PCI. 2004. *PCI Design Handbook: Precast and Prestressed Concrete.* 6th ed. Chicago: Precast/Prestressed Concrete Institute.

Peterman, R. J., J. A. Ramirez, and J. Olek. 2000. Influence of Flexure-Shear Cracking on Strand Development Length in Prestressed Concrete Members. *PCI Journal* 45, no. 5: 76 – 94.

Rose, D. R., and B. W. Russell. 1997. Investigation of Standardized Tests to Measure the Bond Performance of Prestressing Strand. *PCI Journal* 42, no. 4: 56 – 80.

Rueda, E. S., and A. J. Schokker. 2007. Evaluation of Bond Properties in Self-Consolidating Prestressed Beams. In *Self-Consolidating Concrete for Precast Prestressed Applications*, ed. A. Schindler, D. Trejo, and R. Barnes. SP-247-10. Farmington Hills, Michigan: American Concrete Institute: 117 - 122.

Russell, B. W., and N. H. Burns. 1997. Measurement of Transfer Lengths on Pretensioned Concrete Elements. *Journal of Structural Engineering* 123, no. 5: 541 – 549.

Russell, Bruce W., and Ned H. Burns. 1993. Design Guidelines for Transfer,

    Development and Debonding of Large Diameter Seven Wire Strands in

    Pretensioned Concrete Girders. *Research Report 1210-5F*. Austin: Center for

    Transportation Research, The University of Texas at Austin.

Shahawy, Mohsen. 2001. A Critical Evaluation of the AASHTO Provisions for Strand

    Development Length of Prestressed Concrete Members. *PCI Journal* 46, no. 4: 94

    – 116.

Swords, Shane. 2005. Transfer Length in Prestressed Self-Consolidating Concrete. M.S.

    Thesis, Auburn University.

Tabatabai, H. and T. J. Dickson. 1995. "The History of the Prestressing Strand

    Development Length Equation." *Report No. FHWA-RD-93-076.* McLean,

    Virginia: Federal Highway Administration.

Zia, P. and T. Mostafa. 1977. Development Length of Prestressing Strands. *PCI Journal*

    22, no. 5: 54 – 65.

Zia, P., R. A. Nunez, L. A. Mata, and H. M. Dwairi. 2005. "Implementation of Self-

    Consolidating Concrete for Prestressed Girders." In *Seventh International*

    Symposium on Utilization of High-Strength / High Performance Concrete, ed. H.

    G. Russell. Farmington Hills, Michigan: American Concrete Institute: 297 – 314.

APPENDIX A

NOTATION

Report (AASHTO LRFD)	AASHTO Standard	ACI 318-05	Description
A_{ps}	$A_s{}^*$	A_{ps}	area of prestressing steel
α	—	—	proportionality constant (not in AASHTO LRFD)
d_b	D	d_b	nominal diameter of reinforcement
d_v	—	—	distance between centroid of prestressing strand and mid-thickness of the slab
E_c	E_c	E_c	modulus of elasticity of concrete
E_p	—	—	modulus of elasticity of prestressing reinforcement
ε_{max}	—	—	strain in the bottom row of prestressing strands at maximum moment during flexural testing (not in AASHTO LRFD)
$\varepsilon_{max,\,calc}$	—	—	strain in the bottom row of prestressing strands at the nominal resistance of the member (not in AASHTO LRFD)
ε_p	—	—	strain in prestressing reinforcement (not in AASHTO LRFD)
ε_{weight}	—	—	tensile strain in prestressing reinforcement due to self weight (not in AASHTO LRFD)
f'_c	—	—	compressive strength of concrete based on cylinder tests (this report only)
f'_c	f'_c	f'_c	specified compressive strength of concrete (design codes only)
f'_{ci}	—	—	compressive strength of concrete at transfer of prestress force (this report only)
f'_{ci}	f'_{ci}	f'_{ci}	specified compressive strength of concrete at transfer of prestress force (design codes only)
f_p	—	—	stress in prestressing reinforcement (not in AASHTO LRFD)
f_{pbt}	—	—	stress in prestressed reinforcement immediately prior to transfer
f_{pe}	f_{se}	f_{se}	effective stress in prestressed reinforcement after losses
$f_{pe,test}$	—	—	effective stress in prestressed reinforcement after losses immediately prior to flexural testing (not in AASHTO LRFD)

f_{pj}	—	—	stress in prestressed reinforcement immediately after jacking
f_{ps}	f^*_{su}	f_{ps}	stress in prestressed reinforcement at the estimated nominal strength
$f_{ps,calc}$	—	—	stress in prestressed reinforcement at the estimated nominal strength calculated by strain compatibility (not in AASHTO LRFD)
$f_{p,max}$	—	—	stress in prestressed reinforcement calculated by strain compatibility at the maximum moment experienced during flexural testing (not in AASHTO LRFD)
f_{pt}	—	—	stress in prestressed reinforcement immediately after transfer
f_{pu}	f'_s	f_{pu}	specified tensile strength of prestressing reinforcement
f_r	—	f_r	concrete modulus of rupture
f_y	—	—	yield stress of steel reinforcement
I_{tr}	—	—	transformed section moment of inertia (not in AASHTO LRFD)
κ	κ	—	multiplier used in Section 5.11.4 of AASHTO LRFD
l_d	l_d	l_d	development length (only refers to nonprestressed reinforcement in AASHTO Standard and ACI 318)
$l_{d,AASHTO}$	—	—	development length estimated by ACI/AASHTO with calculated properties (not in AASHTO LRFD)
$l_{draw-in}$	—	—	prestressing strand draw-in length due to prestress transfer (not in AASHTO LRFD)
$l_{fb,ACI}$	—	—	flexural bond length according to ACI (not in AASHTO LRFD)
$l_{fb,AASHTO}$	—	—	flexural bond length according to AASHTO (not in AASHTO LRFD)
l_e	—	—	embedment length
l_t	—	—	transfer length (not in AASHTO LRFD)
M_{cr}	—	—	actual cracking moment achieved by specimen during flexural testing
$M_{cr,calc}$	—	—	predicted cracking moment according to strain compatibility (not in AASHTO LRFD)
M_{max}	—	—	maximum moment achieved by specimen during flexural testing (not in AASHTO LRFD)
M_n	—	—	predicted nominal moment capacity
$M_{n,AASHTO}$	—	—	predicted nominal moment capacity according to AASHTO LRFD specifications (not in AASHTO LRFD)
$M_{n,calc}$	—	—	predicted nominal moment capacity according to strain compatibility (not in AASHTO LRFD)
n	—	n	modular ratio
P_c	—	—	cracking load experienced during flexural load testing (not in AASHTO LRFD)
P_s	—	—	service load experienced during flexural load testing (not in AASHTO LRFD)
P_{max}	—	—	maximum load level achieved during pull-out testing (not in AASHTO LRFD)

P_{240}	—	—	load level corresponding to 240 ksi in prestressing strands (not in AASHTO LRFD)
P_{260}	—	—	load level corresponding to 260 ksi in prestressing strands (not in AASHTO LRFD)
P_{270}	—	—	load level corresponding to 270 ksi in prestressing strands (not in AASHTO LRFD)
P_{move}	—	—	load level at which strand first exhibited movement during pull-out testing (not in AASHTO LRFD)
U_t	—	—	average bond stess along transfer length (not in AASHTO LRFD)
V_{nh}	—	V_{nh}	interface shear resistance (not in AASHTO LRFD)
V_{ni}	—	—	interface shear resistance
V_{uh}	—	V_{uh}	interface shear demand (not in AASHTO LRFD)
V_{ui}	—	—	interface shear demand
σ_c	—	—	concrete stress
Δ_{ct}	—	—	total elastic shortening of concrete along transfer length (not in AASHTO LRFD)
$\Delta_{\varepsilon c}$	—	—	change in concrete strain due to transfer of prestress (not in AASHTO LRFD)
$\Delta_{\varepsilon p}$	—	—	change in steel strain due to transfer of prestress (not in AASHTO LRFD)
Δ_{fp}	—	—	change in steel stress due to transfer of prestress (not in AASHTO LRFD)
$\Delta_{p,max}$	—	—	approximate strand pull-out distance (not in AASHTO LRFD)
Δ_{pt}	—	—	total elastic shortening of strand along transfer length (not in AASHTO LRFD)
Δ_o	—	—	distance from the benchmark to the end of the girder prior to prestress release (not in AASHTO LRFD)
Δ_s	—	—	service load deflection (not in AASHTO LRFD)
$\Delta_{s,calc}$	—	—	predicted service load deflection (not in AASHTO LRFD)
Δ_t	—	—	distance from the benchmark to the end of the girder at time, t (not in AASHTO LRFD)
w_c	—	—	unit weight of concrete
Σ_o	—	—	circumference of prestressing strand (not in AASHTO LRFD)

APPENDIX B

CONCRETE MIX DESIGNS

Table B-1: STD-M Mix Design

Design Strength	
f'_{ci} = 5500 psi at 18 hours	
f'_c = 7000 psi at 28 days	
Material	Quantity per yd^3
Cement (Type III)	640 lbs
GGBF Slag (Grade 100)	0 lbs
#78 Crushed Limestone	2034 lbs
Red Bluff Sand	1110 lbs
High-Range, Water-Reducing Admixture	19.2 fl oz
Viscosity-Modifying Admixture	0 fl oz
Air-Entraining Admixture	0.6 fl oz
Retarding Admixture (Delvo)	19.2 fl oz
Water	32.4 gal

Table B-2: SCC-MS Mix Design

Design Strength	
f'$_{ci}$ = 5500 psi at 18 hours	
f'$_c$ = 7000 psi at 28 days	
Material	Quantity per yd^3
Cement (Type III)	553 lbs
GGBF Slag (Grade 100)	237 lbs
#78 Crushed Limestone	1608 lbs
Red Bluff Sand	1317 lbs
High-Range, Water-Reducing Admixture	51 fl oz
Viscosity-Modifying Admixture	16 fl oz
Air-Entraining Admixture	0.6 fl oz
Retarding Admixture (Delvo)	24 fl oz
Water	34.2 gal

Table B-3: SCC-HS Mix Design

Design Strength	
f'$_{ci}$ = 9,000 psi at 18 hours	
f'$_c$ = 13,000 psi at 28 days	
Material	Quantity per yd^3
Cement (Type III)	650 lbs
GGBF Slag (Grade 100)	279 lbs
#78 Crushed Limestone	1601 lbs
Red Bluff Sand	1267 lbs
High-Range, Water-Reducing Admixture	93 fl oz
Viscosity-Modifying Admixture	0 fl oz
Air-Entraining Admixture	0.6 fl oz
Retarding Admixture (Delvo)	28 fl oz
Water	31.2 gal

Table B-4: Cast-in-Place Deck Concrete Mix Design

Design Strength	
f'_c = 4000 psi at 28 days	
Material	Quantity per yd^3
Cement (Type I)	451 lbs
Fly Ash (Class C)	113 lbs
#57 Limestone	1900 lbs
Red Bluff Sand	1297 lbs
Air-Entraining Admixture	2.8 fl oz
WRA, Type A	16.9 fl oz
Water	32.0 gal

Table B-5: Pull-Out Block Concrete Mix Design

Design Strength	
f'_c = 3800 - 5000 psi at 18 hours (heat curing)	
Material	Quantity per yd^3
Cement (Type III)	660 lbs
#78 Crushed Limestone	2011 lbs
Red Bluff Sand	1165 lbs
Normal Range Water Reducer	15 oz
Water	278 lbs

APPENDIX C

FRESH CONCRETE PROPERTIES

Table C-1: Summary of Fresh Concrete Property Testing Results

FRESH PROPERTIES	MIXTURES					
	STD-M		SCC-MS		SCC-HS	
	-1	-2	-1	-2	-1	-2
Slump Flow (in.)	6.75	6.5	26.25	27.75	28	28.25
Unit Weight (lb/ft^3)	Unknown	Unknown	148.5	150.3	153.6	153.2
Air (%)	3.4	3	3.8	1.8	1.5	1.5
VSI	—	—	1.5	1	1	1
T-50 (sec.)	—	—	4.5	3.1	Unknown	5
J-ring (in.)	—	—	26.25	28.6	28	26.25
L-Box (H$_1$/H$_2$)	—	—	0.67	0.86	0.8	Unknown

Figure C-1: Temperature-Development Curves for Girder STD-M-1
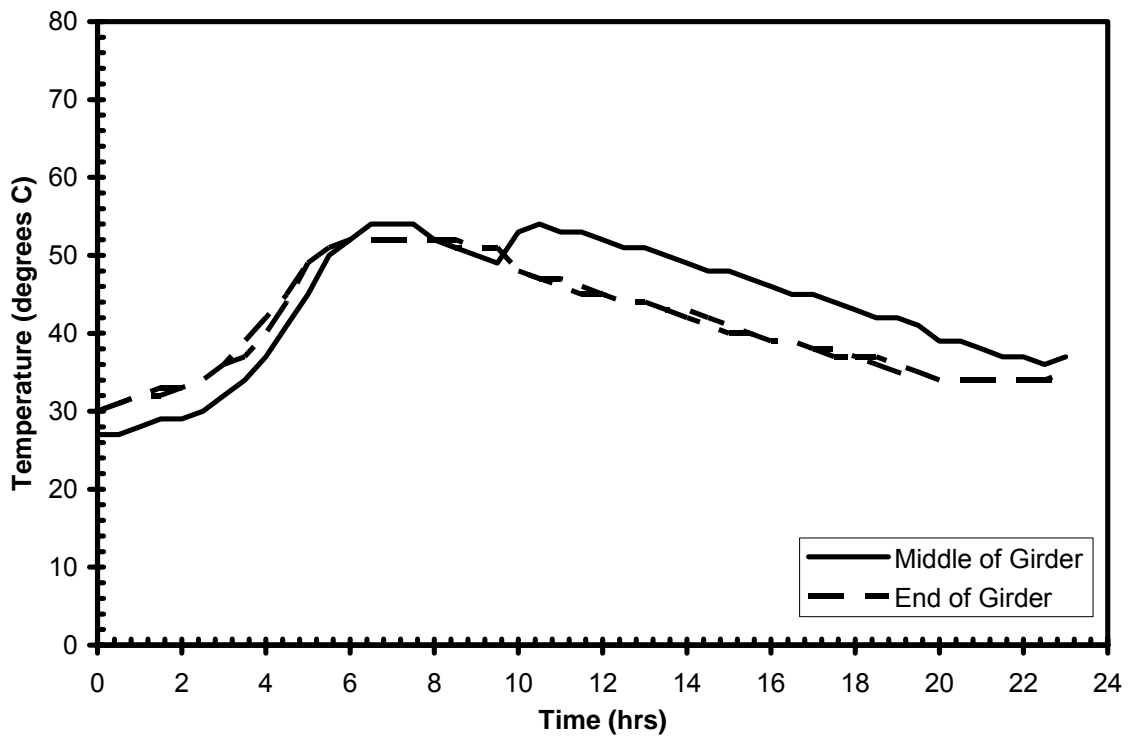
Figure C-2: Temperature-Development Curves for Girder SCC-MS-1

220
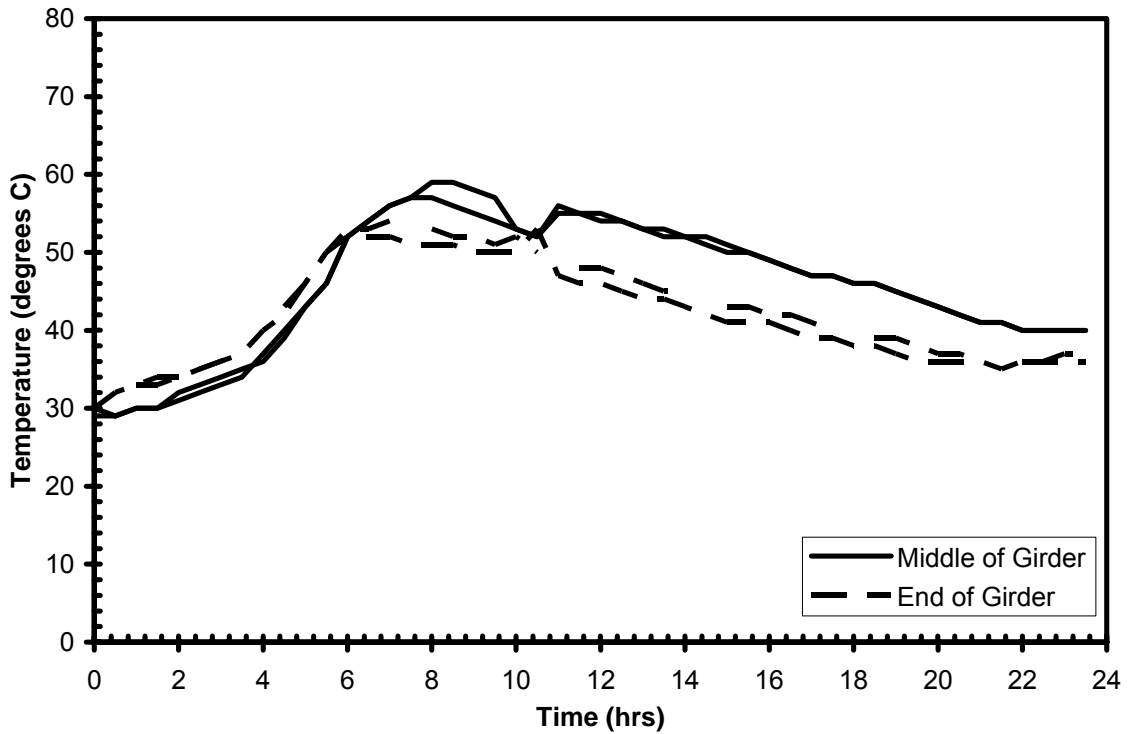
Figure C-3: Temperature-Development Curves for Girder SCC-MS-2
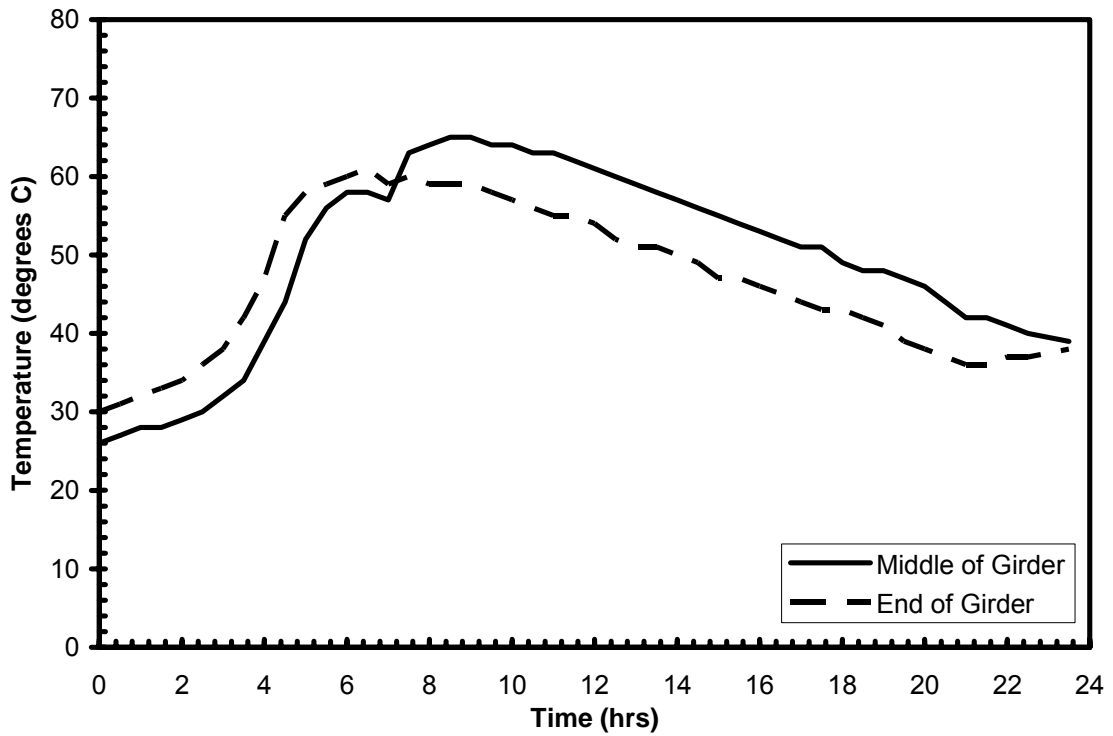
Figure C-4: Temperature-Development Curves for Girder SCC-HS-1
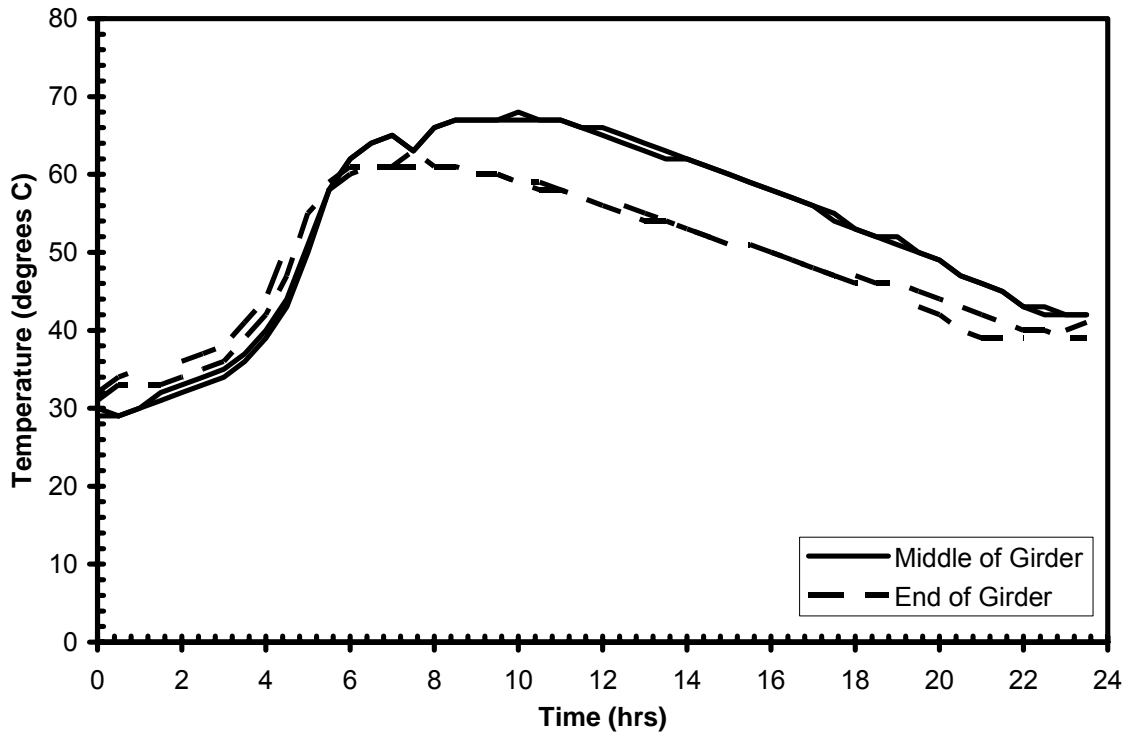
Figure C-5: Temperature-Development Curves for Girder SCC-HS-2

APPENDIX D

HARDENED CONCRETE PROPERTIES

Table D-1: Summary of Hardened Concrete Property Testing Results

HARDENED PROPERTIES		MIXTURES											
		STD-M-1		STD-M-2		SCC-MS-1		SCC-MS-2		SCC-HS-1		SCC-HS-2	
Compressive Strength		f'_c (psi)	E_c (ksi)	f'_c (psi)	E_c (ksi)	f'_c (psi)	E_c (ksi)	f'_c (psi)	E_c (ksi)	f'_c (psi)	E_c (ksi)	f'_c (psi)	E_c (ksi)
Air Cured	Transfer	4990	6050	4860	5550	5110	5200	4500	4950	10190	6750	10720	7150
	7	5790	5900	5740	6050	7110	6100	7210	5850	11710	7350	—	—
	28	6330	6350	6120	5800	8390	6450	8530	6350	12200	7500	12030	7550
	91	6610	6050	6370	6050	8840	5900	9110	6200	12340	7900	—	—
	Post-Test	6720	6150	6540	5800	8850	5850	9160	5900	13080	7100	12810	7200
Match Cured	Transfer	4780	5700	—	—	5540	5250	—	—	10430	7000	—	—
ASTM 6x12	28	6600	6750	7200	7300	9780	7400	9790	7500	13160	8600	13580	8300
CIP Deck (Post-Test)	West End	5720	4950	5370	5350	5480	5350	5080	5300	3720	4100	4820	4550
	East End	5630	5000	5410	5150	5270	5400	5210	5150	3800	3900	4680	4450
Modulus of Rupture		f_r (psi)		f_r (psi)		f_r (psi)		f_r (psi)		f_r (psi)		f_r (psi)	
Air-Cured	Post-Test	900		—	—	840		—	—	940		—	—
ASTM	Post-Test	1110		—	—	1420		—	—	1980		—	—
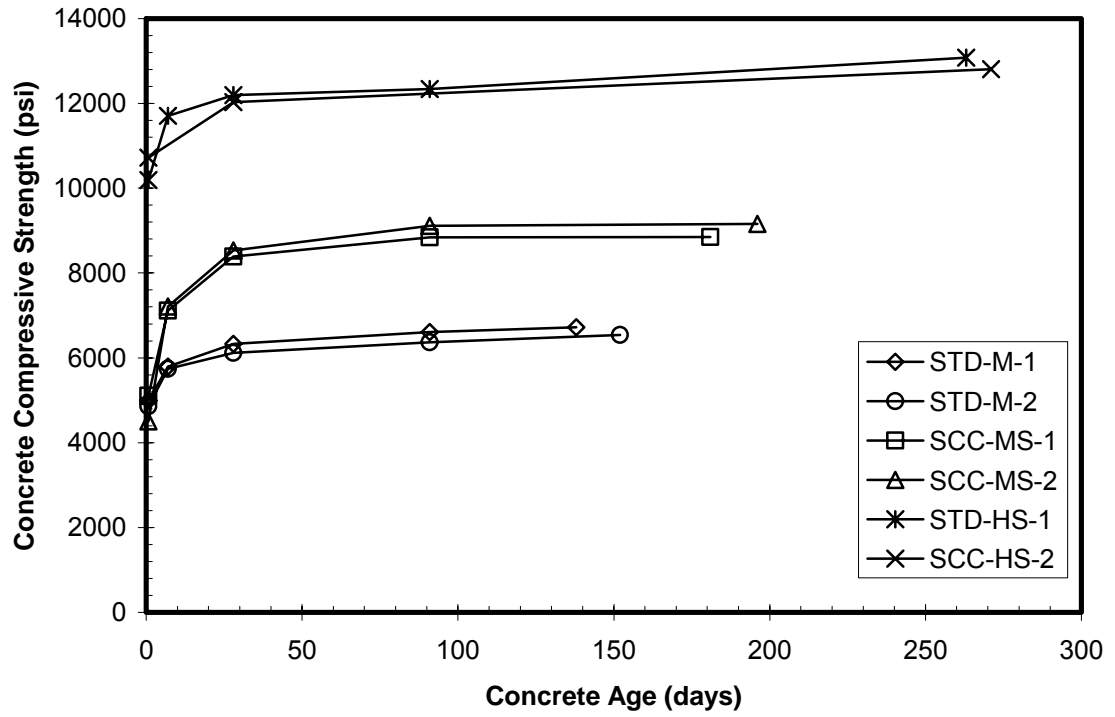
Figure D-2: Air Cured 6 x 12 Cylinder Compressive Strength vs. Concrete Age
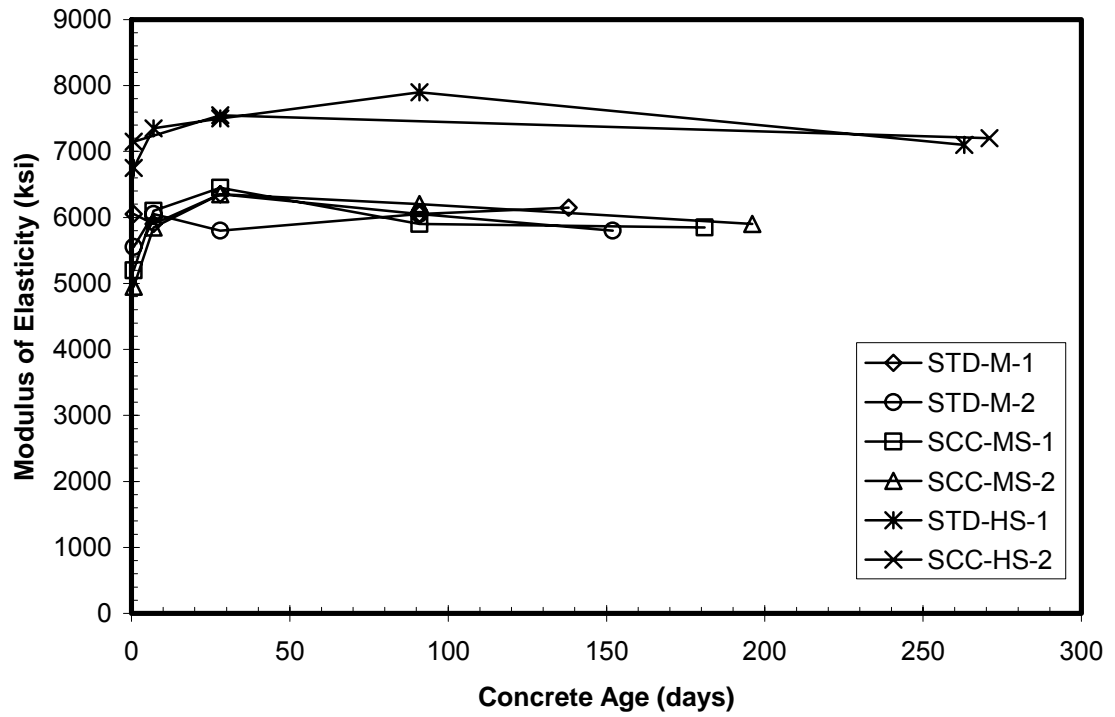
Figure D-3: Air-Cured 6 x 12 Cylinder Elastic Modulus vs. Concrete Age

APPENDIX E

EFFECTIVE STRAND PRESTRESS

Table E-1: Effective Strand Prestress at Measured Transfer Length Ages

Specimen ID	f_{pbt} ksi	f_{pt} ksi	$f_{pe,3}$ ksi	$f_{pe,7}$ ksi	$f_{pe,14}$ ksi	$f_{pe,28}$ ksi	$f_{pe,2\,mon}$ ksi	$f_{pe,3\,mon}$ ksi
STD-M-1W	200	193	186	185	184	182	178	177
STD-M-1E	200	191	184	183	182	180	176	174
STD-M-2E	200	192	185	184	183	181	176	175
STD-M-2W	200	192	185	184	184	182	177	177
SCC-MS-1W	196	187	178	177	176	177	176	175
SCC-MS-1E	196	187	178	176	176	177	175	175
SCC-MS-2E	196	187	178	177	176	177	175	175
SCC-MS-2W	196	188	179	177	176	177	175	175
SCC-HS-1W	202	195	187	185	185	186	185	184
SCC-HS-1E	202	195	187	184	185	185	185	184
SCC-HS-2E	202	195	187	184	185	186	185	184
SCC-HS-2W	202	195	187	184	185	185	185	184

APPENDIX F

CONCRETE SURFACE STRAIN PROFILES
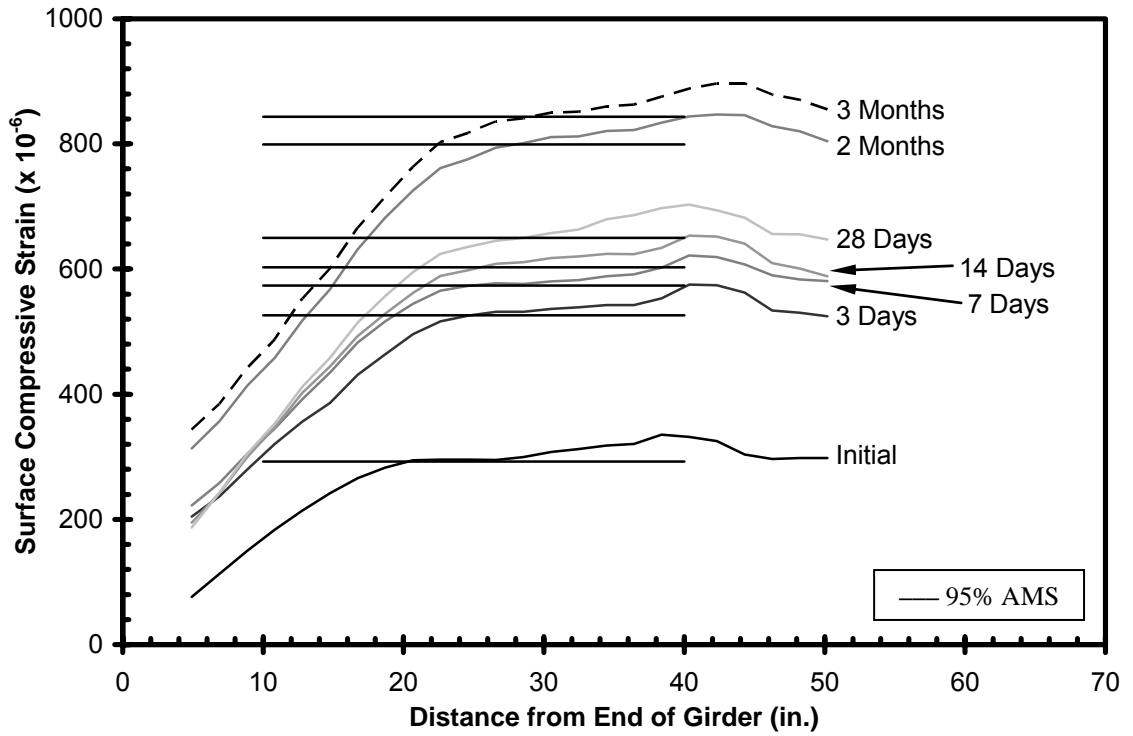
Figure F-1: STD-M-1E Measured Initial and Long-Term Strain Profiles
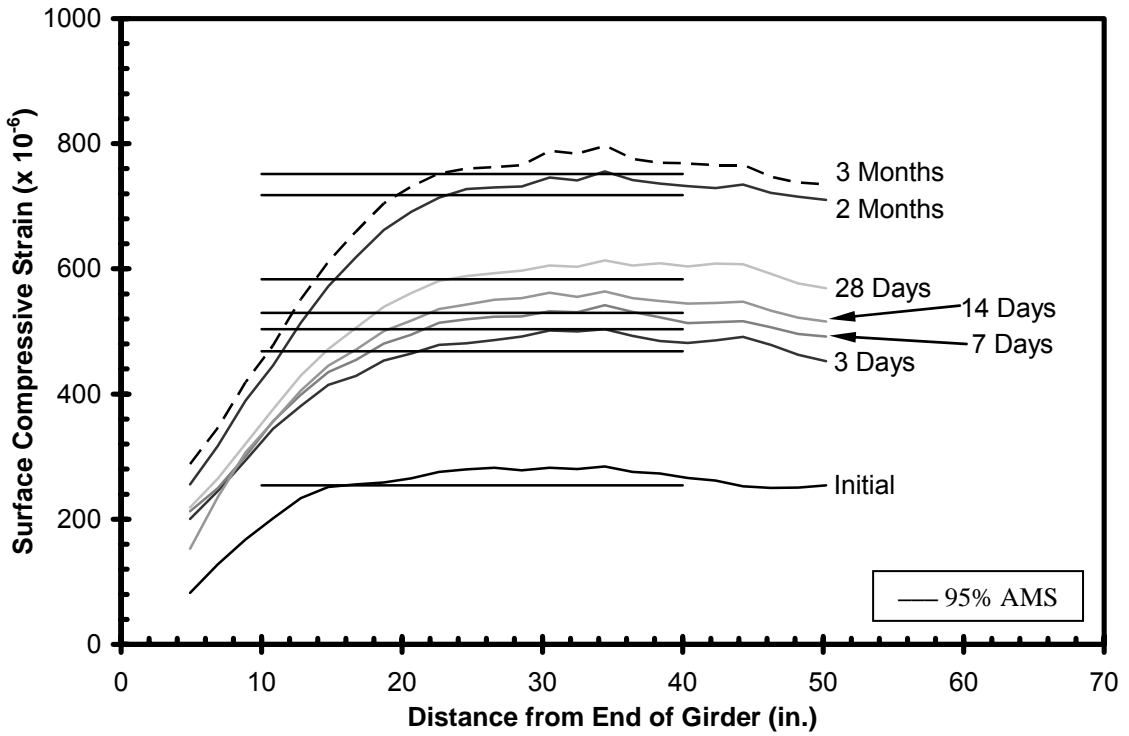
Figure F-2: STD-M-1W Measured Initial and Long-Term Strain Profiles
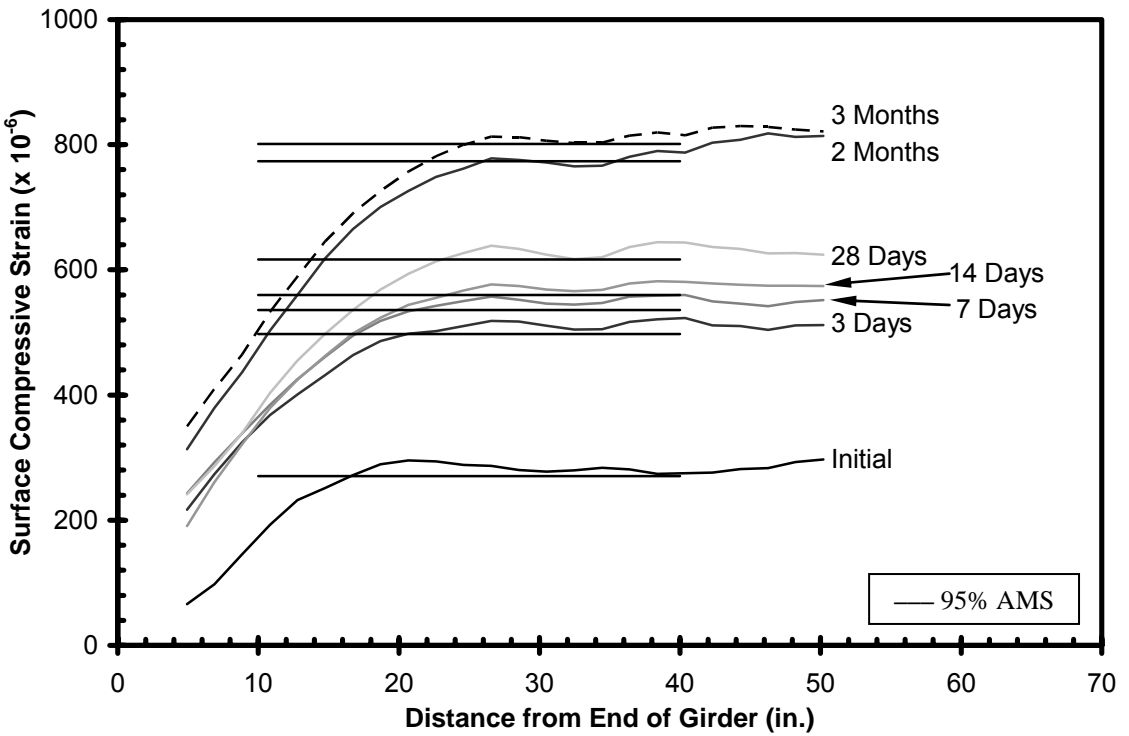
Figure F-3: STD-M-2E Measured Initial and Long-Term Strain Profiles

227
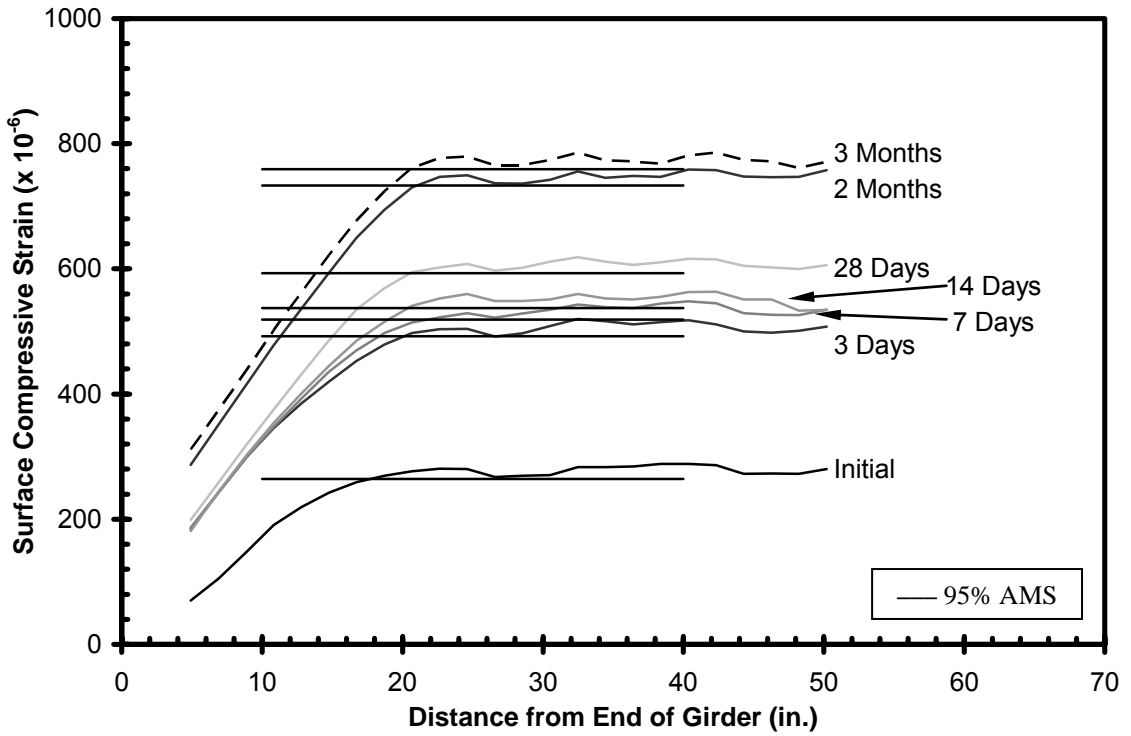
Figure F-4: STD-M-2W Measured Initial and Long-Term Strain Profiles
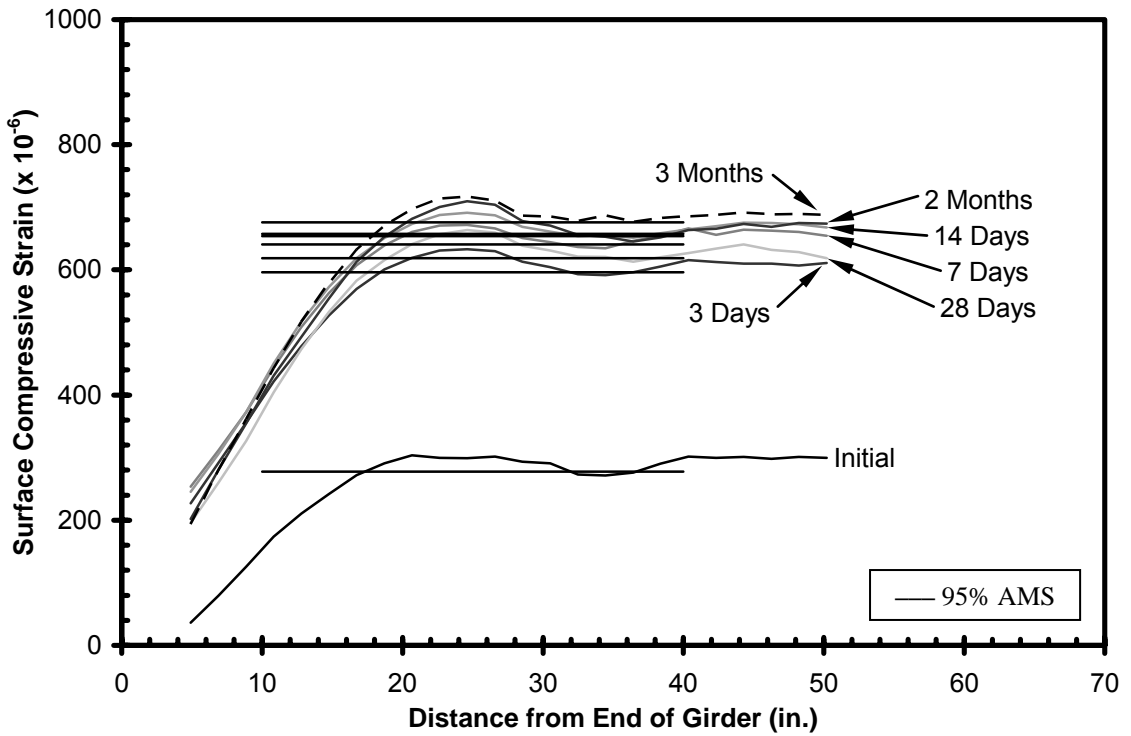
Figure F-5: SCC-MS-1E Measured Initial and Long-Term Strain Profiles
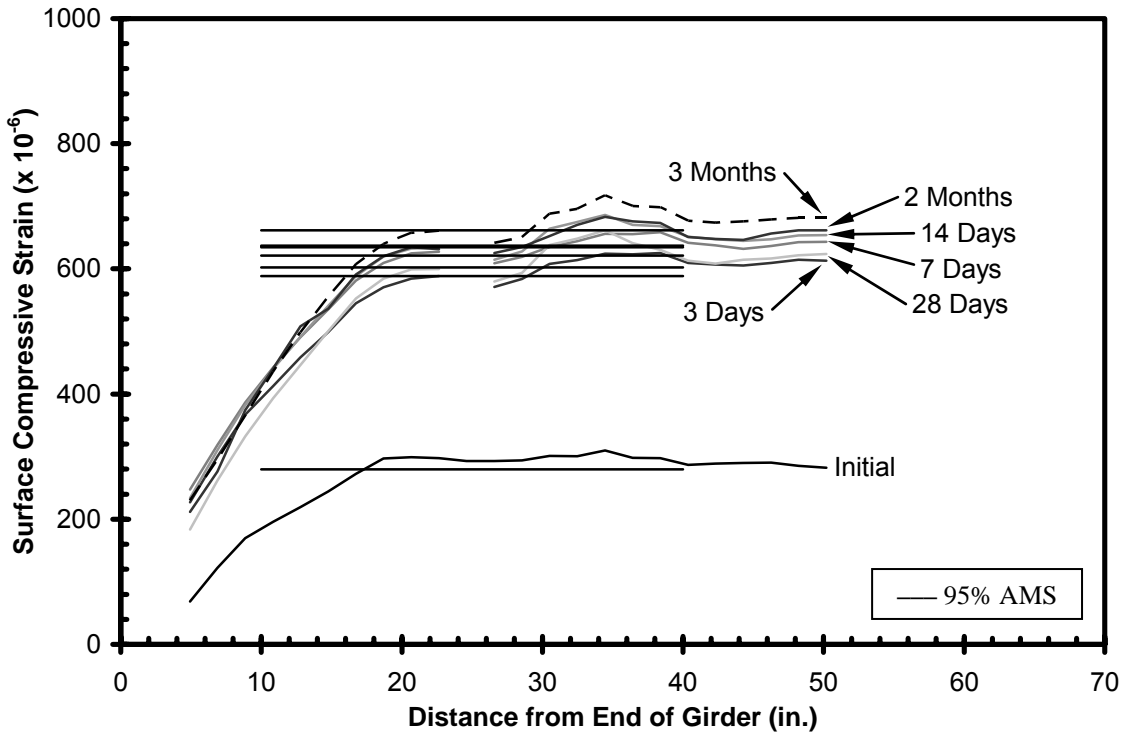
Figure F-6: SCC-MS-1W Measured Initial and Long-Term Strain Profiles
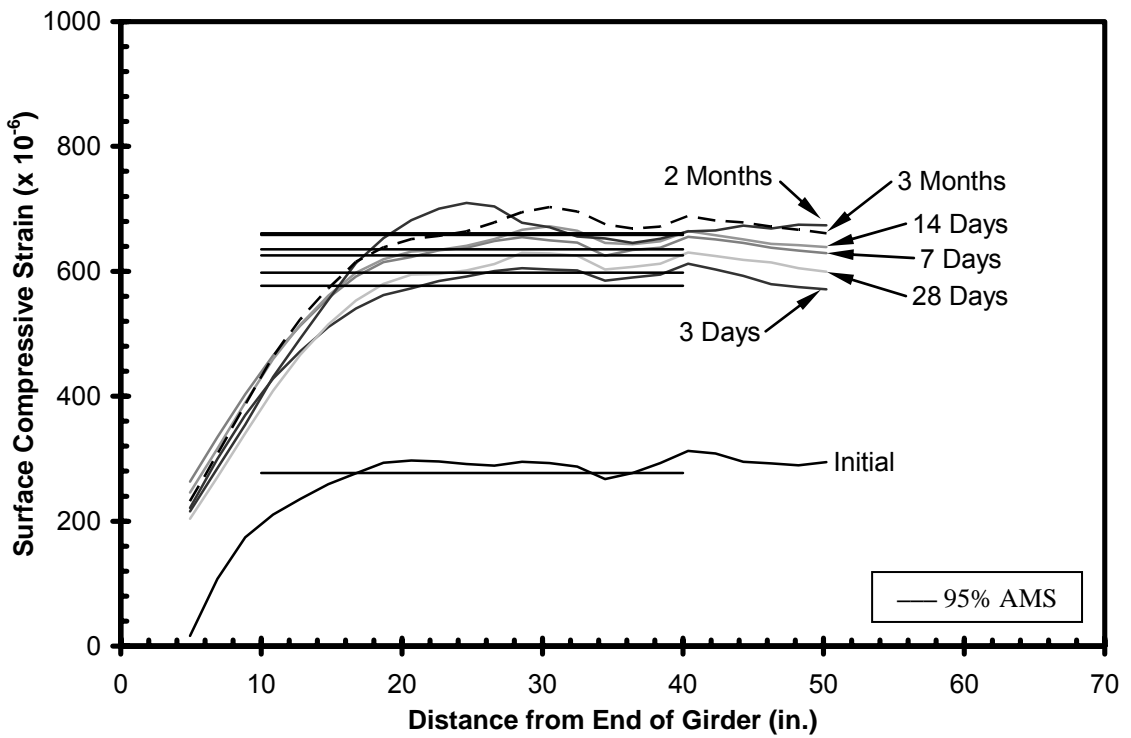
Figure F-7: SCC-MS-2E Measured Initial and Long-Term Strain Profiles

229
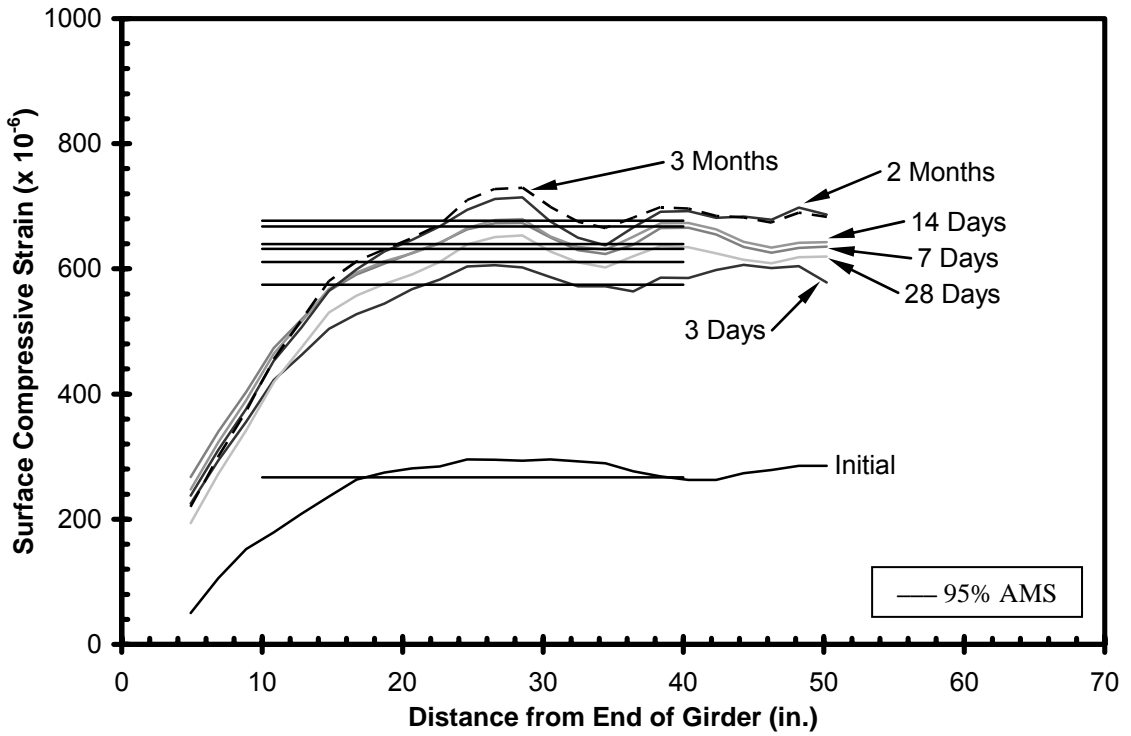
Figure F-8: SCC-MS-2W Measured Initial and Long-Term Strain Profiles
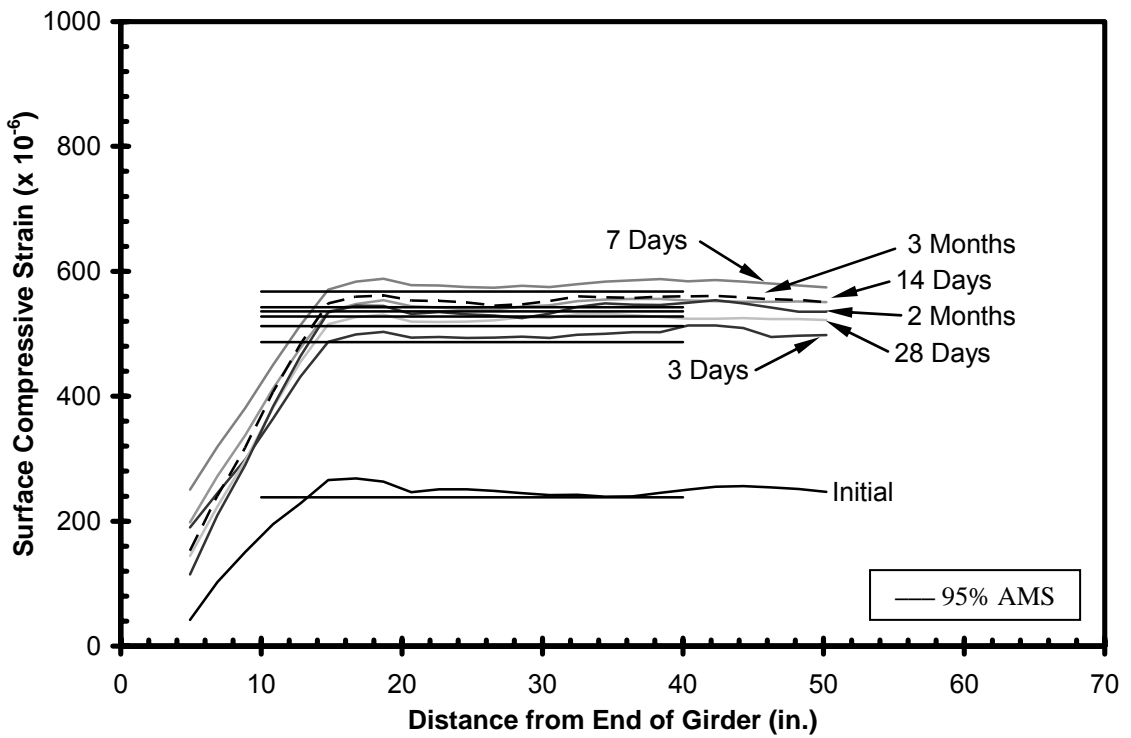
Figure F-9: SCC-HS-1E Measured Initial and Long-Term Strain Profiles
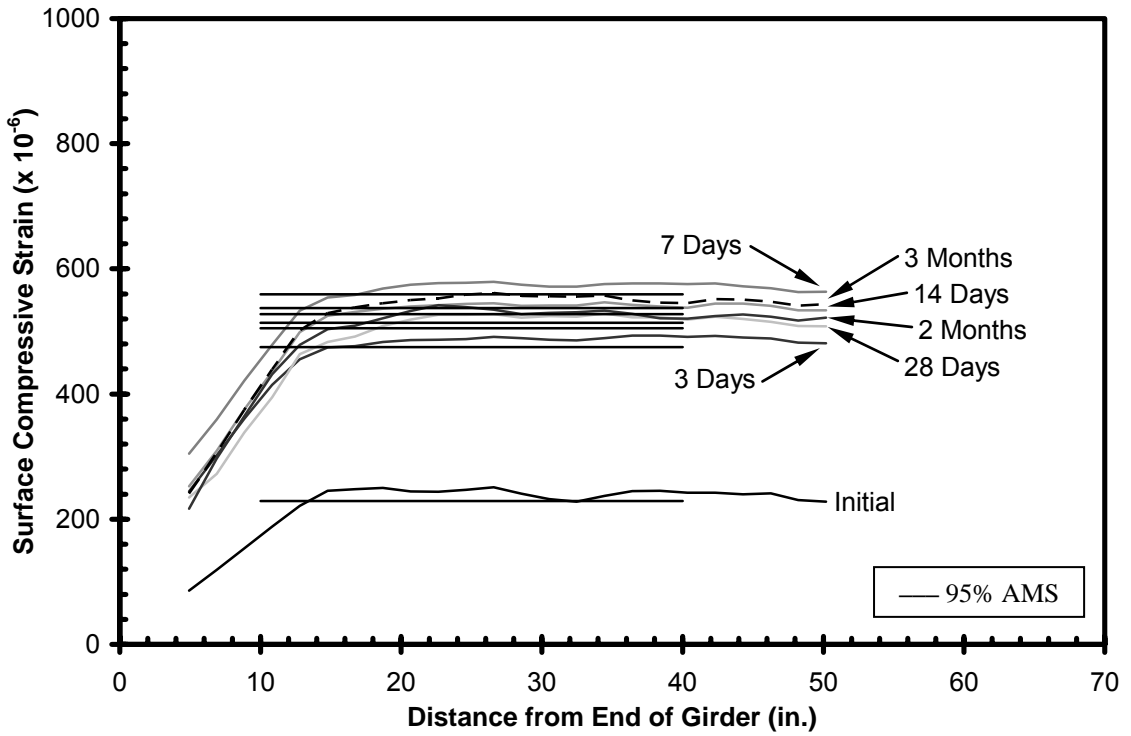
Figure F-10: SCC-HS-1W Measured Initial and Long-Term Strain Profiles
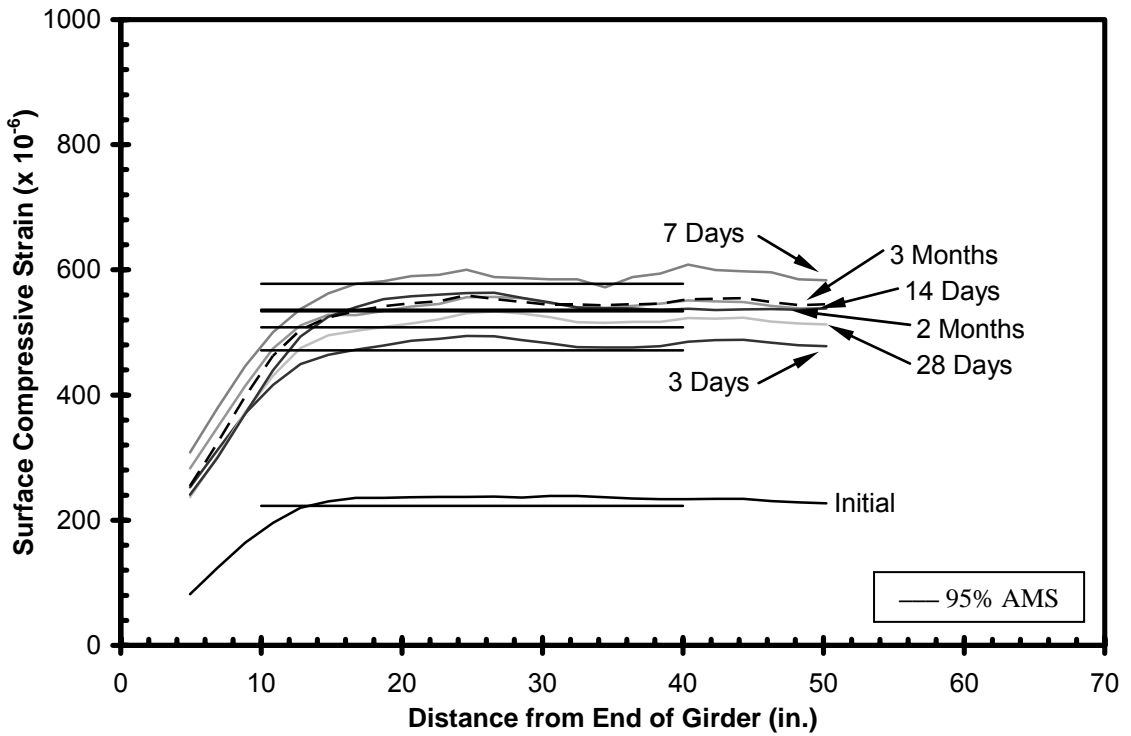
Figure F-11: SCC-HS-2E Measured Initial and Long-Term Strain Profiles

231
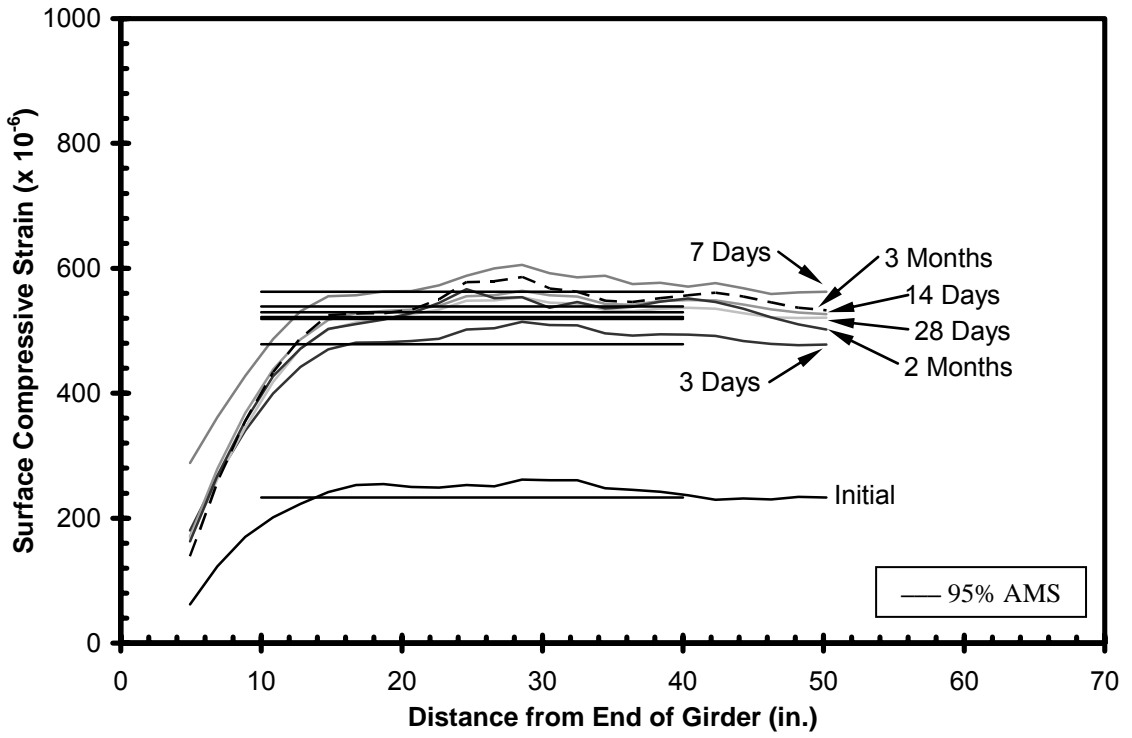
Figure F-12: SCC-HS-2W Measured Initial and Long-Term Strain Profiles

APPENDIX G

STRAND DRAW-IN RESULTS
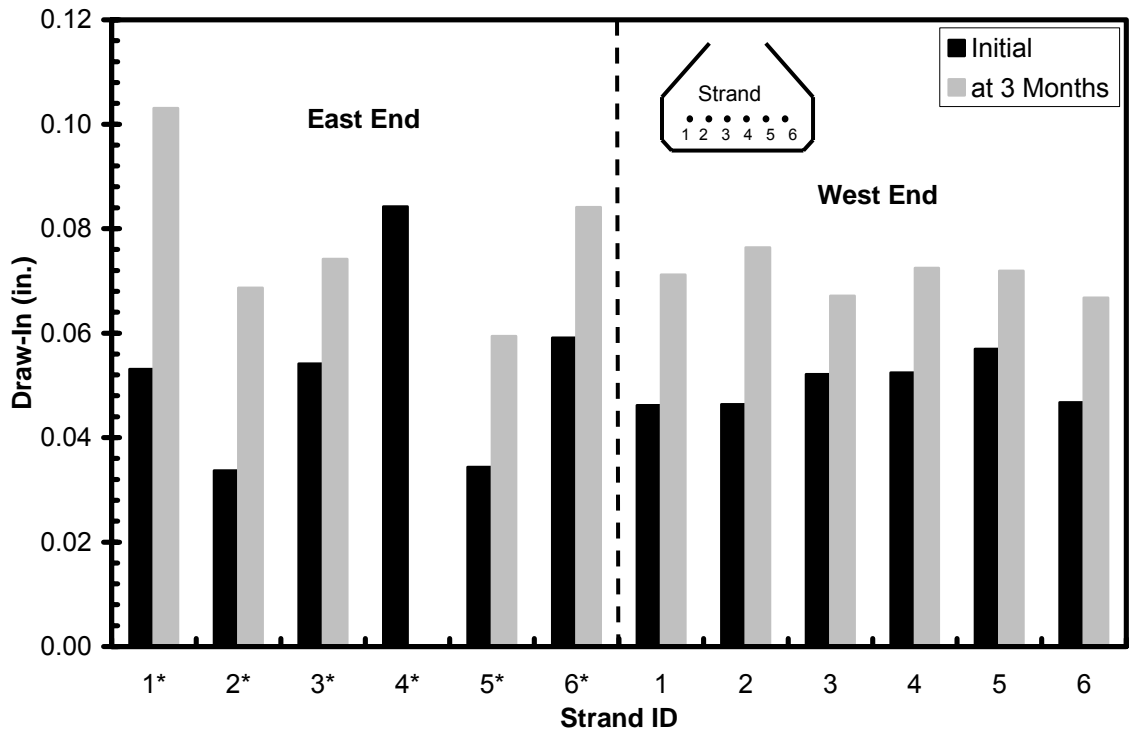
Figure G-1: STD-M-1 Strand Draw-In Results
Note: * Designates cut or "live" end (1E)
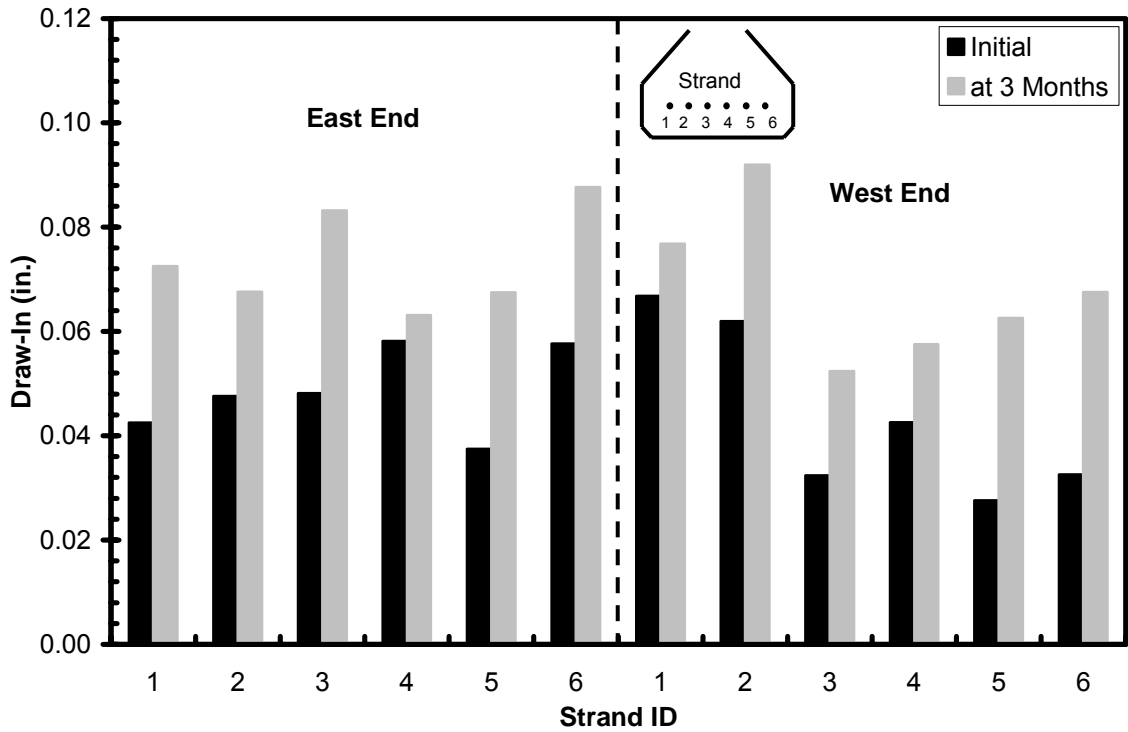
Figure G-2: STD-M-2 Strand Draw-In Results
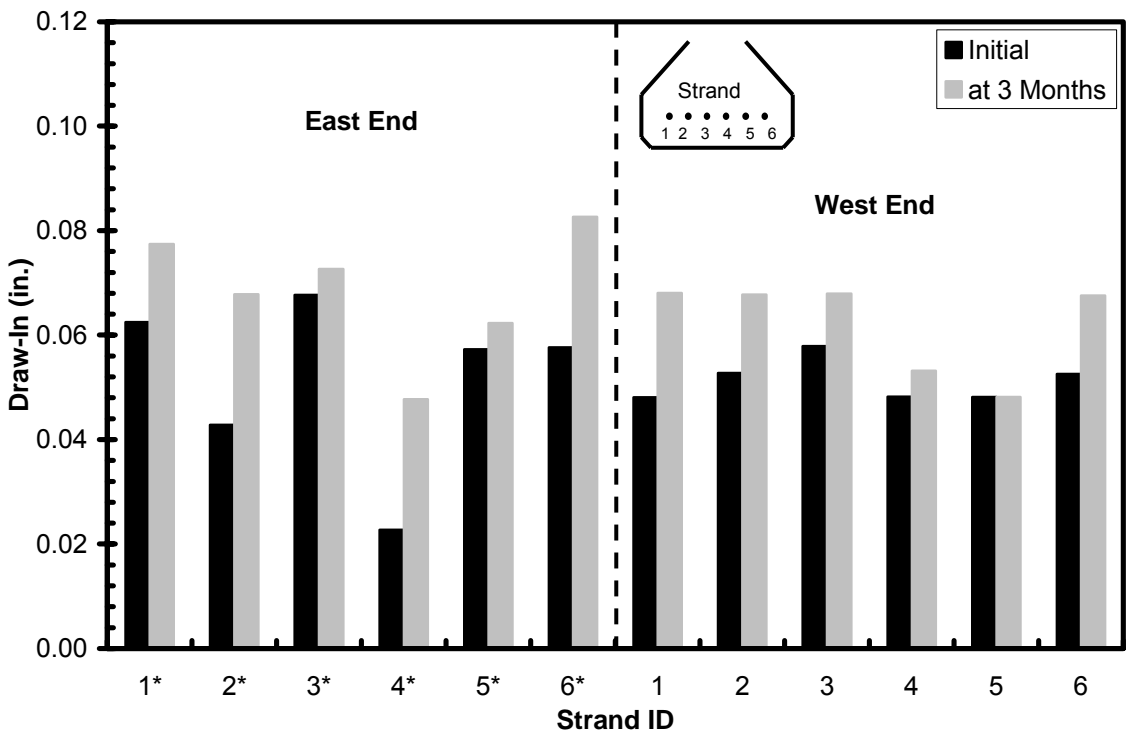
Figure G-3: SCC-MS-1 Strand Draw-In Results
Note: * Designates cut or "live" end (1E)

234
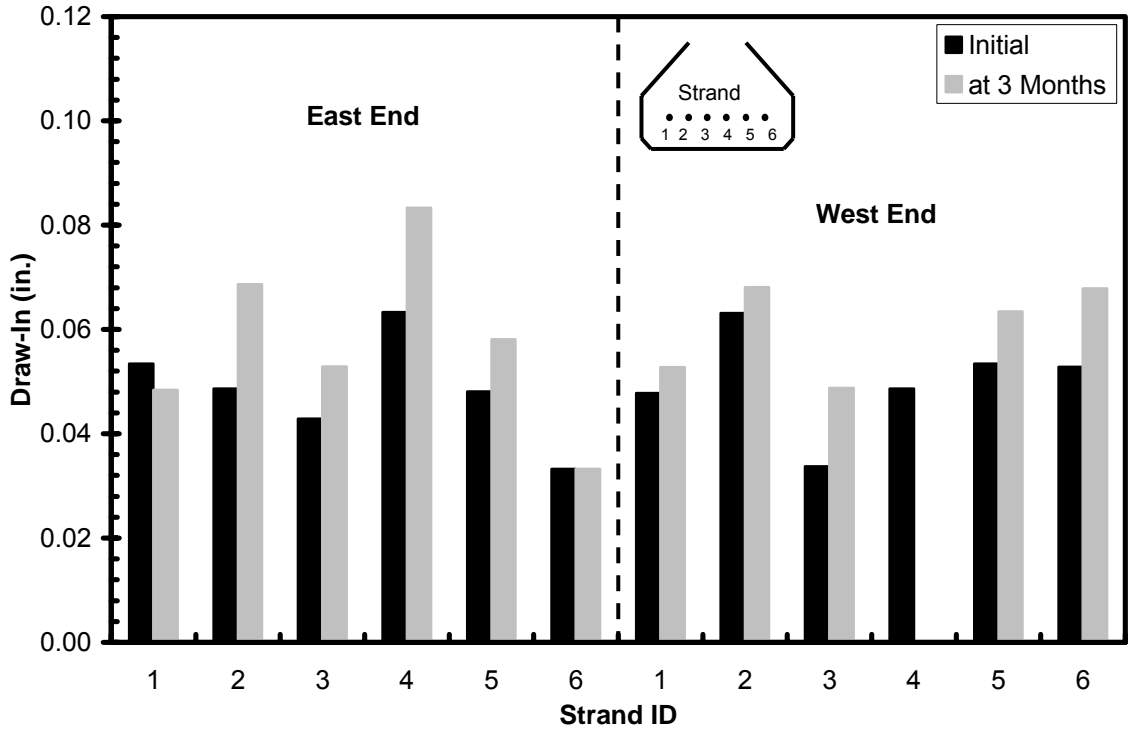
Figure G-4: SCC-MS-2 Strand Draw-In Results
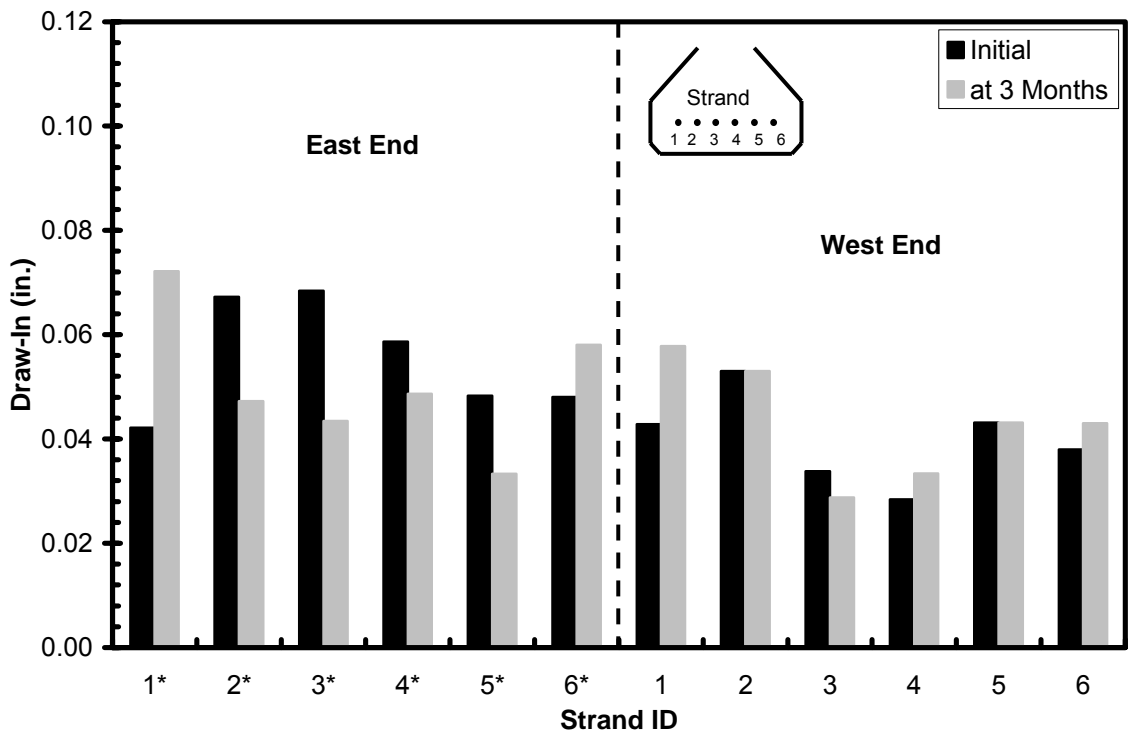
Figure G-5: SCC-HS-1 Strand Draw-In Results
Note: * Designates cut or "live" end (1E)

235
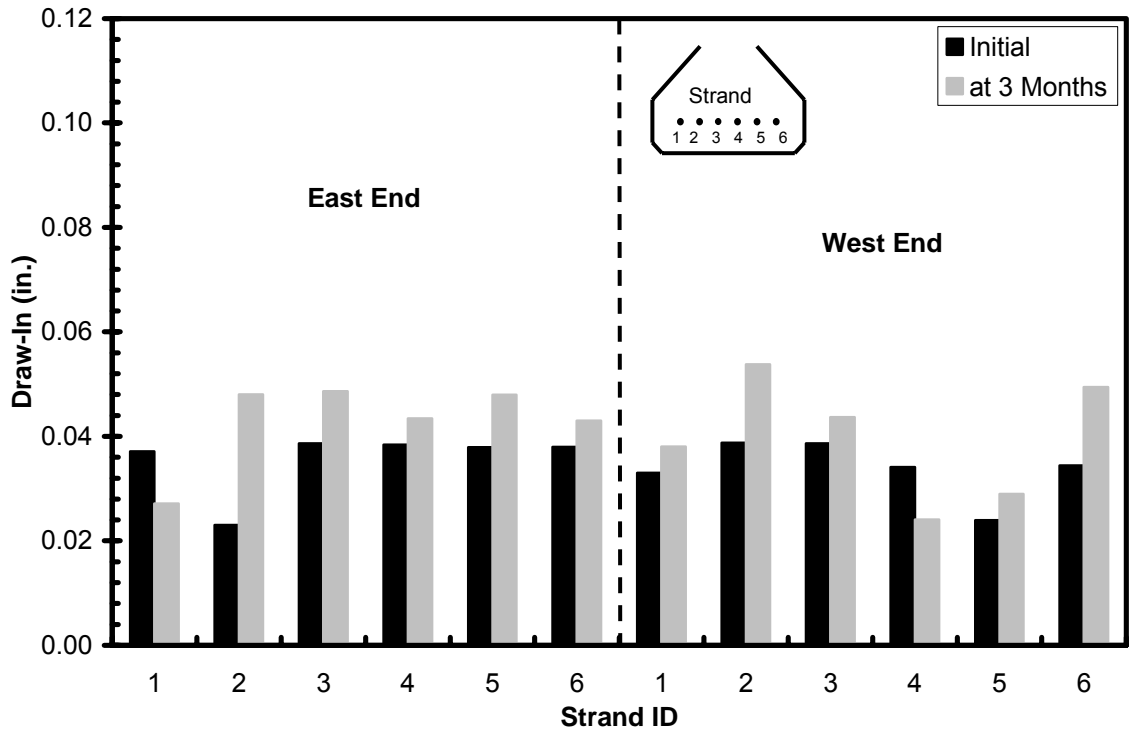
Figure G-6: SCC-HS-2 Strand Draw-In Results

APPENDIX H

LOAD VERSUS DISPLACEMENT DIAGRAMS
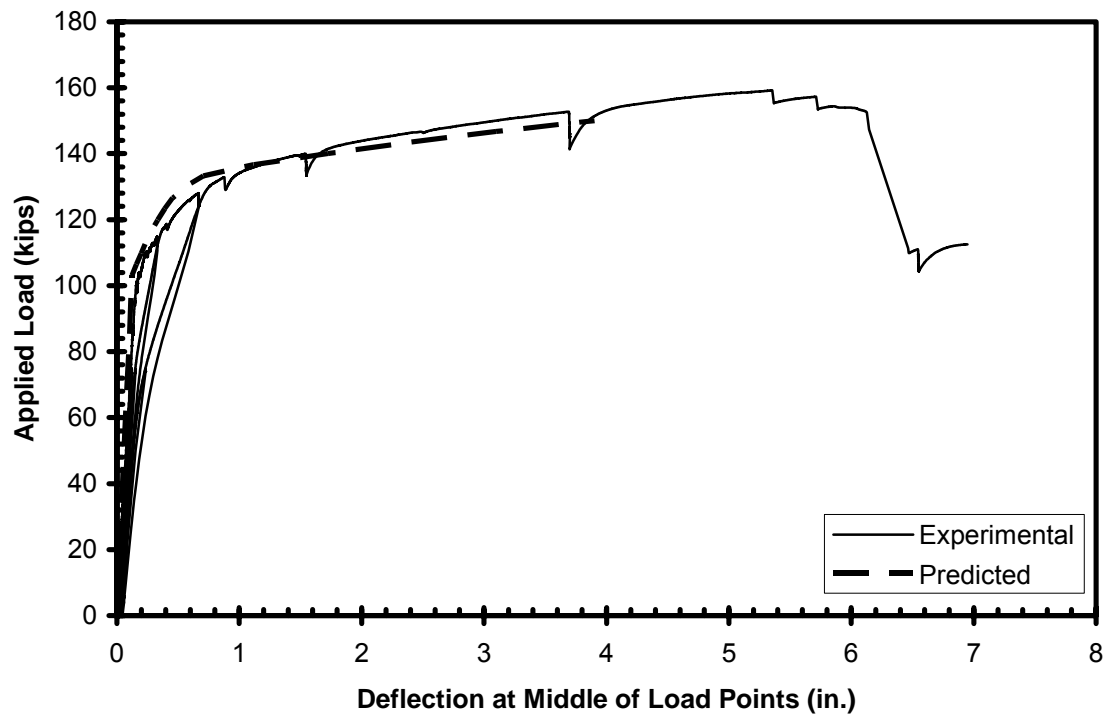
Figure H-1: Load vs. Displacement for STD-M-1E
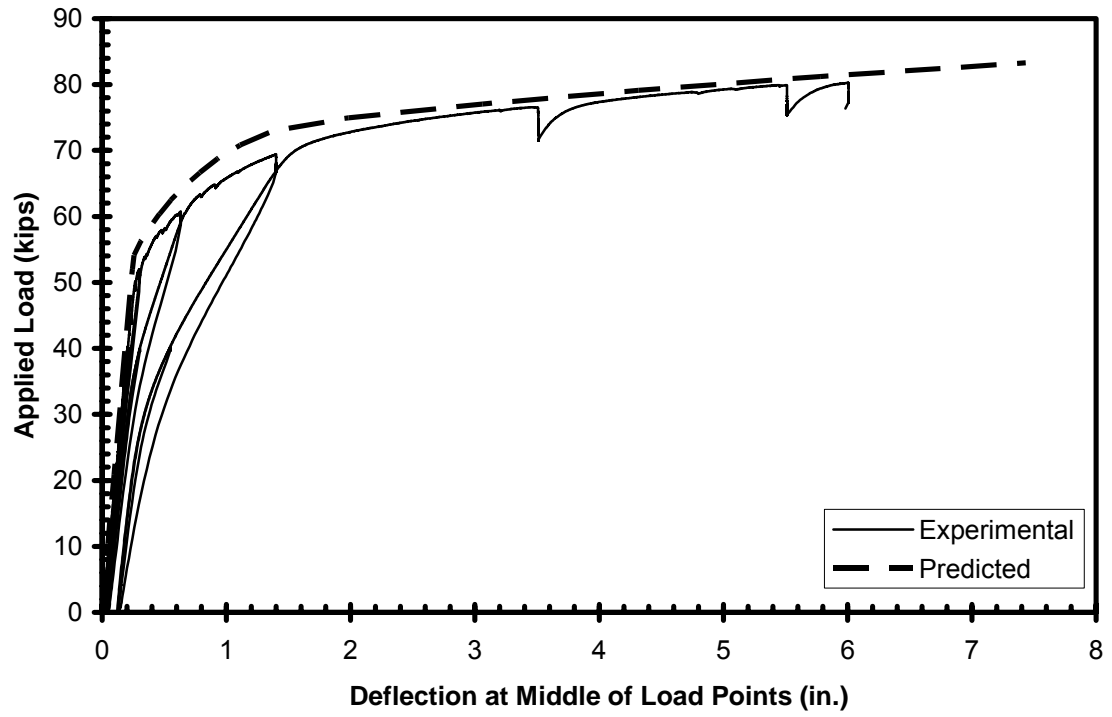
Figure H-2: Load vs. Displacement for STD-M-1W
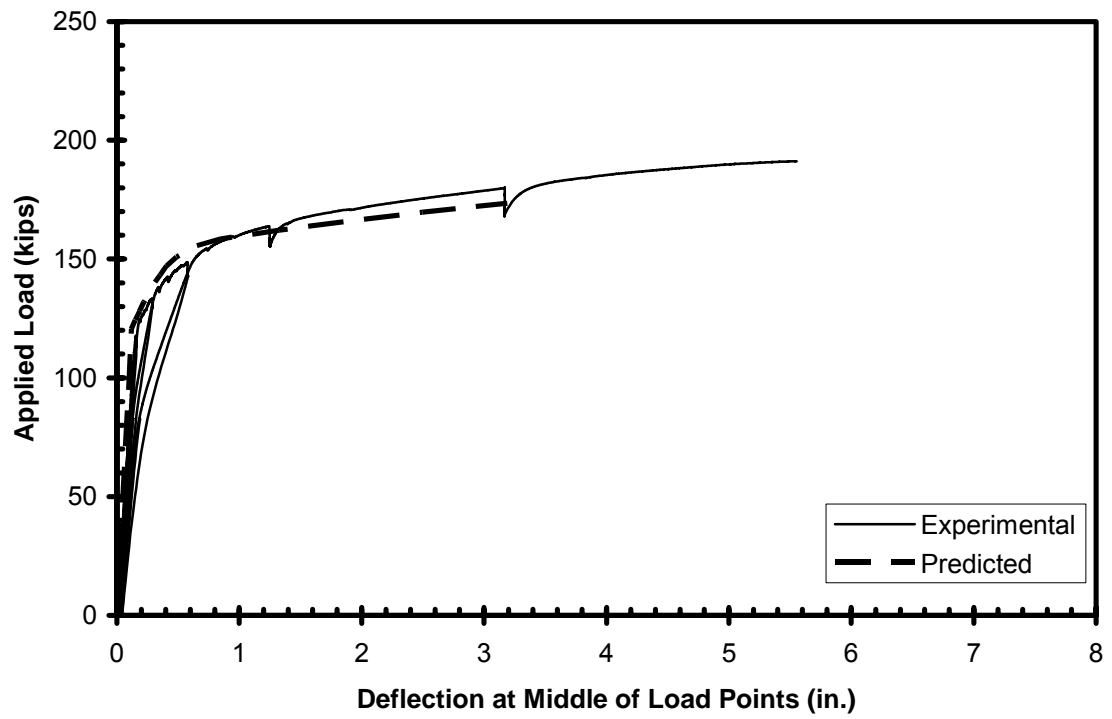
Figure H-3: Load vs. Displacement for STD-M-2E

238
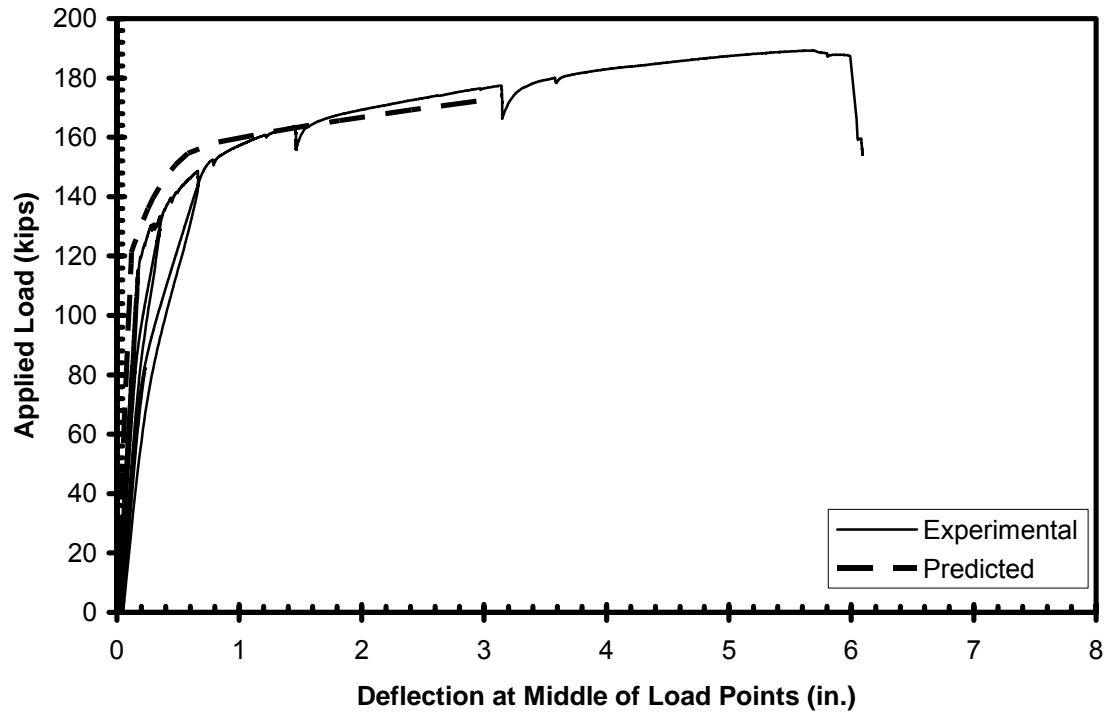
Figure H-4: Load vs. Displacement for STD-M-2W
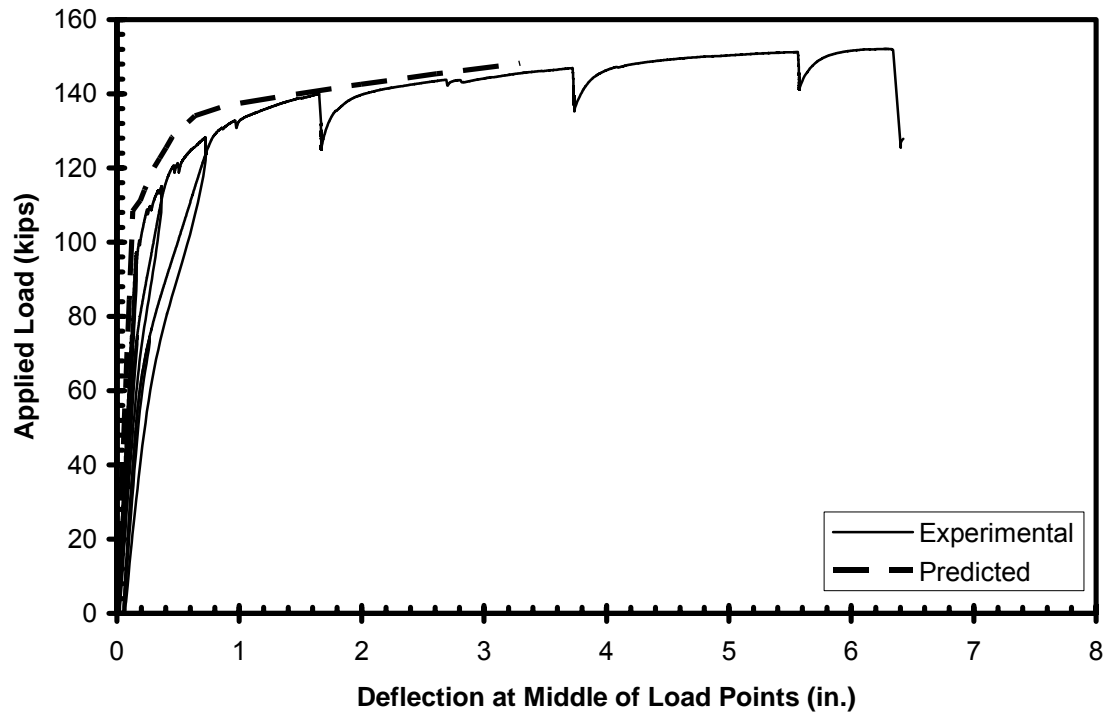
Figure H-5: Load vs. Displacement for SCC-MS-1E

239
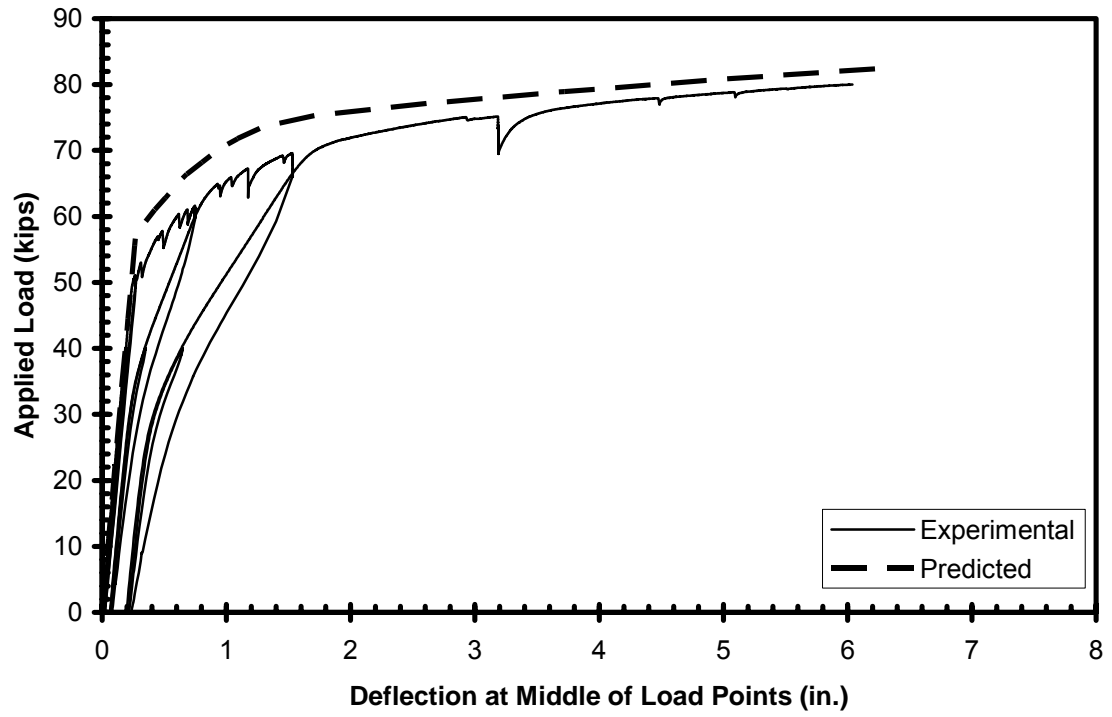
Figure H-6: Load vs. Displacement for SCC-MS-1W
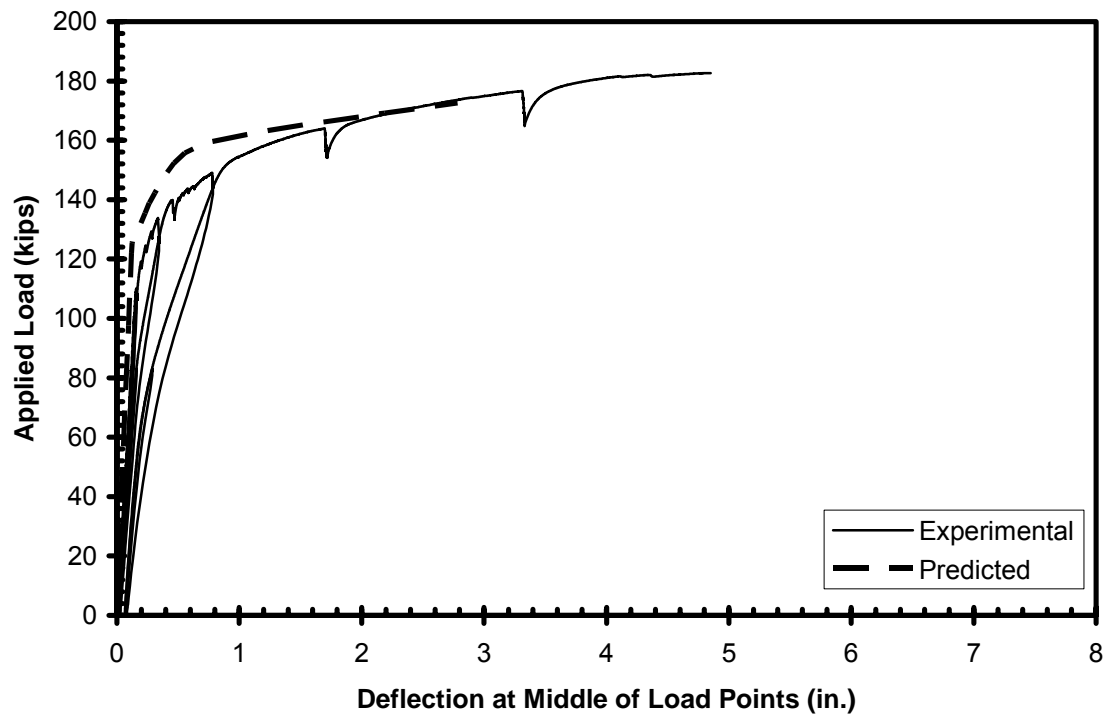
Figure H-7: Load vs. Displacement for SCC-MS-2E

240
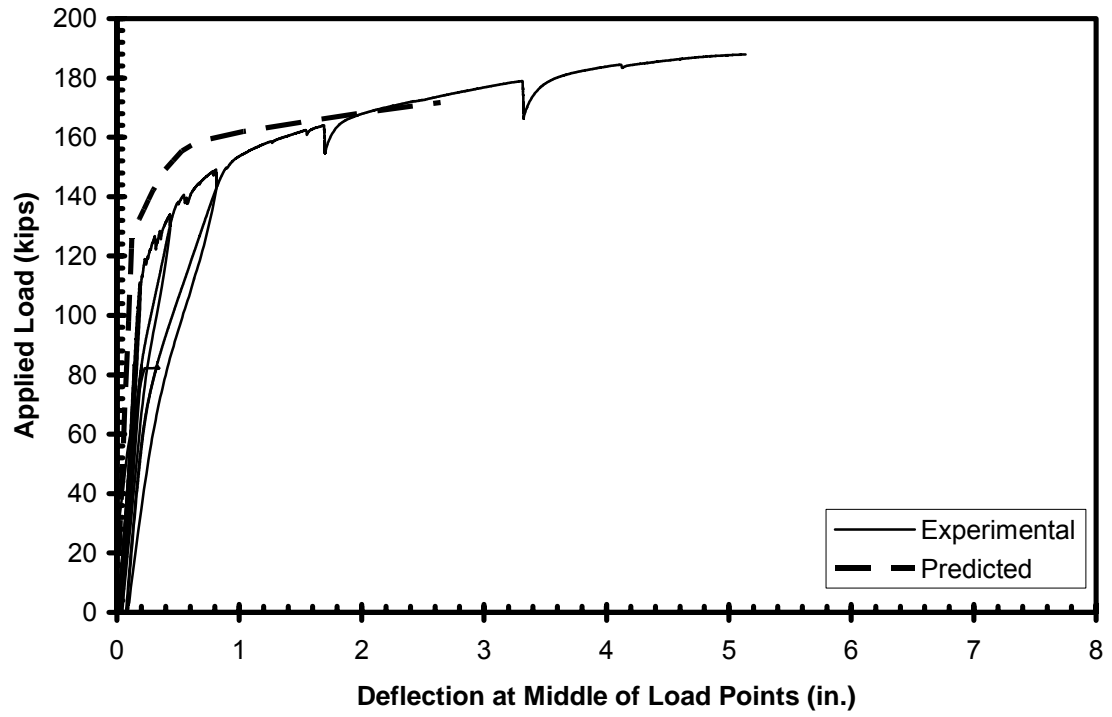
Figure H-8: Load vs. Displacement for SCC-MS-2W
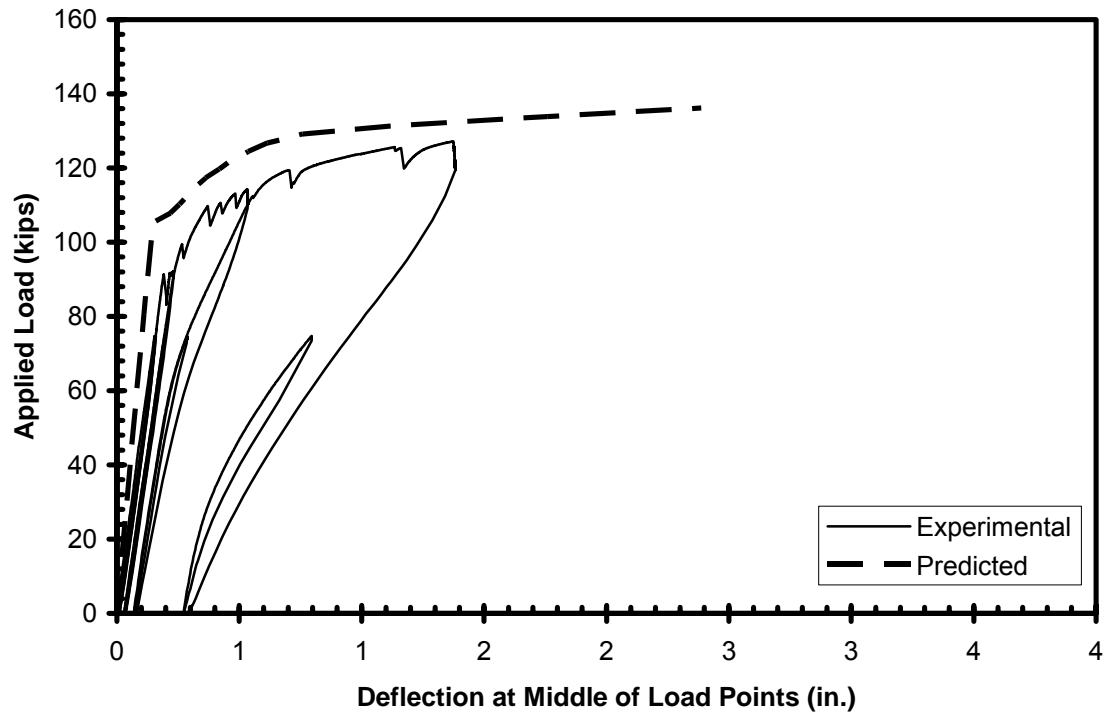
Figure H-9: Load vs. Displacement for SCC-HS-1E Initial Test Configuration

241
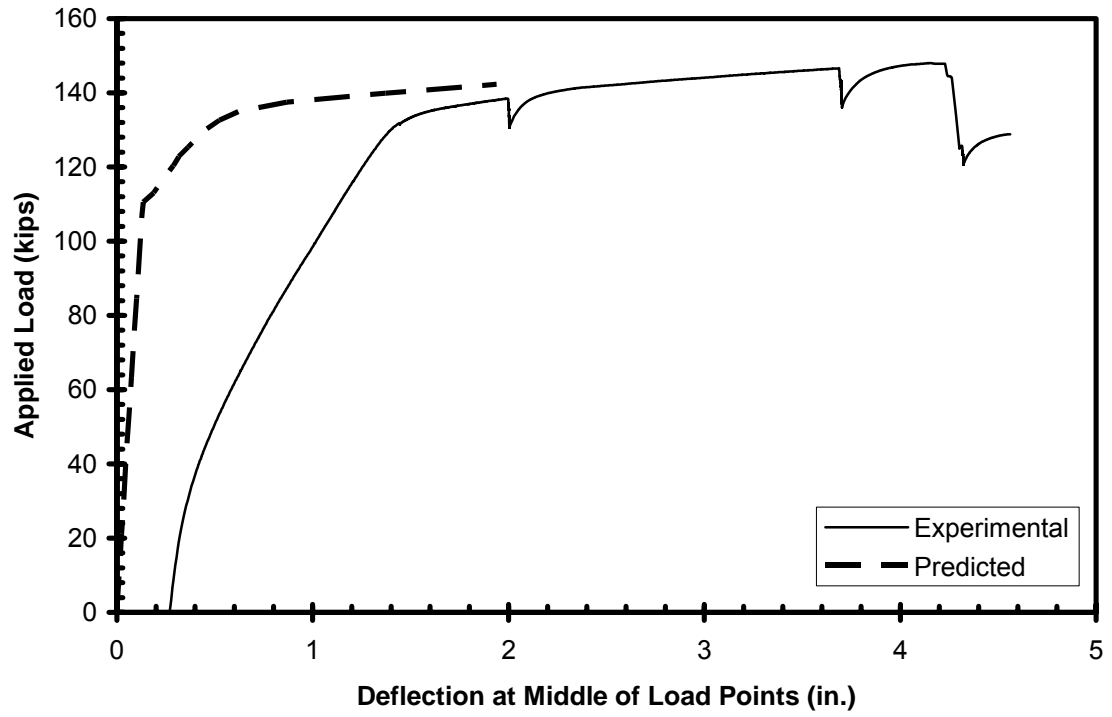
Figure H-10: Load vs. Displacement for SCC-HS-1E Correct Test Configuration
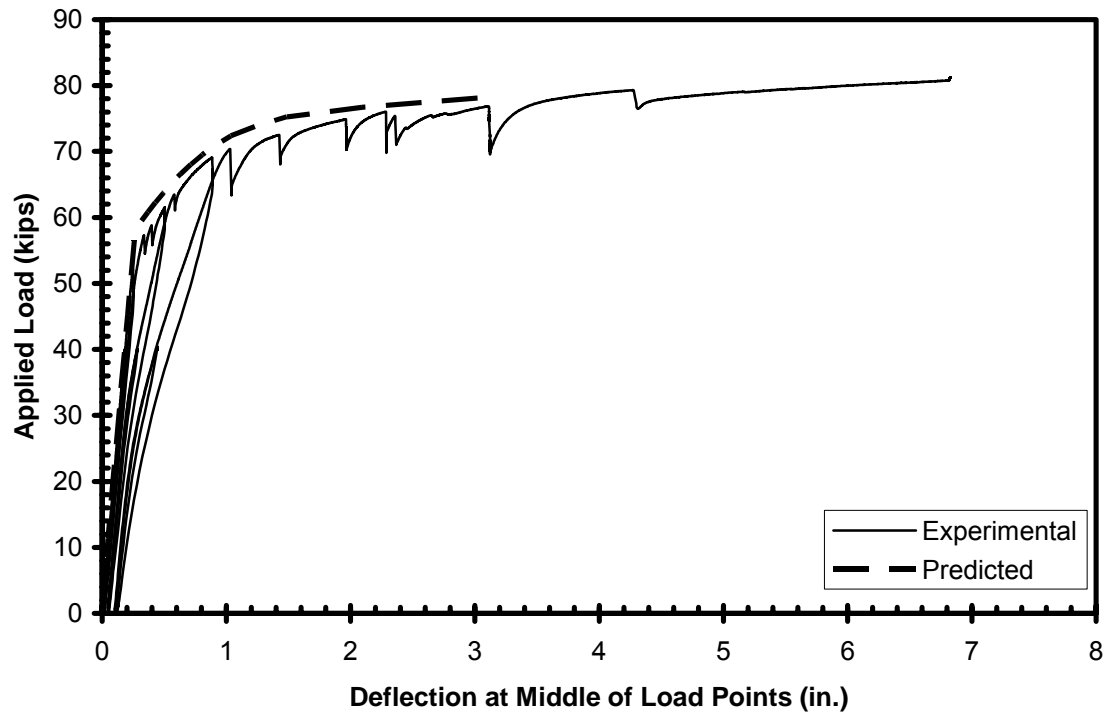
Figure H-11: Load vs. Displacement for SCC-HS-1W

242
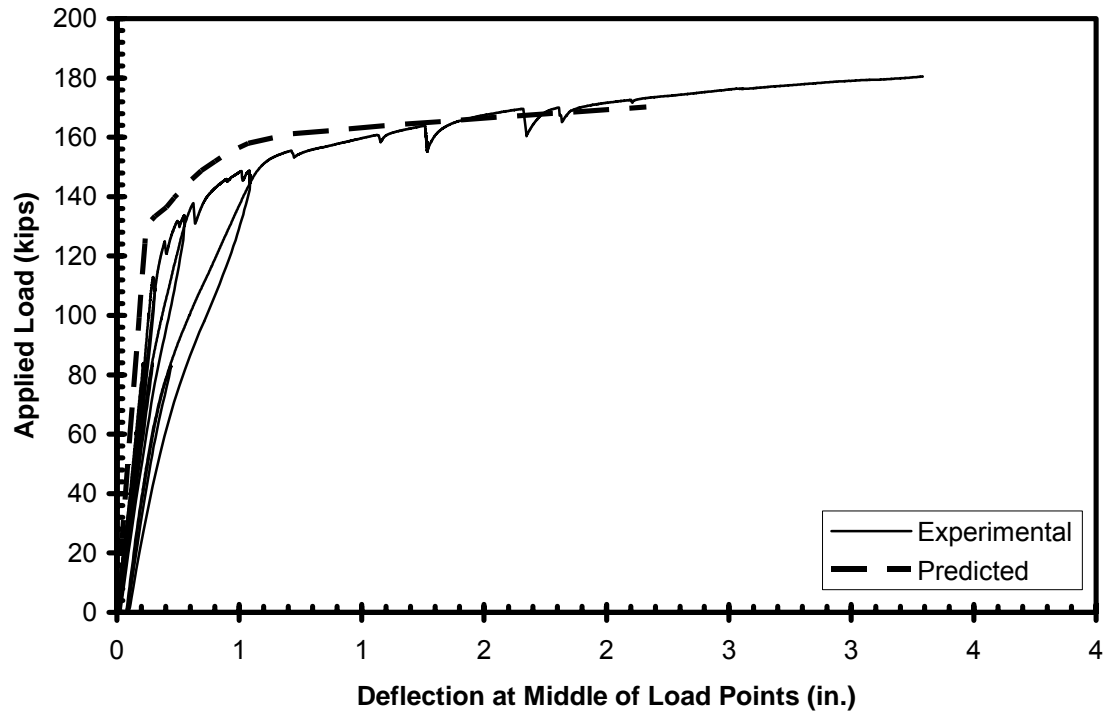
Figure H-12: Load vs. Displacement for SCC-HS-2E
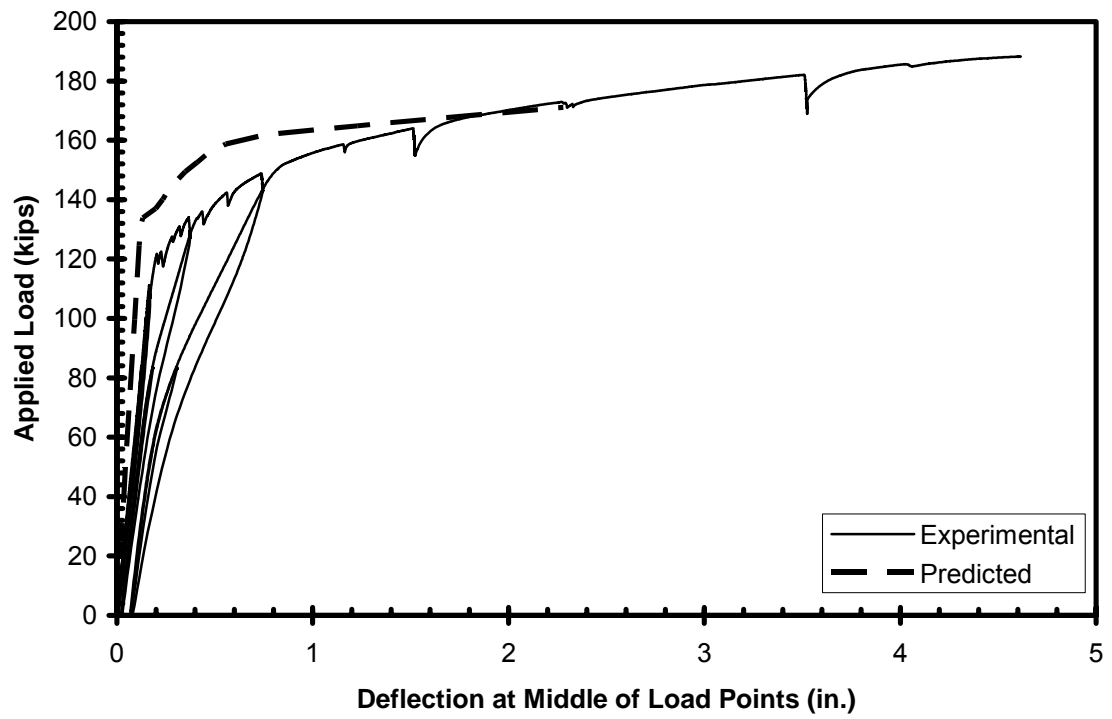
Figure H-13: Load vs. Displacement for SCC-HS-2W

243

APPENDIX I

CRACK PATTERNS
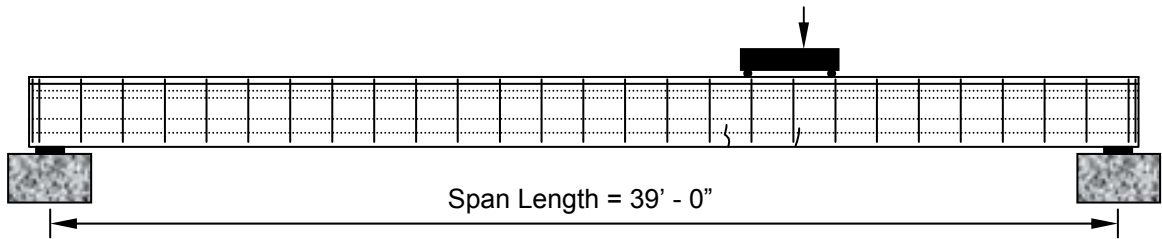
Figure I-1: Crack Pattern at Cracking Load for STD-M-1W
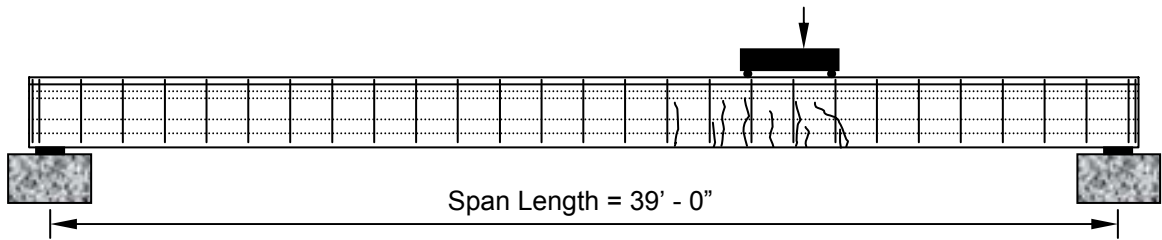
Figure I-2: Crack Pattern at Approx. 240 ksi in Bottom Strands for STD-M-1W
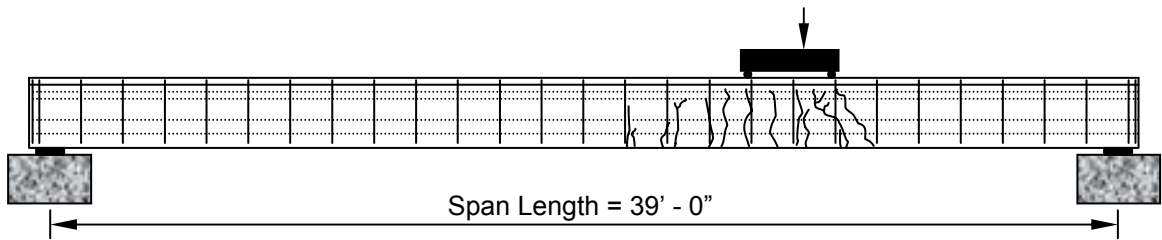
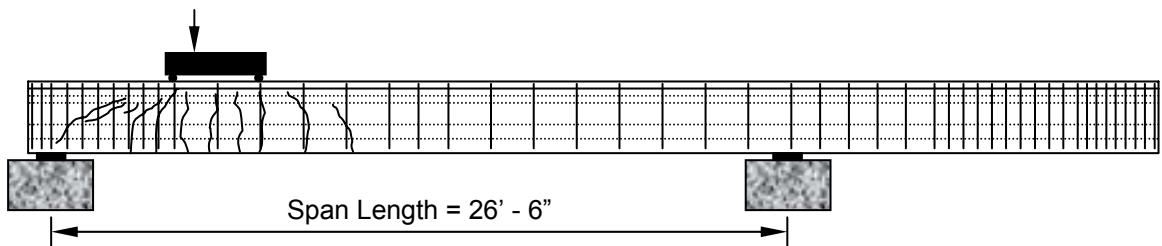

Figure I-3: Crack Pattern at Approx. 260 ksi in Bottom Strands for STD-M-1W

244
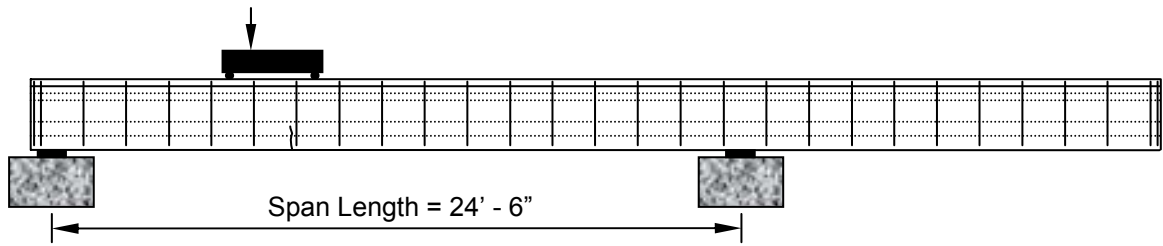
Figure I-4: Crack Pattern at Cracking Load for STD-M-1E
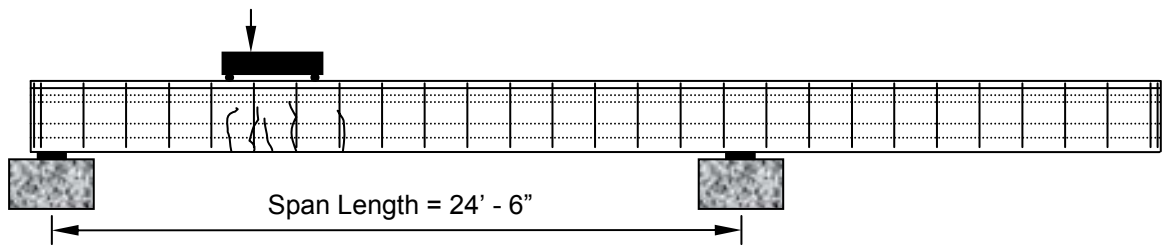
Figure I-5: Crack Pattern at Approx. 240 ksi in Bottom Strands for STD-M-1E
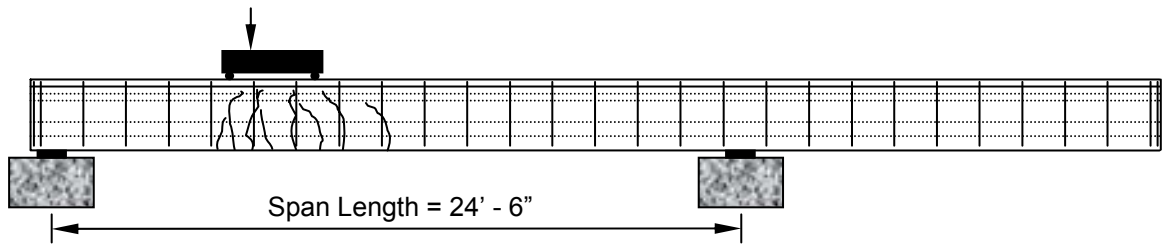
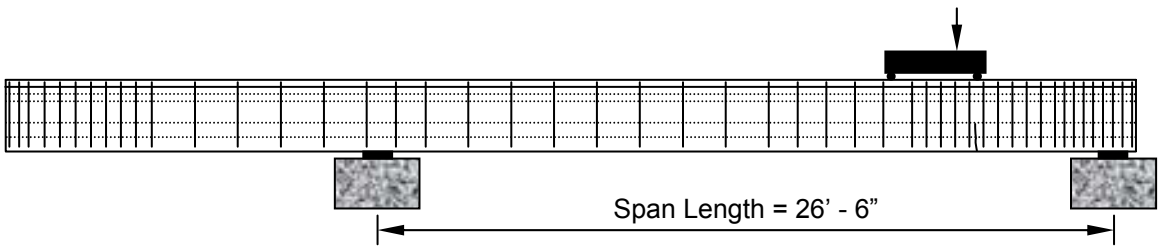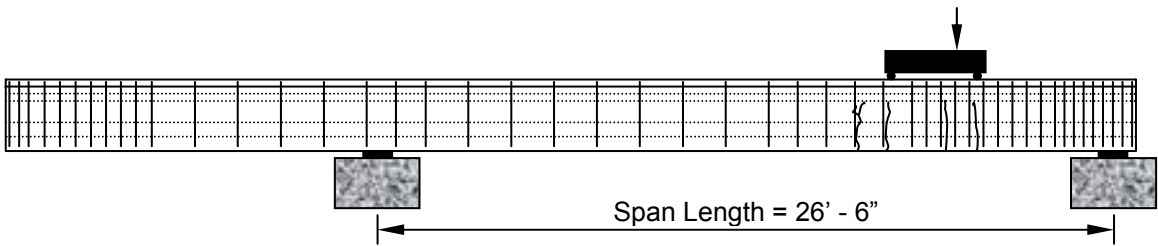**Figure I-6: Crack Pattern at Approx. 260 ksi in Bottom Strands for STD-M-1E**
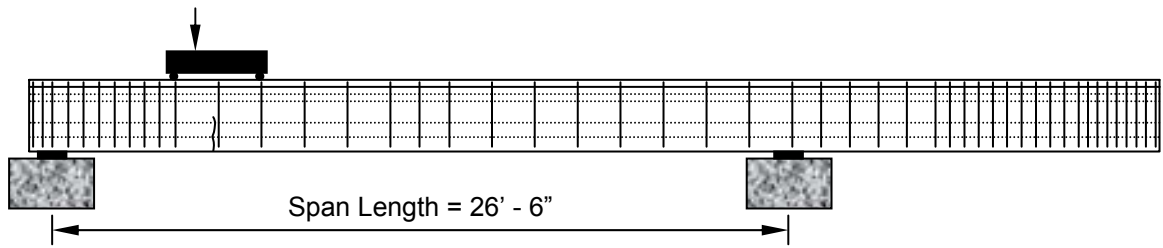
Figure I-7: Crack Pattern at Cracking Load for STD-M-2E
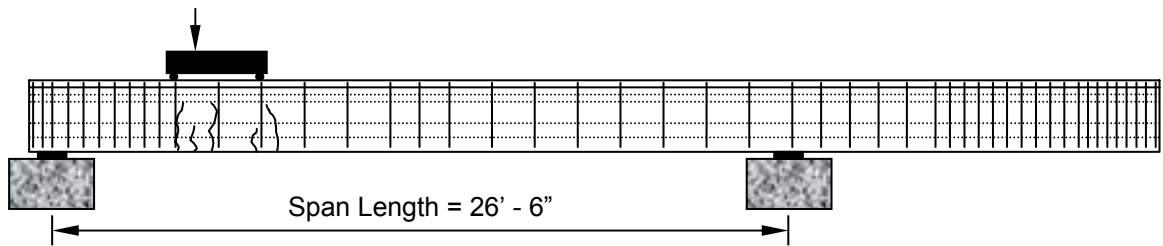
Figure I-8: Crack Pattern at Approx. 240 ksi in Bottom Strands for STD-M-2E
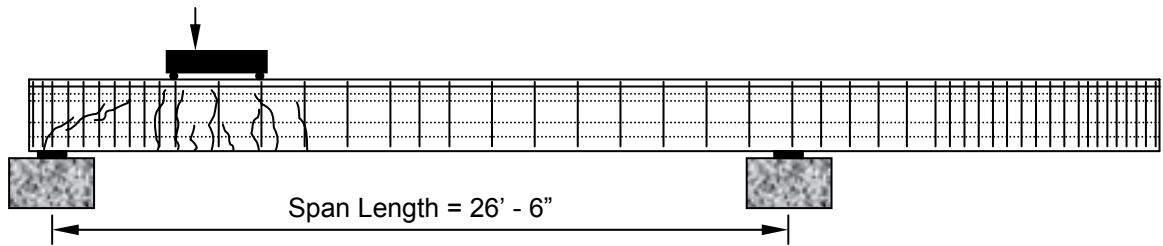
Figure I-9: Crack Pattern at Approx. 260 ksi in Bottom Strands for STD-M-2E

246
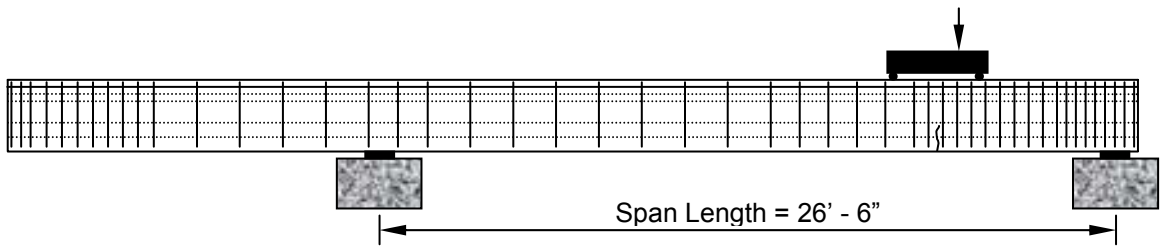
Figure I-10: Crack Pattern at Cracking Load for STD-M-2W
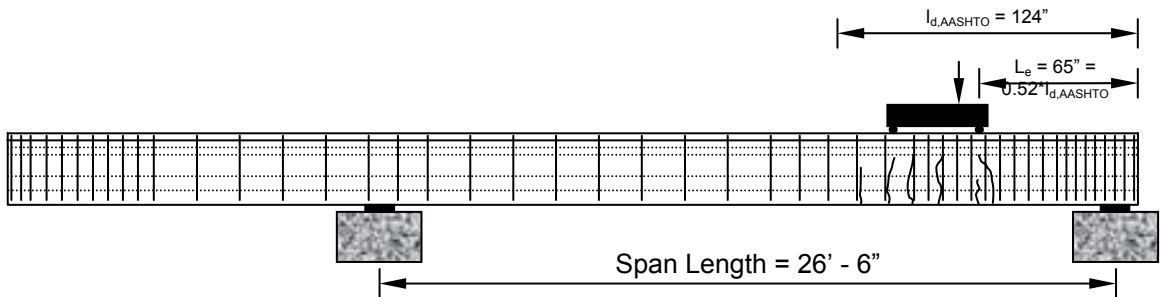
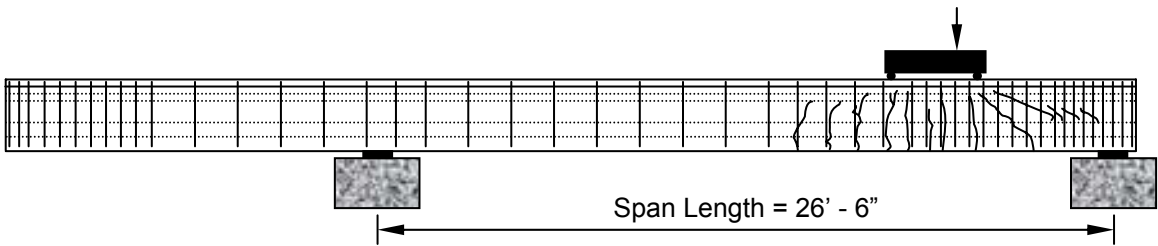**Figure I-11: Crack Pattern at Approx. 240 ksi in Bottom Strands for STD-M-2W**
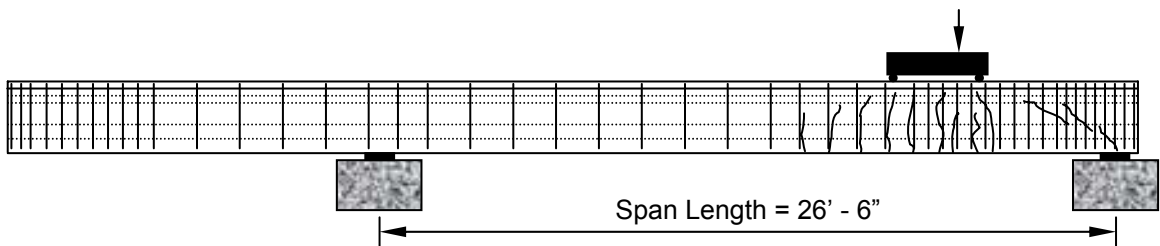
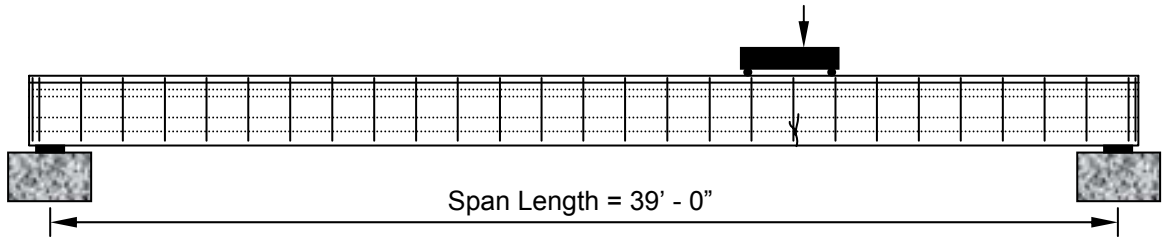**Figure I-12: Crack Pattern at Approx. 260 ksi in Bottom Strands for STD-M-2W**

247
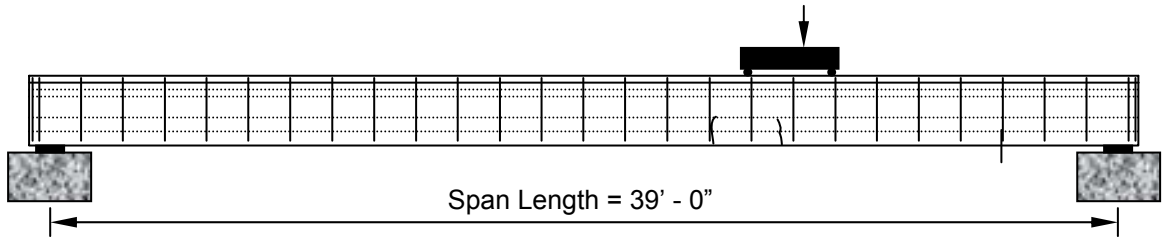
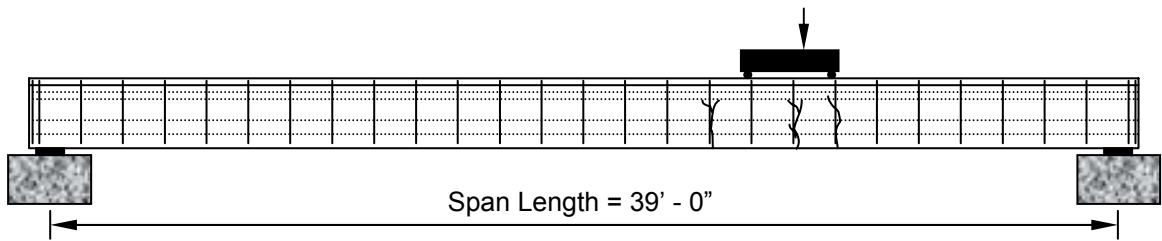**Figure I-13: Crack Pattern at Cracking Load for SCC-MS-1W**
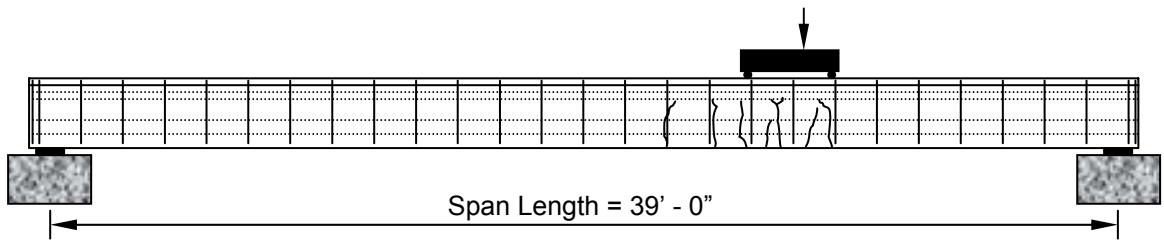
Figure I-14: Crack Pattern at Approx. 240 ksi in Bottom Strands for SCC-MS-1W
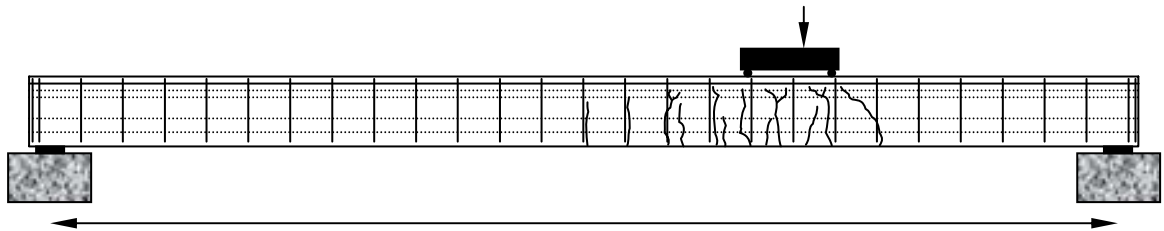
Figure I-15: Crack Pattern at Approx. 260 ksi in Bottom Strands for SCC-MS-1W

248
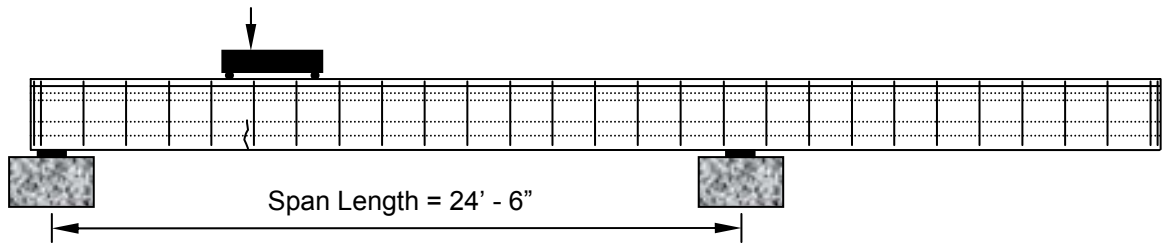
Figure I-16: Crack Pattern at Cracking Load for SCC-MS-1E
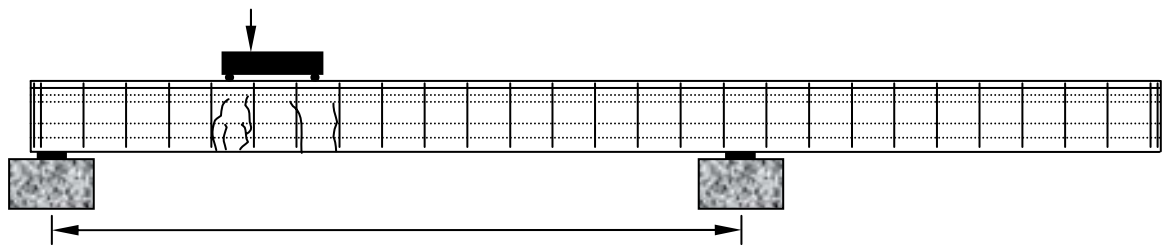
Figure I-17: Crack Pattern at Approx. 240 ksi in Bottom Strands for SCC-MS-1E
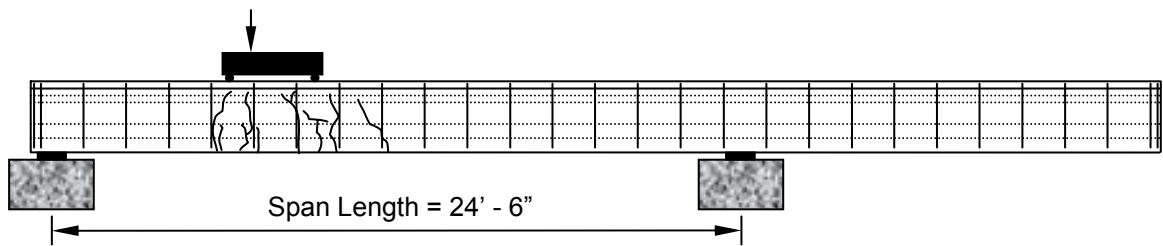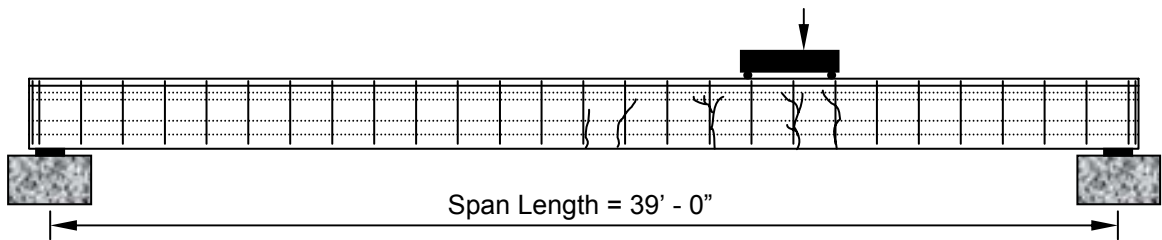

Figure I-18: Crack Pattern at Approx. 260 ksi in Bottom Strands for SCC-MS-1E
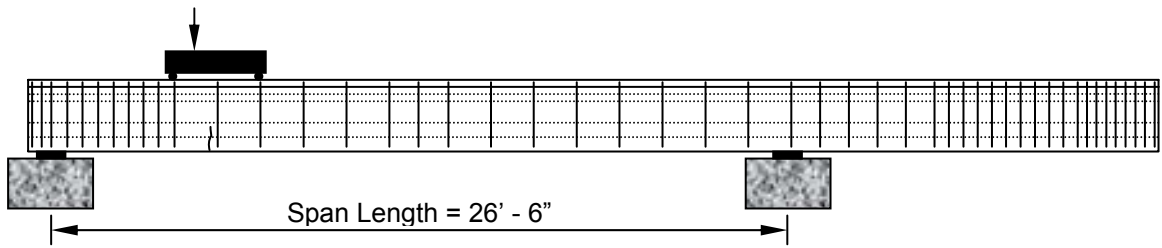
Figure I-19: Crack Pattern at Cracking Load for SCC-MS-2E
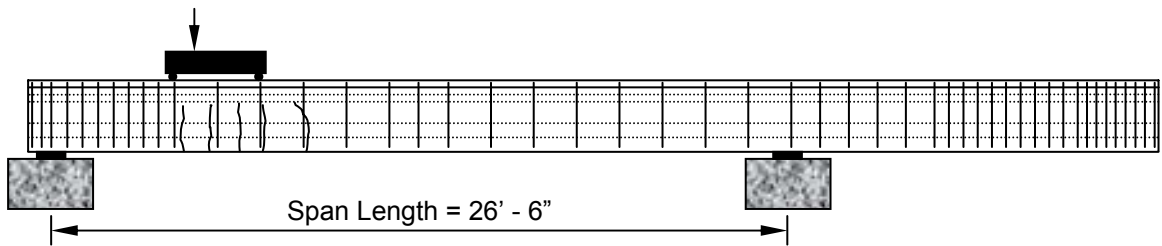
Figure I-20: Crack Pattern at Approx. 240 ksi in Bottom Strands for SCC-MS-2E

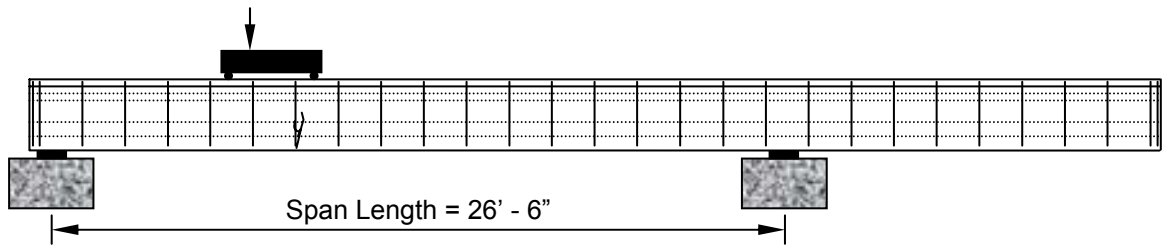**Figure I-21: Crack Pattern at Approx. 260 ksi in Bottom Strands for SCC-MS-2E**

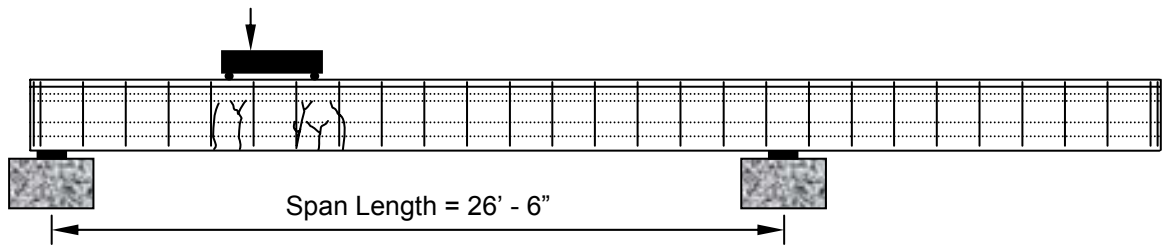**Figure I-22: Crack Pattern at Cracking Load for SCC-MS-2W**

Figure I-23: Crack Pattern at Approx. 240 ksi in Bottom Strands for SCC-MS-2W

Figure I-24: Crack Pattern at Approx. 260 ksi in Bottom Strands for SCC-MS-2W

251

Figure I-25: Crack Pattern at Cracking Load for SCC-HS-1W

Figure I-26: Crack Pattern at Approx. 240 ksi in Bottom Strands for SCC-HS-1W

Figure I-27: Crack Pattern at Approx. 260 ksi in Bottom Strands for SCC-HS-1W

252

Figure I-28: Crack Pattern at Cracking Load for SCC-HS-1E

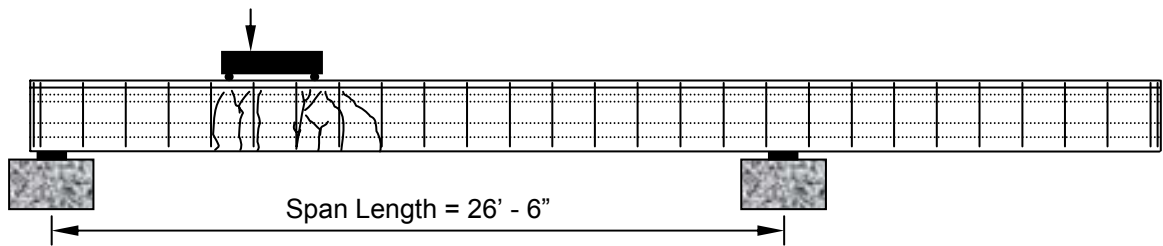**Figure I-29: Crack Pattern at Approx. 240 ksi in Bottom Strands for SCC-HS-1E**

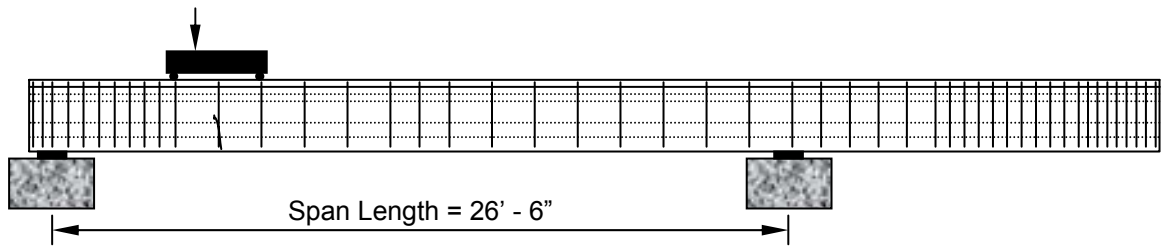**Figure I-30: Crack Pattern at Approx. 260 ksi in Bottom Strands for SCC-HS-1E**

253

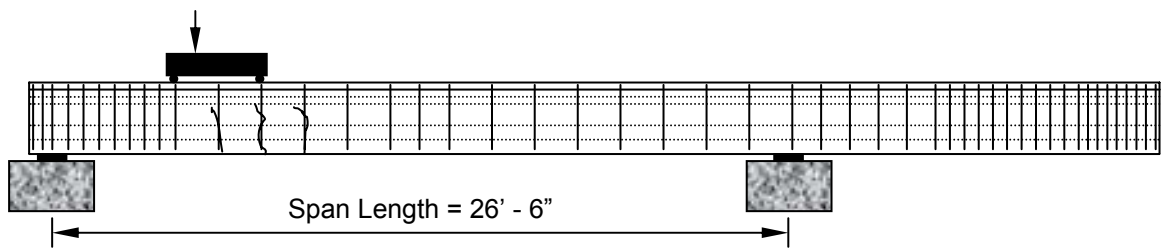**Figure I-31: Crack Pattern at Cracking Load for SCC-HS-2E**

Figure I-32: Crack Pattern at Approx. 240 ksi in Bottom Strands for SCC-HS-2E
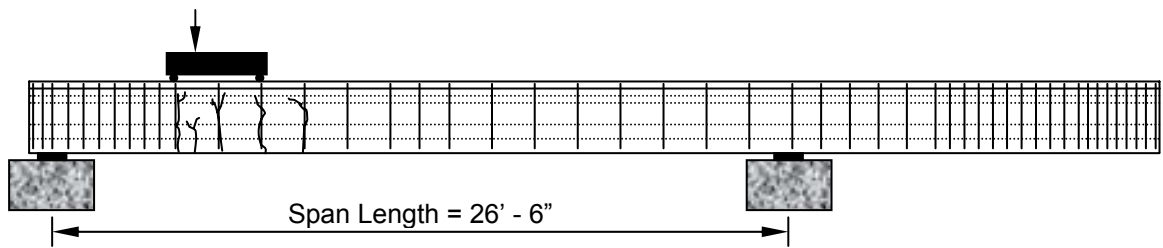

Figure I-33: Crack Pattern at Approx. 260 ksi in Bottom Strands for SCC-HS-2E

Figure I-34: Crack Pattern at Cracking Load for SCC-HS-2W

Figure I-35: Crack Pattern at Approx. 240 ksi in Bottom Strands for SCC-HS-2W

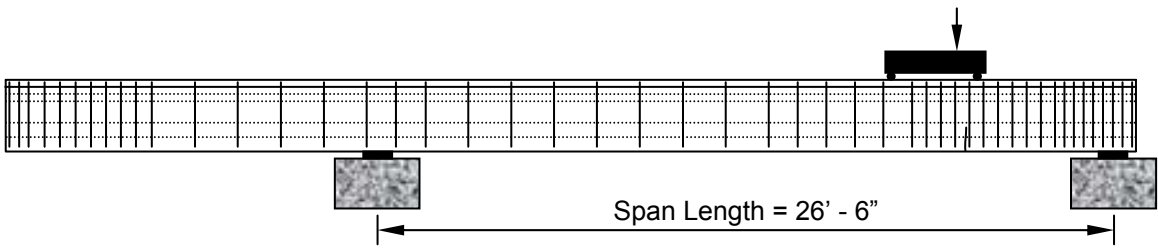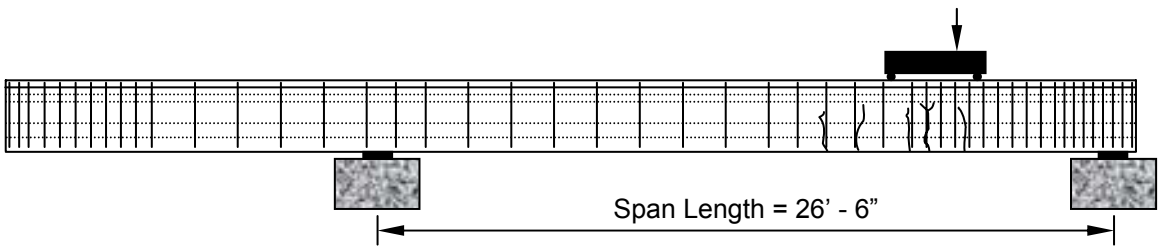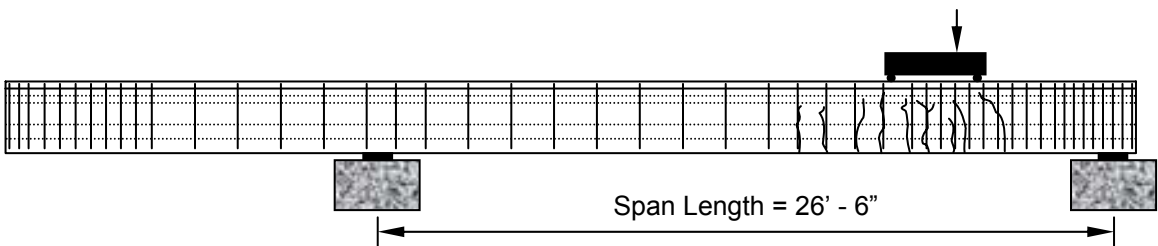**Figure I-36: Crack Pattern at Approx. 260 ksi in Bottom Strands for SCC-HS-2W**

255

APPENDIX J

CRACK WIDTHS

Table J-1: Summary of Crack Widths at Various Load Levels
Note: b. v.= barely visible
Note: *designates incorrect test span

Test Girder	Crack Widths (mm)													
	P_{cr}	Zero	P_s	Zero	P_{240}	Zero	P_s	Zero	P_{260}	Zero	P_s	Zero	P_{270}	P_{max}
STD-M-1W	—	closed	—	closed	0.3	closed	< 0.1	—	0.8	< 0.1	< 0.3	—	2.5	4.0
STD-M-1E	—	—	—	—	0.4	closed	< 0.1	—	0.6	b. v.	0.1	—	2.0	—
STD-M-2E	< 0.1	closed	closed	closed	0.3	closed	< 0.1	closed	0.6	b. v.	< 0.1	—	1.4	> 4.0
STD-M-2W	< 0.1	—	closed	—	0.4	closed	—	—	0.7	—	0.3	—	2.5	> 5.0
SCC-MS-1W	< 0.1	closed	b. v.	—	0.4	b. v.	0.1	b. v.	0.9	0.1	0.4	0.1	3.0	7.0
SCC-MS-1E	< 0.1	closed	b. v.	closed	0.4	< 0.1	< 0.1	b. v.	0.9	< 0.1	0.1	—	2.5	8.0
SCC-MS-2E	< 0.1	closed	0.05	closed	0.5	b. v.	0.1	b. v.	1.0	0.1	0.15	0.05	3.0	> 6.0
SCC-MS-2W	0.1	closed	0.05	closed	0.6	< 0.05	0.1	0.03	0.9	0.05	0.2	—	1.5	6.0
SCC-HS-1W	0.1	closed	< 0.05	closed	0.4	< 0.05	0.1	< 0.05	1.0	0.07	0.4	0.1	2.0	8.0
SCC-HS-1E*	0.15	b. v.	x x	x x	x x	x x	x x	x x	x x	x x	x x	—	2.8	8.0
SCC-HS-2E	< 0.2	closed	b. v.	closed	0.5	—	0.1	b. v.	1.0	0.05	0.25	0.05	3.0	8.0
SCC-HS-2W	0.1	closed	b. v.	closed	0.4	0.02	0.1	0.02	0.9	0.1	0.25	—	2.3	6.0